The Institute of Paper Chemistry

Appleton, Wisconsin

Doctor's Dissertation

Ultrasonic Characterization of Layered Composite Systems

Michael F. Forbes

January, 1986

MEC-03756

ULTRASONIC CHARACTERIZATION OF LAYERED COMPOSITE SYSTEMS

A thesis submitted by

Michael F. Forbes

B.S. 1978, Georgia Institute of Technology

M.S. 1980, Lawrence University

in partial fulfillment of the requirements
of The Institute of Paper Chemistry
for the degree of Doctor of Philosophy
from Lawrence University,
Appleton, Wisconsin

January, 1986

TABLE OF CONTENTS

ABSTRACT

Ultrasonic measurement techniques have provided a nondestructive method for determining the elastic properties of a material. Recently, these techniques have found increased application in the testing of paper and paperboard. It is generally assumed that these materials behave as homogeneous, orthotropic solids. For layered composites, this assumption is not valid.

A layered orthotropic theory was developed to predict ultrasonic wave behavior in layered composites. To test this theory, a number of two and three layer handsheets were produced. Ultrasonic and mechanical tests were performed on all of the composite sheets and individual layers.

It was found that the layered orthotropic theory accurately predicts the ultrasonic behavior of these composites. The in-plane and out-of-plane elastic constants for the composites could be calculated from the elastic constants of the individual layers. The mechanical measurements could also be related to the ultrasonic properties. These results may aid in the development of new ultrasonic test methods.

INTRODUCTION

The objective of this thesis is to better understand the properties of layered composite orthotropic materials. Layered composite materials are used in everything from automotive and aircraft parts to the brown paper bag found in the local supermarket. Although such materials are quite common, the knowledge about their properties is far from complete.

Just as the use of composite materials has increased, so has the use of ultrasonic measuring techniques. Ultrasonic methods for locating flaws in homogeneous materials have been available for many years.[1] Recently, ultrasonic methods have been developed which will measure the elastic properties of heterogeneous materials such as paper and paperboard.[2-10]

One advantage of ultrasonic measurement techniques is that they are nondestructive. Unlike mechanical tests which either degrade or destroy a test specimen, any number of ultrasonic tests can be performed on the same specimen without degradation. Since ultrasonic measurements are nondestructive, they also lend themselves to process control applications.[9] This possibility has recently attracted a great deal of interest from the paper industry.

For the ultrasonic measurement techniques to be most useful they must be able to deal with layered composite materials. For simplicity these materials have generally been treated as though they were homogeneous. Mann,[2] however, found this assumption did not yield consistent results for layered linerboard samples. He discovered this inconsistency while investigating plate wave velocities in these linerboard samples.

In materials such as paper, a specific kind of harmonic vibration known as a plate wave propagates. These plate waves are dispersive, which means that the velocity at which they propagate in a sheet depends upon the wave's frequency. If a plot of velocity versus frequency is made for the various types of plate waves which can propagate in a given sample, a variety of curves are obtained which are known as dispersion curves. Mann[2] observed that the dispersion curves for layered composites cannot be accurately described using single layer models. Since composite materials make up a large portion of the products in the paper industry, it would be beneficial to describe the dispersive behavior of these layered composites.

The purpose of this thesis is to investigate the ultrasonic behavior of layered composite paper materials. There are two primary objectives:

1. **To characterize layered composite systems.** One would like to understand how the mechanical properties of the individual layers affect the mechanical properties of the composite. Mechanical properties of interest include both the three dimensional elastic properties and conventional strength tests.

2. **To develop and test a layered orthotropic model.** One would like to develop a model which would predict the dispersive behavior of plate waves in layered composites. The predictions of this model should then be compared with experimental data.

The experimental portion of this thesis was designed to meet these objectives. A number of layered paperboard sheets were produced using the Formette Dynamique sheet former. The layers in these composites possessed different

densities, anisotropies, and elastic properties. Ultrasonic and mechanical measurements were conducted on all of the composites and on each of the individual layers. The plate wave behavior was also experimentally obtained for all of the composites.

The theoretical portion of this thesis involves developing models which would predict the plate wave behavior of the layered composite papers. Two analytical models were developed by expanding the techniques used by Mann[2] and Shepard.[11] These new models were capable of predicting the behavior of both two and three layer composites.

BACKGROUND

ULTRASONIC MEASUREMENT OF ELASTIC CONSTANTS

Although ultrasonic measurement techniques have found a number of different applications, our discussion will concentrate primarily upon the ultrasonic methods used for measuring the elastic properties of a material. The elastic properties determine the speed at which a specific type of ultrasonic wave will propagate through the material. The determination of elastic properties, therefore, involves measuring the velocities of these ultrasonic waves as they propagate.

Paper and paperboard are generally assumed to behave as orthotropic materials. Orthotropic materials have three principal axes; the properties of the material being different along each of the axes. By definition, the three principal axes are orthogonal and lie perpendicular to the planes of symmetry in the material. The three principal axes in paper are commonly referred to as machine direction, cross direction, and the Z direction. Occasionally, these three axes are also designated as X, Y, and Z or as 1, 2, and 3. Figure 1 shows the convention used to relate these different types of notation for paper materials.

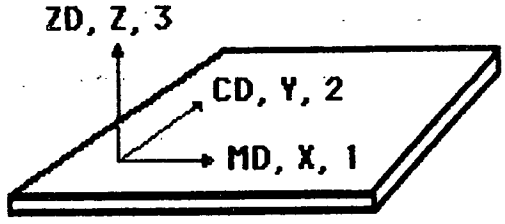

Figure 1. Coordinates for the principal directions of paper.

Consider a cube of material with sides aligned with an orthogonal coordinate system. Three independent stresses may occur at each of the surfaces of the cube. We will assume that the cube is in both translational and rotational equilibrium, and is therefore not undergoing any kind of acceleration. The second order stress tensor for the cube is shown below in Fig. 2.

$$\begin{pmatrix} \sigma_{11} & \sigma_{12} & \sigma_{13} \\ \sigma_{21} & \sigma_{22} & \sigma_{23} \\ \sigma_{31} & \sigma_{32} & \sigma_{33} \end{pmatrix}$$

normal stresses

σ_{11} σ_{22} σ_{33}

shear stresses

σ_{12} σ_{21} σ_{13} σ_{31} σ_{23} σ_{32}

Figure 2. Stress tensor.

Since stress is a second order tensor, it has a double subscript. The first subscript refers to the direction of the normal to the surface on which the stress is acting. The second subscript refers to the direction in which the stress is acting.

It might first appear that 18 different stresses act upon the surfaces of the cube; six surfaces with three stresses acting on each surface. However, since the cube is in both translational and rotational equilibrium, the normal stresses on opposing sides of the cube must be equal in magnitude and opposite in direction. Several of the shear stresses must also have the same values; such that $\sigma_{ij} = \sigma_{ji}$. Therefore, only six independent stresses are needed to describe the stress state of a body in equilibrium.

Writing these stresses in terms of double subscripts can prove a bit tedious. It is a common practice to instead write the six independent values using single subscripts, as shown below:

$$\sigma_1 = \sigma_{11}$$
$$\sigma_2 = \sigma_{22}$$
$$\sigma_3 = \sigma_{33}$$
$$\sigma_4 = \sigma_{23} = \sigma_{32}$$
$$\sigma_5 = \sigma_{13} = \sigma_{31}$$
$$\sigma_6 = \sigma_{12} = \sigma_{21} \qquad (1)$$

These six stresses will of course induce strains within the cube of material. The strains are generally defined in terms of a displacement vector u(x,y,z). The displacement vector describes the change in location of a point in a stressed sample relative to the location of the same point in an unstressed sample. In terms of the displacement vector, the definitions for the six independent strains are:

$$e_1 = e_{11} = \partial u_x/\partial x$$
$$e_2 = e_{22} = \partial u_y/\partial y$$
$$e_3 = e_{33} = \partial u_z/\partial z$$
$$e_4 = e_{23} = e_{32} = (\partial u_x/\partial y + \partial u_y/\partial x)$$
$$e_5 = e_{13} = e_{31} = (\partial u_x/\partial z + \partial u_z/\partial x)$$
$$e_6 = e_{12} = e_{21} = (\partial u_y/\partial z + \partial u_z/\partial y) \qquad (2)$$

The elastic properties of any material can be characterized by the elastic constants relating stresses and strains. This characterization is often made in terms of the engineering constants of Young's moduli, Poisson ratios and shear moduli. This characterization can also be done in terms of the elastic stiffnesses or compliances of the material. As we will see, for ultrasonic measurements it is most convenient to characterize a material in terms of its elastic stiffnesses.

The stiffness tensor (C) defines the stresses in the material as functions of the strains. In matrix form this can be expressed as:

$$(\sigma) = (C)(e) \tag{3}$$

The compliance tensor (S) is the inverse of the stiffness tensor and defines the strains as functions of the stresses.

$$(e) = (S)(\sigma) \tag{4}$$

Instead of the cumbersome four subscripted tensor form C_{ijkl}, the two subscripted stiffness matrix form C_{ij} is employed. The number of nonzero terms in the stiffness matrix depends on the type of material being described. For example, the stiffness matrix for an isotropic material will contain only three different elastic constants. However, for orthotropic materials, such as paper, the stiffness matrix is composed of nine elastic constants. The expanded form of the stiffness matrix is shown below: (One should note that $C_{ij} = C_{ji}$.)

$$\begin{bmatrix} \sigma_1 \\ \sigma_2 \\ \sigma_3 \\ \sigma_4 \\ \sigma_5 \\ \sigma_6 \end{bmatrix} = \begin{bmatrix} C_{11} & C_{12} & C_{13} & 0 & 0 & 0 \\ C_{21} & C_{22} & C_{23} & 0 & 0 & 0 \\ C_{31} & C_{32} & C_{33} & 0 & 0 & 0 \\ 0 & 0 & 0 & C_{44} & 0 & 0 \\ 0 & 0 & 0 & 0 & C_{55} & 0 \\ 0 & 0 & 0 & 0 & 0 & C_{66} \end{bmatrix} \begin{bmatrix} e_1 \\ e_2 \\ e_3 \\ e_4 \\ e_5 \\ e_6 \end{bmatrix} \tag{5}$$

The elastic stiffnesses C_{11}, C_{22}, and C_{33} are the stiffnesses which relate the normal strains e_1, e_2, and e_3 to the normal stresses. These constants are close approximations to the three Young's moduli. Young's modulus is defined as the ratio of normal stress to normal strain when all other stresses are equal to

zero, while C_{11}, C_{22}, and C_{33} are defined as the ratio of normal stress to normal strain when all other strains are equal to zero. Although this difference is small, one should note that these stiffness values are not equal to the corresponding Young's moduli. For example:

$$C_{11} = \frac{\sigma_1}{e_1} \text{ with } e_{2\to6} = 0 \tag{6}$$

while

$$E_x = \frac{\sigma_1}{e_1} \text{ with } \sigma_{2\to6} = 0 \tag{7}$$

The exact relationships for Young's moduli in term of stiffness values is given below in Eq. (8)-(10).

$$E_{11} = \frac{1}{S_{11}} = \frac{C_{11}C_{22}C_{33} + 2\,C_{12}C_{13}C_{23} - C_{11}C_{23}^2 - C_{22}C_{13}^2 - C_{33}C_{12}^2}{C_{22}C_{33} - C_{23}^2} \tag{8}$$

$$E_{22} = \frac{1}{S_{22}} = \frac{C_{11}C_{22}C_{33} + 2\,C_{12}C_{13}C_{23} - C_{11}C_{23}^2 - C_{22}C_{13}^2 - C_{33}C_{12}^2}{C_{11}C_{33} - C_{23}^2} \tag{9}$$

$$E_{33} = \frac{1}{S_{33}} = \frac{C_{11}C_{22}C_{33} + 2\,C_{12}C_{13}C_{23} - C_{11}C_{23}^2 - C_{22}C_{13}^2 - C_{33}C_{12}^2}{C_{11}C_{22} - C_{12}^2} \tag{10}$$

The other diagonal elements of the stiffness matrix are the shear constants C_{44}, C_{55}, and C_{66}. These stiffnesses relate the shear strains to the shear stresses. As seen in Eq. (11)-(13), these values are identical to the engineering shear constants.

$$G_{44} = \frac{1}{S_{44}} = C_{44} \tag{11}$$

$$G_{55} = \frac{1}{S_{55}} = C_{55} \tag{12}$$

$$G_{66} = \frac{1}{S_{66}} = C_{66} \tag{13}$$

The remaining off-diagonal elements of the stiffness matrix are the C_{12}, C_{13}, and C_{23} values. These values are most closely related to Poisson ratios. The exact relationships for the Poisson ratios in terms of the stiffness values are given in Eq. (14)-(19).

$$\nu_{21} = -\frac{S_{12}}{S_{11}} = \frac{C_{12}C_{33} - C_{13}C_{23}}{C_{22}C_{33} - C_{23}^2} \tag{14}$$

$$\nu_{31} = -\frac{S_{13}}{S_{11}} = \frac{C_{13}C_{22} - C_{12}C_{23}}{C_{22}C_{33} - C_{23}^2} \tag{15}$$

$$\nu_{32} = -\frac{S23}{S_{22}} = \frac{C_{23}C_{11} - C_{12}C_{13}}{C_{11}C_{33} - C_{13}^2} \tag{16}$$

$$\nu_{12} = -\frac{S_{12}}{S_{22}} = \frac{C_{12}C_{33} - C_{13}C_{23}}{C_{11}C_{33} - C_{13}^2} \tag{17}$$

$$\nu_{13} = -\frac{S_{13}}{S_{33}} = \frac{C_{13}C_{22} - C_{12}C_{23}}{C_{11}C_{22} - C_{12}^2} \tag{18}$$

$$\nu_{23} = -\frac{S_{23}}{S_{33}} = \frac{C_{23}C_{11} - C_{12}C_{13}}{C_{11}C_{22} - C_{12}^2} \tag{19}$$

If paper is an orthotropic material, its elastic properties can be characterized by nine elastic constants. Ultrasonic methods for obtaining these nine orthotropic elastic stiffnesses have been developed by Mann, et al.[4] These

methods involve measuring the velocities of ultrasonic waves propagating through the material in particular directions. Equations (20)-(28) give the elastic stiffnesses in terms of these particular velocities.

$$C_{11} = \varepsilon V_{LX}^2 \tag{20}$$

$$C_{22} = \varepsilon V_{LY}^2 \tag{21}$$

$$C_{33} = \varepsilon V_{LZ}^2 \tag{22}$$

$$C_{44} = \varepsilon V_{SYZ}^2 \tag{23}$$

$$C_{55} = \varepsilon V_{SXZ}^2 \tag{24}$$

$$C_{66} = \varepsilon V_{SXY}^2 \tag{25}$$

$$C_{13} = (C_{33}\ (C_{11} - \varepsilon V_{SOX}))^{1/2} \tag{26}$$

$$C_{23} = (C_{33}\ (C_{22} - \varepsilon V_{SOY}))^{1/2} \tag{27}$$

$$C_{12} = ((2\ \varepsilon V_S^2(45°) - \tfrac{1}{2}\ (C_{11}+C_{22}) - C_{66})^2 - ((C_{11}-C_{22})/2)^2)^{1/2} - C_{66} \tag{28}$$

where

V_{LX} = velocity of a bulk longitudinal wave traveling in the X direction

V_{LY} = velocity of a bulk longitudinal wave traveling in the Y direction

V_{LZ} = velocity of a bulk longitudinal wave traveling in the Z direction

V_{SXZ} = velocity of an X displacement shear wave traveling in the Z direction

V_{SYZ} = velocity of an Y displacement shear wave traveling in the Z direction

V_{SXY} = velocity of an X displacement shear wave traveling in the Y direction

V_{SOX} = velocity of a low frequency plate wave traveling in the X direction

V_{SOY} = velocity of a low frequency plate wave traveling in the Y direction

V_S45 = velocity of a bulk shear wave traveling at 45° to the X and Y directions

and ρ = apparent density of the material

These three velocities allowed the determination of the three Z direction orthotropic elastic constants C_{33}, C_{44}, and C_{55}.

Since Mann treated paper as a three dimensional orthotropic material, his intent was to determine all nine of the orthotropic elastic constants. He determined the four in-plane ultrasonic constants using a modified Morgan test device. Two additional orthotropic elastic constants were still needed. These were the constants C_{13} and C_{23}.

From Eq. (26)-(27) we see that to obtain the constants C_{13} and C_{23}, the low frequency plate wave velocities V_{SOX} and V_{SOY} must be measured. Plate waves are particular mechanical vibrations which can propagate in thin materials such as paper. Unlike the bulk waves which travel at a velocity which is independent of frequency, plate wave velocities exhibit a frequency dependence known as dispersion. Although the next chapter will deal with plate waves in greater depth, it is important to realize that bulk waves and plate waves are two different types of mechanical vibration.

The velocities actually obtained from Morgan type instruments are not the true bulk longitudinal wave velocities, V_{LX} and V_{LY}, but rather are the low frequency plate wave velocities, V_{SOX} and V_{SOY}. Although for most uses the differences between the bulk wave and low frequency plate wave velocities are insignificant, the values for the elastic constants C_{13} and C_{23} are determined by the differences in these two types of velocities. A method was therefore needed to obtain the bulk in-plane ultrasonic velocities.

Mann[2] obtained these bulk in-plane velocities by measuring the velocity of a longitudinal bulk wave propagating through a stack of sheets. By supplying these bulk velocities into Eq. (26) and (27) he was able to calculate reasonable

Some of the first investigations using ultrasonic measurement in paper were conducted by Craver and Taylor.[5,6] By neglecting any Z direction stresses, they found it easier to characterize a planar orthotropic material. Instead of the nine elastic constants required to characterize a three dimensional orthotropic material, only four elastic constants (C_{11}, C_{22}, C_{12}, and C_{66}) are required to characterize a planar orthotropic material.

Craver and Taylor developed the relationships for the three planar elastic constants E_x, E_y, and G_{xy} in terms of the ultrasonic velocities. They used the sonic moduli values of ρV_{LX}^2 and ρV_{LY}^2 as approximations to the values E_x and E_y. Here the terms V_{Lx} and V_{Ly} represent the velocities of longitudinal waves traveling in the X and Y directions, respectively, and ρ represents the apparent density of the material.

The device which Craver and Taylor used to make their measurements was the Morgan Dynamic Modulus Tester.[12] This consists of two bender type transducers being placed against one surface of the sheet. The tips of these transducers vibrate back and forth along a single line and this motion is coupled into the sheet. A 10 kHz triangular shaped pulse is transmitted from one of the transducers and is received by the other transducer. The electronics of the system measures the time delay between the sent and received signals. By measuring these delays at different transducer spacings, it is possible to calculate the velocity of the wave traveling in the sheet.

The motion of the transducers is polarized along one axis. By rotating the transducers it is possible to transmit either shear or longitudinal waves in a given direction. Propagation of these shear and longitudinal waves along the

appropriate axis allows determination of all four planar ultrasonic elastic constants.

Baum and Bornhoeft[7] also used the Morgan device to measure the in-plane Poisson ratios for paper. In addition to the velocities measured by Craver and Taylor, they also measured a shear wave at 45° with respect to the machine and cross-machine directions. Using this velocity in conjunction with the other in-plane velocities, they were able to calculate the in-plane Poisson ratios. They found good agreement between the ultrasonically determined Poisson ratios and those determined using a biaxial tensile tester.

Craver and Taylor[5] also found a relationship between the elastic modulus values measured ultrasonically and the elastic modulus and strength values measured on a standard tensile tester. A similar correlation between ultrasonic measurements and tensile measurements was obtained by Chatterjee.[13] A theoretical explanation for this correlation has been presented by Waterhouse.[14] The fact that a failure phenomenon such as tensile strength can be correlated with a nondestructive elastic measurement is quite interesting. This result has encouraged the development of an ultrasonic device to function as an on-line measure of tensile strength.

Papadakis[15] and Lu[16] both describe a number of different untried methods for performing on-line ultrasonic measurements. Luukkala et al.[8] developed a noncontacting method for producing plate waves in paper which might be used for making on-line measurements. None of these devices have been tested on moving webs.

Baum and Habeger[9] have reported good results from an on-machine device developed at The Institute of Paper Chemistry. This device consists of ultrasonic transducers mounted in wheels which contact the moving sheet. Delay time measurements are made for ultrasonic waves traveling in both the MD and CD directions. Knowing that $C_{ii} = \rho V_{Li}^2$, extensional stiffness is defined as $\underline{ES_i}$ = (caliper) C_{ii} = (basis weight) V_{Li}^2. By obtaining these velocities in addition to the basis weight, it is possible to estimate the tensile strength of the sheet from the on-line measurements.

Realistically, paper and paperboard cannot be considered planar materials. Though paper is a thin material, it does possess a thickness dimension. In many applications in the paper industry such as printing and converting, the Z direction properties have a large effect upon the end-use performance of the sheet. A method for characterizing these Z direction properties would prove most useful.

Mann[2] was one of the first investigators to use ultrasonic techniques to measure Z direction properties. He treated paper as a three dimensional orthotropic material. To obtain the Z direction elastic properties, it was necessary to measure the ultrasonic velocity of waves traveling in the Z direction of the sheet. These measurements were obtained by placing an ultrasonic transducer on either side of the sheet and transmitting a sinusoidal wave pulse from one of the transducers. The delay time for the wave to traverse the sheet was measured. The caliper of the sheet was then divided by this delay time to yield the Z direction velocity.

Mann needed to make three different velocity measurements in the Z direction; one longitudinal velocity and two shear velocities. The shear wave displacements were polarized to occur either in the X-Z plane or in the Y-Z plane.

values for the constants C_{13} and C_{23}. Mann also measured the longitudinal velocities using a single layer method. He obtained bulk velocities from the single layer method that were similar to the velocities obtained from the stacks of sheets. The single layer method's main advantage was that it eliminated the tedious task of constructing stacks of sheets.

Fleischman[17] also attempted to obtain values for C_{13} and C_{23}. He tried to measure the bulk wave velocities in his samples by using the single sheet method developed by Mann. This technique yielded only limited success. Fleischman concluded that accurate values for C_{13} and C_{23} could only be obtained by constructing stacks of sheets.

Ultrasonic measurement techniques can be applied to paper and paperboard materials. These materials behave as three dimensional orthotropic materials and seven of the nine orthotropic elastic constants can be obtained experimentally. We will now see that these elastic constants can also be used to predict the plate wave behavior of the material.

THEORETICAL DISPERSION CURVES

Plate waves are dispersive waves which can propagate in materials such as paper. This dispersive nature is a function of the elastic constants and thickness of the material. This frequency-velocity function is not one smooth curve, but rather a series of separate curves. Mann[2] calculated these separate dispersion curves for a sample of milk carton stock. The curves representing the behavior of plate waves propagating in the CD of the sheet are shown in Fig. 3.

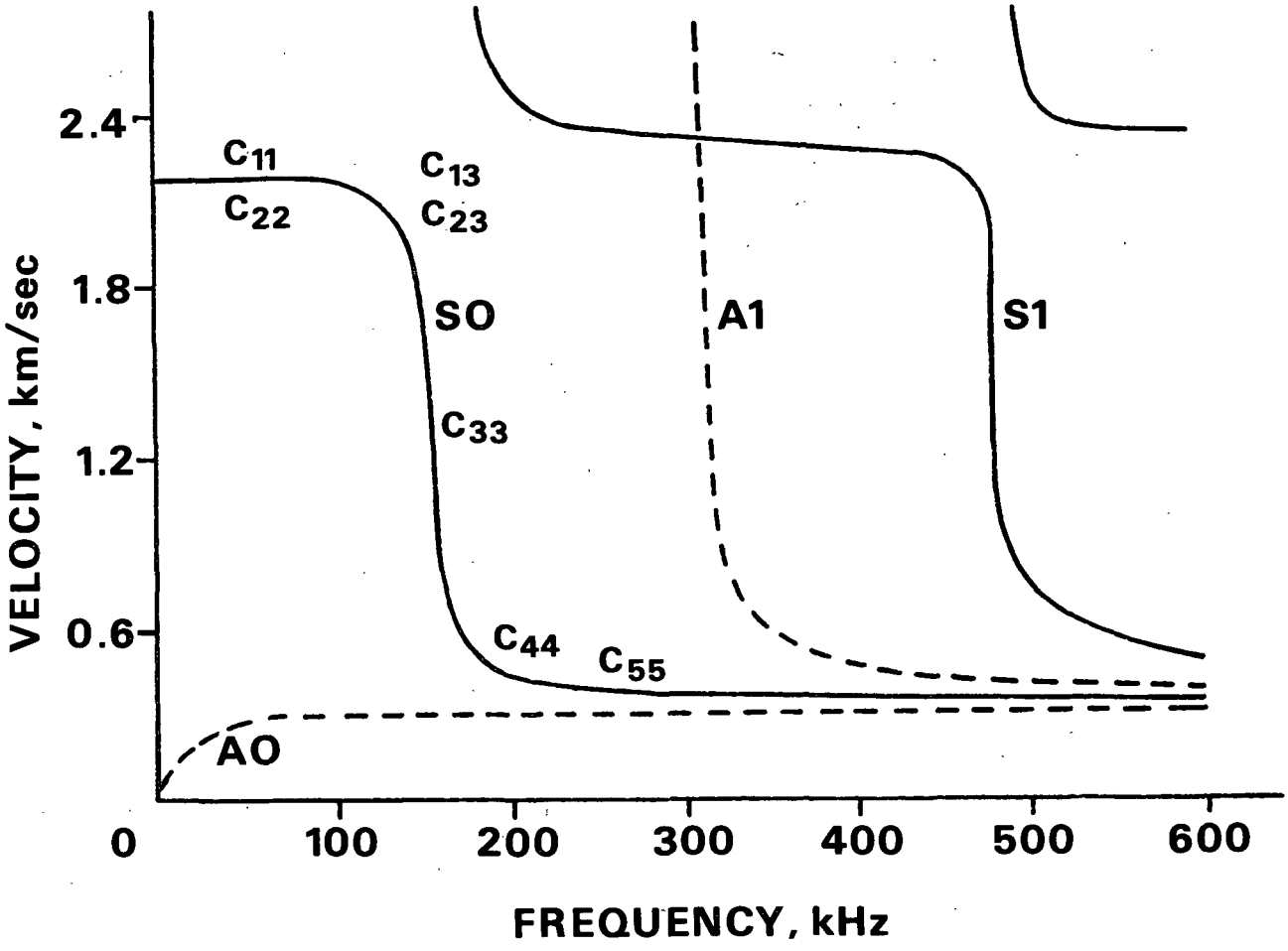

Figure 3. CD dispersion curves for Mann's[2] milk carton stock sample.

Mann[2] found that for each of the curves in Fig. 3, a different kind of displacement was occurring in the sample. Plate waves on the SO curve induced symmetrical displacements in the sheet, while plate waves on the AO curve induced antisymmetrical displacements. The other curves represented higher order modes of displacements similar to either of the SO or AO curves. The S(n) curves represented symmetrical displacements and the A(n) curves represented antisymmetrical displacements. Mann found the displacements which occur for these modes and some of these displacements are shown in Fig. 4.

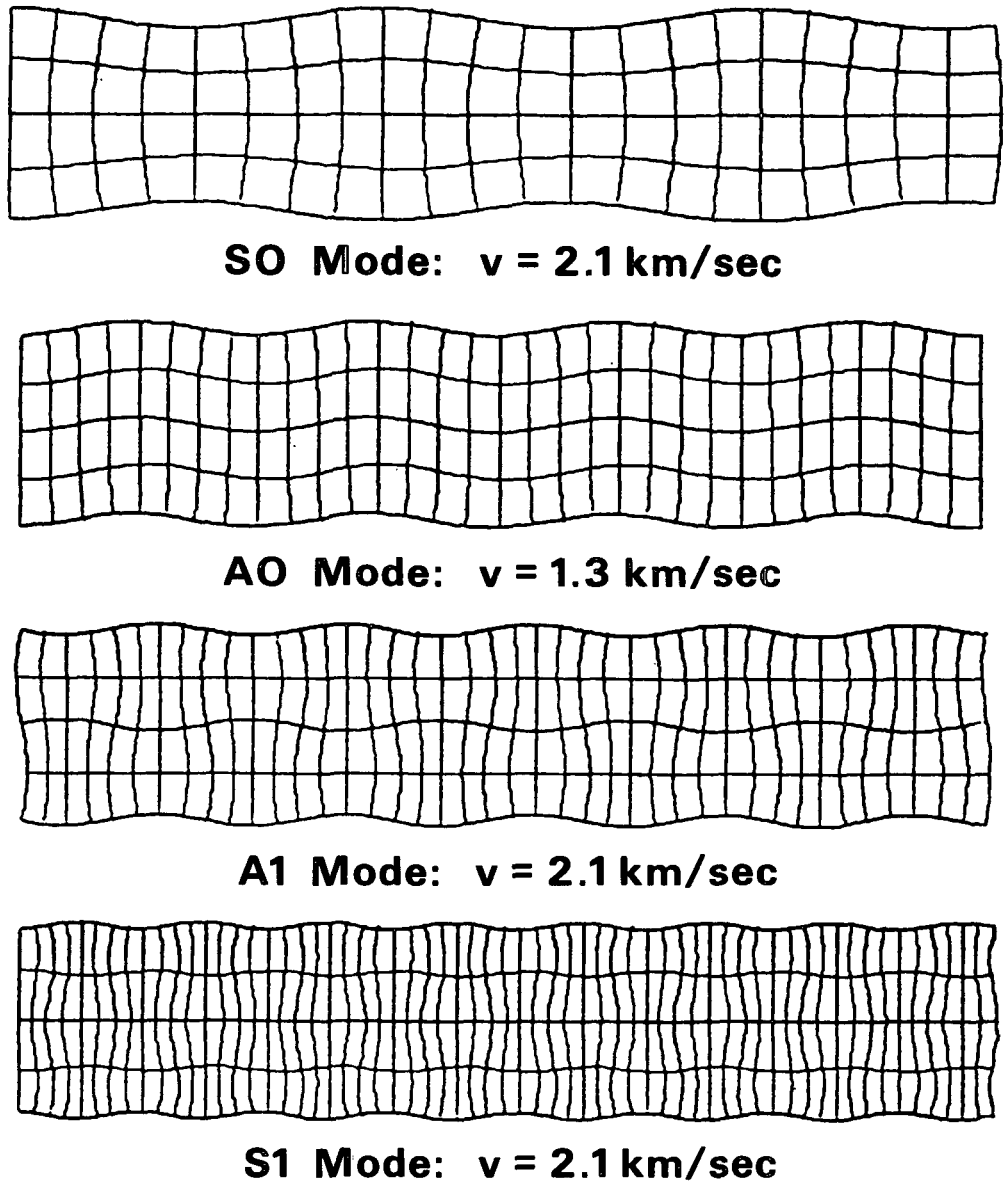

Figure 4. Plate wave displacements for various modes of the dispersion curves as calculated by Mann[2].

Mann was one of the first investigators to study plate wave vibrations in paper. He used a model[18] which predicted dispersion curves for an orthotropic material. From the bulk orthotropic elastic stiffness values, Mann was able to calculate the theoretical dispersion curves for the material.

With his model, Mann was able to observe how the various stiffnesses affected the shape of the curves. In Fig. 3, the stiffnesses are shown in the regions of the curves most affected by those particular constants. Here the constants C_{11}, C_{33}, C_{13}, and C_{55} apply to a plate wave propagating in the X direction of the sample, while the constants C_{22}, C_{33}, C_{23}, and C_{44} would apply to similar curves for a plate wave propagating in the Y direction of the sample.

The model used by Mann assumed that plate waves are actually a combination of bulk waves traveling in the sample. As noted earlier, bulk waves are non-dispersive. They travel through a volume of material at a velocity which is independent of frequency. It might seem unreasonable to assume that these non-dispersive waves could produce the dispersive behavior common to plate waves. We will see how this dispersion occurs.

A rather interesting phenomenon takes place when a bulk wave impinges upon a free surface of the material. Instead of the wave simply being reflected from the interface, two waves are reflected. This phenomenon is known as mode conversion. For example, say a longitudinal wave impinges on a surface of the sample; instead of only a longitudinal wave being reflected, both a longitudinal and shear wave are reflected from the interface. Similarly, when a shear wave strikes a surface, both a longitudinal and shear wave are reflected. The only time mode conversion does not occur is when the displacements of an incident shear wave are parallel to the surface of the sheet. In this case, only the shear wave is reflected.

In thin materials such as paper, multiple reflections occur at both surfaces of the sheet. A single bulk wave impinging on one surface of the sheet will be converted to a large number of shear and longitudinal waves by these

multiple reflections. It is possible that some combinations of longitudinal and shear waves might produce interference patterns.

Mann's model[2] used an analytic technique known as the method of partial waves. This method had previously been used by Solie and Auld[18] for studying the plate wave behavior of plates with cubic symmetry. This method assumes that a number of bulk waves propagate in the sample, and that these waves are coupled by their reflections at the surfaces of the plate. The boundary conditions assume that all normal and shear stresses at the surfaces of the plate equal zero. The displacements of these bulk waves add constructively to yield the displacements of the plate wave. For this kind of interference to occur, the component of the individual wave vectors in the direction that the plate wave is traveling must be equal to the wave vector of the plate wave.

Consider a plate wave propagating in the X direction of the sample. Four bulk waves are chosen such that the X components of their wave vectors are the same as the wave vector for the plate wave, K_x. This is illustrated in Fig. 5.

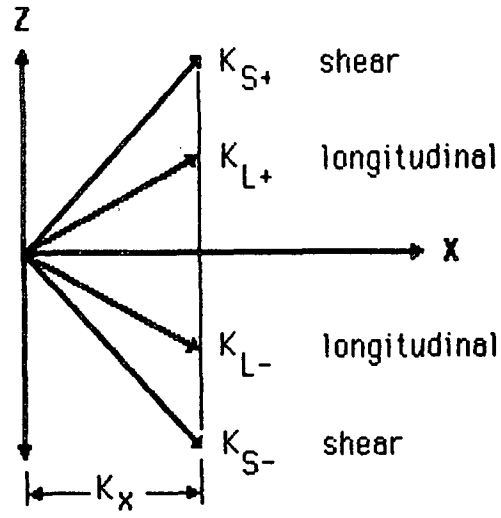

Figure 5. Wave vectors for single layer plate wave model.

To construct a plate wave traveling in the X direction we must first find a solution to the equations of motion. From Kolsky,[19] the general equations of motion are:

$$\rho \frac{d^2U_1}{dt^2} = \frac{d}{dx}\sigma_1 + \frac{d}{dy}\sigma_6 + \frac{d}{dz}\sigma_5 \tag{29}$$

$$\rho \frac{d^2U_2}{dt^2} = \frac{d}{dx}\sigma_6 + \frac{d}{dy}\sigma_2 + \frac{d}{dz}\sigma_4 \tag{30}$$

$$\rho \frac{d^2U_3}{dt^2} = \frac{d}{dx}\sigma_5 + \frac{d}{dy}\sigma_4 + \frac{d}{dz}\sigma_3 \tag{31}$$

Here U_1, U_2, and U_3 represent the components of the displacement vector $u(U_1, U_2, U_3)$ in the X, Y, and Z directions, respectively.

If the plate wave displacements are planar and are confined to the X-Z plane, the displacements in the Y direction will equal zero. If all displacements in the Y direction equal zero, all of the partials with respect to the Y direction will also equal zero and the displacement equations become:

$$\rho \frac{d^2U_1}{dt^2} = \frac{d}{dx}\sigma_1 + \frac{d}{dy}\sigma_5 \tag{32}$$

$$\rho \frac{d^2U_3}{dt^2} = \frac{d}{dx}\sigma_5 + \frac{d}{dy}\sigma_3 \tag{33}$$

If the generalized Hooke's law equations [Eq. (5)] are substituted into Eq. (32) and (33), one obtains the equations of motion in terms of the elastic stiffnesses and the strains. If the definitions of strains [Eq. (2)] are also substituted onto these equations, the equations of motion become:

$$\rho \frac{d^2U_1}{dt^2} = C_{11} \frac{d^2U_1}{dx^2} + C_{13} \frac{d^2U_3}{dxdz} + C_{55} \left(\frac{d^2U_1}{dz^2} + \frac{d^2U_3}{dxdz} \right) \tag{34}$$

$$\rho \frac{d^2U_3}{dt^2} = C_{33} \frac{d^2U_3}{dz^2} + C_{13} \frac{d^2U_1}{dxdz} + C_{55} \left(\frac{d^2U_1}{dxdz} + \frac{d^2U_3}{dx^2} \right) \tag{35}$$

Assuming plane wave solutions for these equations of the form:

$$U_1 = U_{1A} \exp [i(K_x X + K_z Z - \omega t)] \tag{36}$$

$$U_3 = U_{3A} \exp [i(K_x X + K_z Z - \omega t)] \tag{37}$$

Substituting these solutions into the equations of motion yields:

$$\rho U_{1A} \omega^2 = C_{11} U_{1A} K_x^2 + (C_{55} + C_{13}) U_{3A} K_x K_z + C_{55} U_{1A} K_z^2 \tag{38}$$

$$\rho U_{3A} \omega^2 = C_{55} U_{3A} K_x^2 + (C_{55} + C_{13}) U_{1A} K_x K_z + C_{33} U_{3A} K_z^2 \tag{39}$$

Eliminating U_{1A} and U_{3A} gives:

$$(C_{55} + C_{13})\, 2K_x^2 K_z^2 = (\rho\omega^2 - C_{11}K_x^2 - C_{55}K_z^2)\,(\rho\omega^2 - C_{55}K_x^2 - C_{33}K_z^2) \tag{40}$$

The solutions to this equation are:

$$K_z^2 = \frac{K_x^2}{2} \left[-B \pm (B2 - 4D)^{1/2} \right] \tag{41}$$

where:

$$B = \frac{\rho}{C_{33}C_{55}} \left[C_{33} \left(\frac{C_{11}}{\rho} - \frac{\omega^2}{K_x^2} \right) - \frac{C_{13}}{\rho} (2C_{55} + C_{13}) - C_{55} \frac{\omega^2}{K_x^2} \right] \tag{42}$$

and

$$D = \frac{\rho}{C_{33}C_{55}} \left[\frac{\omega^2}{K_x^2} - \frac{C_{55}}{\rho} \right] \left[\frac{\omega^2}{K_x^2} - \frac{C_{11}}{\rho} \right] \tag{43}$$

For any given value of wave number K_x and frequency ω, four values of K_z exist. These values correspond to four different bulk waves propagating in the

layer. Two of these bulk waves are longitudinal waves, one propagating in the positive Z direction and the other propagating in the negative Z direction. The two other bulk waves are shear waves, one propagating in the positive Z direction and the other propagating in the negative Z direction.

The amplitude of the Z direction displacements can be related to the amplitude of the X direction displacements. Taking Eq. (38) and (39) and solving for the ratio of the amplitudes yields:

$$\frac{U_{3A}}{U_{1A}} = \frac{(\omega^2 - C_{11}K_x^2 - C_{55}K_{z\pm}^2)}{(C_{55} + C_{13})K_xK_{z\pm}} = \tan\phi_{\pm} \tag{44}$$

We will use the terms $\tan\phi_+$ and $\tan\phi_-$ to designate the ratios which correspond to positive and negative roots for K_z, respectively.

Plate wave solutions are chosen which are linear combinations of the four solutions to Eq. (41). M, N, P, and Q designate the relative magnitudes of these four waves. The assumed plate wave solutions are therefore:

$$u_x = e^{i(k_xx-\omega t)}\,(Me^{ik_{z+}z} + Ne^{-ik_{z+}z} + Pe^{ik_{z-}z} + Qe^{-ik_{z-}z}) \tag{45}$$

$$u_z = e^{i(k_xx-\omega t)}\,[\tan\phi_+(Me^{ik_{z+}z} - Ne^{-ik_{z+}z}) + \tan\phi_-(Pe^{ik_{z-}z} - Qe^{-ik_{z-}z})] \tag{46}$$

If the caliper of the sheet is taken to be equal to T, then the surfaces of the sheet are located at Z = ± T/2. The boundary conditions must require that there is zero normal stress and zero shear stress at the surfaces of the sheet. These boundary conditions are:

$$\sigma_3 = C_{33}\frac{\partial u_z}{\partial z} + C_{13}\frac{\partial u_x}{\partial x} = 0 \tag{47}$$

$$\sigma_5 = C_{55}\left(\frac{\partial u_z}{\partial x} + \frac{\partial u_x}{\partial z}\right) = 0 \tag{48}$$

If the plate wave solutions are substituted into Eq. (47) and (48) for $Z = \pm T/2$, a series of four equations in four unknowns is obtained. In matrix form, these equations are:

$$\begin{bmatrix} G_+e^{1/2ik_{z+}T} + G_+e^{-1/2ik_{z+}T} + G_-e^{1/2ik_{z-}T} + G_-e^{-1/2ik_{z-}T} \\ G_+e^{-1/2ik_{z+}T} + G_+e^{1/2ik_{z+}T} + G_-e^{-1/2ik_{z-}T} + G_-e^{1/2ik_{z-}T} \\ H_+e^{1/2ik_{z+}T} - H_+e^{-1/2ik_{z+}T} + H_-e^{1/2ik_{z-}T} - H_-e^{-1/2ik_{z-}T} \\ H_+e^{-1/2ik_{z+}T} - H_+e^{1/2ik_{z+}T} + H_-e^{-1/2ik_{z-}T} - H_-e^{1/2ik_{z-}T} \end{bmatrix} \begin{bmatrix} M \\ N \\ P \\ Q \end{bmatrix} = 0 \quad (49)$$

where

$$G_\pm = C_{33}k_{z\pm}\tan\phi_\pm + C_{13}k_x \quad (50)$$

$$H_\pm = k_{z\pm} + k_x \tan\phi_\pm \quad (51)$$

Nontrivial solutions exist if and only if the determinant of the matrix equals zero. This requirement reduces to the equation:

$$[\tan(1/2k_{z+}T)/\tan(1/2k_{z-}T)] = [H_-G_+/H_+G_-]^{\pm 1} \quad (52)$$

Equation (52) describes the dispersive behavior of plate waves traveling in the sheet. Solutions of Eq. (52) are found for only specific values of K_x and ω. Since plate wave velocity equals ω/K_x, these solutions are the combinations of frequency and velocity found on the dispersion curves.

This was the method which Mann used to calculate the theoretical dispersion curves shown in Fig. 3. He measured the elastic constants of the material using ultrasonic techniques; he measured the caliper and basis weight of the sample; and he supplied these values to a computer program which calculated the values of frequency and velocity which gave solutions to Eq. (52). He then used these points to plot the dispersion curves for the sample.

Mann also measured the dispersion curves for his samples experimentally, using a noncontacting technique originally developed by Luukkala, et al.[8] This method generates plate waves by impinging an ultrasonic plane wave upon the surface of the sample. This technique is shown in Fig. 6.

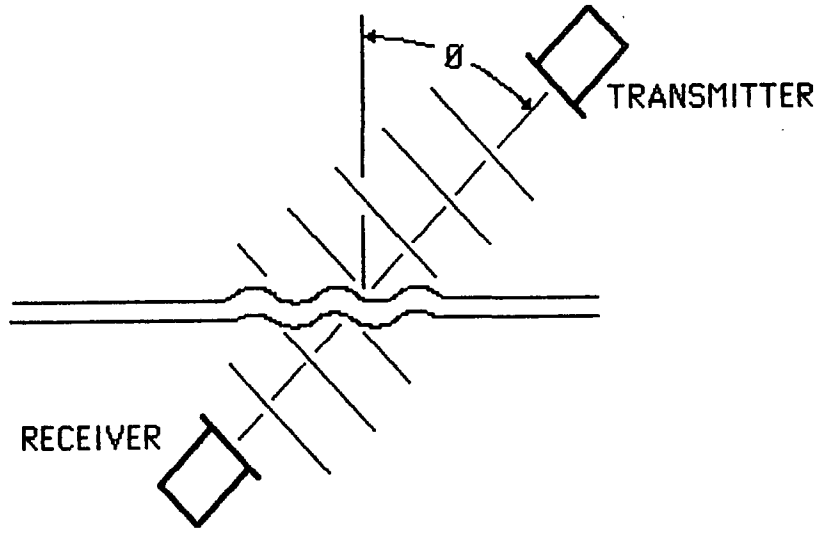

Figure 6. Plate wave resonance device.

Plate waves are generated as the transmitter and receiver are rotated with respect to the sample. At some angle ϕ_{max} and frequency ω, a resonance may occur within the sample. This resonance is detected by an increase in the amplitude of the received signal. At resonance, the projection of the wave fronts of the transmitted ultrasound propagates along the sample at the same velocity as a plate wave propagating in the sample. Knowing the velocity of sound in air and the angle ϕ_{max}, it is possible to calculate the velocity of the plate wave at frequency ω from the equation:

$$\text{Velocity}_{\text{Plate Wave}} = \frac{\text{Velocity}_{\text{Air}}}{\text{Sin } \phi_{max}} \tag{53}$$

With these experimental values, Mann was able to test the predictions of his model. For his milk carton stock, the agreement between the theory and the data was quite good. However, for his linerboard samples, the results were not as good. The dispersion curves for one of his linerboard samples are shown in Fig. 7.

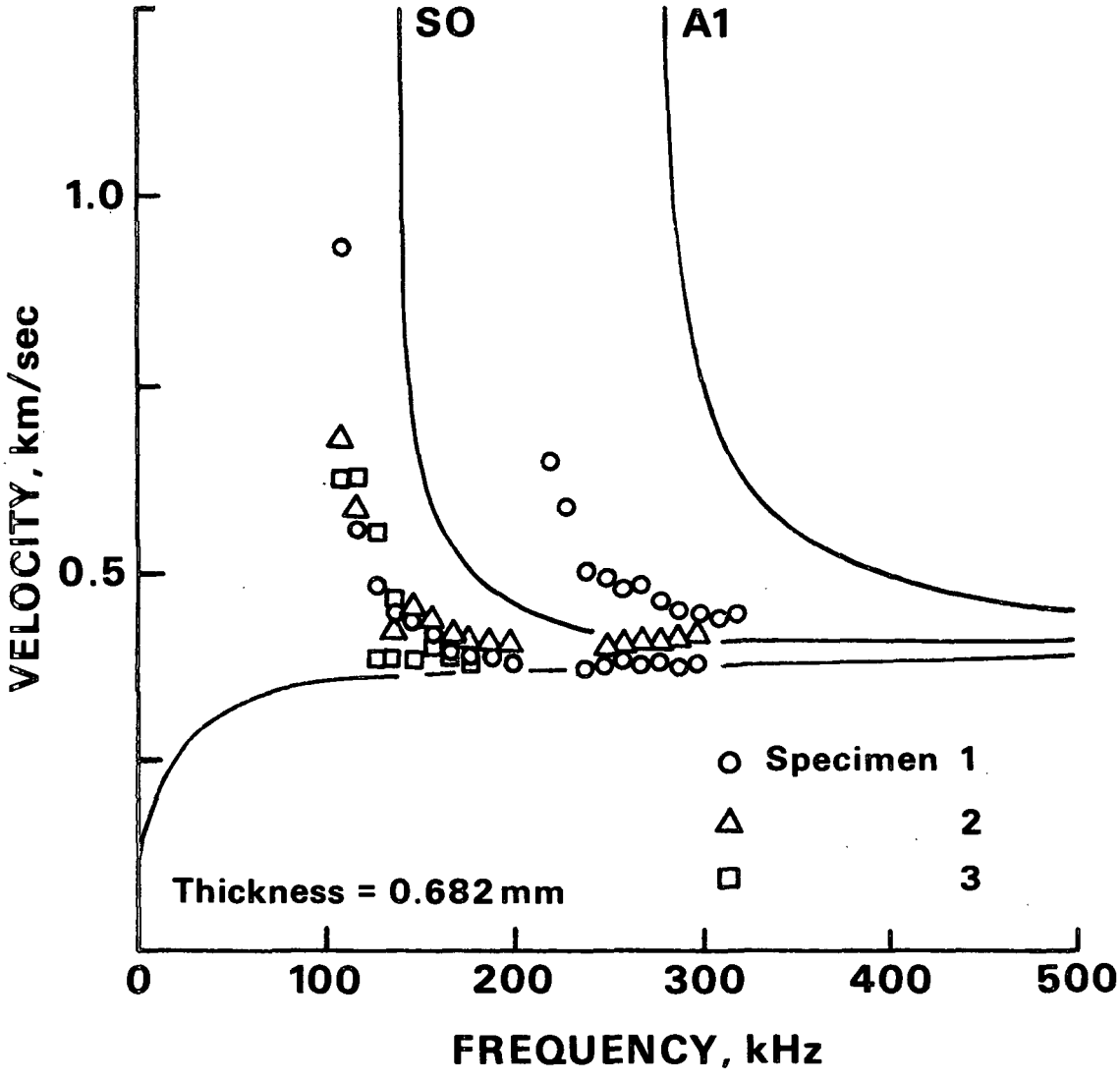

Figure 7. Dispersion curves for one of Mann's[2] linerboard samples.

Upon investigation, Mann found that this linerboard sample was produced on a two headbox paper machine. The sample was therefore not a homogeneous orthotropic layer, but was rather a two layer composite material. Since Mann's theory did not deal with such a composite, it is not surprising that this theory did not fit his experimental results.

Shepard[11] was one of the first to attempt to calculate the dispersion curves for a two layer composite. He attempted to model the plate wave behavior of a coated paper. His theoretical model consisted of an isotropic layer of material perfectly bonded to an orthotropic layer. He assumed continuity of stress and strain across the interface between the two layers for these "perfectly" bonded composites.

Shepard's model expanded upon the model of Mann. Plate wave solutions similar to those in Eq. (45) and (46) were choosen for each of the layers in Shepard's model. These solutions were:

$$U_X = \exp[i(K_X X - wt.)]\,[M\exp(iK_Z{+}Z) + N\exp(-iK_Z{-}Z) + P\exp(iK_Z{+}Z) + Q\exp(-iK_Z{-}Z)] \tag{54}$$

$$U_Z = \exp[i(K_X X - wt.)]\,[\tan\phi{+}\{M\exp(iK_{Z+}Z) + N\exp(-iK_{Z-}Z)\} + \tan\phi{-}\{P\exp(iK_{Z+}Z) + Q\exp(-iK_{Z-}Z)\}] \tag{55}$$

$$U'_X = \exp[i(K_X X - wt.)]\,[M'\exp(ik'_{Z+}Z) + N'\exp(-iK'_{Z-}Z) + P'\exp(iK_{Z+}Z) + Q'\exp(-iK_{Z-}Z)] \tag{56}$$

$$U'_Z = \exp[i(K_X X - wt.)]\,[\tan'\phi{+}\{M'\exp(iK'_{Z+}Z) + N'\exp(-iK'_{Z-}Z)\} + \tan'\phi{-}[P'\exp(iK'_{Z+}Z) + Q'\exp(-iK'_{Z-}Z)\}] \tag{57}$$

For the composite, Shepard let Z = 0 represent the interface between the layers. Here the unprimed values refer to the orthotropic layer while the

primed values refer to the isotropic layer. Z = g represents the top surface of the orthotropic layer and Z = -f represents the bottom surface of the isotropic layer. Shepard used the same four boundary conditions used by Mann and shown in Eq. (47) and (48).

In addition to those boundary conditions, he also assumed continuity of stress and strain across the interface between the two layers. These additional boundary conditions are:

$$U_1(X,0,t) = U_1'(X,0,t) \tag{58}$$

$$U_3(X,0,t) = U_3'(X,0,t) \tag{59}$$

$$\sigma_3(X,0,t) = \sigma(3'(X,0,t) \tag{60}$$

$$\sigma_5(X,0,t) = \sigma_5'(X,0,t) \tag{61}$$

Here the definitions of σ_3 and σ_5 are the same as those given in Eq. (47) and (48).

By substituting the plate wave solutions into the boundary conditions, Shepard obtained a series of eight equations in eight unknowns. In matrix form, these equations are:

$$\begin{bmatrix}
1 & 1 & 1 & 1 & -1 & -1 & -1 & -1 \\
\tan\phi_+ & -\tan\phi_+ & \tan\phi_- & -\tan\phi_- & -\tan'\phi_+ & \tan'\phi_+ & -\tan'\phi_- & \tan'\phi_- \\
G_+ & G_+ & G_- & G_- & -G'_+ & -G'_+ & -G'_- & -G'_- \\
C_{55}H_+ & -C_{55}H_+ & C_{55}H_- & -C_{55}H_- & -C_{55}H'_+ & C_{55}H'_+ & -C_{55}H'_- & C_{55}H'_- \\
G_+\exp(iKz+g) & G_+\exp(-iKz+g) & G_-\exp(iKz-g) & G_-\exp(-iKz-g) & 0 & 0 & 0 & 0 \\
0 & 0 & 0 & 0 & G'_+\exp(-iKz+f) & G'_+\exp(iKz+f) & G'_-\exp(-iKz-f) & G'_-\exp(iKz-f) \\
H_+\exp(iKz+g) & H_+\exp(-iKz+g) & H_-\exp(iKz-g) & H_-\exp(-iKz-g) & 0 & 0 & 0 & 0 \\
0 & 0 & 0 & 0 & H'_+\exp(-iK'z+f) & H'_+\exp(iK'z+f) & H'_-\exp(-iK'z-f) & H'_-\exp(iK'z-f)
\end{bmatrix}
\begin{Bmatrix} M \\ N \\ P \\ Q \\ M' \\ N' \\ P' \\ Q' \end{Bmatrix} = 0 \tag{62}$$

Here

$$G_{\pm} = C_{33}K_{z\pm}\tan\phi_{\pm} + C_{13}K_x \quad (63)$$

$$H_{\pm} = K_{z\pm} + K_x\tan\phi_{=} \quad (64)$$

$$G'_{\pm} = C'_{33}K'_{z\pm}\tan'\phi_{\pm} + C'_{13}K_x \quad (65)$$

$$H'_{\pm} = K'_{z\pm} + K_x\tan'\phi_{\pm} \quad (66)$$

Shepard was unable to further simplify the dispersion relationship into an algebraic equation. However, he was able to numerically determine the values of velocity and frequency which made the determinant go to zero. By supplying the model with the appropriate elastic constants for each of the layers, Shepard was able to calculate the theoretical dispersion curves for a number of different composites.

Unlike Mann, Shepard was only able to test the low frequency region of the SO mode plate wave curve for his samples. Although good agreement between the theory and the experimental data was found in this region of the curves, Fig. 7 shows that the main disparity for Mann's composite linerboard sample was found in the fall-off region of the SO mode. Because Shepard was working with thin samples, the fall-off regions of the curves fell at relatively high frequencies. At these frequencies, it was impossible to obtain the plate wave data for his samples. However, he was able to compare the fall-off regions calculated by his model with the predictions of an impedance model.[11] He found good agreement between the fall-off regions predicted by these two different models. Although Shepard's layered model appears successful, he was unable to fully test the model against experimental data.

One of the objectives of this thesis is to develop a model to calculate the dispersion curves for a composite constructed of two orthotropic layers. This

model will be obtained by modifying Shepard's model. The theoretical dispersion curves will then be compared with experimental data for actual two layer composites.

THE BENDING OF LAYERED COMPOSITES

Many paper products can be classified as layered composites. Many board grades produced today are formed on multiple headbox machines, often with different grades of pulp in each of the various layers. Coated papers might also be considered as layered composite materials. The production of composite materials will continue to grow in the years to come.

There are two principal motivations for manufacturing layered composites. The first is to manufacture a product which either could not otherwise be produced or would be prohibitively expensive to produce as a single layer material. The second is to use the layering process to optimize the properties of the product to meet the requirements of a specific end-use application. In either case, the ability to accurately characterize the properties of the layered composite would be most beneficial.

The property of layered composites which has received the most attention has been bending stiffness. From classical mechanics,[20] one finds that the bending stiffness for a composite beam is given by:

$$EI_{Composite} = \sum_{i=I}^{n} E_i I_i \tag{67}$$

The $E_i I_i$ values for the individual layers are taken relative to the neutral plane of the composite. When a beam is bent, part of the beam is in tension and

part is in compression. Between these two regions of stress there lies a plane of points which experience no stress. This plane is referred to as the neutral plane (Fig. 8).

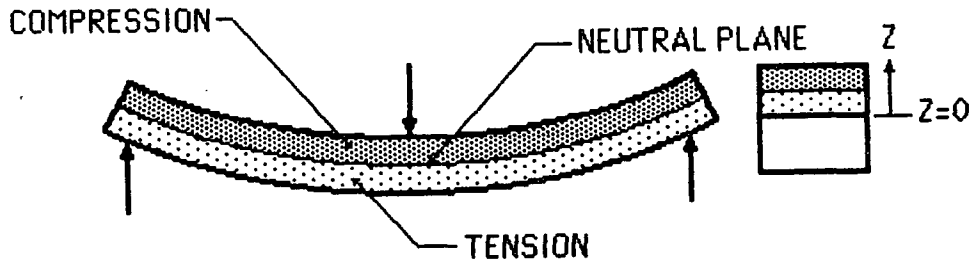

Figure 8. The neutral plane.

The location of the neutral plane can be calculated from the equation:

$$Z_c = [\Sigma A_i(E_i/E_1)R_i]/[\Sigma A_i(E_i/E_1)] \qquad (68)$$

Here A_i is the cross-sectional area of the layer i, (E_i/E_1) is the ratio of Young's modulus for the layer i to the Young's modulus of layer 1, R_i is the distance (Z) the centroid of layer i is from the arbitrary reference point Z = 0, and Z_c is the location of the neutral plane relative to the point Z = 0. Here, layer 1 refers to the layer in the composite chosen as a reference value for Young's modulus. Regardless of which layer in the composite is chosen as layer 1, the value of Z_c will remain the same. Although Eq. (67) and (68) are quite simple, finding the location of the neutral plane of the composite and calculating the individual layer moments is quite tedious.

Carlsson and Fellers[21] reported a simplified method for calculating the bending stiffness of layered composites. The bending stiffness value for the composite, S_b, is obtained from the equation:

$$S_b = D - \frac{B^2}{A} \tag{69}$$

Where:

$$A = \sum_{k=1}^{n} (E_x)_k \ (R_k - R_{k-1}) \tag{70}$$

$$B = \frac{1}{2} \sum_{k=1}^{n} (E_x)_k \ (R_k^2 - R_{k-1}^2) \tag{71}$$

$$D = \frac{1}{3} \sum_{k=1}^{n} (E_x)_k \ (R_k^3 - R_{k-1}^3) \tag{72}$$

The main advantage of Carlsson and Fellers' method for determining bending stiffness is that it does not require the calculation of the composite's neutral axis. The apparent difference between the units of Eq. (67) and (69) occurs because Eq. (67) applies to the bending stiffness of a beam of finite width, while Eq. (69) is derived from a planar bending model. This planar bending analysis yields a bending stiffness which is normalized with respect to the composite's width.

The bending model of Carlsson and Fellers yields the bending stiffness values for composites under the conditions of pure bending. However, many of the test methods for bending stiffness induce shear forces as well as bending moments in the sample.[22,23] The results of these tests will not necessarily follow the classical model for a beam in pure bending.

The four point bending test[24] ideally offers a bending test which is free of shear stresses. Although a small shear load is induced into the sample by the strain gage displacement measurement, this shear load is generally negligible. The bending stiffness results obtained from a four point bending test may be assumed to represent the bending stiffness values for a beam in pure bending.

EXPERIMENTAL

HANDSHEETS

The goal of this thesis is to characterize layered composite systems. To do this, a number of suitable paper composites must first be obtained. One approach would be to select composites which are available commercially. Although a large number of commercial samples are available, the construction and properties of the individual layers of these composites are either unknown or unsuitable for experimental work. A study of commercially available composites would also present difficulties in characterizing the individual layer properties. To obtain the single layer properties, the various layers of the composite would have to be separated by some mechanical means. Separation of the individual layers of a composite, without affecting the properties of the layers, has proven a difficult task.[25]

The approach used in this work was to produce layered composites which possess the desired characteristics. The composites could be constructed from either two or three single orthotropic layers. The bonding between layers, however, must be strong enough to ensure continuity of stress and displacement across the interface.

To improve energy transmission when making plate wave resonance measurements, it is desirable for each layer to have a low density. The energy of the ultrasonic wave which can be transmitted between air and the sheet depends upon the relative acoustic impedances of air and paper. The energy transfer between two materials is greatest when the two acoustic impedances are nearly identical. The energy transfer decreases as the differences between the two impedances

increases. The acoustic impendance of a material is directly related to the material's density.[26] Air has a relatively low density and low acoustic impedance. To efficiently couple the energy of an ultrasonic wave from air into a sheet of paper, the sheet should therefore have a low density and a low acoustic impendance.

The Institute's Formette Dynamique was selected as the means for producing these layered structures. The Formette is a machine which produces oriented handsheets by spraying a pulp slurry upon the interior of a rotating cylindrical screen. By varying the pressure at the spraying nozzle and the rotational speed of the screen it is possible to vary the degree of fiber orientation within the sheet.

The elastic properties of the sheet change with fiber orientation.[17] The anisotropy of the sheet, or the ratio of the MD modulus to the CD modulus, is affected by the degree that the fibers are oriented to the MD of the sheet. As the degree of fiber orientation increases, the anisotropy of the sheet also increases. By altering the fiber orientation, therefore, it is possible to alter the anisotropy of the sheet.

It is possible to produce two and three layer sheets directly inside the Formette. However, as noted earlier, it is difficult to obtain the single layer properties for these composites. Although the forming conditions for a single layer could be matched closely to the forming conditions for one of the layers in the composite, fines migration and differences in forming conditions might alter the properties of the two sheets. Sheets with basis weights in excess of 400 g/m^2 could not be formed using the Formette. Thus, since high basis weight composites were of interest, no composites were actually formed within the Formette.

Single layer oriented handsheets were produced using the Formette and portions of these sheets were wet pressed together into layered composites. Each single layer Formette sheet was cut into four 8 x 8 inch sheets. Two of these pieces were wet pressed into layered composites and two of the sheets were retained as single layers. Since the composites and single layer sheets were pressed and dried under identical conditions, the single layer sheets should be representative of the single layers within the composite.

Two dissimilar pulps were selected for producing the layered composites. The first was a refined unbleached softwood kraft pulp (350 CSF) and the second was a repulped newsprint furnish (180 CSF). The softwood kraft pulp was obtained from Domtar as dry-lap market pulp. The newsprint was obtained from the Appleton Post Crescent. Fiber analysis of the newsprint furnish revealed that the pulp was 90% softwood and 10% hardwood and that the furnish had been mechanically pulped. Since these pulps possessed different elastic properties, they could be used to construct composites with significantly different layer properties.

The first series of composites were two layer sheets. A 2^4 factorial design was chosen as the basis for producing these sheets. All of the composites were composed of the kraft layer (S) and the newsprint layer (G), with two levels of basis weight and fiber orientation for each layer. The single layers or composite sheets were stacked between blotters and pressed in a Baldwin platen press at a pressure of 860 psi for twenty minutes. The pressed sheets were then dried using the Institute's cylinder dryer. A listing of the two layer sheets and their compositions appears in Table 1.

Table 1. Composition of two layer 1182 series of samples.

	Mechanical Pulp Layer				Chemical Pulp Layer			
	Basis Weight		Anisotropy		Basis Weight		Anisotropy	
Sample	High	Low	High	Low	High	Low	High	Low
GS1		x		x		x		x
GS2	x			x		x		x
GS3		x	x			x		x
GS4	x		x			x		x
GS5		x		x	x			x
GS6	x			x	x			x
GS7		x	x		x			x
GS8	x		x		x			x
GS9		x		x		x	x	
GS10	x			x		x	x	
GS11		x	x			x	x	
GS12	x		x			x	x	
GS13		x		x	x		x	
GS14	x			x	x		x	
GS15		x	x		x		x	
GS16	x		x		x		x	

Basis weight - High ≈ 400 g/m,^{2} - Low ≈ 200 g/m^2
Orientation - High R ≈ 2, - Low R ≈ 1

A second series of two and three layer composites was also produced. As before, single layer sheets were produced on the Formette, using the same two pulp types. This time the kraft pulp freeness was 310 CSF and the freeness for the newsprint was 240 CSF. Two different levels of basis weight and two levels of fiber orientation were again selected for each pulp type. However, instead of aligning the direction of orientation of each of the layers in the composite, the single layers for the two different pulp types were cross laminated. The machine direction for the newsprint furnish, for example, was aligned with the cross direction of the kraft furnish. The purpose of this cross lamination was to increase the differences between the individual layer properties in the

composite. The direction designated as the "machine" direction for these composites was the one aligned with the machine direction of the kraft single layers. These sheets were pressed at 625 psi for 20 minutes and then dried in the Institute roll dryer. The pressing pressure was reduced to lower the densities of these sheets. A listing of the composition of all of these sheets appears in Table 2.

Table 2. Composition of three layer 883 series of samples.

	Layer 1						Layer 2						Layer 3					
	Pulp		B. W.		Anis.		Pulp		B. W.		Anis.		Pulp		B. W.		Anis.	
Sample	T	K	H	L	H	L	T	K	H	L	H	L	T	K	H	L	H	L
TK1	x		x			x	x		x			x	x		x			x
TK2		x	x			x		x	x			x		x	x			x
TK3	x		x		x			x	x		x		x		x		x	
TK4		x	x		x		x		x		x			x	x		x	
TK5	x		x		x			x	x		x			x	x		x	
TK6		x	x		x		x		x		x		x		x		x	
TK7		x		x	x		2		x		x			x		x	x	
TK8	x			x	x			2	x		x		x			x	x	
TK9	x		x			x		x	x		x		x		x		x	
TK10		x	x			x	x		x		x			x	x		x	
TK11	x		x		x			x	x			x		x	x		x	
TK12		x	x		x		x		x			x	x		x		x	
TK13	2			x	x			2		x	x		2			x	x	
TK14	2			x		x	2			x		x	2			x		x
TK15		2		x		x		2		x		x		2		x		x
TK16	2			x	x			x	x			x	2			x	x	
TK17		2		x	x		x		x			x		2		x	x	
TK18		2		x	x		2			x	x			2		x	x	

Definitions:

H - High
L - Low
T - Newsprint
K - Kraft
2 - Two identical layers pressed together

Basis weight: High ≈ 250 g/m^2; Low ≈ 125 g/m^2

Orientation: High R ≈ 2; Low R ≈ 1

Prior to testing, all of the sheets were conditioned at 15% RH for 24 hours and then conditioned at 50% RH for 48 hours. The basis weight of the sheets was determined by weighing the full sample size of the conditioned sheets. After trimming, this sample size was 20.32 x 20.32 cm.

ULTRASONIC MEASUREMENT TECHNIQUES - ELASTIC CONSTANTS

Equations (20)-(28) show that the elastic constants of an orthotropic material can be obtained by measuring specific ultrasonic velocities. Determining these velocities involves measuring the time it takes for an ultrasonic wave to travel a given distance in the material. We will now discuss the equipment and techniques required to make these "time of flight" measurements.

In-Plane Elastic Constants

The low frequency plate wave velocities are measured using the IPC ultrasonic modulus tester.[27] This device measures the time required for an ultrasonic wave to travel between two points on the sample. Although a number of different techniques have been used to obtain these time delays, the technique that is currently being used at IPC[28] is shown in Fig. 9. An Apple IIE computer is used both to coordinate the testing procedure and to analyze the resulting data. For each measurement cycle, the computer first triggers the function generator to supply a single 60 kHz sinusoidal pulse to the middle transducer of the system. The signal from one of the receiving transducers is amplified, digitized, and sent back to the computer. The computer then signals the function generator to send a second 60 kHz pulse to the sending transducer. The received signal from the other transducer is then amplified, digitized, and sent to the computer. The computer is programmed to allow enough time to elapse between pulses so that

the reflections of the first signal do not interfere with the second pulse. A photograph of the in-plane measurement apparatus is shown in Fig. 10.

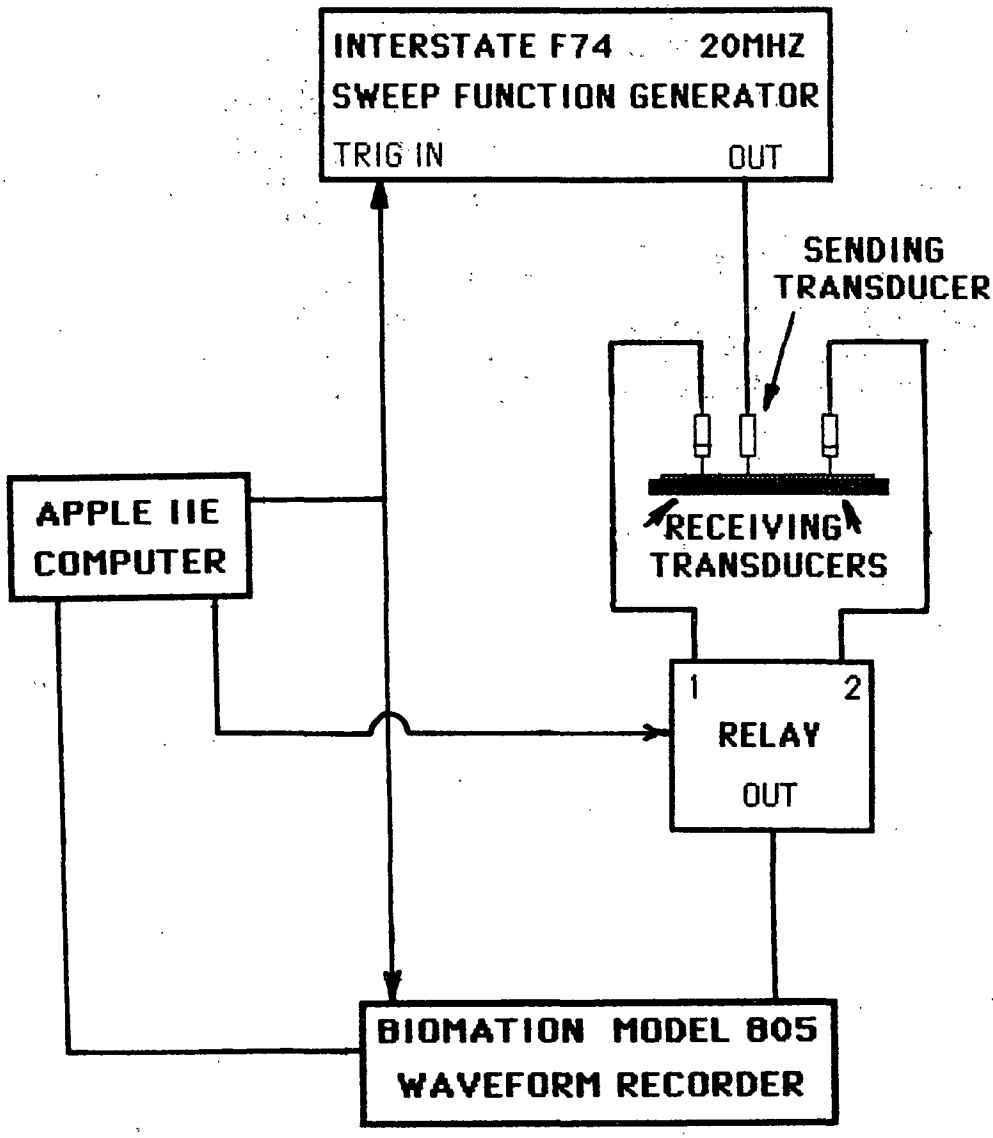

Figure 9. The in-plane velocity measurement device.

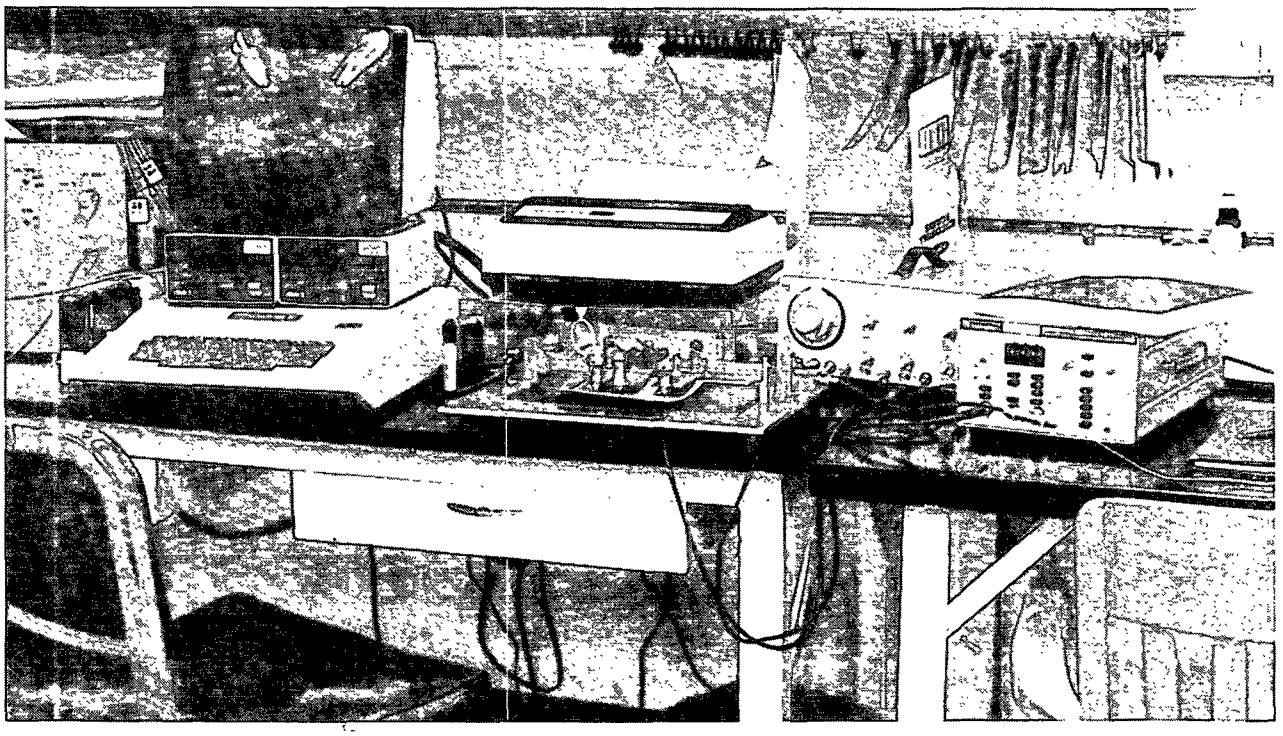

Figure 10. Photograph of the in-plane velocity measurement device.

The computer does a cross-correlation between the two digitized signals and calculates the delay time. All other delays due to the measurement system will be the same for both signals and therefore will not affect the calculated delay time. Knowing the delay time between the two signals (T), and the two transducer spacings (D_1 and D_2), the velocity is:

$$\text{Velocity} = (D_2 - D_1)/T \tag{73}$$

This method for measuring velocities has a number of advantages. One advantage is that the transducers always remain in fixed positions. Previous measuring techniques involved different transducer spacings which required the operator to physically move the transducers. This was time consuming and introduced possible errors in the transducer spacing. Using fixed position transducers allows the test to be performed more easily and reduces the chance of an error in transducer spacing.

Another advantage of this method is that it is easy to conduct signal averaging at each test position on the sample. Instead of performing only one velocity measurement, the computer can be instructed to perform a number of tests at each position and then average the results. Since each test only takes about one second, averaging several tests at each point does not require a prohibitive length of time. This kind of averaging improves the cross-correlation between the two averaged digitized signals and therefore improves the accuracy of the delay time measurement.

The in-plane velocities are low frequency plate waves propagating within the sample. The mechanical disturbance is produced using Pomona Electronics Model 3753 "bender" type transducers. The small, rounded tips of these transducers essentially make point contact with the surface of the sheet. When the transducers are positioned such that the motion of the tips are aligned with the line between transducers, a longitudinal plate wave is propagated between transducers. When the motion of the tips is oriented perpendicular to the line between transducers, a bulk shear wave is transmitted between transducers. This same kind of test arrangement can be used to obtain the V_{SXY} and $V_{S45°}$ velocities.

The in-plane shear plate wave velocities are the same as the velocities of bulk shear waves propagating in the plane of the sheet. However, the in-plane longitudinal wave velocities are for dispersive plate waves. The measurements are made at 60 kHz to ensure that these longitudinal velocities fall along the low frequency plateau region of the SO mode, as shown in Fig. 3. Since the plateau region of the curves is relatively flat, the measured velocities are relatively insensitive to small changes in frequency.

Out-of Plane Elastic Constants

When attempting to measure Z direction ultrasonic velocities, one must know the caliper of the sample and the length of time required for the ultrasonic wave to propagate through the sample. Ideally, these two measurements should be made at the same time and at the same place on the sample. A device which will make both measurements simultaneously has been developed at The Institute of Paper Chemistry. The device which is shown schematically in Fig. 11, is basically an IPC caliper tester in which the platens have been replaced with ultrasonic transducers.

When using this arrangement to measure the Z direction longitudinal velocity, the two transducers are 5 MHz longitudinal transducers and the items labeled "pillows" are actually pieces of soft rubber. The function generator sends a short pulse of 1 MHz ultrasound to both the sending transducer and the oscilloscope. The signal obtained at the receiving transducer is amplified and sent to another channel of the oscilloscope. By comparing the signals on the oscilloscope it is possible to determine the time delay of the received signal with respect to the transmitted signal. The caliper of the sample is measured at the same location as the delay time measurement. By dividing the caliper by the delay time, one obtains the desired Z direction velocity.

There are delays in the measuring system other than the delay of the ultrasound traveling through the sample. These nonpaper delay times must be subtracted from the measured values to obtain the delay times through the sample. The most obvious method for obtaining these other delays would be to measure the time delay obtained when no sample is placed between the transducers. Unfortunately, this method cannot be used because the two soft rubber pillows

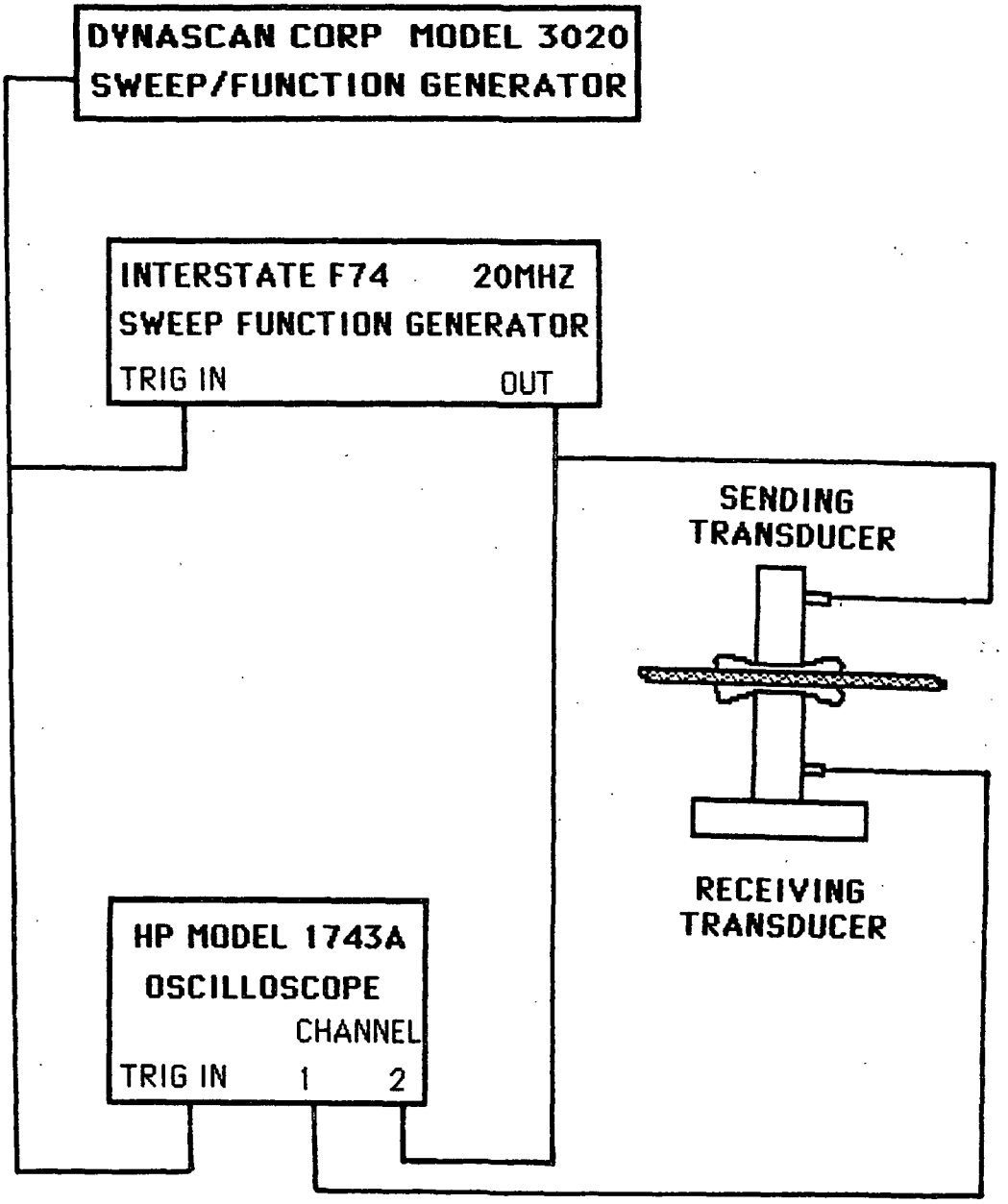

Figure 11. The out-of-plane velocity measurement device.

deform differently when they are placed against one another than they do when placed on either side of a sample.

The method used involves measuring the delay time of an ultrasonic wave traveling through a thin piece of aluminum foil. The foil allows the soft rubber pillows to deform against a rigid surface. Since the caliper of the foil and the velocity of sound in aluminum are known, it is possible to calculate the delay time through the foil. However, because the velocity of sound in aluminum is very high and the caliper of the foil is quite low, it is often possible to neglect the delay through the foil.

High frequency ultrasound is required to make accurate Z direction measurements. A high frequency, short wavelength ultrasonic wave allows the first peak of the wave to be transmitted cleanly through the sample without interference from reflections from the sheet's surfaces. For this reason, the wavelength of the ultrasound should always be shorter than the caliper of the sample. It would appear that going to higher and higher frequencies would improve the accuracy of the Z direction velocity measurements. However, there is an upper limit to the frequencies which can be used. As the wavelength of the ultrasound begins to approach dimensions of fiber width, scattering begins to take place from the fibers in the sample and the signal is severely attenuated. For typical paper systems, this usually occurs at frequencies around 1.5 to 2.0 MHz.

So far we have only discussed the longitudinal Z direction velocity measurements. Shear measurements are made in a device which is very similar to the device used for longitudinal measurements. The transducers used to make shear measurements, however, vibrate in the plane of the paper, rather than perpendicular to the sheet. Rubber cannot be used as a couplant, because rubber

does not transmit shear. No couplant is required for thick samples, but for thin or very rough samples, a couplant is necessary.[29] Fluid filled "pillows" are employed. The basic arrangement of the device and the electronics for handling the signals remains essentially the same as those shown in Fig. 11. A photograph showing both the longitudinal and shear out-of-plane modulus testers is shown in Fig. 12.

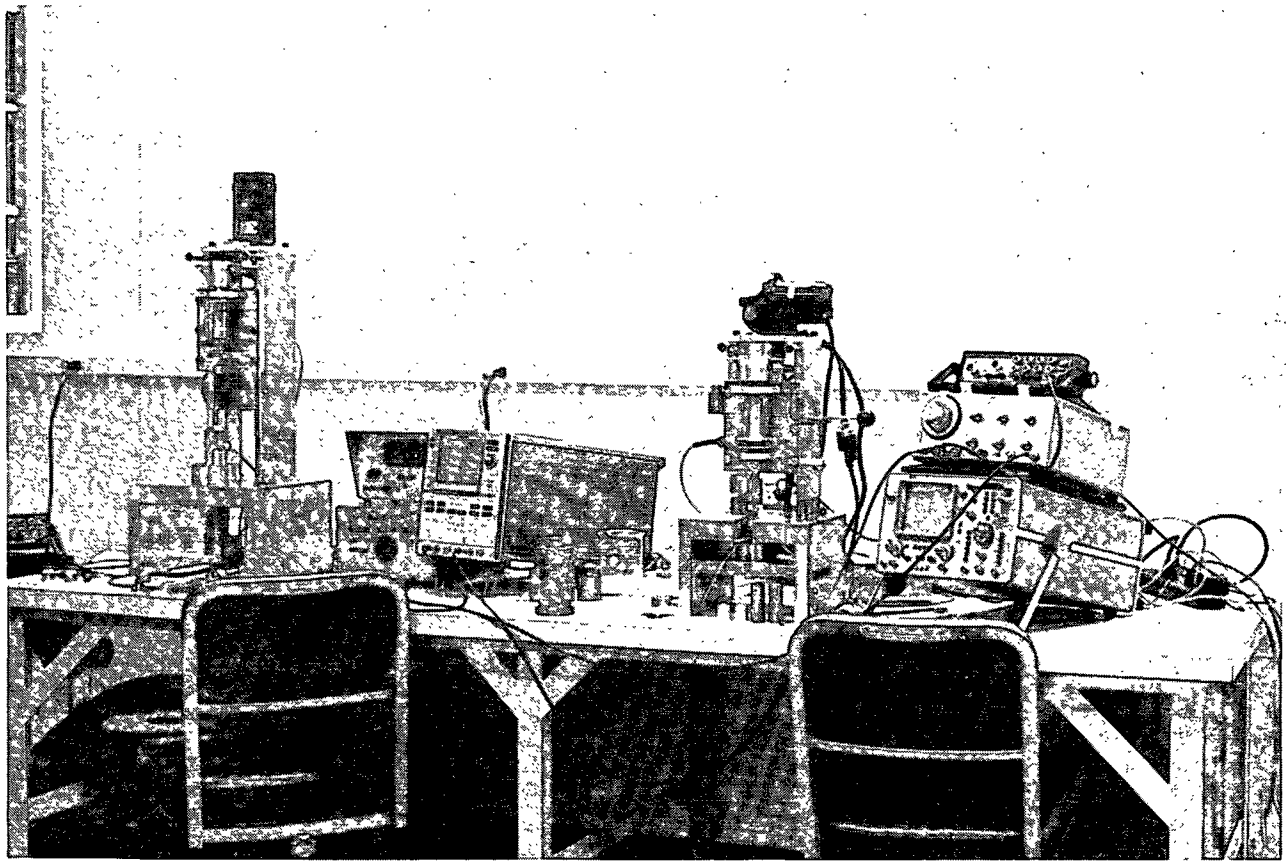

Figure 12. Photograph showing both the longitudinal and shear out-of-plane velocity measurement devices.

The fluid filled pillows are used primarily to improve the shear coupling between the sample and the transducers. Coupling shear waves into paper materials has long been a problem when making Z direction velocity measurements. The hard surfaces of the transducers simply do not transmit a large percentage of the shear wave energy into the sample.

The main advantage of using the fluid filled pillows is that the sample is not contaminated with the coupling material. The pillows are constructed by placing a known quantity of diluted polybutene oil between two films of polyethylene and sealing the edges together. The coupling material does not come in contact with the sample, but it still effectively couples the shear wave between the transducers and the sheet.

With respect to normal time frames, polybutene behaves as a viscous fluid. As the transducers are loaded, the polyethylene film conforms to the surface of sample and the fluid flows to fill the many small depressions on the sample surface. The film and fluid are therefore placed in intimate contact with the sheet. By adjusting the viscosity of the polybutene, one can tailor the flow of the fluid to the surface roughness of the sample.

At ultrasonic frequencies, polybutene behaves as though it were a solid, providing an excellent shear couplant between the transducers and the sheet. The fluid filled pillows therefore provide a good method for coupling shear energy into the sample without contaminating the surface and possibly changing the elastic properties of the sample.

The fluid filled pillows do present additional difficulties in measuring path length and system time delays. Although more time consuming than the methods used for the Z direction longitudinal measurements, the methods give good results. The methods are described in detail by Wink and Habeger.[29]

We have discussed the methods involved for obtaining seven of the nine orthotropic elastic constants. These measurements were performed on all of the composite and single layer sheets described earlier. The elastic constants were used in the orthotropic models to calculate the theoretical dispersion curves

for the composites. We next discuss how the experimental dispersion curves were obtained.

Plate Wave Measurement Device

One of the objectives of this thesis is to predict dispersion curves for layered composites. To test the predictions it is necessary to have some experimental technique for measuring the velocities of plate waves propagating in the composites. Mann[2] modified a technique originally used by Luukkala, et al.[8] to obtain these velocities. The work described here improves upon Mann's technique.

The device used for measuring plate wave velocities is shown in Fig. 13. The main differences between this device and that used by Mann lie in the ultrasonic transducers and the lock-in amplifier. Since Mann reported that air currents had significant effects upon the measurements, the sample and transducer arrangement was enclosed within a glove box. A photograph of the plate wave device appears in Fig. 14.

Figure 14 shows that the two transducers are not equal distances from the sample. Ideally, the sending transducer should be located as far from the sample as possible so that the incident waves are very nearly plane waves. Due to attenuation of the ultrasound in air and the physical size of the glove box, the distance between the sending transducer and the sheet was reduced to 12 inches. The distance from the sheet to the receiving transducer was only four inches. Since the receiving transducer only measures the amplitude of the signal, it is desirable to place it as close to the sheet as possible to reduce the amount of attenuation of the signal by air.

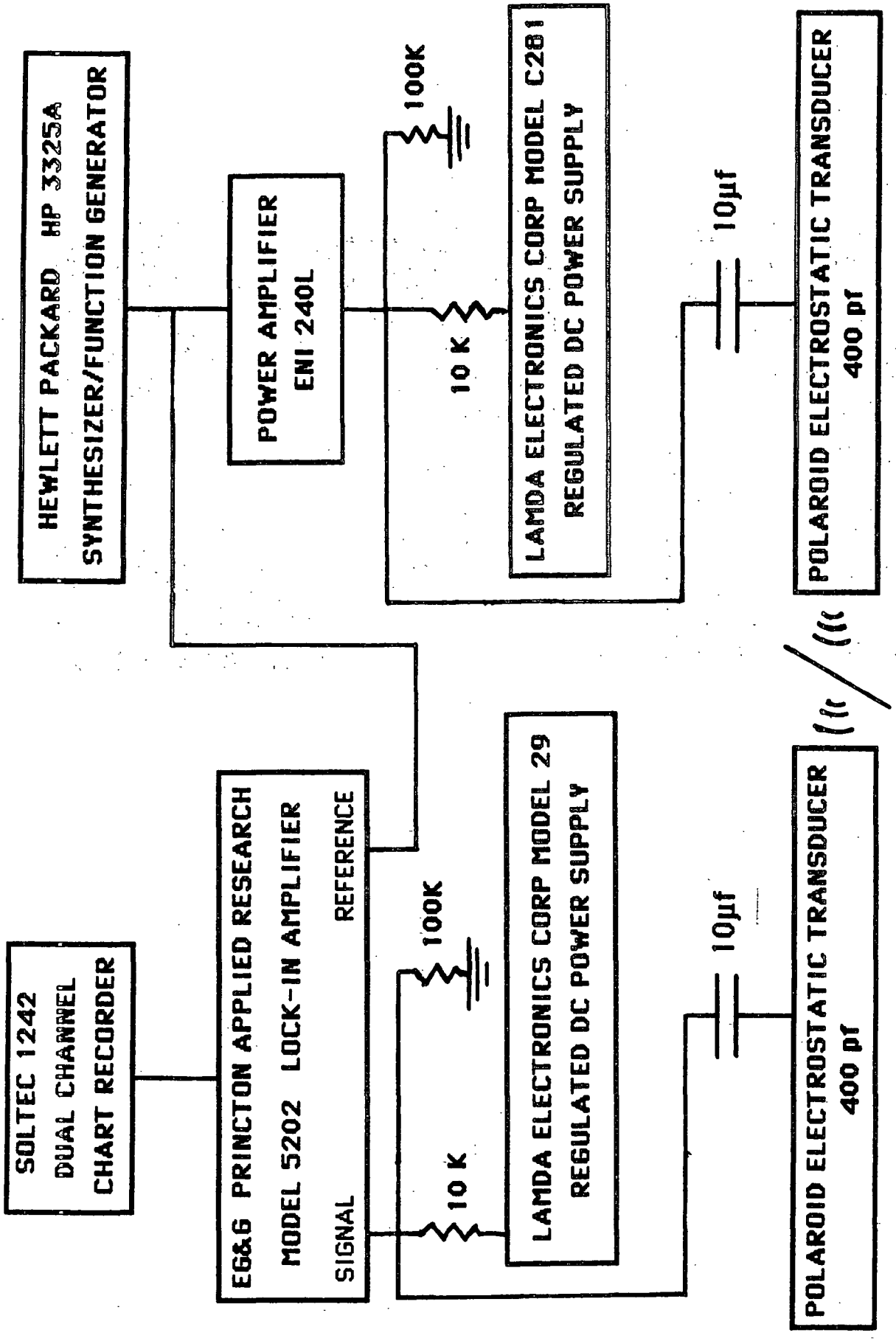

Figure 13. The plate wave resonance device.

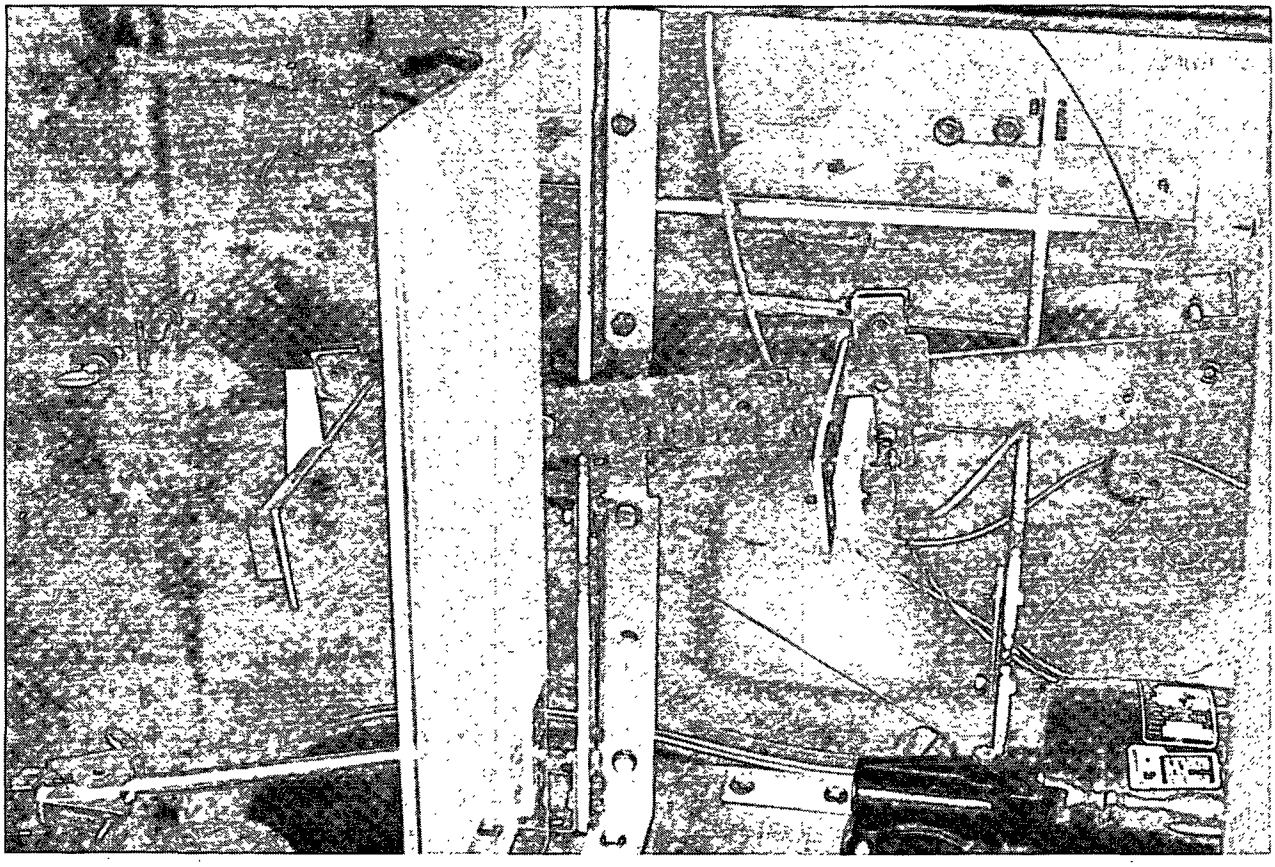

Figure 14. Photograph of transducer and sheet position for the plate wave resonance device.

The transducers used were electrostatic transducers manufactured by the Polaroid Corporation for use in their ultrasonic ranging cameras. These transducers were designed to operate within a narrow frequency range around 50 kHz, but by modifying the backplates it was possible to increase the frequency range to about 400 kHZ. This modification involved removing a spiral grooved backplate supplied by Polaroid, and replacing it with aluminum disks which were roughened slightly by rubbing them with 400 grit Carborundum powder. The modified transducers were quite stable and their response did not change with time. This stability was a considerable improvement over the electret transducers employed by Mann.

The operation of the plate wave device is quite simple. The frequency synthesizer supplies a continuous sine wave signal to both the power amplifier and lock-in amplifier. The amplified signal produces an ultrasonic wave at the sending transducer which impinges upon the sample at an angle, ϕ. The receiving transducer picks up the transmitted signal and sends it to the lock-in amplifier. The lock-in amplifier uses the signal from the frequency generator as a reference and amplifies only that frequency in the received signal. A major advantage of the lock-in amplifier is that it removes all extraneous signals.

The amplitude of the received signal and the angle of the transducers is recorded using the chart recorder. The angle of the transducers is obtained via a calibrated potentiometer attached to the rotating transducer arm. Typical chart traces for the received signal and potentiometer output are shown in Fig. 15. The angle ϕ_{max} is determined by comparing the location of the peaks in the received signal with the potentiometer output.

Figure 14 shows that the potentiometer curve goes both up and down. The resonance measurement is first performed as ϕ is slowly changed from 70° to 10°, and then is repeated as ϕ is changed from 10° back to 70°. For each measurement, therefore, two sets of resonance curves are obtained. The average of these resonance values of ϕ yield the values for ϕ_{max}.

Figure 15 shows two sets of resonance peaks. The outer peaks correspond to a point on the A0 mode dispersion curve, and the inner peaks correspond to a point on the S0 mode dispersion curve. At low frequencies, only the A0 mode peaks will appear. As frequency is increased the S0 mode peaks will begin to appear at low values of ϕ. As frequency increases further, the S0 peaks will

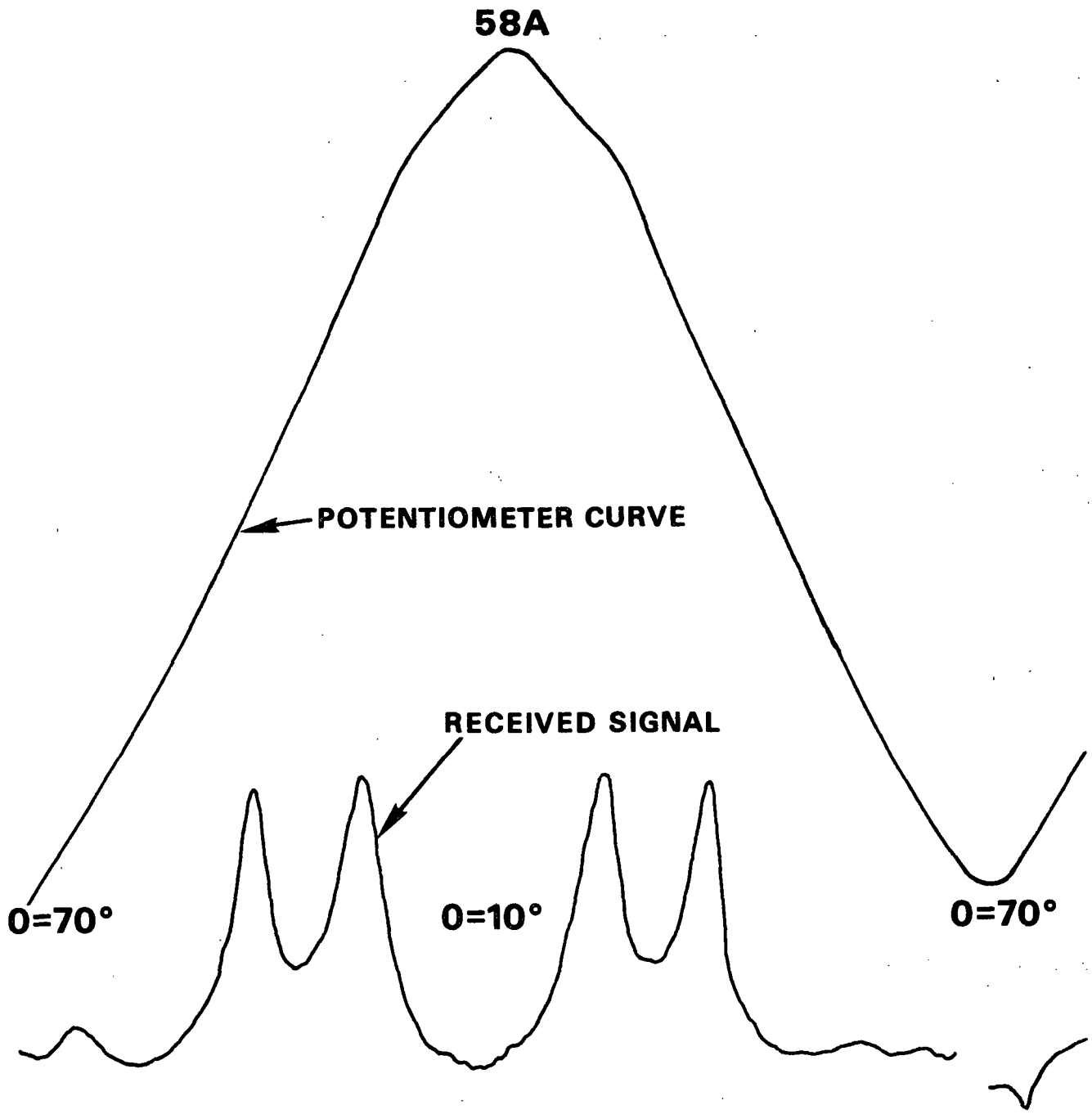

Figure 15. Plate wave resonance curves.

move to higher values of ϕ until they are nearly on top of the A0 peaks. As frequency is increased further, another set of peaks may appear at low values of ϕ. These peaks correspond to points on the A1 mode dispersion curve. After obtaining the values for ϕ_{max}, the velocities of the plate waves can be calculated from Eq. (53).

Plate wave measurements at frequencies higher than 300 to 350 kHz are usually not possible due to the attenuation of ultrasound as it travels through air. This frequency limitation makes detection of the fall-off regions of the dispersion curves difficult. The "fall-off" regions of the dispersion curves (see Fig. 3) occur when a longitudinal standing wave develops in the Z direction of the sample. The frequency at which this standing wave develops is a function of C_{33} and the caliper of the sample. As C_{33} increases, the "fall-off" frequency also increases. Similarly, as the caliper of the sample decreases, the "fall-off" frequency also increases. In order for the initial "fall-off" region of the dispersion curves to be in the 100 to 350 kHz frequency range, the sample should have both a high caliper and a low C_{33} stiffness.

The plate wave technique also has some velocity limitations, since from Eq. (53) it is evident that the measured plate wave velocity can never be less than the velocity of sound in air. A velocity of 1000 m/sec is the practical upper velocity limit for this technique. Above this velocity, the transducers are located almost perpendicular to the sample. At these angles $\sin\phi$ is nearly zero and the resonance peaks become broad, making determination of the maxima difficult.

One method for improving the velocity range would be to use a gas other than air. Since the sample and transducer arrangement was located inside a

glove box to reduce the effects of air currents, introducing different gases into the glove box did not require major alterations to the apparatus.

One problem in using gases other than air, however, is maintaining the moisture content of the sample. A changing moisture content drastically changes the elastic properties of the sample. Thus when using a gas other than air, the gas was bubbled through a saturated salt solution to maintain a 50% RH level. The gas within the glove box was also recirculated through the salt solution to maintain this relative humidity and to improve mixing.

The first gas investigated was helium. Since the velocity of sound in helium is approximately three times higher than in air, it seemed reasonable that helium should increase the velocity range of the plate wave technique by a factor of three. This was not the case, however, because even though the velocity of sound in helium is higher than in air, helium is much less dense. The less dense helium was unable to transmit as much energy into the sample, and no improvement in the upper velocity range was realized.

Freon was also tried in an attempt to extend the lower velocity range of the technique. The measurements in freon did reproduce the velocity measurements attained in air. However, since the low velocity plate waves for the layered composites could be attained using air, no particular advantage was obtained by making measurements in freon.

Mann observed that the received signal was significantly affected by air currents. Several tests were conducted to determine the effect of air currents on the plate wave measurements and it was found that the lock-in amplifier eliminates these effects. The plate wave device, therefore, does not have to be operated inside a glove box. Since air currents do not affect the measurements

when using the lock-in amplifier, it may be possible to use this technique for the on-line measurement of the elastic properties of paper.

MECHANICAL MEASUREMENTS

In addition to the various ultrasonic measurements, a number of mechanical measurements were also performed on the samples. These measurements included tensile strengths, STFI compressive strengths, Taber bending stiffnesses and four point bending stiffnesses. Since previous work had found relationships between elastic parameters and these strength or end-use measurements, it was of interest to see whether these same relationships held for layered composites.

A problem in carrying out the mechanical measurements was the eight-inch sample size. To allow as many test strips as possible to be cut from each sample, all of the test strips were cut 12.7 cm long and 1.5 cm wide. Although these strip dimensions were not the TAPPI recommended values for several of the tests, the results obtained from these dimensions can be related back to data obtained from TAPPI sample sizes.

The tensile tests were performed on a standard Instron instrument in accordance with TAPPI Standard Procedure, except that a 10.16 cm span length was used for the measurements instead of the usual 20.32 cm span. The usual crosshead speed is also reduced to maintain the same strain rate within the sample. The tensile strength values obtained on shorter span samples will normally be slightly higher than the values obtained on longer samples. The deviation from the standard 2.54 cm specimen width has a negligible effect upon the tensile stress values.

The STFI compression test requires samples which are 15 mm wide, and therefore the test specimen size was appropriate for this test. A problem did develop for a number of the layered composites, however, in that the compressive strengths for some of the composites exceeded the upper limits of the compression tester. Several attempts were made to try to increase the range of the tester without success. In order to measure the compressive strengths it was necessary to decrease the specimen size to a 1.27-cm width. A number of tests were run on both the 1.27-cm and 1.5-cm specimens. After correcting for the difference in width, it was found that the compression values obtained were the same for both test widths. The overloading problem did not occur for any of the single layer samples, and these samples were all tested using the 1.5-cm specimen width.

The Taber stiffness values were also obtained using 1.5-cm-wide samples. The Taber test is a cantilever beam bending test. Although the specimens tested here are longer and narrower than the regular Taber sample size, it is easy to calculate the bending stiffness values for samples of any size.

A main disadvantage of the Taber stiffness test is that it is not a pure bending test. In addition to applying bending moments, a cantilever bending test also applies shear forces to the test span. The resulting "bending stiffness" is therefore the result of both bending moments and shear stresses.

To eliminate the shear effects, a four point beam bending apparatus was constructed. This allows the center span of the sample to experience only pure bending moments. The design of this device is shown in Fig. 16.

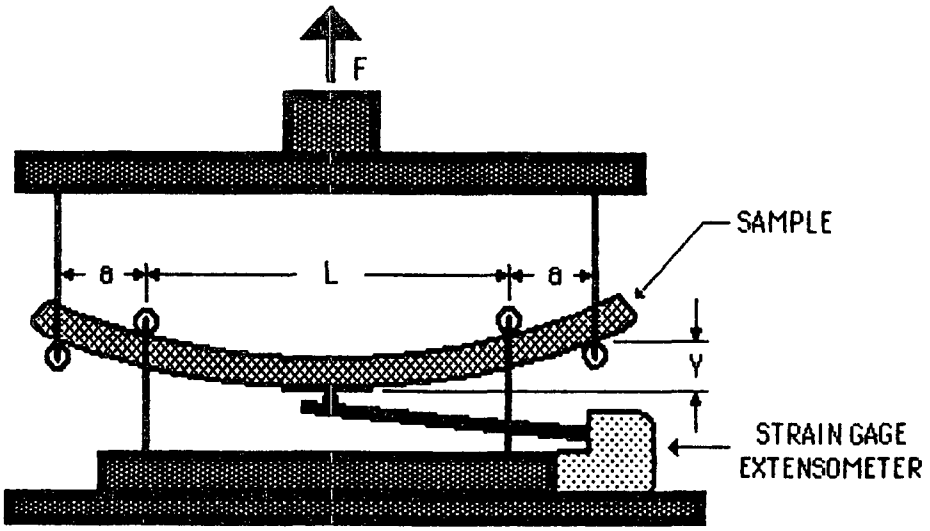

Figure 16. Four point bending device.

This device was installed in an Instron Model 1125 with a "B" load cell. The center span deflection was measured by the strain gage extensometer (Instron number G-51-17-A) and the force F was measured by the load cell. From these two values it is possible to calculate the bending stiffness value for the sample from the equation:

$$EI = \frac{F\,L^2\,a}{16\,Y} \tag{74}$$

EI = bending stiffness, N-mm^2

F = load measured on Instron, N

Y = displacement measured by displacement transducer, mm

L = 76.2 mm

a = 0.762 mm

The strain gage extensometer exerted a small load on the center span of the sample. For the composite sheets, this load was negligible. Four point bending measurements were not made on the single layer sheets, because for the lower basis weight sheets this load was no longer negligible.

THEORETICAL DISPERSION CURVES

One of the objectives of this thesis was to develop a method for predicting the plate wave behavior of layered composite materials. The work of Mann[2] and Shepard[3] provides the basis for developing such a method. Their models must be modified and expanded to deal with two and three layered orthotropic composites.

The two layer orthotropic model can be obtained from Shepard's two layer model.[3] Shepard's boundary conditions were:

1. Zero normal and shear stresses at the surfaces of the composite.
2. Continuity of stress and displacement at the interfaces between layers.

Shepard's model treats composites constructed from one orthotropic layer and one isotropic layer. By altering the elastic constants, however, it is possible to model a composite constructed from two orthotropic layers. Such a theoretical model yields a series of eight equations in eight unknowns which are identical to Eq. (62). As before, nontrivial solutions to these equations exist only when the value of the determinant equals zero. By adding and subtracting various rows and columns, the determinant of the matrix can be reduced to the form shown in Fig. 17.

A numerical solution must be employed to determine the values of K_x and ω which make the determinant go to zero. Shepard used a search method which calculated the value of the determinant for a grid of velocity and frequency values. When the sign of the determinant changed between two adjacent grid points, the determinant was calculated for a point half way between the first two points. This halving process continued for nine iterations. Since calculating the

determinant for each grid point and each half step iteration requires a large amount of computer time, other search methods were investigated.

$$
\begin{vmatrix}
1 & 0 & 1 & 0 & -1 & 0 & -1 & 0 \\
0 & -\tan \varnothing_{+} & 0 & -\tan \varnothing_{-} & 0 & \tan \acute{\varnothing}_{+} & 0 & \tan \acute{\varnothing}_{-} \\
G_{+} & 0 & G_{-} & 0 & -\acute{G}_{+} & 0 & -\acute{G}_{-} & 0 \\
0 & -C_{55}H_{+} & 0 & -C_{55}H_{-} & 0 & \acute{C}_{55}\acute{H}_{+} & 0 & \acute{C}_{55}\acute{H}_{-} \\
G_{+}\cos(iKz+g) & G_{+}\,i\sin(-iKz+g) & G_{-}\cos(iKz-g) & G_{-}\,i\sin(-iKz-g) & 0 & 0 & 0 & 0 \\
0 & 0 & 0 & 0 & \acute{G}_{+}\cos(-i\acute{K}z+f) & \acute{G}_{+}\,i\sin(i\acute{K}z+f) & \acute{G}_{-}\cos(-i\acute{K}z-f) & \acute{G}_{-}\,i\sin(i\acute{K}z-f) \\
H_{+}\,i\sin(iKz+g) & H_{+}\cos(-iKz+g) & H_{-}\,i\sin(iKz-g) & H_{-}\cos(-iKz-g) & 0 & 0 & 0 & 0 \\
0 & 0 & 0 & 0 & \acute{H}_{+}\,i\sin(-i\acute{K}z+f) & \acute{H}_{+}\cos(i\acute{K}z+f) & \acute{H}_{-}\,i\sin(-i\acute{K}z-f) & \acute{H}_{-}\cos(i\acute{K}z-f)
\end{vmatrix}
$$

Figure 17. Determinant for a two layer composite.

The search method chosen basically traces the dispersion curves rather than testing grid points (30). A linear search is initially made along the edges of the frequency-velocity space. When the value of the determinant goes to zero at some point, a search for a second zero point is initiated in the area of the first point. Once two points have been established, a third point is sought

along the line of the first two points. This process continues tracing the dispersion curve until the edge of the frequency-velocity space is encountered again. The program then returns to the linear search until another dispersion curve is found. The code for this search method appears in the computer program listings found in Appendix IV.

This search method has two advantages over the grid search method. First, it reduces the amount of computer time required by about a factor of three. Second, it allows the low velocity regions of the dispersion curves to be calculated at higher frequencies. In the low velocity and high frequency region of the curves, the value of the determinant changes quite rapidly. Using the grid search method, the value of the determinant calculated for the grid point is often larger than the capacity of the machine. Using the tracing method, such wide swings in the value of the determinant are eliminated.

An attempt was made to expand the two layer model to treat the loss of bonding between the layers of the composite. In this case, instead of assuming continuity of shear stress and shear displacements across the interface between layers, the shear stresses at the interface were set equal to zero. The boundary conditions of continuity of stress and displacement across the interface, namely:

$$U_x = U'_x \tag{75}$$

and

$$\sigma_5 = \sigma'_5 \tag{76}$$

are replaced by:

$$\sigma_5 = 0 \tag{77}$$

$$\sigma'_5 = 0 \tag{78}$$

These two new boundary conditions yield the simplified determinant shown in Fig. 18. The zeros of this determinant are found using the same search method described above. The results are presented later.

$$\begin{vmatrix}
0 & 0 & 0 & 0 & 0 & C'_{55}H'_{+} & 0 & C'_{55}H'_{-} \\
0 & -\tan\phi_{+} & 0 & -\tan\phi_{-} & 0 & \tan\phi'_{+} & 0 & \tan\phi'_{-} \\
2G_{+} & 0 & 2G_{-} & 0 & -2G'_{+} & 0 & -2G'_{-} & 0 \\
0 & -C_{55}H_{+} & 0 & -C_{55}H_{-} & 0 & 0 & 0 & 0 \\
G_{+}\cos(iKz+g) & G_{+}\sin(-iKz+g) & G_{-}\cos(iKz-g) & G_{-}\sin(-iKz-g) & 0 & 0 & 0 & 0 \\
0 & 0 & 0 & 0 & G'_{+}\cos(-iKz+f) & G'_{+}\sin(iKz+f) & G'_{-}\cos(-iKz-f) & G'_{-}\sin(iKz-f) \\
H_{+}\sin(iKz+g) & H_{+}\cos(-iKz+g) & H_{-}\sin(iKz-g) & H_{-}\cos(-iKz-g) & 0 & 0 & 0 & 0 \\
0 & 0 & 0 & 0 & H'_{+}\sin(-iKz+f) & H'_{+}\cos(iKz+f) & H'_{-}\sin(-iKz-f) & H'_{-}\cos(iKz-f)
\end{vmatrix}$$

Figure 18. Determinant for a two layer composite with slip between the layers.

So far we have only addressed dispersion curves for a two layer composite. The next step is to develop a method for calculating the dispersion curves for a three layer composite. The same basic boundary conditions will be assumed that were used for the two layer composites.

The basic arrangement of the three layer composite and the relative Z direction positions are shown in Fig. 19.

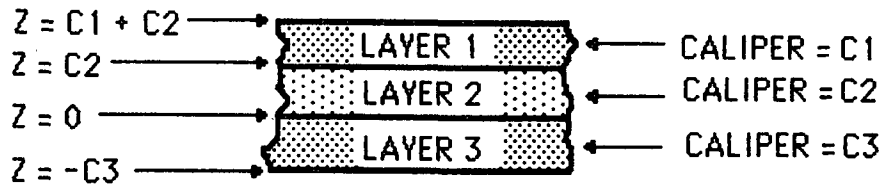

Figure 19. Construction of the three layer composite.

The value of Z = 0 has been arbitrarily assigned to the interface between layers 2 and 3. Layers 1, 2, and 3 have calipers C1, C2, and C3, respectively. All Z values other than Z = 0 are given in terms of the layer calipers.

For the sake of simplicity, let us consider a plate wave propagating in the X direction of the sheet. (As noted earlier, the same procedure can be followed to obtain the determinant for a plate wave propagating in the Y direction of the sheet if the appropriate stiffness values are substituted.) Initially, this three layer model follows the development of Mann's single layer model as shown in Eq. (29)-(44). If we consider four bulk waves propagating in each of the three individual layers, all twelve bulk waves must interact to produce a plate wave in the composite. With this in mind, we now construct the assumed wave equations. These are:

$$U_X(1) = \exp[i(K_X X-\omega t)][M_1\exp(iK_{Z1+}Z) + N_1\exp_{-iK_{Z1-}Z}) + \\ + P_1\exp(iK_{Z1+}Z) + Q_1\exp(-iK_{Z1-}Z)] \qquad (79)$$

$$U_Z(1) = \exp[i(K_X X-\omega t)][\tan\phi_{1+}[M_1\exp(iK_{Z1+}Z) + N_1\exp(-iK_{Z1-}Z)] + \\ + \tan\phi_{1-}[P_1\exp(iK_{Z1+}Z + Q_1\exp(-iK_{Z1-}Z)]] \qquad (80)$$

$$U_X(2) = \exp[i(K_X X-\omega t)][M_2\exp(iK_{Z2+}Z) + N_2\exp(-iK_{Z2-}Z) + + P_2\exp(iK_{Z2+}Z) + Q_2\exp(-iK_{Z2-}Z)] \quad (81)$$

$$U_Z(2) = \exp[i(K_X X-\omega t)][\tan\phi_{2+}[M_2\exp(iK_{Z2+}Z) + N_2\exp(-iK_{Z2-}Z)] + + \tan\phi_{2-}[P_2\exp(iK_{Z2+}Z) + Q_2\exp(-iK_{Z2-}Z)]] \quad (82)$$

$$U_X(3) = \exp[i(K_X X-\omega t)][M_3\exp(iK_{Z3+}Z) + N_3\exp(-iK_{Z3-}Z) + + P_3\exp(iK_{Z3+}Z) + Q_3\exp(-iK_{Z3-}Z)] \quad (83)$$

$$U_Z(3) = \exp[i(K_X X-\omega t)][\tan\phi_{3+}[M_3\exp(iK_{Z3+}Z) + N_3\exp(-iK_{Z3-}Z)] + + \tan\phi_{3-}[P_3\exp(iK_{Z3+}Z + Q_3\exp(-iK_{Z3-}Z)]] \quad (84)$$

These equations look very similar to Eq. (54)-(57). However, instead of using primed and unprimed values (such as M and M') to distinguish between layers, Eq. (79)-(84) use subscripted values (such as M_1, M_2, and M_3) to designate the values for a given layer.

Equations (79)-(84) must satisfy the boundary conditions of zero stress at the surfaces of the composite and continuity of stress and displacements across the interfaces between layers. There are twelve boundary conditions for the three layer composite. These are:

AT $Z = C1 + C2$

$$\sigma_3(1) = 0 \quad (85)$$

$$\sigma_5(1) = 0 \quad (86)$$

AT $Z = -C3$

$$\sigma_3(3) = 0 \quad (87)$$

$$\sigma_5(3) = 0 \quad (88)$$

AT $Z = 0$

$$U_X(2) = U_X(3) \quad (89)$$

$$U_Z(2) = U_Z(3) \quad (90)$$

$$\sigma_3(2) = \sigma_3(3) \quad (91)$$

$$\sigma_5(2) = \sigma_5(3) \quad (92)$$

AT Z = C2

$$U_X(1) = U_X(2) \tag{93}$$

$$U_Z(1) = U_Z(2) \tag{94}$$

$$\sigma_3(1) = \sigma_3(2) \tag{95}$$

$$\sigma_5(1) = \sigma_5(2) \tag{96}$$

Substituting Eq. (79)-(84) into these boundary conditions yields a series of twelve equations in twelve unknowns. The matrix of these twelve equations is shown in Fig. 20.

exp (KZ1+* C2)	- exp (KZ1+* C2)	exp (KZ1-* C2)	- exp (KZ1-* C2)	- exp (KZ2+* C2)	exp (KZ2+* C2)	- exp (KZ2-* C2)	exp (KZ2-* C2)	0	0	0	0
0	0	0	0	-1	-1	-1	-1	1	1	1	1
TAN1+ exp (KZ1+* C2)	-TAN1+ exp (KZ1+* C2)	TAN1- exp (KZ1-* C2)	-TAN1- exp (KZ1-* C2)	-TAN2+ exp (KZ2+* C2)	TAN2+ exp (KZ2+* C2)	-TAN2- exp (KZ2-* C2)	TAN2- exp (KZ2-* C2)	0	0	0	0
0	0	0	0	-TAN2+	TAN2+	-TAN2-	TAN2-	TAN3+	-TAN3+	TAN3-	-TAN3-
G1+ exp (KZ1+* C2)	G1+ exp (KZ1+* C2)	G1- exp (KZ1-* C2)	G1- exp (KZ1-* C2)	-G2+ exp (KZ2+* C2)	-G2+ exp (KZ2+* C2)	-G2- exp (KZ2-* C2)	-G2- exp (KZ2-* C2)	0	0	0	0
0	0	0	0	-G2+	-G2+	-G2-	-G2-	G3+	G3+	G3-	G3-
C55(1) H1+ exp (KZ1+* C2)	-C55(1) H1+ exp (KZ1+* C2)	C55(1) H1- exp (KZ1-* C2)	-C55(1) H1- exp (KZ1-* C2)	-C55(2) H2+ exp (KZ2+* C2)	C55(2) H2+ exp (KZ2+* C2)	-C55(2) H2- exp (KZ2-* C2)	C55(2) H2- exp (KZ2-* C2)	0	0	0	0
0	0	0	0	-C55(2) H2+	C55(2) H2+	-C55(2) H2-	C55(2) H2-	C55(3) H3+	-C55(3) H3+	C55(3) H3-	-C55(3) H3-
G1+ exp ((KZ1+)* (C1+ C2))	G1+ exp ((KZ1+)* (C1+ C2))	G1- exp ((KZ1-)* (C1+ C2))	G1- exp ((KZ1-)* (C1+ C2))	0	0	0	0	0	0	0	0
0	0	0	0	0	0	0	0	G3+ exp (KZ3+* C3)	G3+ exp (KZ3+* C3)	G3- exp (KZ3-* C3)	G3- exp (KZ3-* C3)
H1+ exp (KZ1P* AZ + BZ)	-H1+ exp (KZ1P* AZ + BZ)	H1- exp (KZ1N* AZ + BZ)	-H1- exp (KZ1N* AZ + BZ)	0	0	0	0	0	0	0	0
0	0	0	0	0	0	0	0	H3+ exp (KZ3+* C3)	-H3+ exp (KZ3+* C3)	H3- exp (KZ3-* C3)	-H3- exp (KZ3-* C3)

Figure 20. Determinant for the three layer composite.

The twelve equations have a nontrivial solution if and only if the determinant equals zero. As with the two layer model, values of frequency and velocity must be found which give the determinant a value of zero. To reduce the amount of computer time required to calculate the determinant, it was simplified by adding and subtracting various rows and columns. The reduced form of this determinant appears in Fig. 21.

2 COS (KZ1+* C2)	-ISIN (KZ1+* C2)	2 COS (KZ1-* C2)	-ISIN (KZ1-* C2)	- 2 COS (KZ2+* C2)	ISIN (KZ2+* C2)	- 2 COS (KZ2-* C2)	ISIN (KZ2-* C2)	0	0	0	0
0	0	0	0	-2	0	-2	0	2	0	2	0
2 TAN1+ ISIN (KZ1+* C2)	-TAN1+ COS (KZ1+* C2)	2 TAN1- ISIN (KZ1-* C2)	-TAN1- COS (KZ1-* C2)	-2TAN2+ ISIN (KZ2+* C2)	TAN2+ COS (KZ2+* C2)	-2TAN2- ISIN (KZ2-* C2)	TAN2- COS (KZ2-* C2)	0	0	0	0
0	0	0	0	0	TAN2+	0	TAN2-	0	-TAN3+	0	-TAN3-
2 G1+ COS (KZ1+* C2)	-G1+ ISIN (KZ1+* C2)	2 G1- COS (KZ1-* C2)	-G1- ISIN (KZ1-* C2)	-2G2+ COS (KZ2+* C2)	G2+ ISIN (KZ2+* C2)	-2G2- COS (KZ2-* C2)	G2- ISIN (KZ2-* C2)	0	0	0	0
0	0	0	0	-2G2+	0	-2G2-	0	2G3+	0	2G3-	0
2C55(1) H1+ ISIN (KZ1+* C2)	-C55(1) H1+ COS (KZ1+* C2)	2C55(1) H1- ISIN (KZ1-* C2)	-C55(1) H1- COS (KZ1-* C2)	-2C55(2) H2+ ISIN (KZ2+* C2)	C55(2) H2+ COS (KZ2+* C2)	-2C55(2) H2- ISIN (KZ2-* C2)	C55(2) H2- COS (KZ2-* C2)	0	0	0	0
0	0	0	0	0	C55(2) H2+	0	C55(2) H2-	0	-C55(3) H3+	0	-C55(3) H3-
2 G1+ COS ((KZ1+)* C1+ C2))	-G1+ ISIN ((KZ1+)* (C1+ C2))	2 G1- COS ((KZ1-)* (C1+ C2))	-G1- ISIN ((KZ1-)* (C1+ C2))	0	0	0	0	0	0	0	0
0	0	0	0	0	0	0	0	2G3+ COS (KZ3+* C3)	G3+ ISIN (KZ3+* C3)	2G3- COS (KZ3-* C3)	G3- ISIN (KZ3-* C3)
2H1+ ISIN (KZ1P* C1+ C2))	-H1+ COS (KZ1P* (C1+ C2))	2H1- ISIN (KZ1N* (C1+ C2))	-H1- COS (KZ1N* (C1+ C2))	0	0	0	0	0	0	0	0
0	0	0	0	0	0	0	0	-2H3+ ISIN (KZ3+* C3)	-H3+ COS (KZ3+* C3)	-2H3- ISIN (KZ3-* C3)	-H3- COS (KZ3-* C3)

Figure 21. Reduced form of the three layer determinant.

Examples of these symbols are given below.

$$G1\pm = [C_{33}]]KZ1\pm][TAN1\pm] + C_{13}K_x \qquad H2\pm = KZ2\pm + K_x[TAN2\pm] \tag{97}$$

where $KZ1\pm = KZ\pm$ for layer 1

$KZ2\pm = KZ\pm$ for layer 2

$TAN1\pm = \tan\phi\pm$ for layer 1

$TAN2\pm = \tan\phi\pm$ for layer 2

These symbols represent the same kinds of quantities as the $G\pm$ and $H\pm$ in Eq. (63)-(66). The only difference lies in the numbers used to designate the layer number.

The search method used for the three layer model was the same as that employed for the two layer model. As expected, the three layer model required about twice as much computer time as the two layer model. Some reduction in computer time can be obtained by increasing the spacing between points while tracing the curves. If the spacing is made too large, however, the tracing program can become "lost" and can begin following a different plate wave mode. For the Burroughs 6900, the processor time required to calculate the three layer dispersion curves generally ranged between 10 and 15 minutes.

We have developed methods for calculating the theoretical dispersion curves for two- and three-layer composite systems. Earlier we described a method for experimentally measuring the dispersion curves for these kinds of composites. We are now prepared to compare the experimental results with the theoretical predictions.

RESULTS AND DISCUSSION

The results presented here are divided into three separate parts. The first part is a comparison of the experimental dispersion curves with the predictions of the layered orthotropic models. The second part discusses relationships between the ultrasonic elastic constants of the layers and the ultrasonic elastic constants of the layered composite. Last, a comparison is made between the single layer and composite sheet elastic constants and the other test results.

The ultrasonic velocity data and the corresponding elastic constants appear in Appendix I. The data for the other measurements appear in Appendix II. The plate wave resonance data and the corresponding theoretical dispersion curves appear in Appendix III. The FORTRAN code for the two and three layer computer models appears in Appendix IV.

As noted earlier, it is difficult to experimentally determine values for C_{13} and C_{23}. For small values of these constants, the shapes of the dispersion curves do not change significantly. A series of dispersion curves were produced using different values for C_{13} ranging from 0 to 0.3 GPa. The shape of the dispersion curves did not change significantly over this range of C_{13} values. The one exception was $C_{13} = 0$, which produced problems in calculating the value of the determinant. The values $C_{13} = C_{23} = 0.03$ GPa were chosen partly because they were within the realm of values which did not change the shape of the dispersion curves, and partly because for such small values of C_{13} and C_{23} the low frequency SO velocities are nearly identical with the in-plane bulk velocities. These C_{13} and C_{23} values were used to calculate all of the dispersion curves in Appendix III.

DISPERSIVE BEHAVIOR OF COMPOSITES

From the density data shown in Appendix I, it appears that the densities of the composites are not equal to the densities calculated from the individual layer properties. Though some differences are noted in the basis weight data, the main reason for this difference in density is due to the caliper data. The calipers of the composites are less than the sum of the calipers of the layers. Due to the surface roughness of the layers, for hard platen caliper measurements this result is not uncommon.[31] The rubber platen caliper measurement[32] ideally should compensate for this surface roughness effect. For these particular sheets, it appears that this roughness effect has not been completely eliminated.

Another possible explanation for some of the disagreement in the dispersion curves is that the drying conditions for the composites and the individual layers was not the same. The same drying tension was applied to both kinds of sheets. Since the composites were higher basis weight sheets, it is possible that they exhibited more shrinking during drying. If this is true, the basis weight of the composites should be greater than the sum of the basis weights of the individual layers. The data in Appendix I shows that this is not the case. From the basis weight data it appears that the shrinkage which occurred during drying occurred approximately the same for the composites and the single layers.

Figure 22 shows the densities of the composites plotted against the densities calculated from the single layer properties. If the properties of the individual layers were representative of the layers in the composite, all of the points in Fig. 22 should fall along the one-to-one correspondence line. However, this is not the case.

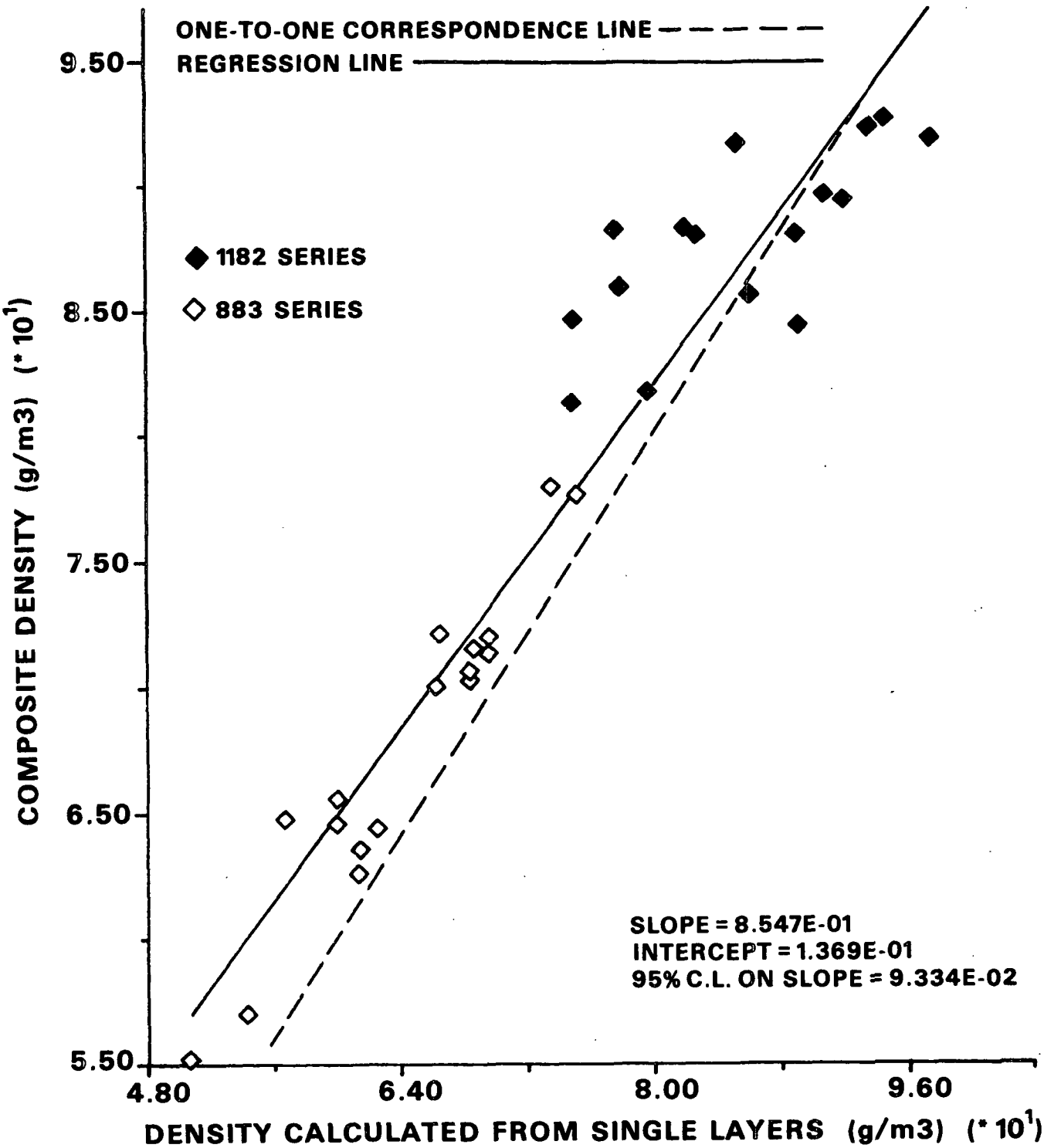

Figure 22. Composite density versus the density calculated from the individual layer properties.

The data for the 1182 series of samples scatters on either side of the one-to-one line. This scatter is mostly due to the large differences in densities for the bleached kraft (S) single layers. As noted earlier, some of this difference in densities may be the result of the surface roughness of the samples. Some of this density variation may also be due to the pressing conditions for the samples. Although the sheets were all pressed under identical pressures for a period of twenty minutes, if the basis weight of the sheet affected its densification, some of the variation in densities may be due to this basis weight effect. However, this basis weight effect does not explain the large differences in densities for sheets of approximately the same basis weight, such as Samples S1 and S3. It is possible that some of these differences may have resulted from transferring the sheets from the Formette to the platen press or from the platen press to the dryer. Although care was taken to handle the wet sheets as carefully as possible, it is impossible to avoid producing some stresses within the sheet.

Figure 22 also shows the density data for the 883 series of samples. These data are less scattered than the 1182 data and they all fall above the one-to-one correspondence line. The calipers for all of the 883 composites are less than the sums of the calipers for the layers. As noted earlier, this result would be expected if the rubber platen caliper device did not completely compensate for the surface roughness of the single layers. This difference in caliper would also be more noticeable for the 883 series of samples, since these samples were constructed from a larger number of layers.

From the results shown in Appendix III, a comparison can be made between the experimental dispersion curves and the theoretical curves obtained from the layered orthotropic models. In general, the experimental data points agree

quite well with the theoretical curves for both the two and three layer composites. However, for some of the curves, this agreement is not as good. This disagreement can be attributed to the differences in densities between the individual layers and the composites.

As noted earlier, the caliper of the sample has a significant effect on the fall-off regions of the dispersion curves. A higher caliper will shift the fall-off regions of the curves to lower frequencies. Since the sum of the single layer calipers is generally larger than the caliper of the composite, a dispersion curve model using the single layer properties will calculate the fall-off regions of the curves to fall at lower frequencies than a model which uses the composite's properties. The two and three layer models will therefore predict that the fall-off regions will occur at frequencies lower than those predicted by a single layer model. For the experimental data shown in Appendix III, the lower frequency fall-off regions obtained from the layered models fits the data better than the single layer models.

The differences in densities also affect the low frequency plateau regions of the SO and AO dispersion curves. Some of the deviations between the experimental points and the theoretical curves in these regions may be explained by differences in density. The composite properties which govern these regions of the curves are either the basis weight or caliper average of the individual layer properties. These averages will be discussed in detail in the next chapter.

Theoretical dispersion curves were calculated for the 1182 and 883 samples in both the MD and CD. The sample TK7 was the only sample for which the dispersion curves could not be easily calculated. The values of the determinant were such that the tracing search method became easily lost. It appears that the

12 x 12 determinant for this particular sample is ill conditioned for solution by the three layer theoretical model.

Because it is difficult to discuss all of the dispersion curves in Appendix III, we will now limit our discussion to the samples TK3 and TK6. One reason for selecting these two samples is that the density and caliper problems discussed earlier are less severe. A second reason for selecting these samples is that they are constructed from the same kinds of layers. The difference between these samples lies in the arrangement of the layers. These samples will therefore offer the opportunity to examine the effect of two and three layer construction upon the shape of the dispersion curves. They will also offer the opportunity to compare the theoretical dispersion curves for single layer, two layer, and three layer orthotropic models.

We will first look at the plate wave data for sample TK6CD. From Table 2 we see that sample TK6 is a three layer sample in which two of the adjacent layers are the same. Therefore, although it was produced using three layers, sample TK6 is really constructed as a two layer composite. The CD denotes that the plate wave measurements were made in the cross direction of the sample.

Figure 23 shows the data for the sample TK6CD. The theoretical curve was generated using the elastic constants of the composite in a single layer model. By a single layer model we mean that the elastic constants of the composite are measured as though it were a single layer sheet. These constants are used in a single layer plate wave model, such as Mann's, to calculate the dispersion curves. Figure 23 shows that the single layer theoretical curve fits the data fairly well in the plateau regions, but it predicts a higher fall-off frequency region than is observed experimentally. That is the same behavior noted by Mann with his linerboard samples.

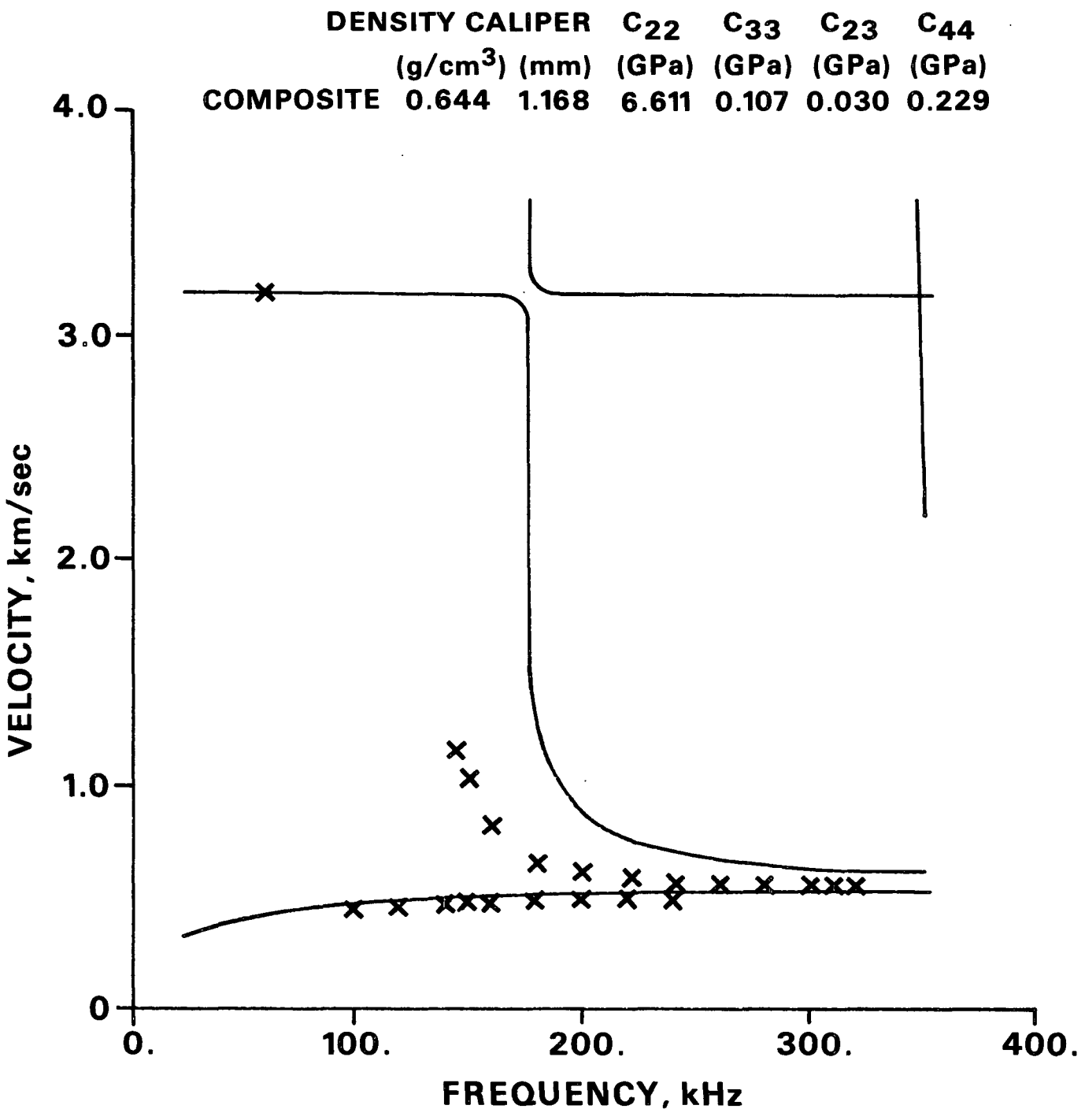

Figure 23. Dispersion curves for sample TK6CD using a single layer model.

Figure 24 shows the data for the same sample TK6CD plotted with the predictions of the two layer orthotropic model. Here the constants for the individual layers of the composite are used in a layered orthotropic plate wave model to

generate the theoretical dispersion curves. The plateau regions for the layered model still fit the data, but the layered orthotropic model does a much better job in predicting the frequencies at which the "fall-off" regions occur.

	DENSITY (g/cm^3)	CALIPER (mm)	C_{22} (GPa)	C_{33} (GPa)	C_{23} (GPa)	C_{44} (GPa)
LAYER 1	0.566	0.890	6.404	0.071	0.030	0.146
LAYER 2	0.785	0.316	5.862	0.312	0.030	0.226

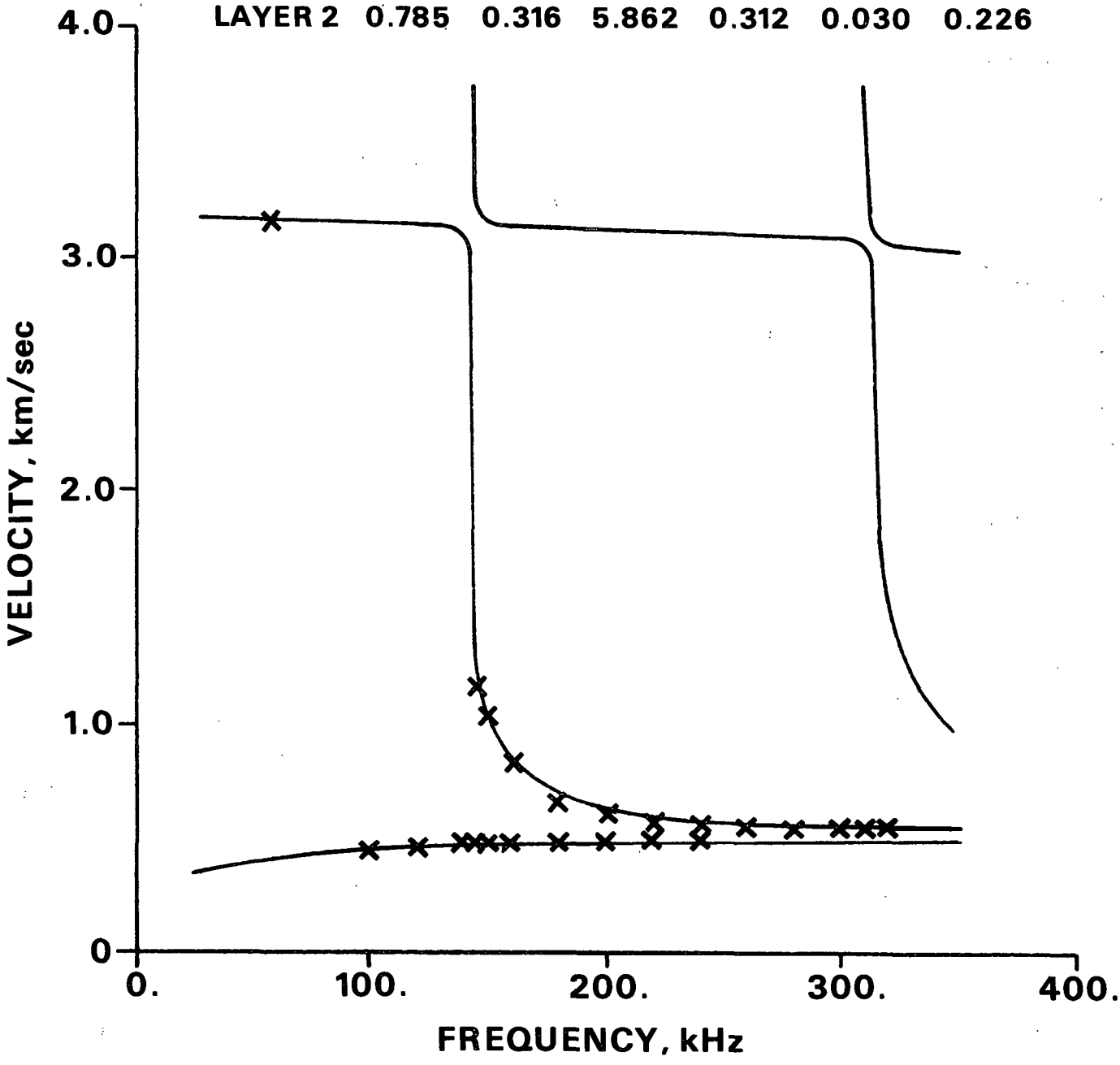

Figure 24. Dispersion curves for sample TK6CD using a two layer model.

Figure 25 shows the data for sample TK3CD. Table 2 shows that sample TK3 is constructed from the same layers as sample TK6, but that the layers in TK3 are arranged to yield a three layer composite. Figure 26 shows that a single layer theoretical curve accurately predicts the low frequency fall-off region of the curve and the plateau regions. However, the single layer model apparently does not predict the higher order fall-off regions, as it does not account for the single point at higher frequencies.

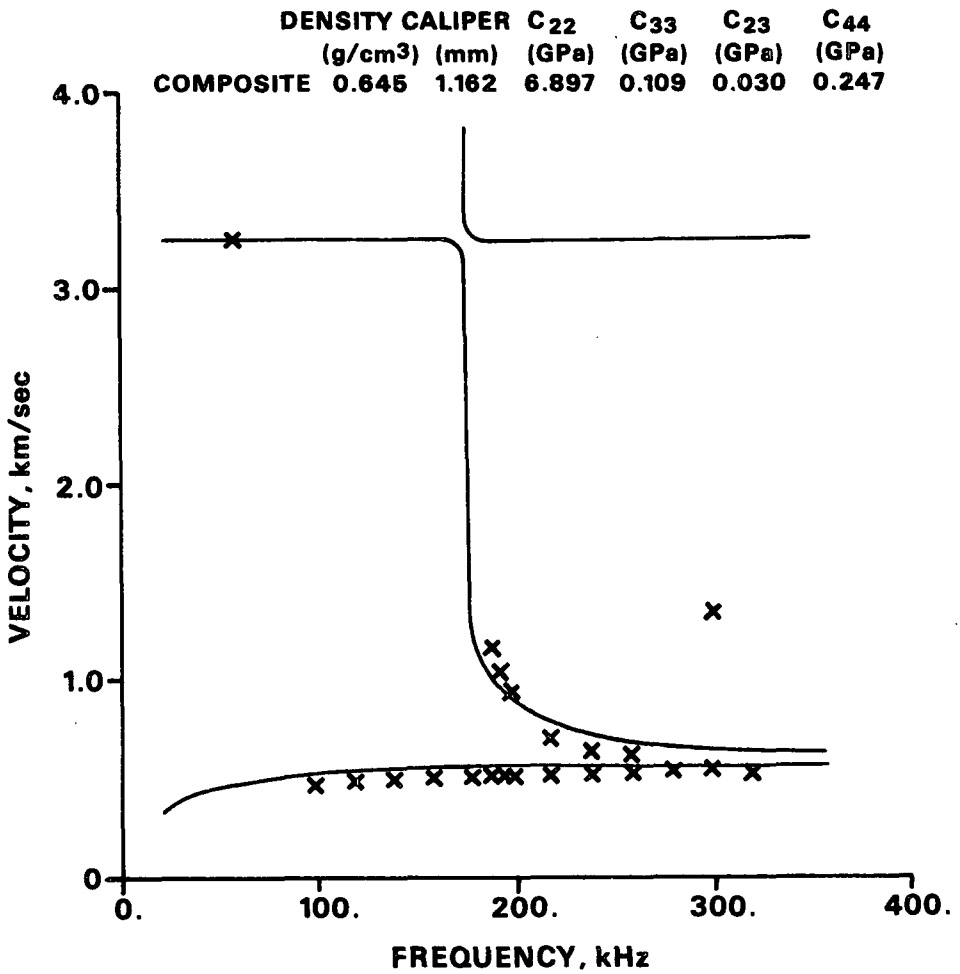

Figure 25. Dispersion curves for sample TK3CD using a single layer model.

Figure 26 shows the data for the same three layer sample TK3CD plotted against the three layer orthotropic model, using the elastic constants for the individual layers. The layered model accurately predicts the plateau regions and the "fall-off" regions of the dispersion curves. The single point at high frequencies is accounted for in this case. It appears that an advantage of the layered orthotropic model, over the single layer orthotropic model, for describing the dispersive behavior of layered composite materials lies in its ability to predict the "fall-off" regions of the dispersion curves.

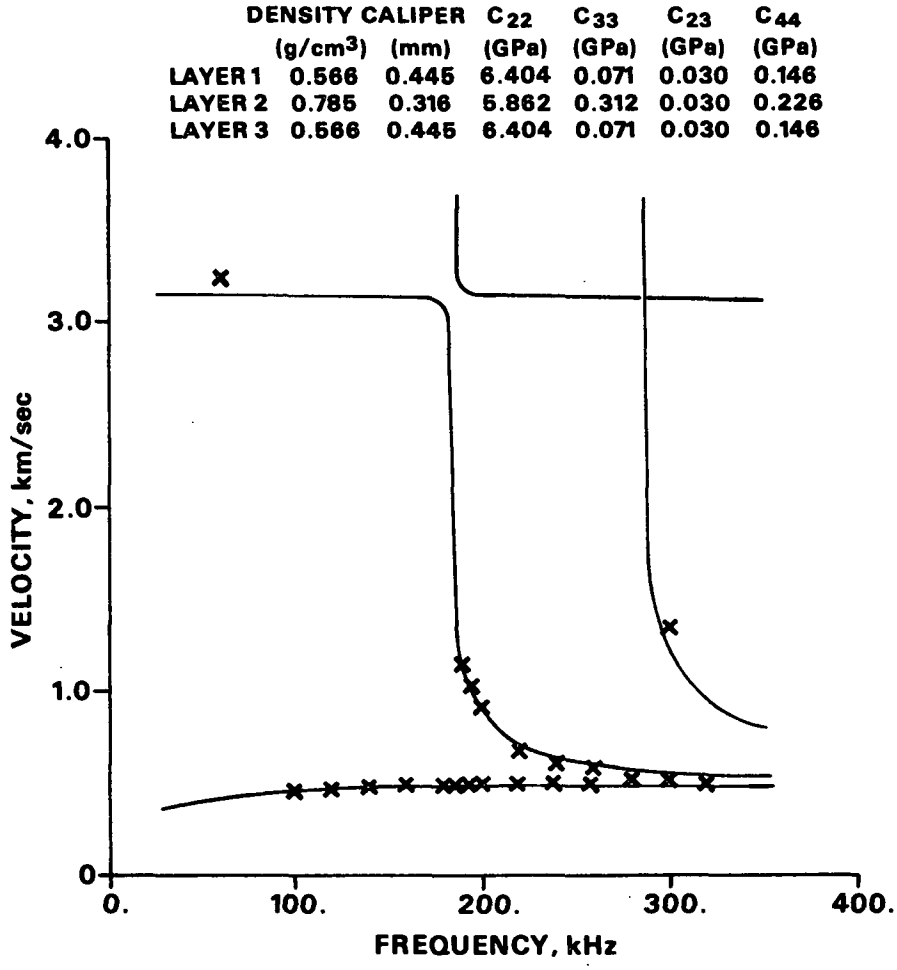

Figure 26. Dispersion curves for sample TK3CD using a three layer model.

It has been noted earlier that these fall-off regions in the dispersion curves are determined by a standing wave developing within the Z direction of the material. For single layer materials, the fall-off regions occur at integral multiples of some frequency. At such frequencies integral multiples of half wavelengths of the Z direction longitudinal wave "fit" within the thickness direction of the material. For layered composites, one must also consider the difference in acoustic impedance between layers and the resulting phase shifts in waves crossing the interfaces. The fall-off regions for the layered composite dispersion curves are determined by standing wave development in the Z direction of the composite, but the frequencies at which these standing waves exist are also determined by impedance differences between the layers. Therefore, for layered composites, one would not necessarily expect these fall-off regions to occur at integral multiples of frequency.

DISPERSION CURVES - THE EFFECT OF LAYER SLIP

In the preceding discussion it was noted that differences in acoustic impedance between layers will affect the shape of the dispersion curve. The layered orthotropic model assumes continuity of stress and displacement across the interface between layers. For commercially produced composites it is unlikely that these boundary conditions are always met. It is of interest, therefore, to investigate how bonding between layers affects the shape of the dispersion curve.

In the general case of layer slip, the layers are neither totally bonded or totally unbonded. In this case, a kind of "friction factor" might be used to describe the bonding between layers. However, for this work, only the simple condition of zero bonding between layers was investigated.

As shown earlier in Fig. 17, it was relatively simple to incorporate boundary conditions of zero shear stress at the interface between the two layers. The theoretical dispersion curves from such a model are shown in Fig. 27. The dotted line in Fig. 27 represents the dispersion curve predicted by the model when there is no slippage (perfect bonding) between the layers. The difference between slippage and no slippage appears only in the low frequency region of the curves, below the "fall-off" frequency. The two models overlap in the other regions of the curves.

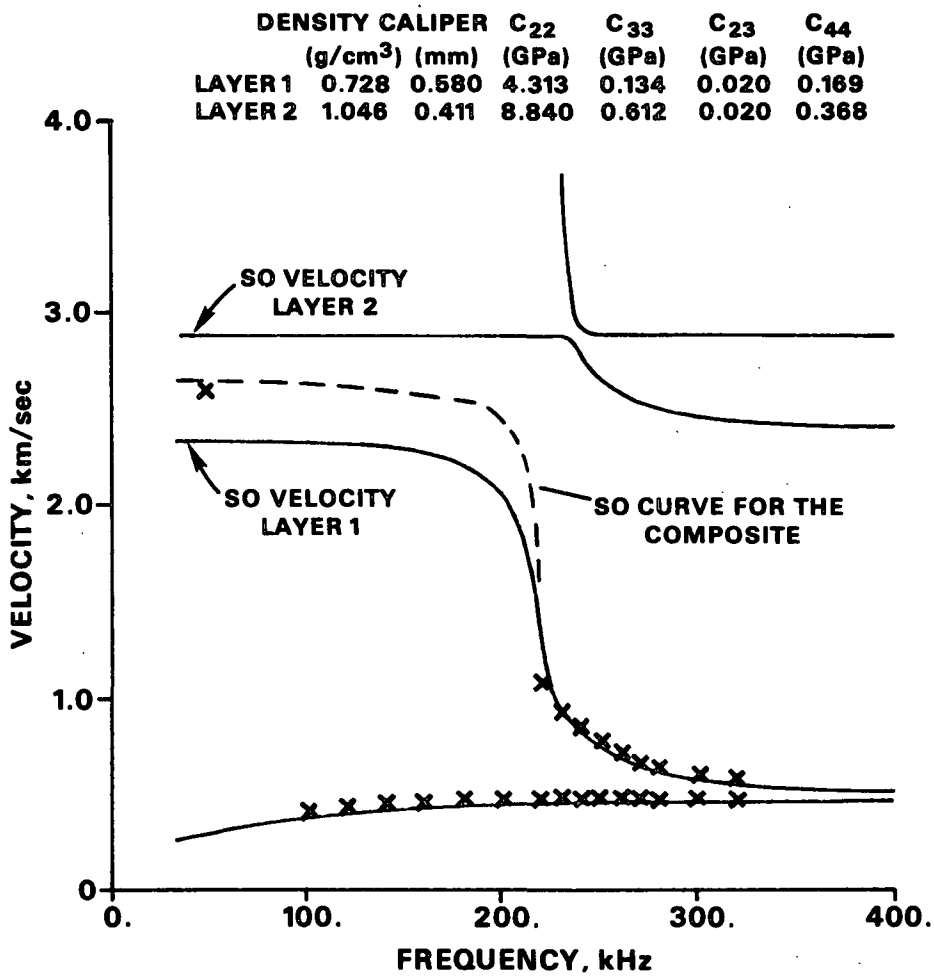

Figure 27. Dispersion curves for sample GS16CD, assuming slippage occurs between the layers of the sample.

For the unbonded model, the low frequency, high velocity plate wave mode separates into two separate plate waves, one propagating in each of the layers. The other regions of the dispersion curve are relatively unaffected by the lack of interface bonding. These results are interesting, and seem to agree with other experimental observations. For example, when measuring the in-plane ultrasonic velocities of a material, one finds that the measurement is relatively insensitive to the type of material used to back the sample. If two single layer sheets are stacked together and the ultrasonic transducers are placed in contact with the top sheet, only the velocity of the top sheet will be measured. If the order of the sheets is reversed, the measured velocity will always be that of the sheet contacting the transducers. The theoretical prediction for two unbonded sheets, that the low frequency-high velocity plate wave modes propagate independently, is in agreement with the above observation.

At higher frequencies (lower velocities) the curves remain unaffected by the loss of bonding. These regions of the curves are determined by the velocity of surface waves propagating in the layers.[33] The displacements induced by these surface waves are localized at the outer surfaces of the sheet. Since these surface waves have little interaction with the interface between the layers, it would appear reasonable that this region of the dispersion curves would be little affected by the loss of layer bonding.

Figure 27 indicates that the "fall-off" regions of the dispersion curves remain unchanged with a loss of layer bonding. It was noted earlier that the "fall-off" regions of the curves occur when a longitudinal displacement standing wave develops in the Z direction of the sheet. While the theoretical slip model assumed zero bonding between layers, it did assume that the layers still remained in intimate contact. The perpendicular Z direction displacements in

one layer could therefore produce Z direction displacements within the other layer. Under the conditions for a longitudinal standing wave produced in the composite, one can visualize how the physical contact between layers might be sufficient for the standing wave to exist.

The preceding discussion has dealt with the plate wave behavior of layered orthotropic materials. Experimental data are still fairly difficult to obtain. Because of the frequency and velocity limitations of the method, the plate wave technique of Luukkala is most applicable to thick, low density materials. The technique is, therefore, not applicable to a large number of commercial paper and paperboard materials.

There are other ultrasonic measurement techniques. Ultrasonic measurements of the elastic constants of a material have already found a fair amount of application within the paper industry. In the next section we will discuss how these techniques can be applied to layered composite materials.

ULTRASONIC ELASTIC CONSTANTS

As noted earlier, seven of the nine ultrasonic elastic stiffness values were obtained for the single layer samples as well as for the composite sheets. The ultrasonic velocity data and the resulting ultrasonic stiffness values all appear in Appendix I.

When investigating the properties of layered composite materials, one is interested in how the properties of the individual layers affect the properties of the composite as a whole. In this discussion we consider the in-plane and out-of-plane composite elastic properties separately. Let us begin by looking at the in-plane elastic properties.

The description presented here was originally developed by Habeger.[34]

We know that $$V_i^2 = \frac{C_i}{\rho_i} \tag{98}$$

where C_i = stiffness of layer i

ρ_i = density of layer i

V_i = velocity of layer i

If T_i = caliper of layer i

then $$V_i^2 \frac{C_i T_i}{\rho_i T_i} = \frac{\text{extensional stiffness}}{\text{basis weight}} \tag{99}$$

Consider a three layer composite (see Fig. 28).

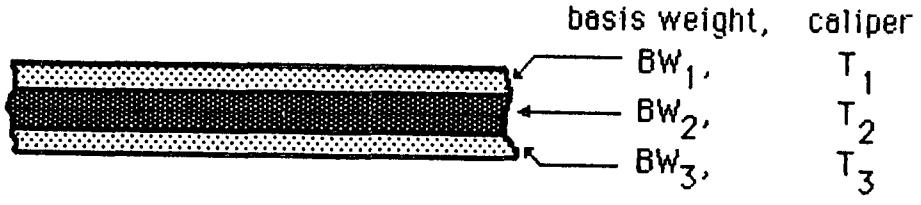

Figure 28. A theoretical three layer composite.

$$V_{composite} = \frac{\text{total stiffness}}{\text{total mass}} = \frac{C_1T_1 + C_2T_2 + C_3T_3}{\rho_1T_1 + \rho_2T_2 + \rho_3T_3} \tag{100}$$

$$V^2_{composite} = \frac{V_1^2T_1q_1 + V_2^2T_2q_2 + V_3^2T_3q_3}{\rho_1T_1 + \rho_2T_2 + \rho_3T_3} \tag{101}$$

But since $T_i\rho_i = BW_i$

$$V^2_{composite} = \frac{V_1^2BW_1 + V_2^2BW_2 + V_3^2BW_3}{\sum_{i=1}^{3} BW_i} \tag{102}$$

The square of the in-plane velocity for each of the individual layers is "basis weight averaged" to yield the square of the in-plane velocity in the composite. We can experimentally determine whether this kind of averaging actually occurs in layered composites.

Figure 29 shows the composite C_{11}/ρ values plotted against the basis weight average of the single layer values for both series of composites. Figure 30 shows the C_{22}/ρ values for the same samples. The correlations in these figures are for all of the data points from both data sets. As predicted, the data points on these plots fall close to the one-to-one correspondence line. The in-plane ultrasonic elastic properties seem to follow this kind of basis weight averaging.

The same kind of basis weight average should work for the in-plane shear stiffness values. Figure 31 shows the C_{66}/ρ values for the composite plotted against the basis weight average of the values for the single layers. As with the other in-plane values, the points fall near the one-to-one correspondence line. Although a relationship does appear to exist, the data are quite scattered. There is no apparent reason why the shear data should be more scattered than the longitudinal data.

In this study, caliper was measured using rubber covered platens. The rubber conforms to the surface of the sample and reduces the effect of surface roughness on caliper. However, the rubber platen caliper device did not eliminate this effect completely. The caliper data in Appendix I shows that the sum of the single layer calipers is generally larger than the caliper of the composite. This surface roughness effect is most evident for the 883 series of samples, due to the larger number of layers and interfaces in these samples.

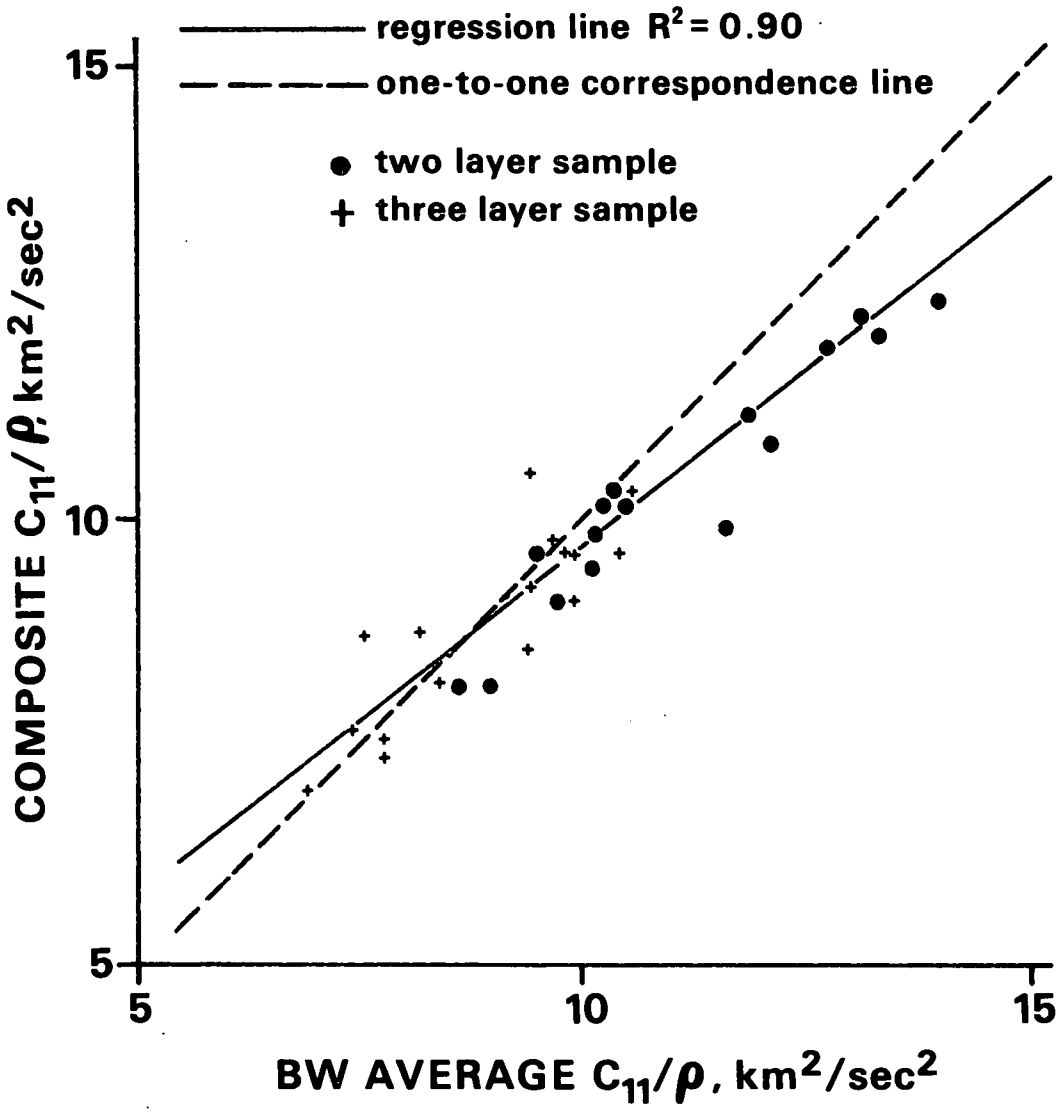

Figure 29. C_{11}/ρ of the composite versus the basis weight average C_{11}/ρ of the single layers.

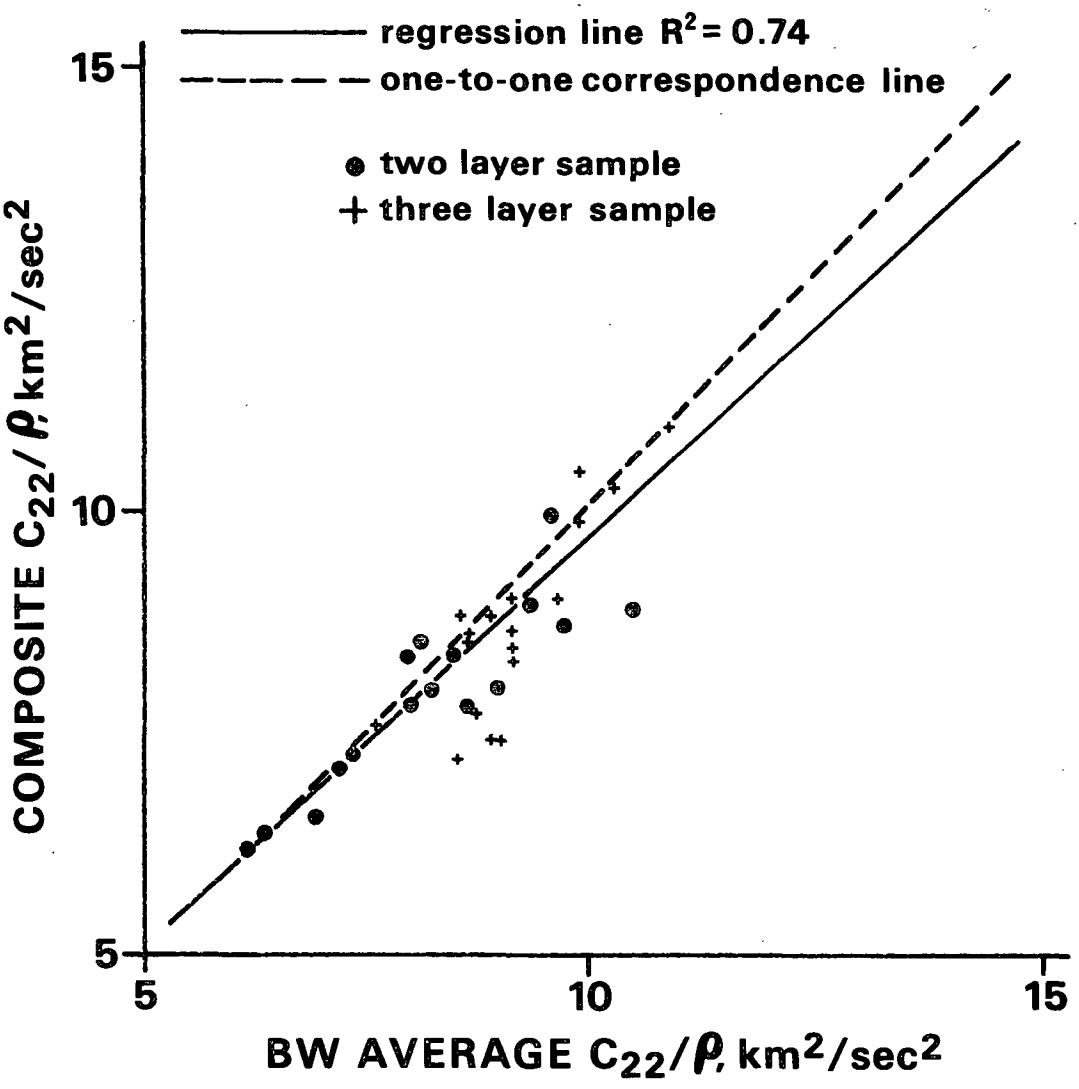

Figure 30. C_{22}/ρ of the composite versus the basis weight average C_{22}/ρ of the single layers.

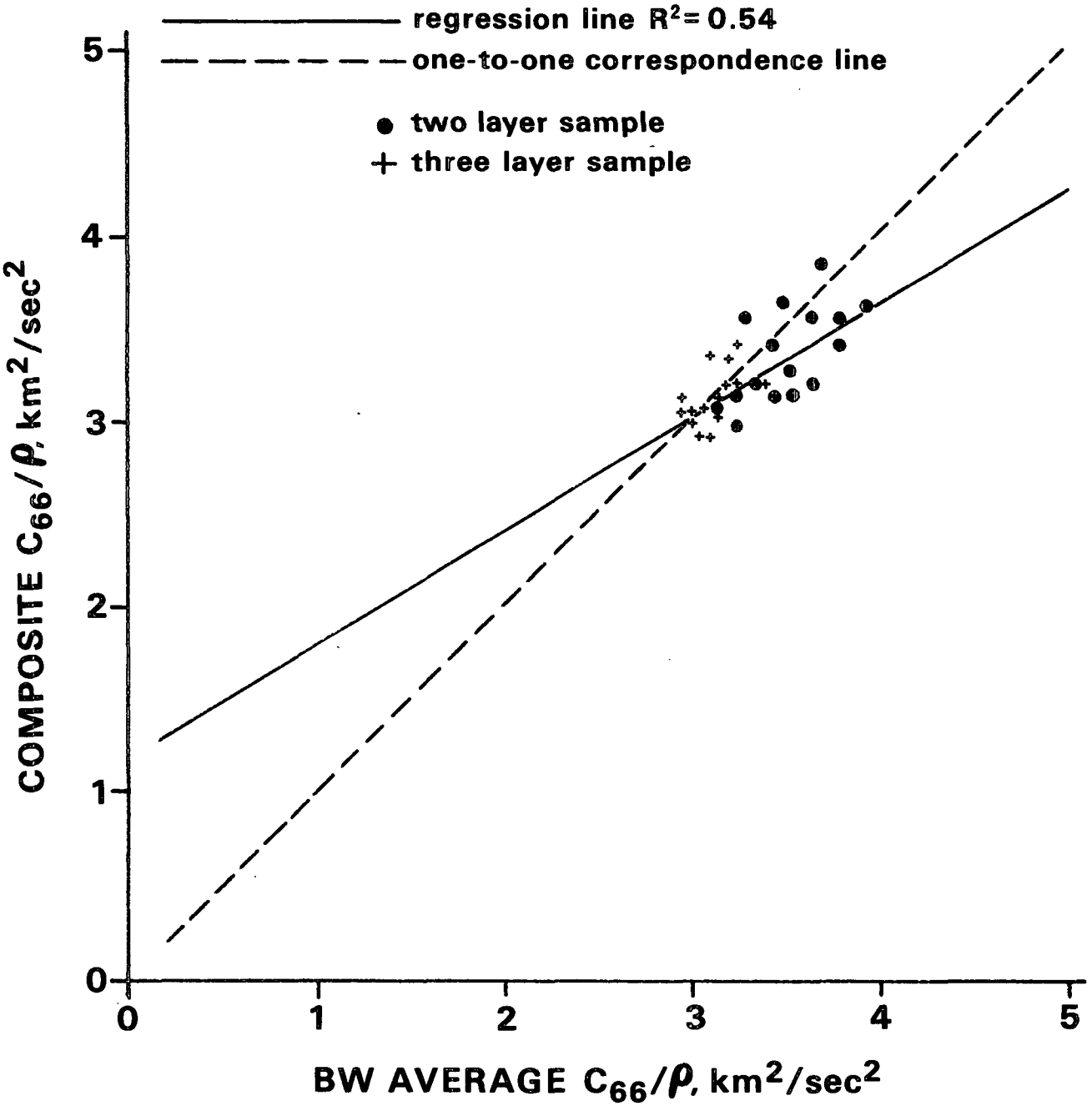

Figure 31. C_{66}/ρ of the composite versus the basis weight average C_{66}/ρ of the single layers.

Now let us consider the Z direction properties. For an ultrasonic wave propagating in the Z direction of a layered composite, the time it takes for the wave to propagate through the composite should be equal to the sum of the times it takes to travel through each of the layers. Therefore:

$$t_{composite} = t_1 + t_2 + t_3 + \ldots \tag{103}$$

Since time is equal to distance over velocity (T_i/V_i),

$$\frac{T_{composite}}{V_{composite}} = \frac{T_1}{V_1} + \frac{T_2}{V_2} + \frac{T_3}{V_3} + \ldots \tag{104}$$

$$V_{composite} = \frac{T_{composite}}{\frac{T_1}{V_1} + \frac{T_2}{V_2} + \frac{T_3}{V_3} + \ldots} \tag{105}$$

Figure 32 shows the composite out-of-plane longitudinal velocity versus the caliper average of the single layer velocities. In these figures all of the points fall quite close to the one-to-one correspondence line. There is also less scatter than in the in-plane longitudinal velocity results. Part of this difference is due to the out-of-plane results being velocities while the in-plane results are velocity squared. Figure 32 shows that Eq. (105) accurately predicts the out-of-plane longitudinal velocity for the composite.

Figures 33 and 34 show the composite out-of-plane shear velocities plotted against the predictions of Eq. (105). This shear data are very scattered. Although the data points fall near the one-to-one correspondence line, one cannot confidently say that the out-of-plane shear velocities follow these predictions.

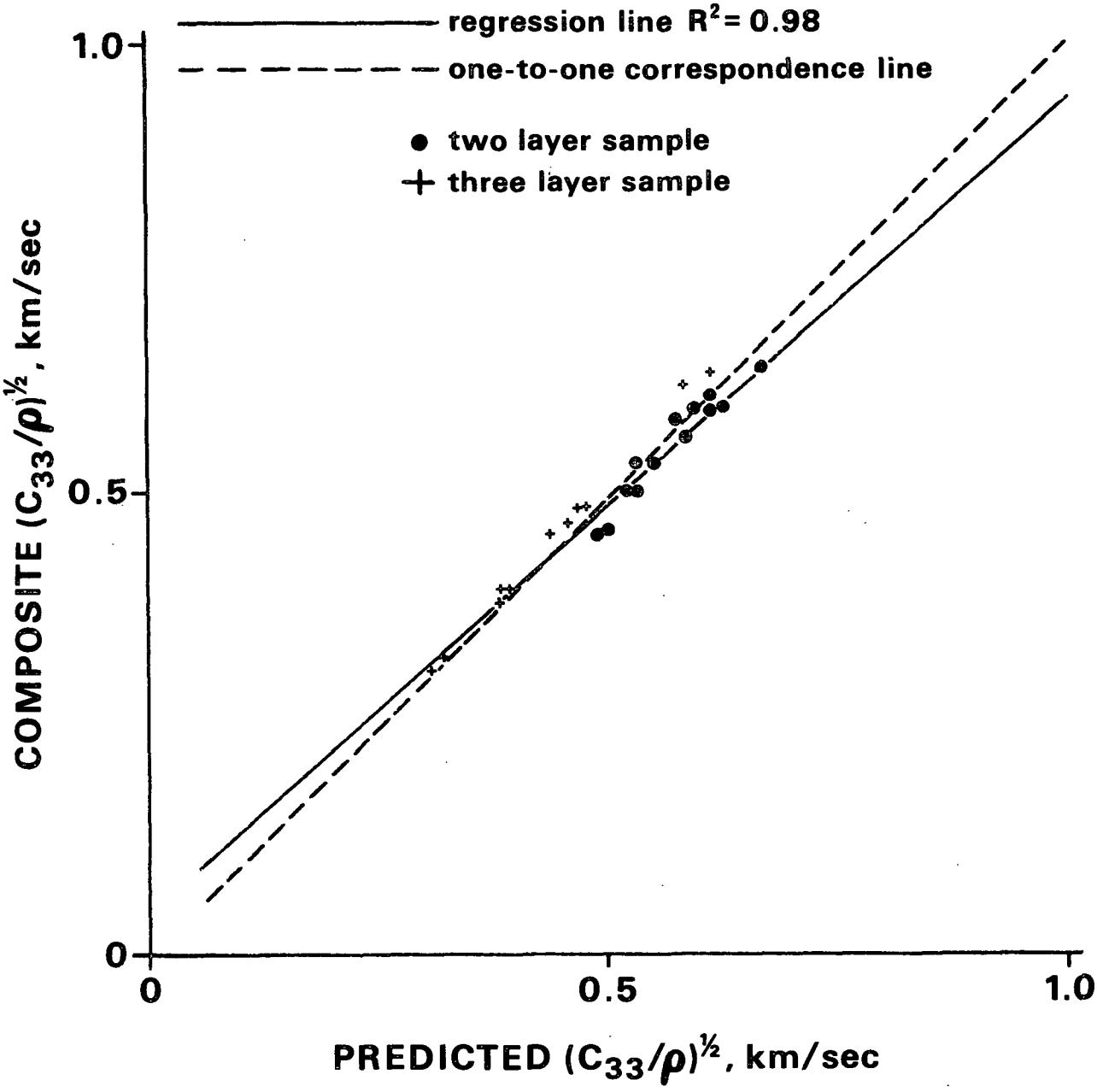

Figure 32. $(C_{33}/\rho)^{1/2}$ of the composite versus the caliper average $(C_{33}/\rho)^{1/2}$ of the single layers.

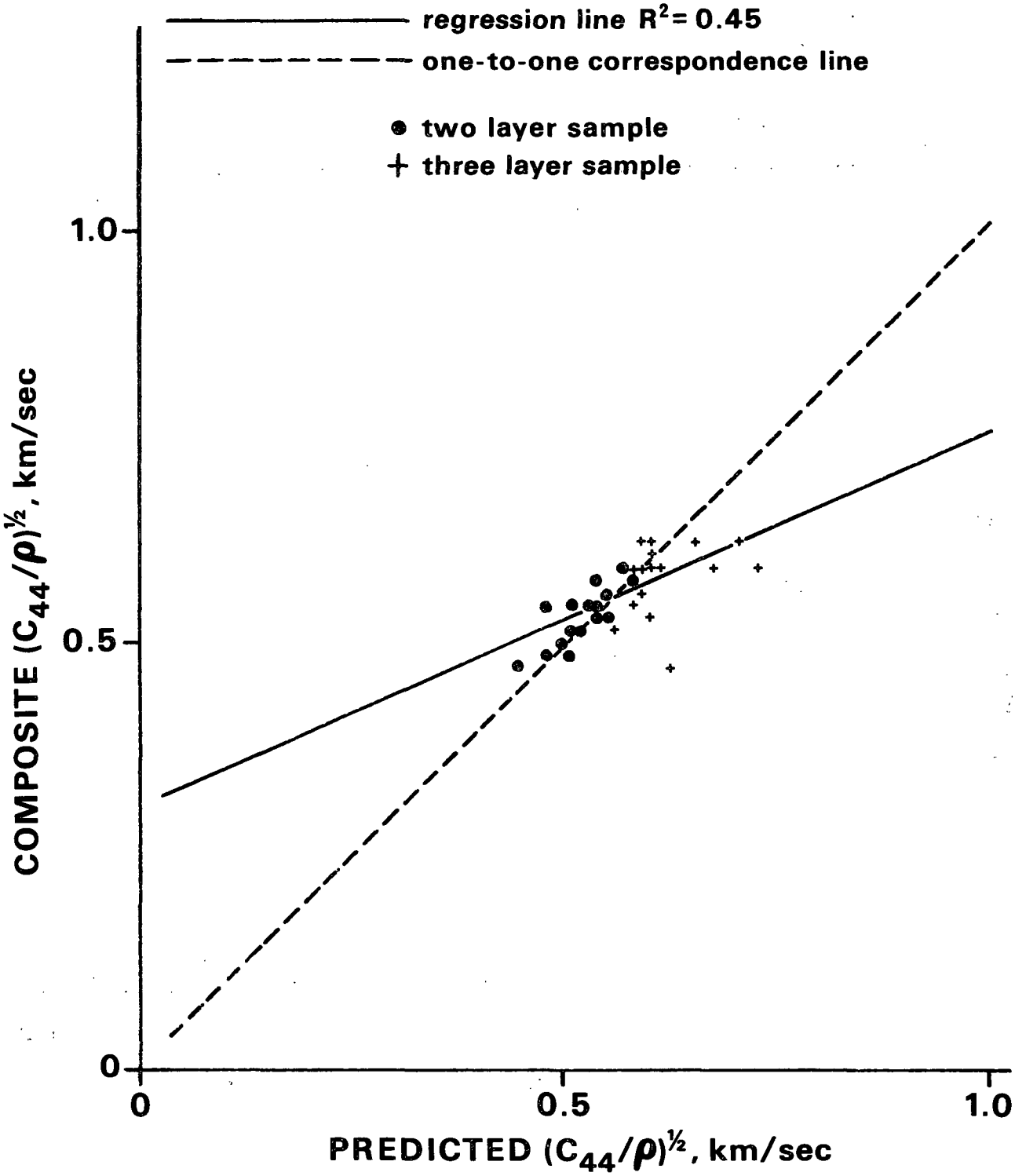

Figure 33. $(C_{44}/\rho)^{1/2}$ of the composite versus the caliper average $(C_{44}/\rho)^{1/2}$ of the single layers.

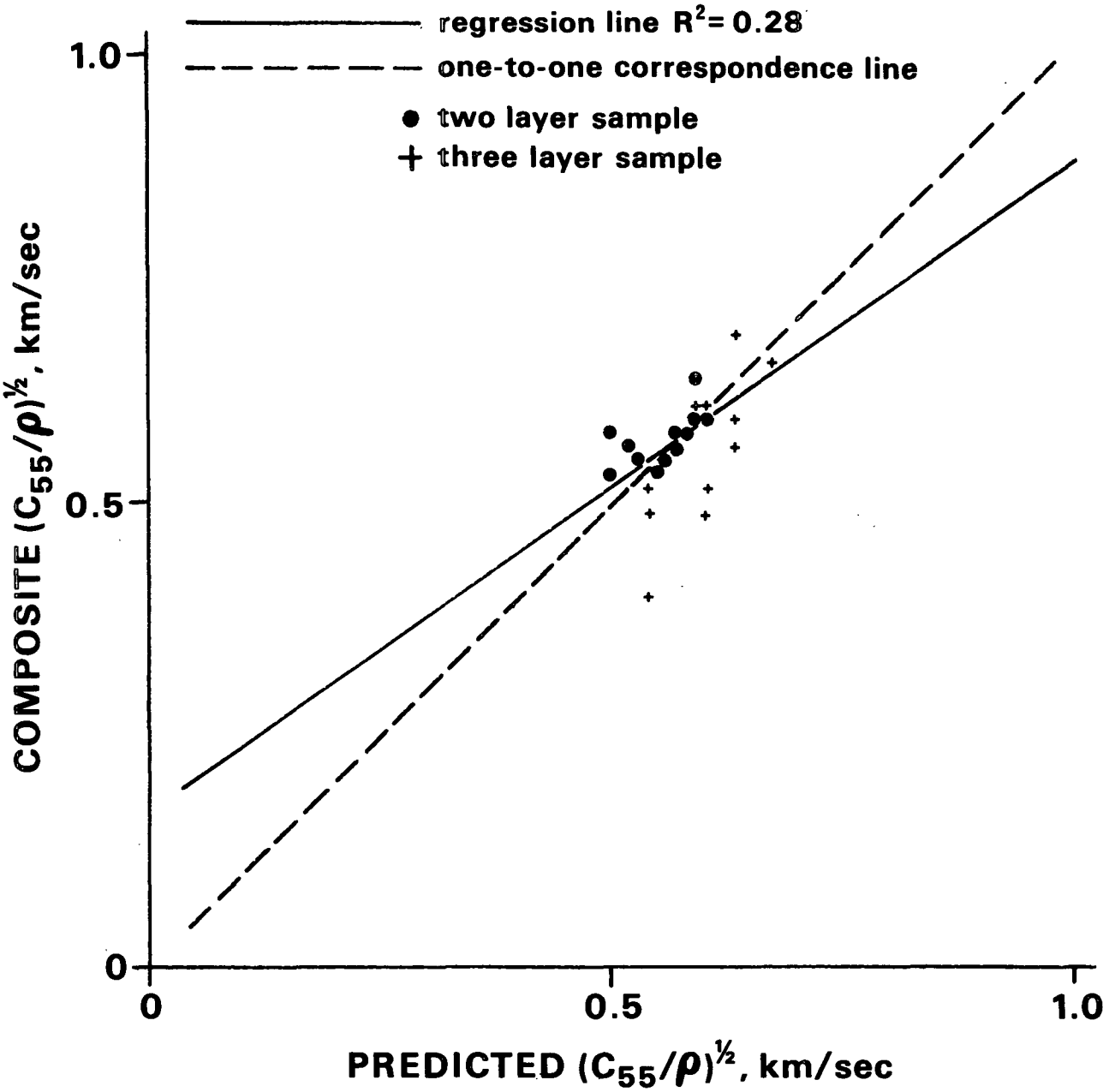

Figure 34. $(C_{55}/\rho)^{1/2}$ of the composite versus the caliper average $(C_{55}/\rho)^{1/2}$ of the single layers.

Reduced bonding at the interface between layers might explain the large amount of scatter in the Z direction shear velocity measurements. Any differences in layer bonding within the sheet will have a significant effect upon the measured shear velocities. If the degree of layer bonding varied throughout the sheet, this variation would induce scatter in the velocity data. Ideally, one would like to characterize the properties of the interface at specific locations to account for these kinds of variations. At this time, no appropriate technique is available for performing this characterization.

Summary

The elastic stiffnesses for the composite can be predicted from the elastic stiffnesses of the individual layers via simple calculations. For the in-plane values, C_{11} and C_{22}, the results follow a basis weight average, while C_{33} obeys a caliper type average. The shear values seem to follow similar trends (i.e., a basis weight average for the in-plane value C_{66} and a caliper average for the out-of-plane values, C_{44} and C_{55}), but there is much more scatter in the shear data.

ULTRASONIC AND MECHANICAL PROPERTIES

Tensile Strength

As noted earlier, Baum, et al.[9] found an empirical relationship between tensile strength and extensional stiffness. This relationship held for single layer sheets. It would be interesting to see whether this relationship also holds for our layered composite materials.

In the preceding section we found that the square of the velocity of an in-plane longitudinal wave in the composite was linearly related to a basis weight average of the single layer velocities squared. We might expect, therefore,

that the tensile strength of the composite owuld also be related to a basis weight average of the single layer velocities. If so, we also might expect the tensile strength of the composite to be proportional to the sum of the single layer tensile strengths.

Since $$(BW \times V^2)_{composite} = \sum_{i=1}^{n} (BW_i \times V_i^2) \quad (106)$$

becomes $$TS_{composite} = \sum_{i=1}^{n} a_i TS_i \quad (107)$$

where a_i is the proportionality constant for each layer i.

If the proportionality constants, a_i, were equal for all of the layers, the tensile strength of the composite would just be the sum of the single layer tensile strengths.

The above discussion suggests three specific questions:

1. Does the composite extensional stiffness correlate with the composite's tensile strength?
2. Does the sum of the extensional stiffnesses for the individual layers correlate with the composite's tensile strength?
3. Does the sum of the tensile strengths for the individual layers equal the tensile strength of the composite?

For this discussion, the term "single layer model" will be used to describe treating the layered composites as though they were homogeneous, single layer sheets. The elastic and strength properties of the composites will be then taken to be the properties of the composite as a whole. The term "layered model" will refer to modeling the behavior of the composite as a function of the individual layer properties.

Figures 35 and 36 show the composite tensile strength plotted against the composite extensional stiffness. A good correlation exists for both the machine direction and the cross direction. In addition, within the 95% confidence limits on the slopes, the machine direction and cross direction slopes are the same. All of the MD and CD data would fall on a single straight line if plotted together.

The next question is whether the sum of the single layer extensional stiffnesses correlates with the composite's tensile strength. Figures 37 and 38 show the tensile strength of the composite plotted against the sum of the individual layer extensional stiffnesses. As above, the data follow a linear relationship. Comparison of Fig. 35 and 36 with Fig. 37 and 38 suggests that there is not much difference in the fit of the data points. The tensile data for the composite are described equally well in terms of either the composite extensional stiffness or the sum of the individual layer stiffnesses.

Figures 39 and 40 show that the tensile strength of the composite also seems to correlate with the tensile strengths of the individual layers for the (two layer) 1182 series of samples, in both the MD and CD, respectively. However, Fig. 41 and 42 show that such correlations were not found for the (three layer) 883 series of samples.

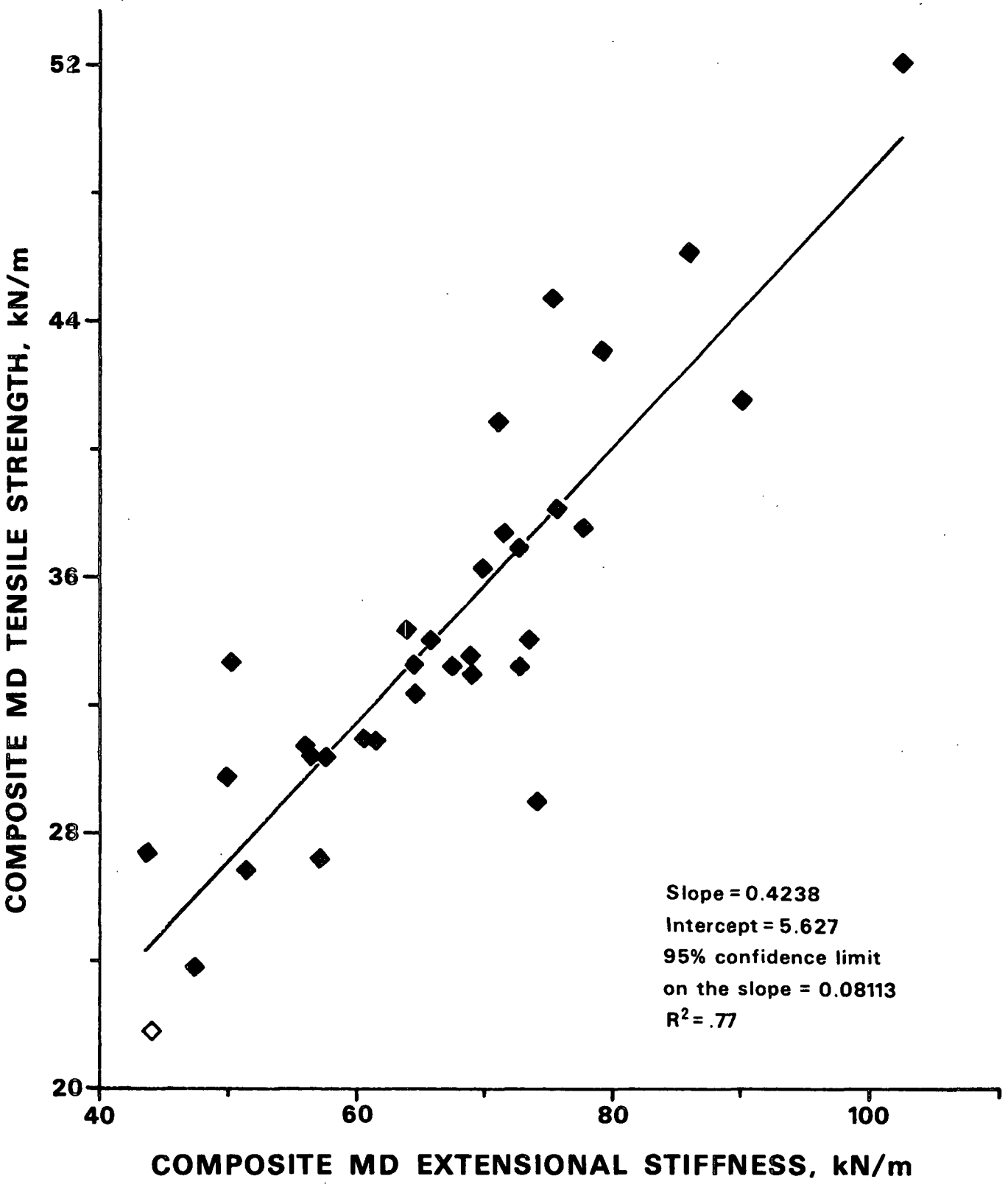

Figure 35. Composite MD tensile strength versus the composite MD extensional stiffness. Data for both the 1182 and 883 series of samples.

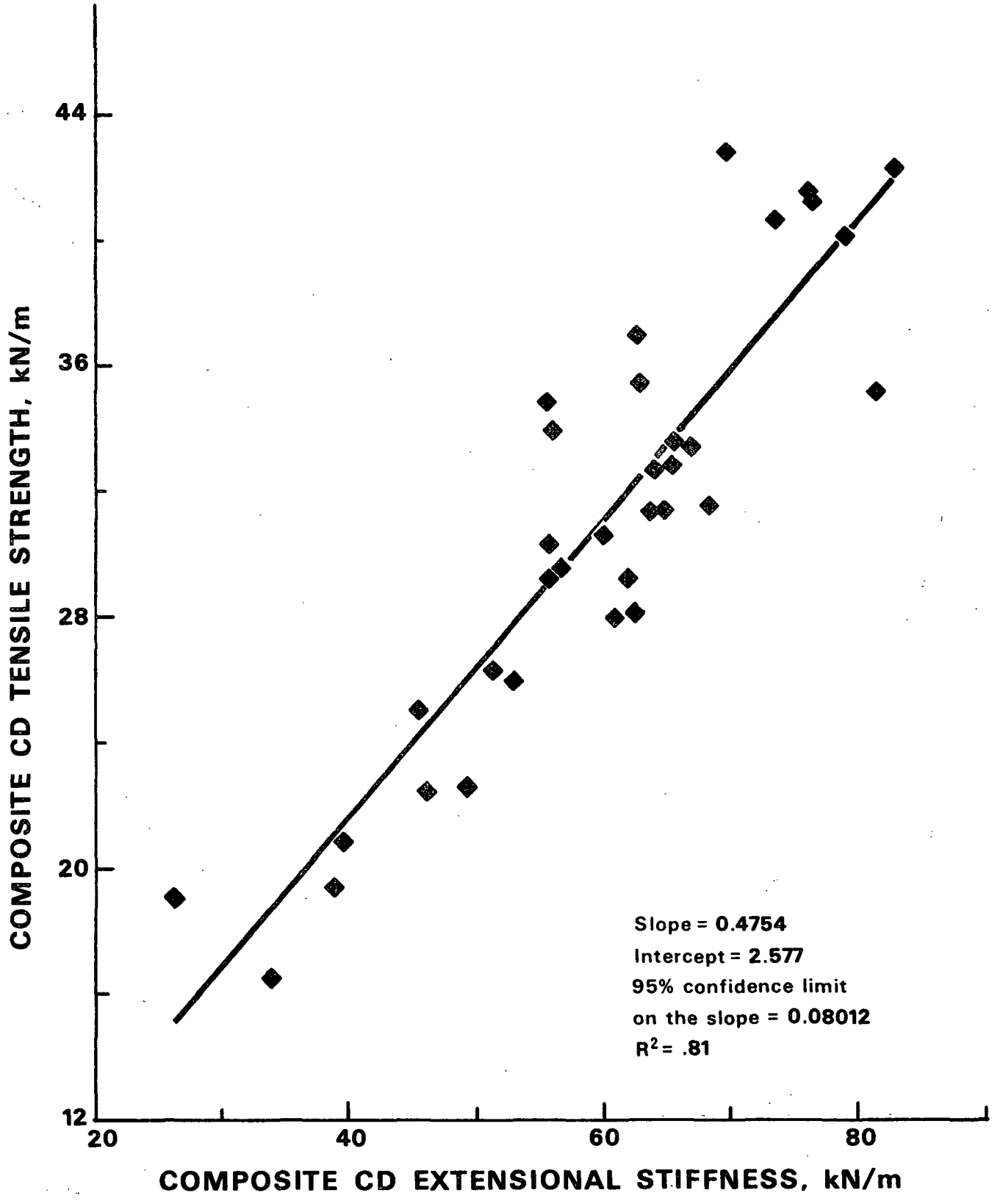

Figure 36. Composite CD tensile strength versus the composite CD extensional stiffness. Data for both the 1182 and 883 series of samples.

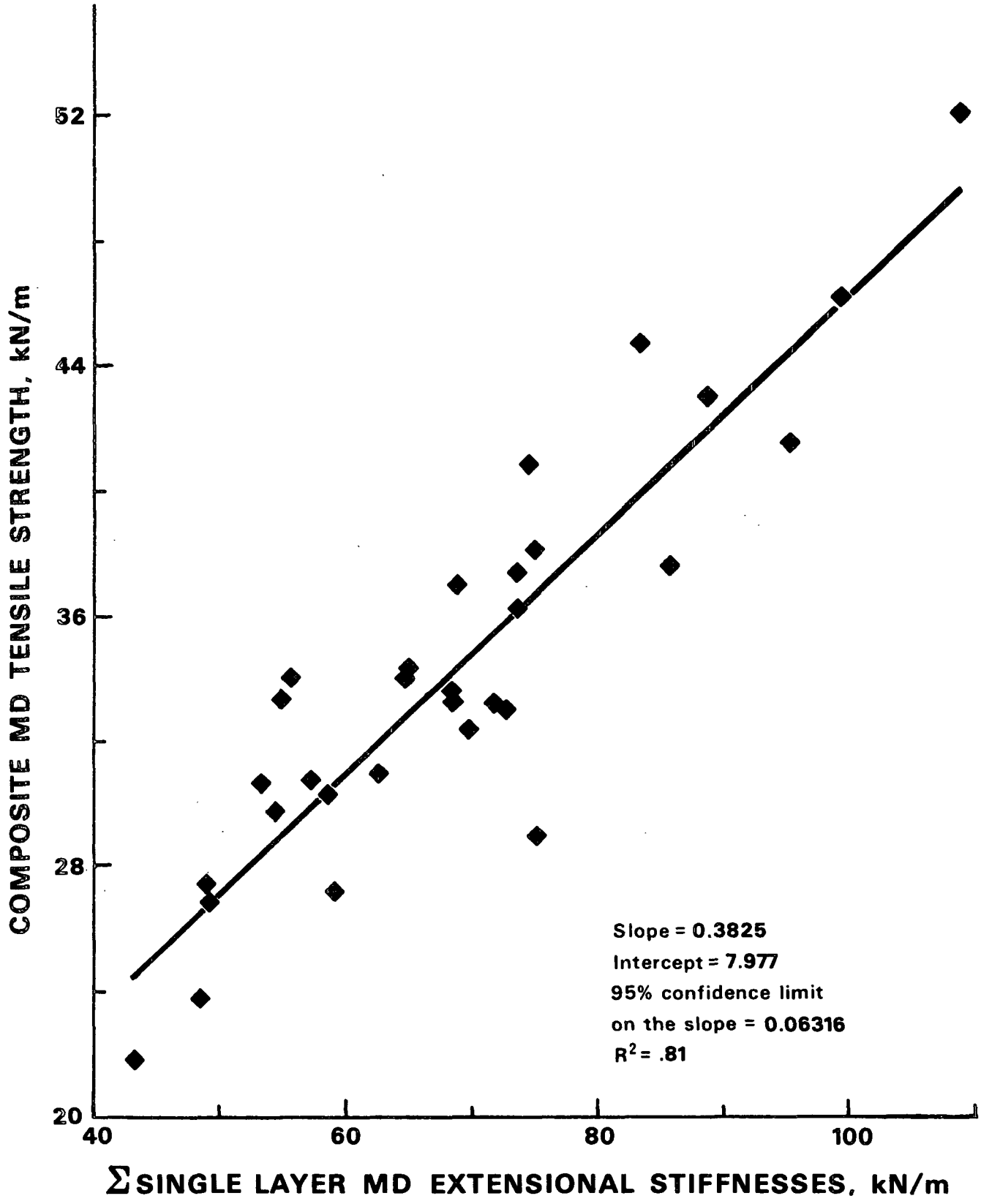

Figure 37. Composite MD tensile strength versus the sum of single layer MD extensional stiffnesses. Data for both the 1182 and 883 series of samples.

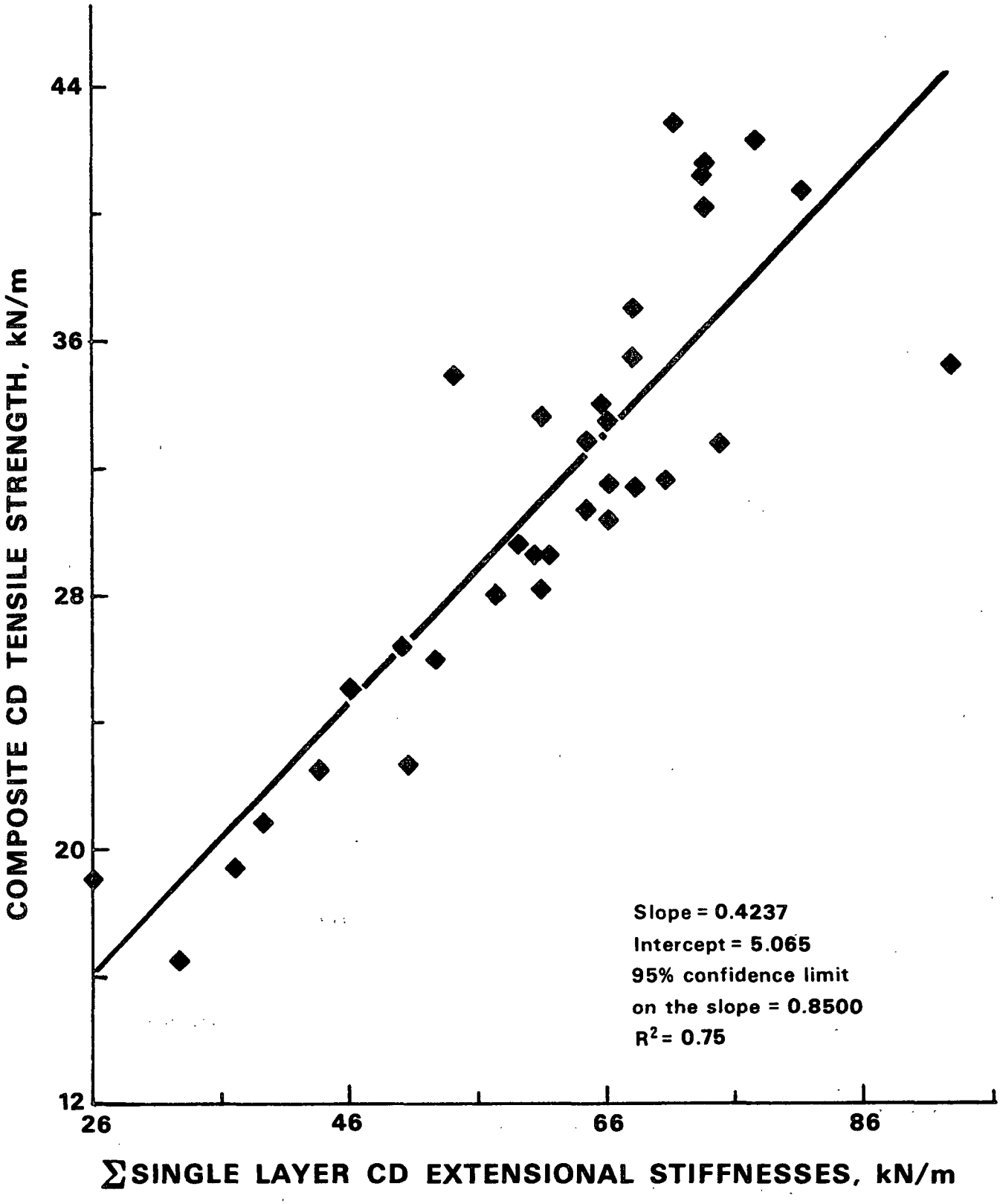

Figure 38. Composite CD tensile strength versus the sum of single layer CD extensional stiffnesses. Data for both the 1182 and 883 series of samples.

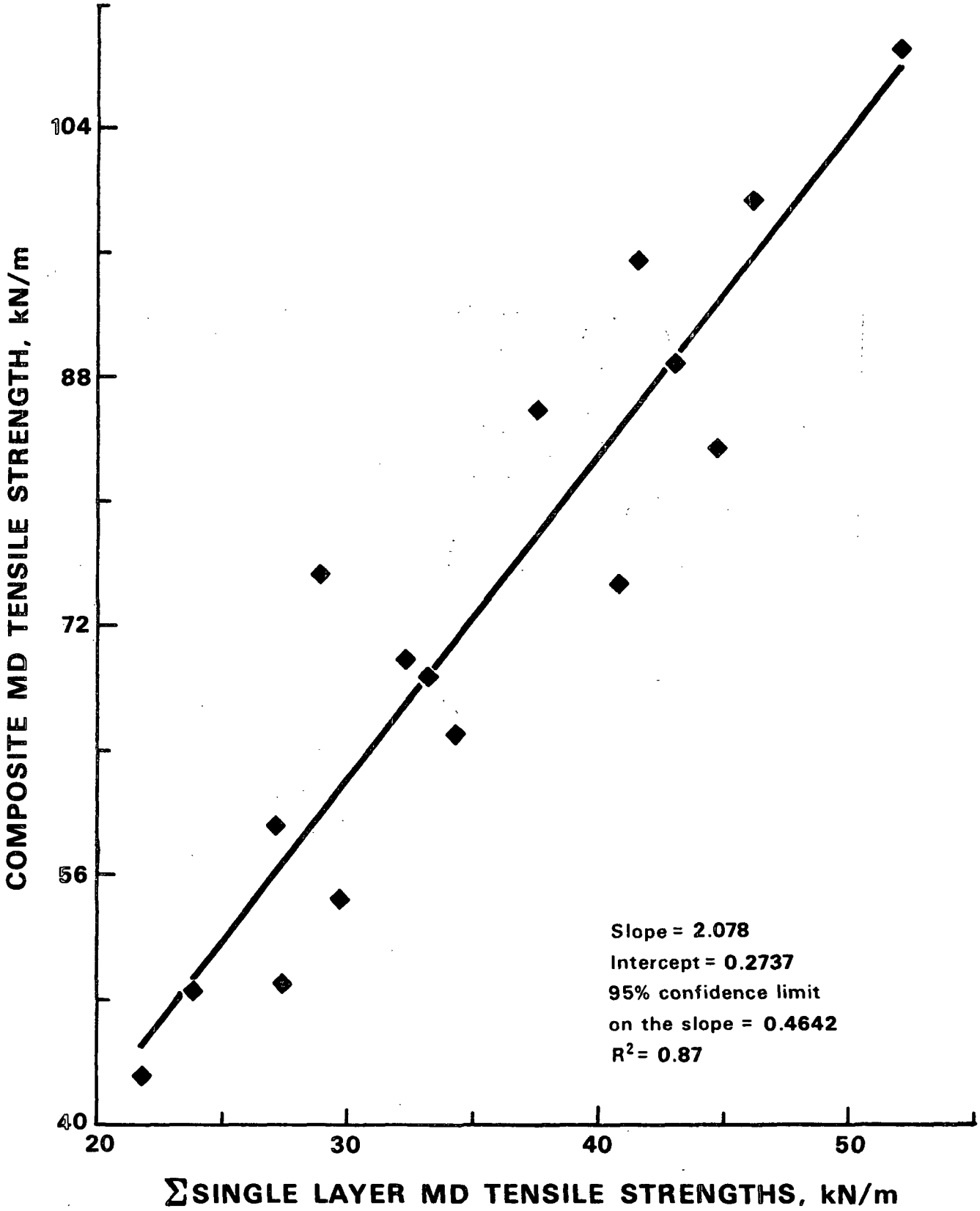

Figure 39. Composite MD tensile strength versus the sum of single layer MD tensile strengths. Data for the 1182 series of samples.

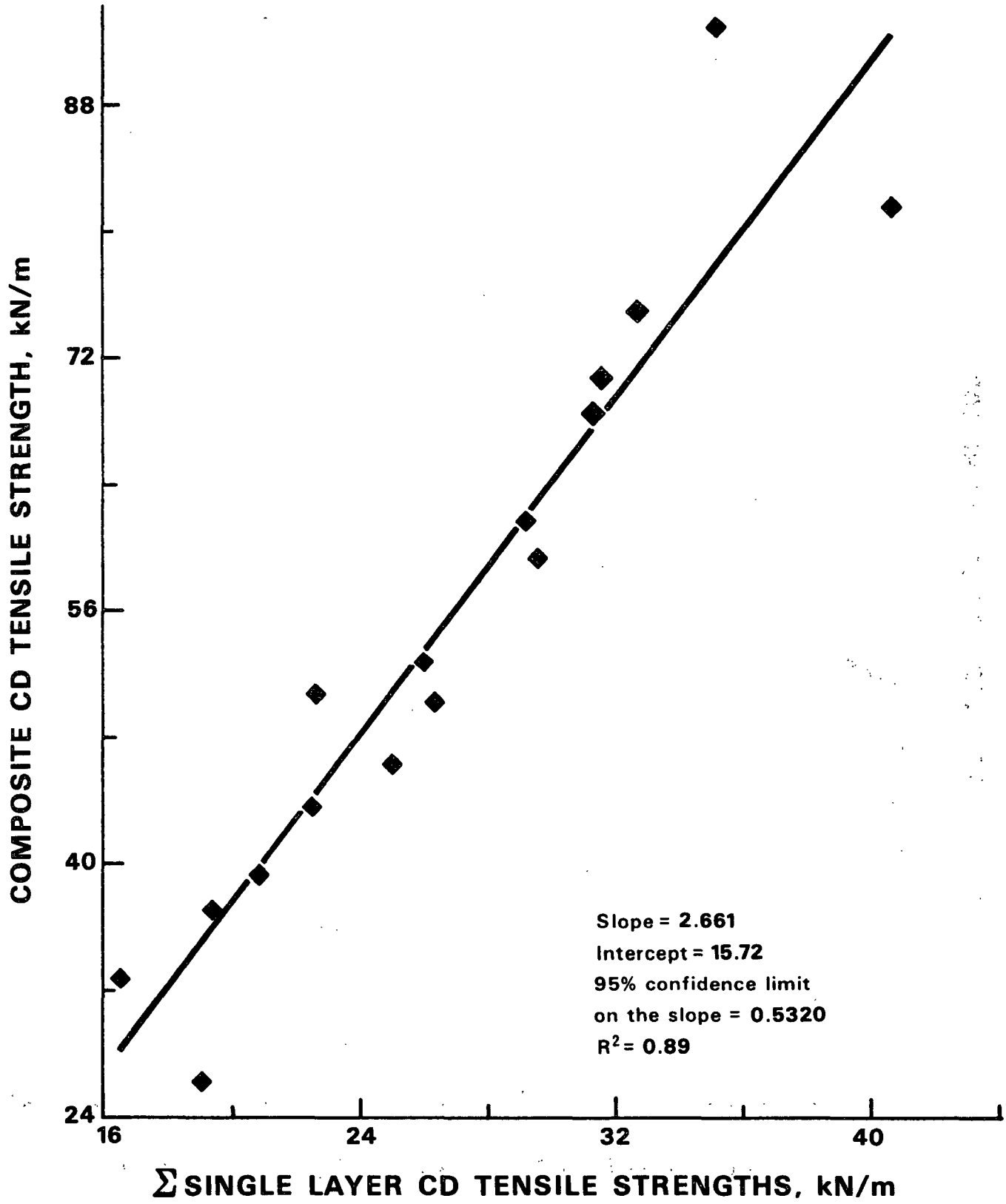

Figure 40. Composite CD tensile strength versus the sum of single layer CD tensile strengths. Data for the 1182 series of samples.

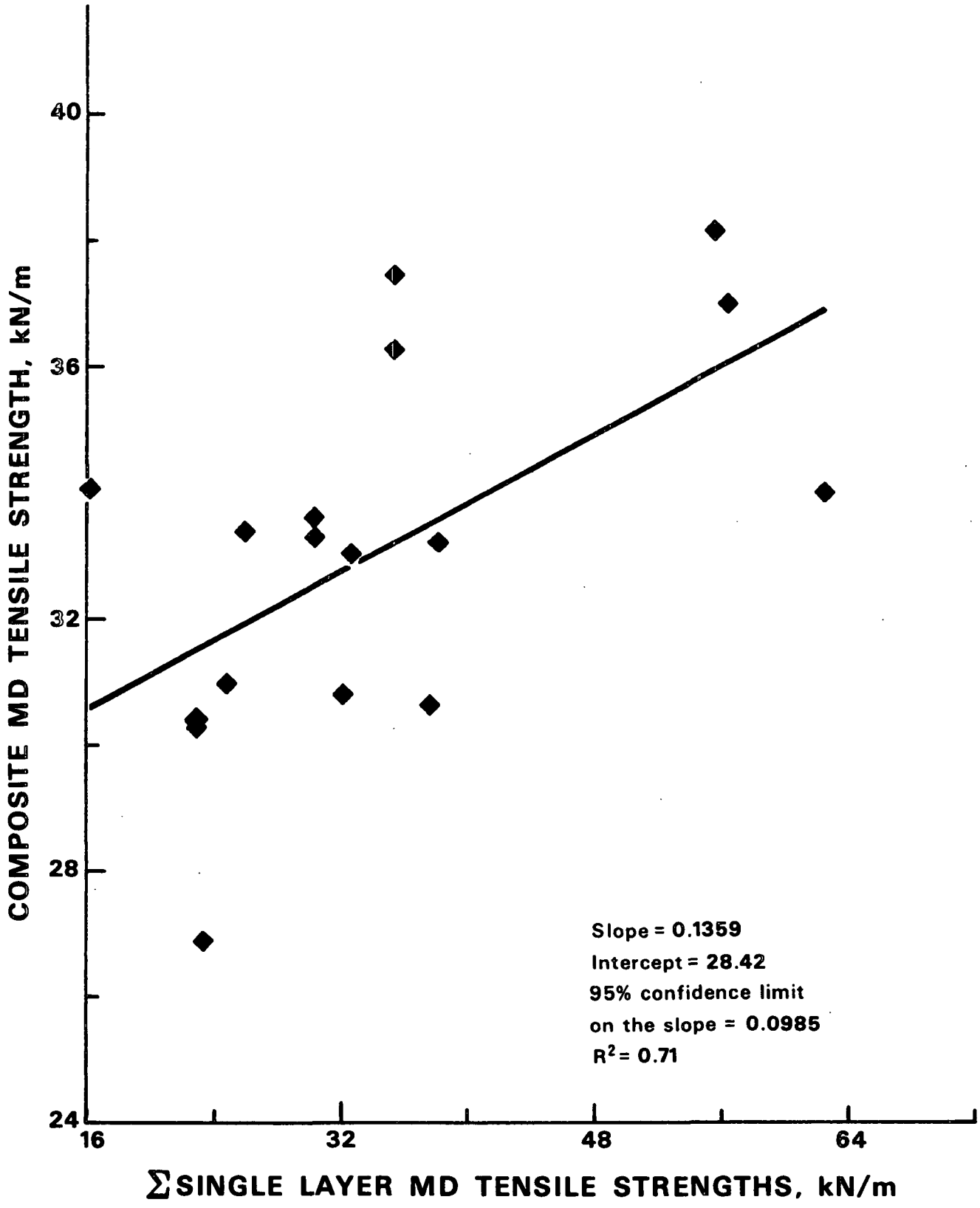

Figure 41. Composite MD tensile strength versus the sum of single layer MD tensile strengths. Data for the 883 series of samples.

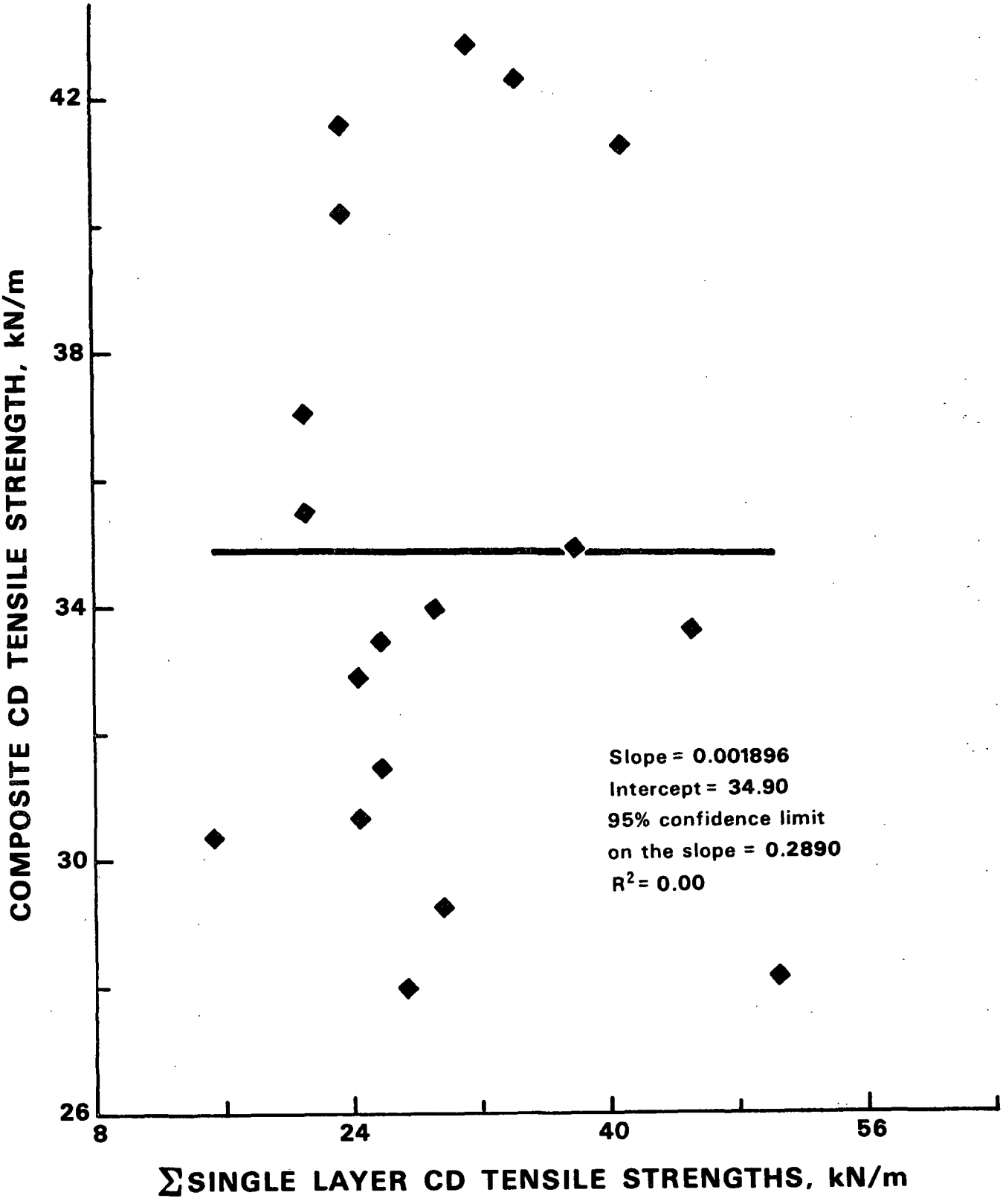

Figure 42. Composite CD tensile strength versus the sum of single layer CD tensile strengths. Data for the 883 series of samples.

Compressive Strength

Edge compressive strength or STFI compressive strength is an important attribute of linerboard, since it can be related to box performance. Generally, linerboard is also a two layered composite material, produced using multiple headboxes. It is important, therefore, to investigate how the single layer properties affect the compressive strengths of the composite. Figures 43 and 44 show the compressive strengths for the composites plotted against the sum of the compressive strengths of the individual layers for the two layered 1182 series samples. There is a very high correlation between these values in both the machine and cross machine directions. The compressive strength of the composite can be expressed as the sum of the compressive strengths of the individual layers.

Figures 45 and 46 show similar graphs for the 883 samples, in the MD and CD, respectively. A relationship is apparent, even though these results show a significantly larger amount of scatter. The cause of the scatter is unknown.

Figures 47 and 48 show the compressive strengths for the composites plotted against the extensional stiffness values of the composites for both the MD and CD, respectively, for both the 1182 and 883 data.

Figures 49 and 50 show the MD and CD compressive strengths, respectively, of the composite plotted against the sum of the extensional stiffness values for the individual layers in the composite. Again, the data fall along a straight line. When these results are compared with those in Fig. 47 and 48, the corresponding machine and cross machine direction plots appear almost identical. It would appear that either the layered model or the single layer model predicts the STFI compressive strength values equally well.

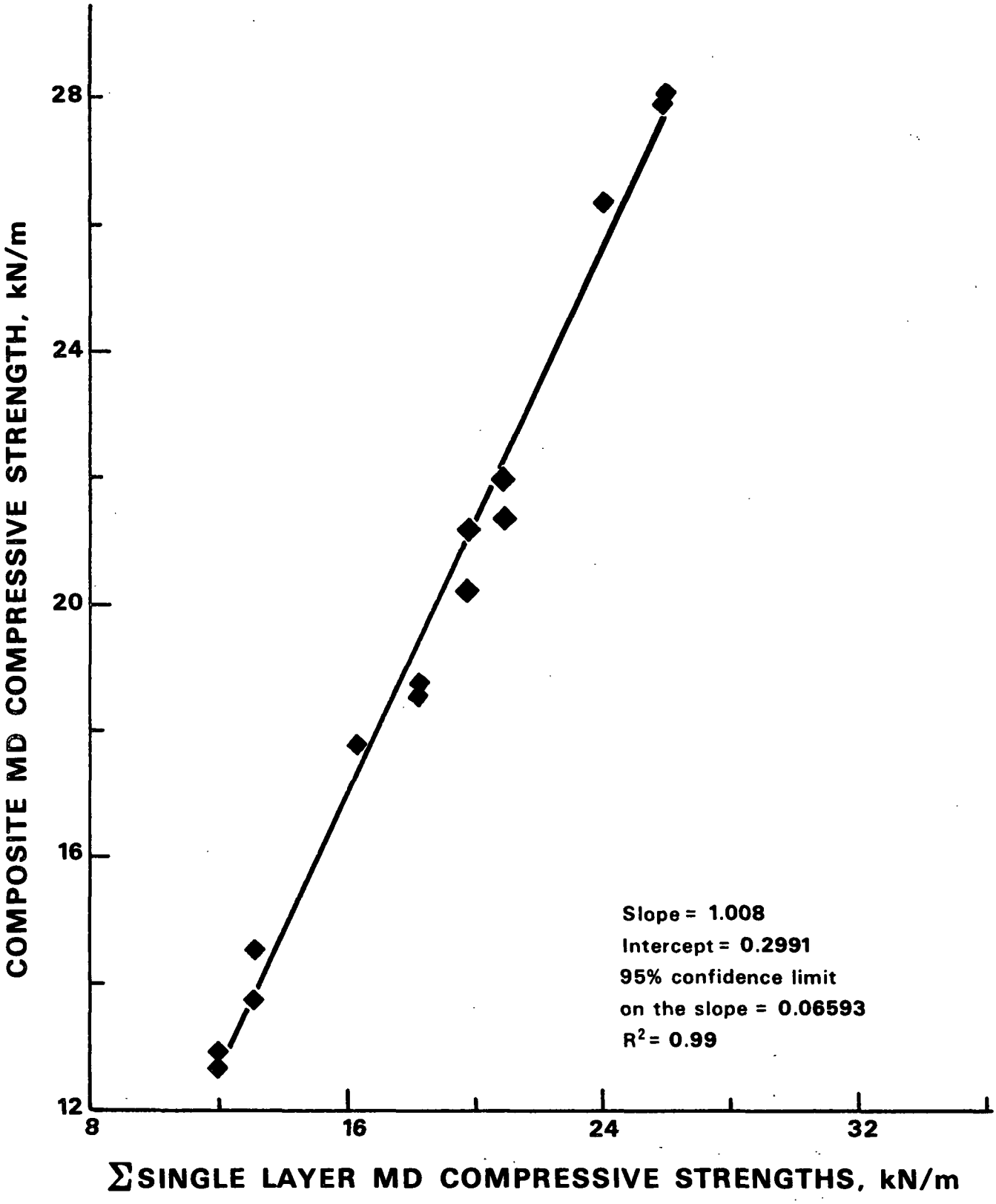

Figure 43. Composite MD compressive strength versus the sum of single layer MD compressive strengths. Data for the 1182 series of samples.

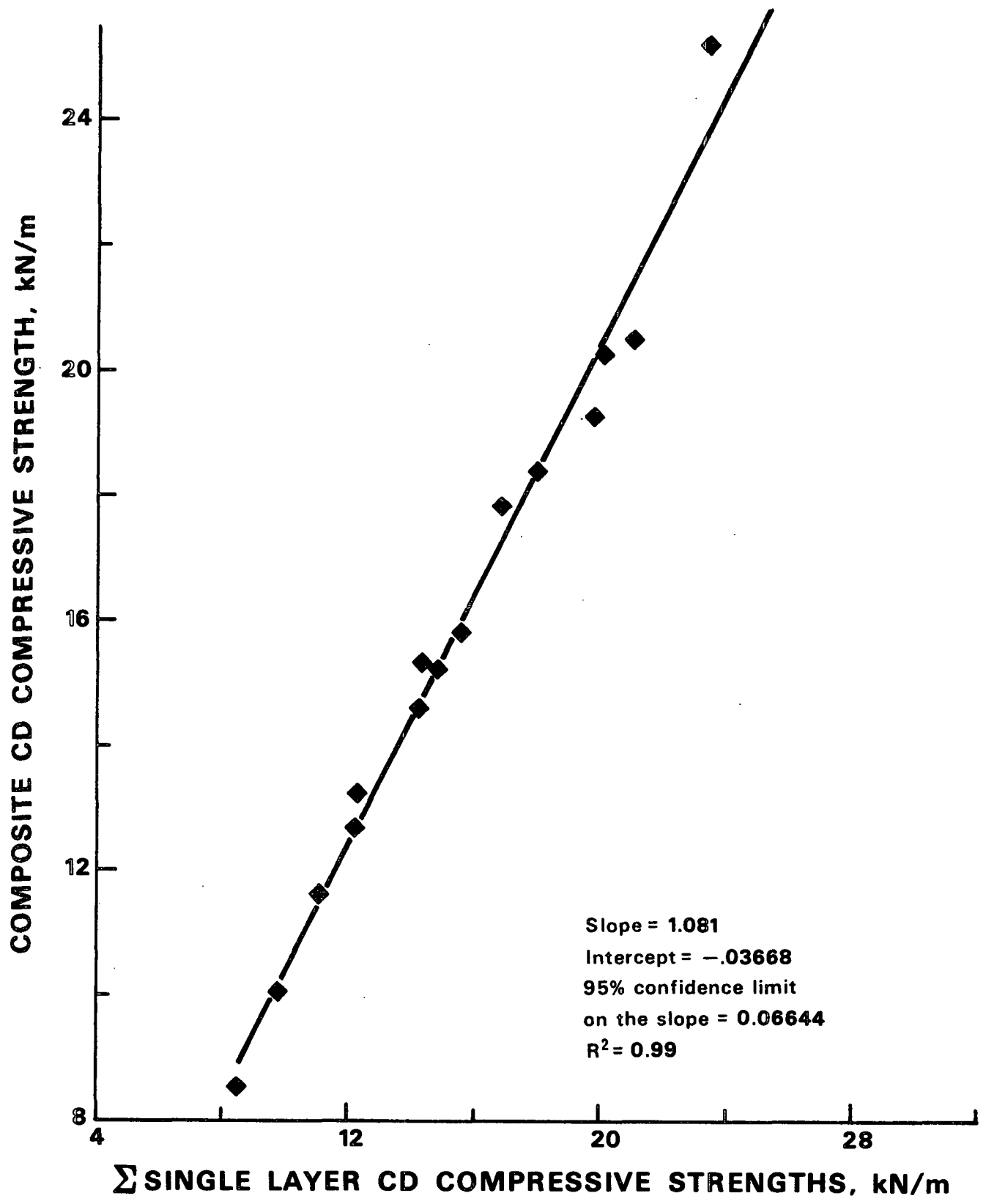

Figure 44. Composite CD compressive strength versus the sum of single layer CD compressive strengths. Data for the 1182 series of samples.

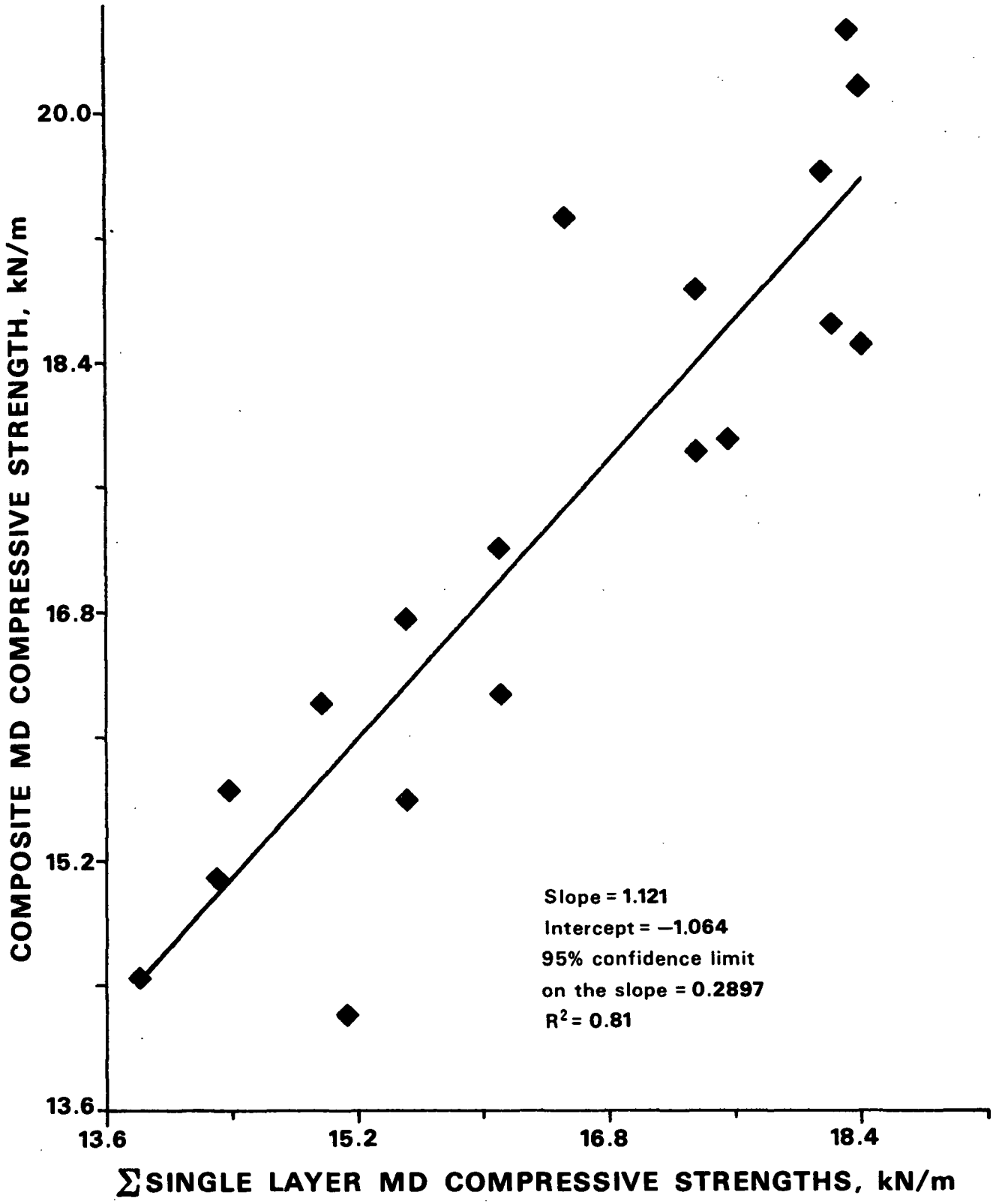

Figure 45. Composite MD compressive strength versus the sum of single layer MD compressive strengths. Data for the 883 series of samples.

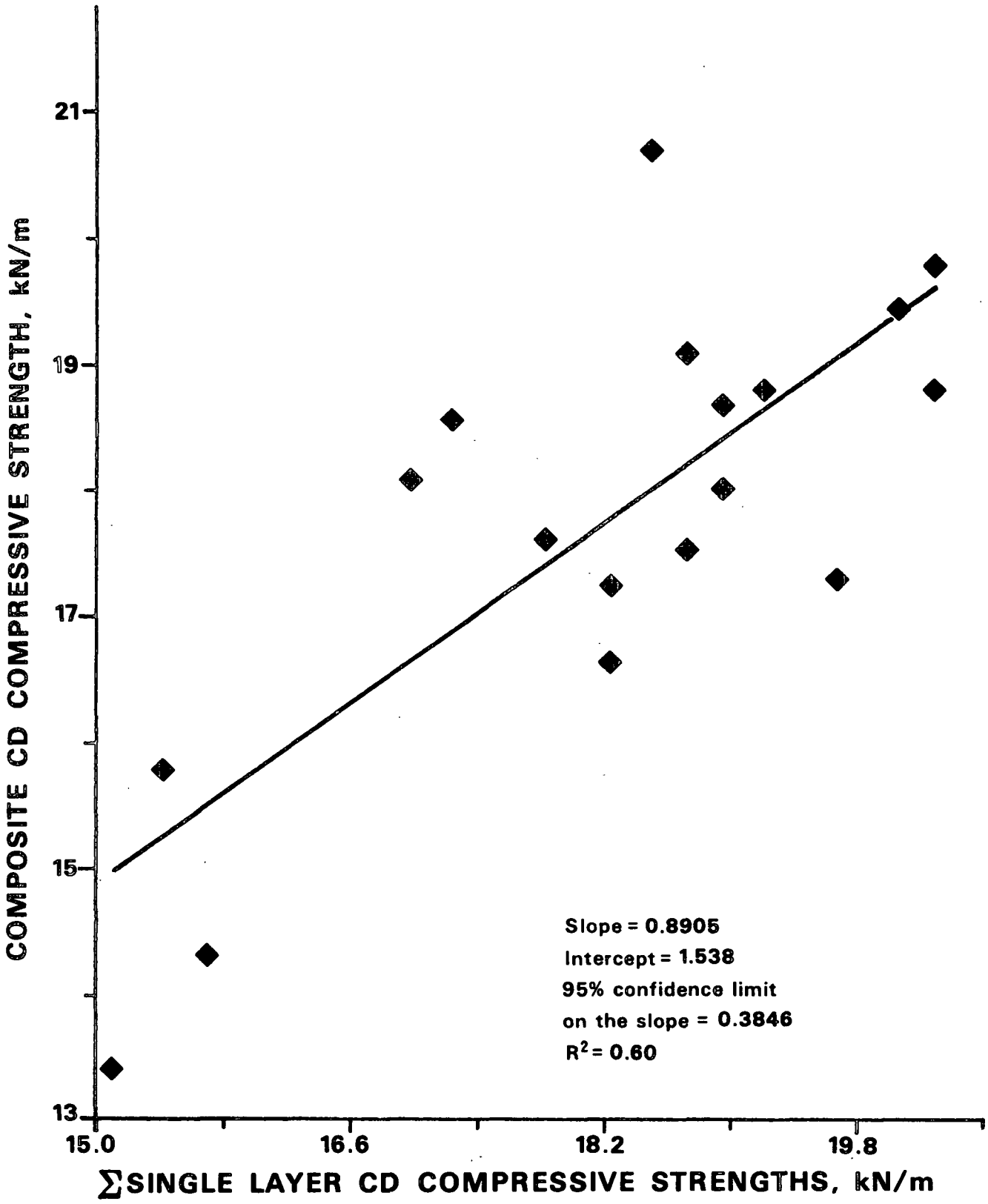

Figure 46. Composite CD compressive strength versus the sum of single layer CD compressive strengths. Data for the 883 series of samples.

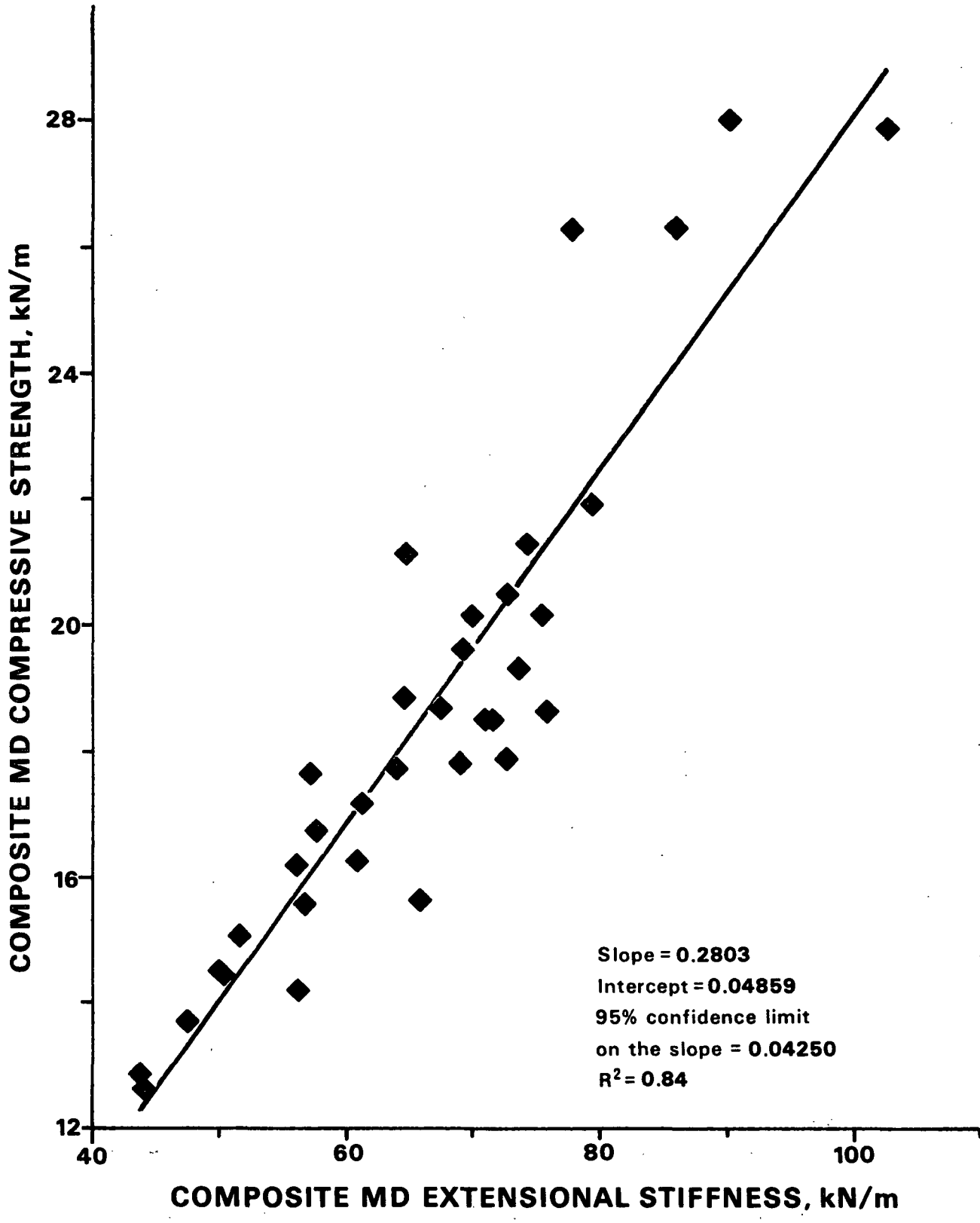

Figure 47. Composite MD compressive strength versus composite MD extensional stiffness. Data for both the 1182 and 883 series of samples.

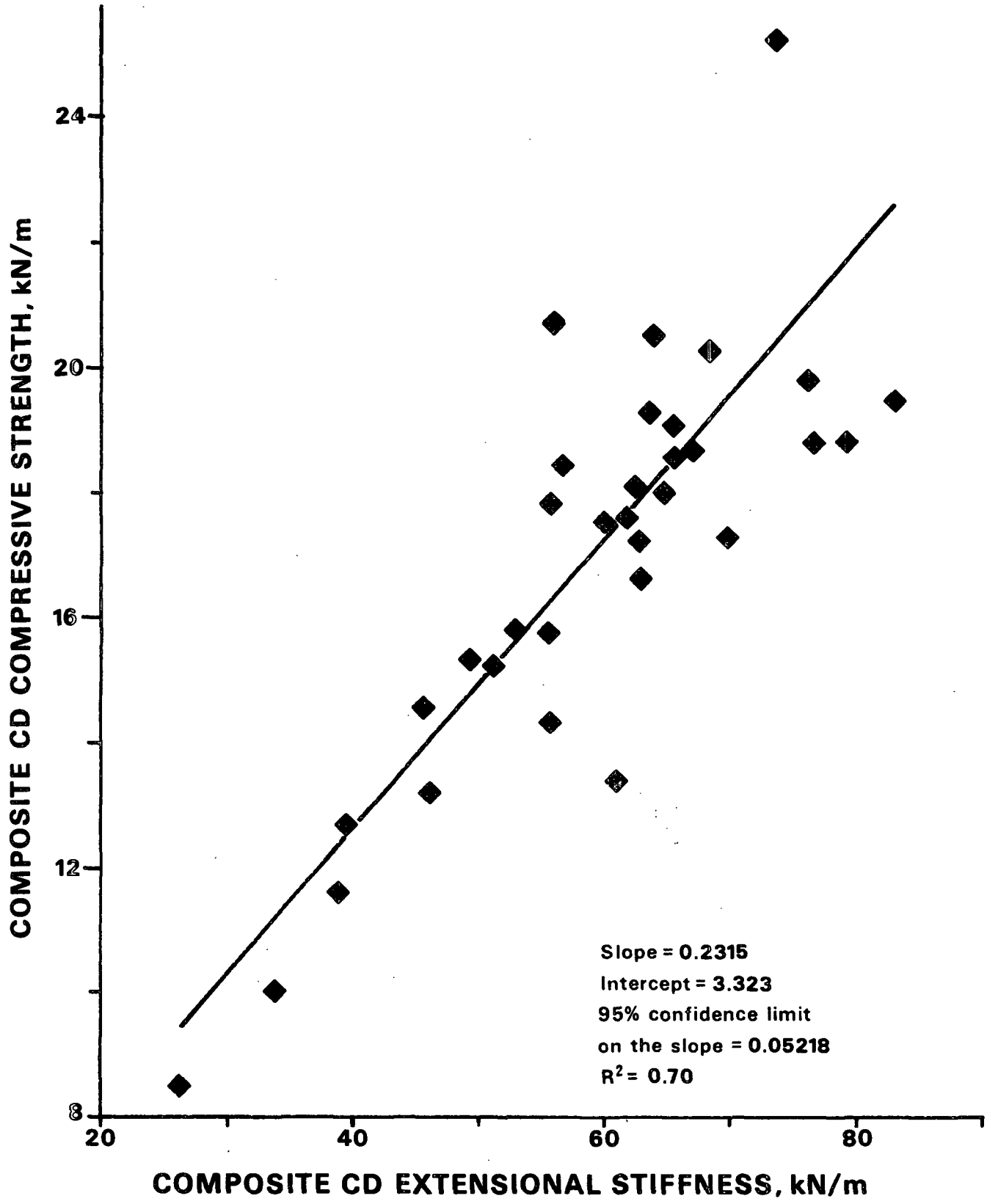

Figure 48. Composite CD compressive strength versus composite CD extensional stiffness. Data for both the 1182 and 883 series of samples.

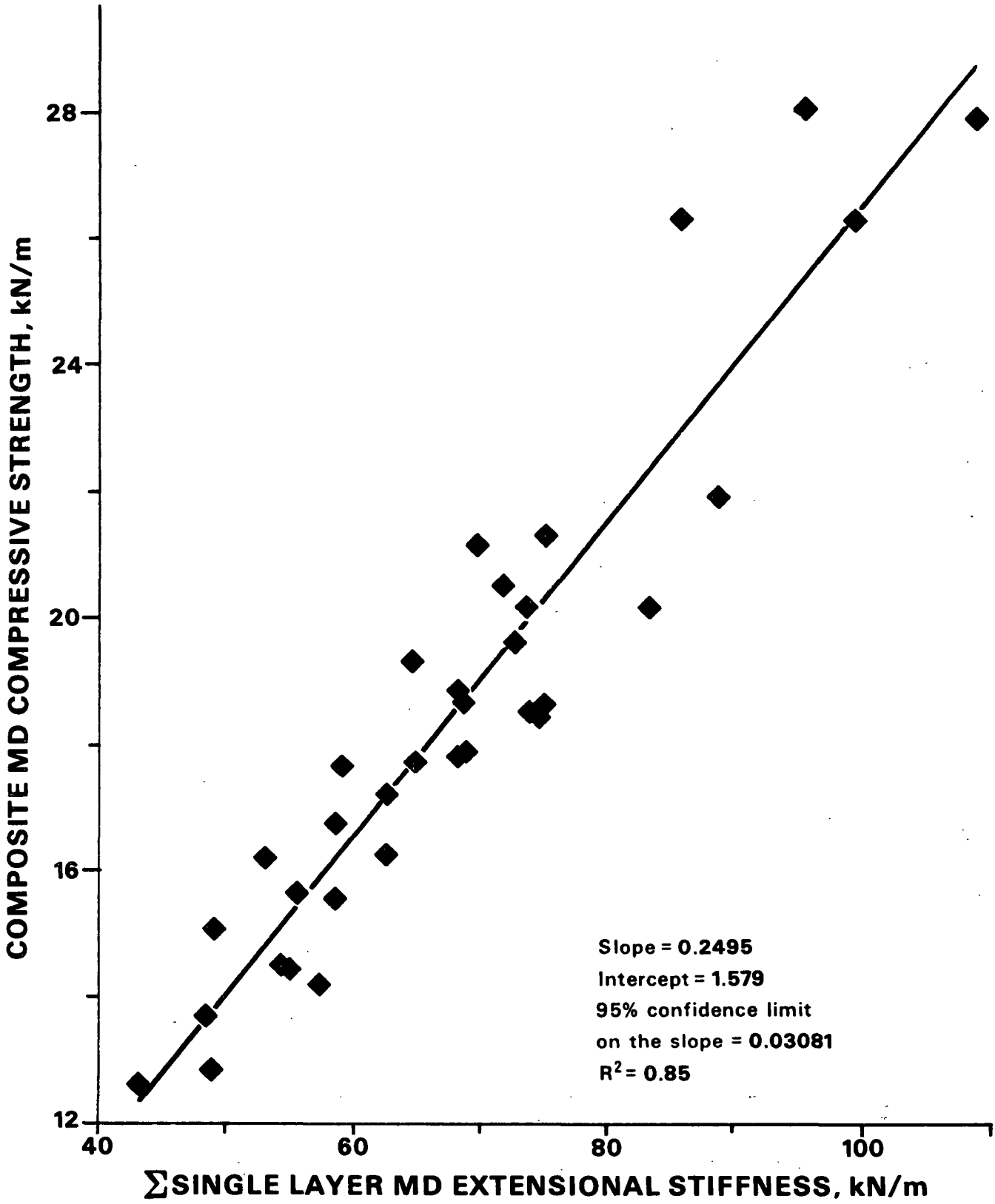

Figure 49. Composite MD compressive strength versus the sum of single layer MD extensional stiffness. Data for both the 1182 and 883 series of samples.

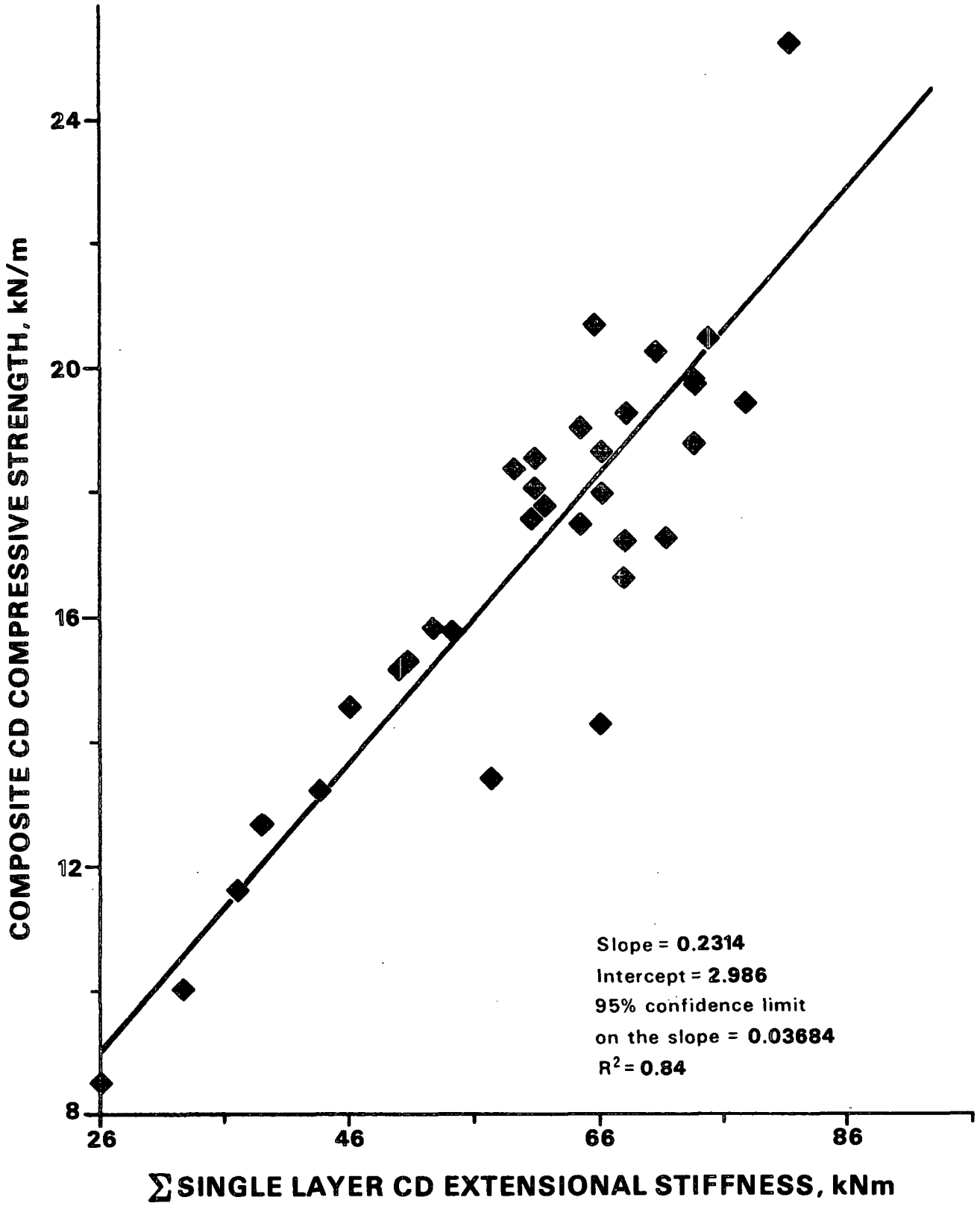

Figure 50. Composite CD compressive strength versus the sum of single layer CD extensional stiffness. Data for both the 1182 and 883 series of samples.

According to the model of Habeger, et al.,[35] the compressive strength should be related to the product of an in-plane and out-of-plane elastic parameter. For example, CD compressive strength would be related to the product $(E_{CD}G_{CD-ZD})^{1/2}$, or $(C_{22}C_{44})^{1/2}$. However, inclusion of the out-of-plane values here did not improve the correlations.

Taber and Four Point Bending

As in the case of tensile and compressive strengths, our main concern here is to determine how the properties of the individual layers affect the bending properties of the composite. It is well known that the flexural rigidity of a layered composite can be expressed as:

$$EI_{composite} = \sum_{i=I}^{n} (EI)_i \qquad (108)$$

where $(EI)_i$ is the flexural rigidity for layer i.

E is Young's modulus and I is the moment of inertia for the layer in question. For layer i, the moment of inertia is taken with respect to the neutral axis of the composite. It is of interest to see this equation holds for the Young's moduli values determined ultrasonically.

Figures 51 and 52 show the Taber stiffness values for the composite plotted against the EI value of the composite for the MD and CD directions, respectively. A reasonably good correlation exists between these two values in the cross machine direction, but the correlation is not as good in the machine direction data. The probable reason for this difference is that the three-layer samples were cross laminated to accentuate the differences in layer properties.

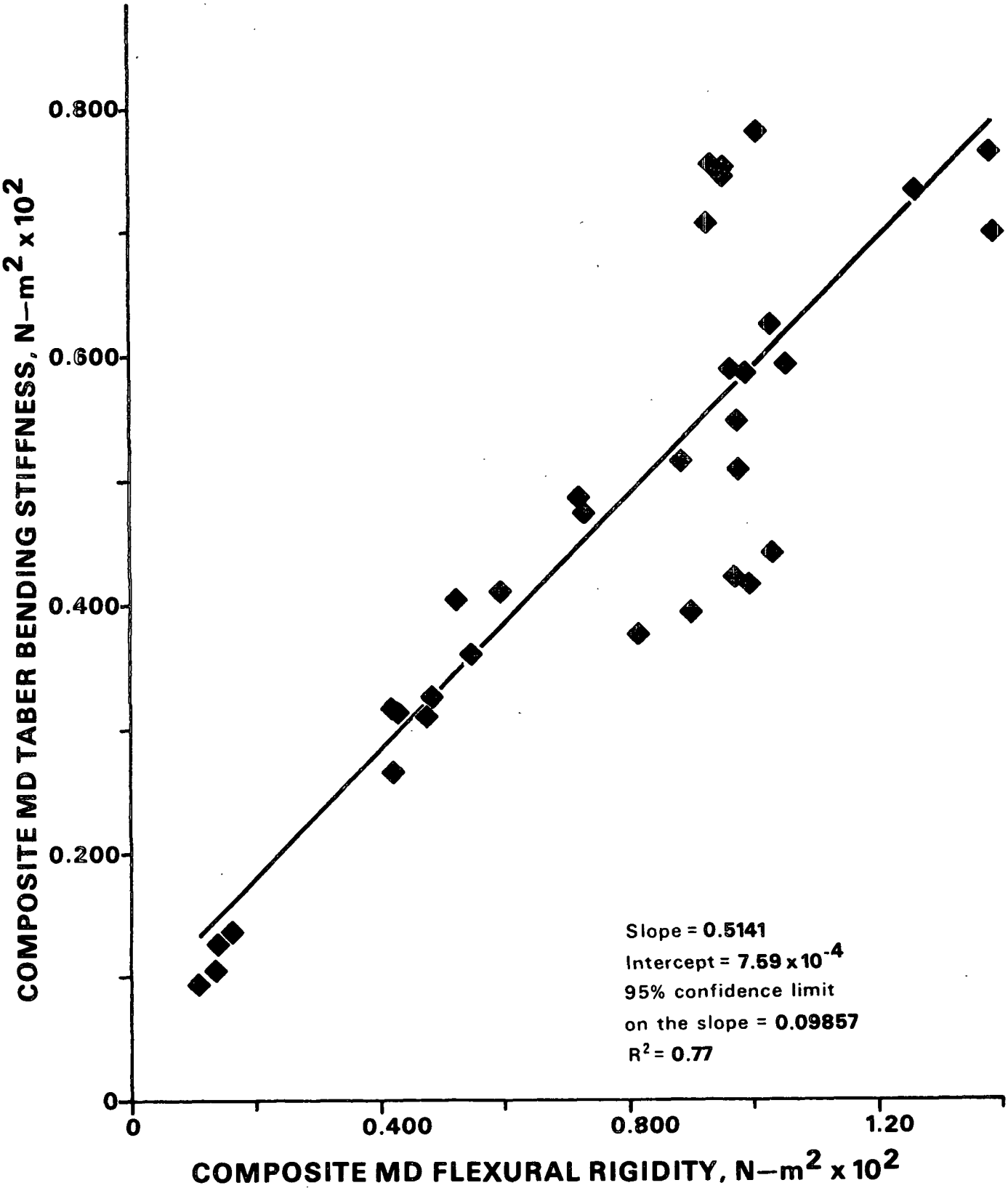

Figure 51. Composite MD Taber bending stiffness versus composite MD flexural rigidity (E measured ultrasonically). Data for both the 1182 and 883 series of samples.

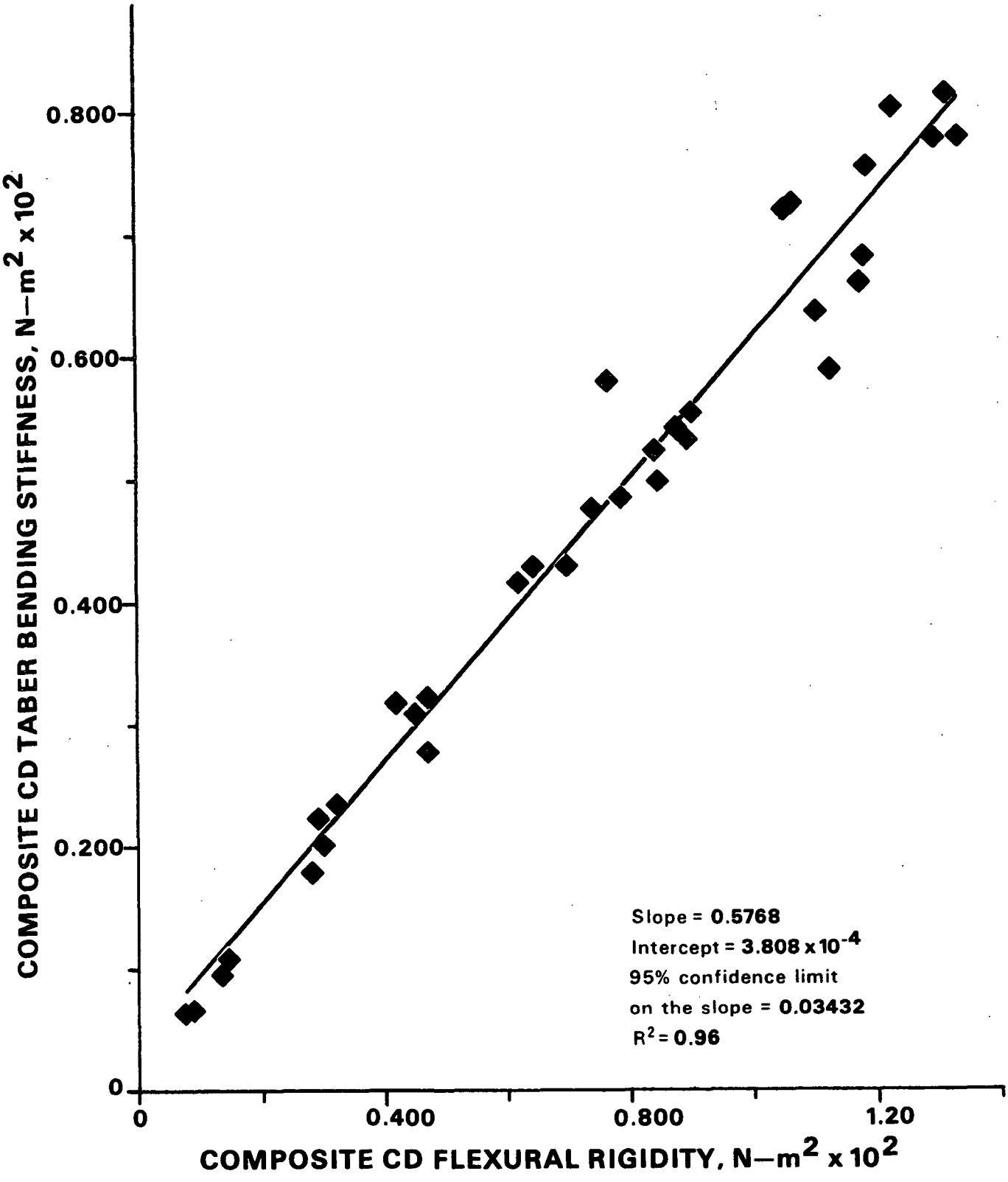

Figure 52. Composite CD Taber bending stiffness versus composite CD flexural rigidity (E measured ultrasonically). Data for both the 1182 and 883 series of samples.

The differences in the scatter of data is most likely due to the relative differences in these individual layer properties. If one investigates the composite construction for each of the data points in Fig. 51, the data points which deviate the farthest from the expected values belong to the three layer composites. One might expect this kind of behavior in the three layer samples because they would be the samples most likely to show an "I beam" effect, due to the large differences in the properties of the layers which are located away from the neutral plane. The flexural rigidity of a beam is most affected by the properties of the layers located furthest from the neutral plane (i.e., the layers with the largest I values).

It would appear that the bending properties of the three layer composites could be accounted for by summing the EI values for each of the individual layers. Figures 53 and 54 show the Taber stiffness values plotted against the sum of the individual layer EI values for the MD and CD directions, respectively. The fit of the data is good in both cases. Comparing Fig. 53 with the results in Fig. 51, the fit of the machine direction data has improved considerably. As expected, a layered model predicts the bending behavior of the layered composite better than a single layer model.

Figures 55 and 56 show the results for the four point bending tests. As with the Taber stiffness values, the cross machine values exhibit a far better fit than the machine direction values. The machine direction plots in Fig. 51 and 55 are practically identical.

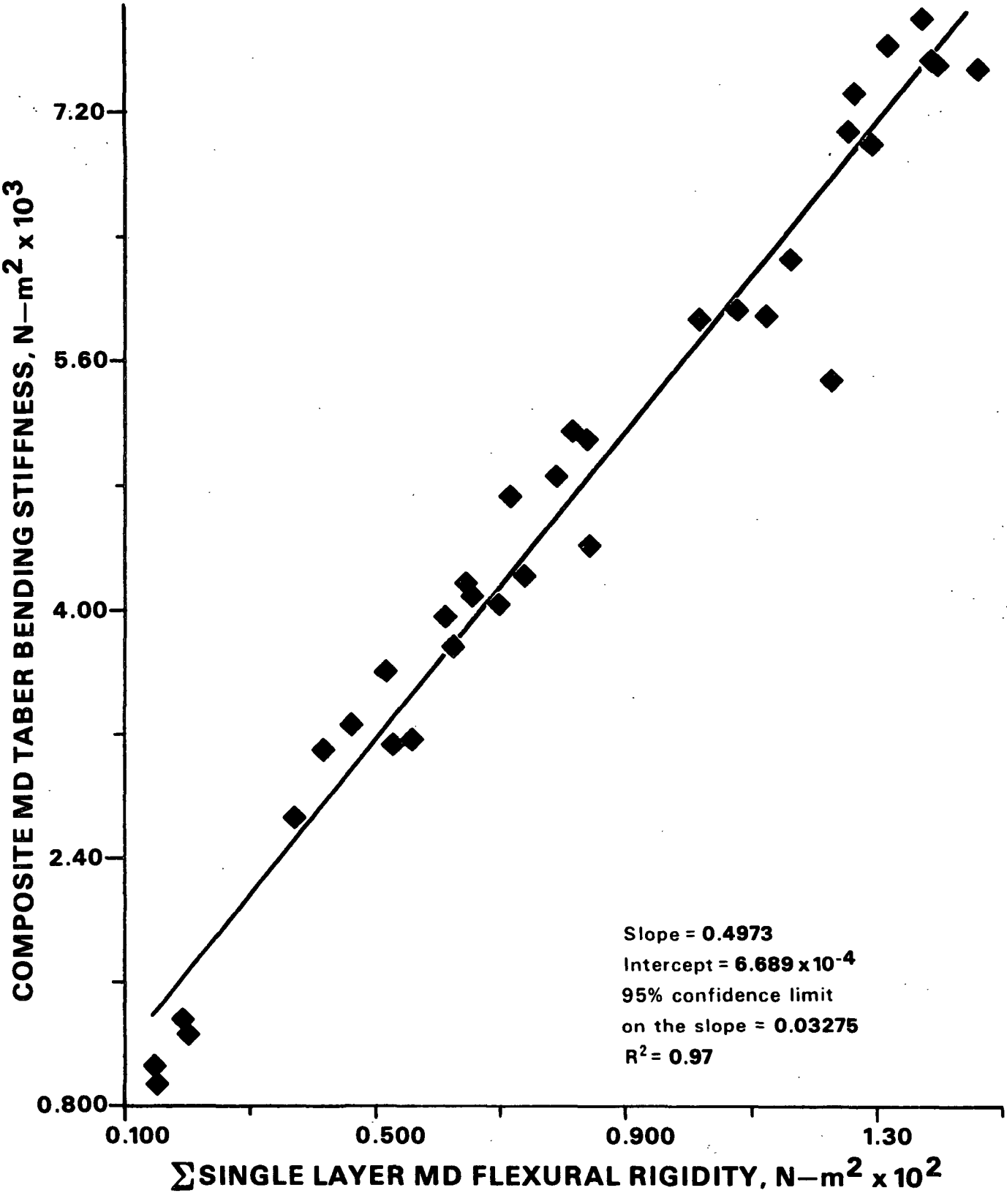

Figure 53. Composite MD Taber bending stiffness versus the sum of single layer MD flexural rigidity (E measured ultrasonically). Data for both the 1182 and 883 series of samples.

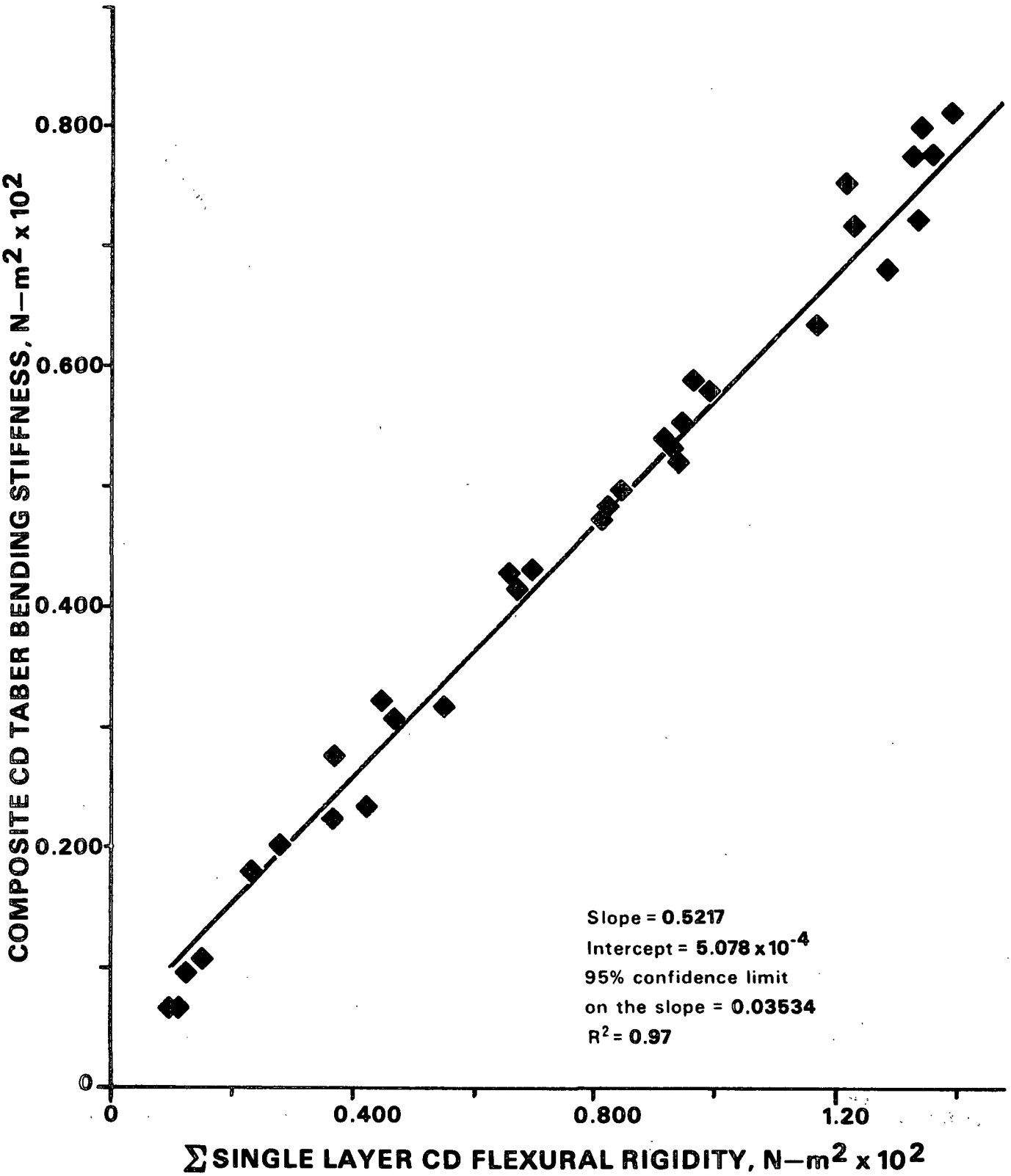

Figure 54. Composite CD Taber bending stiffness versus the sum of single layer CD flexural rigidity (E measured ultrasonically). Data for both the 1182 and 883 series of samples.

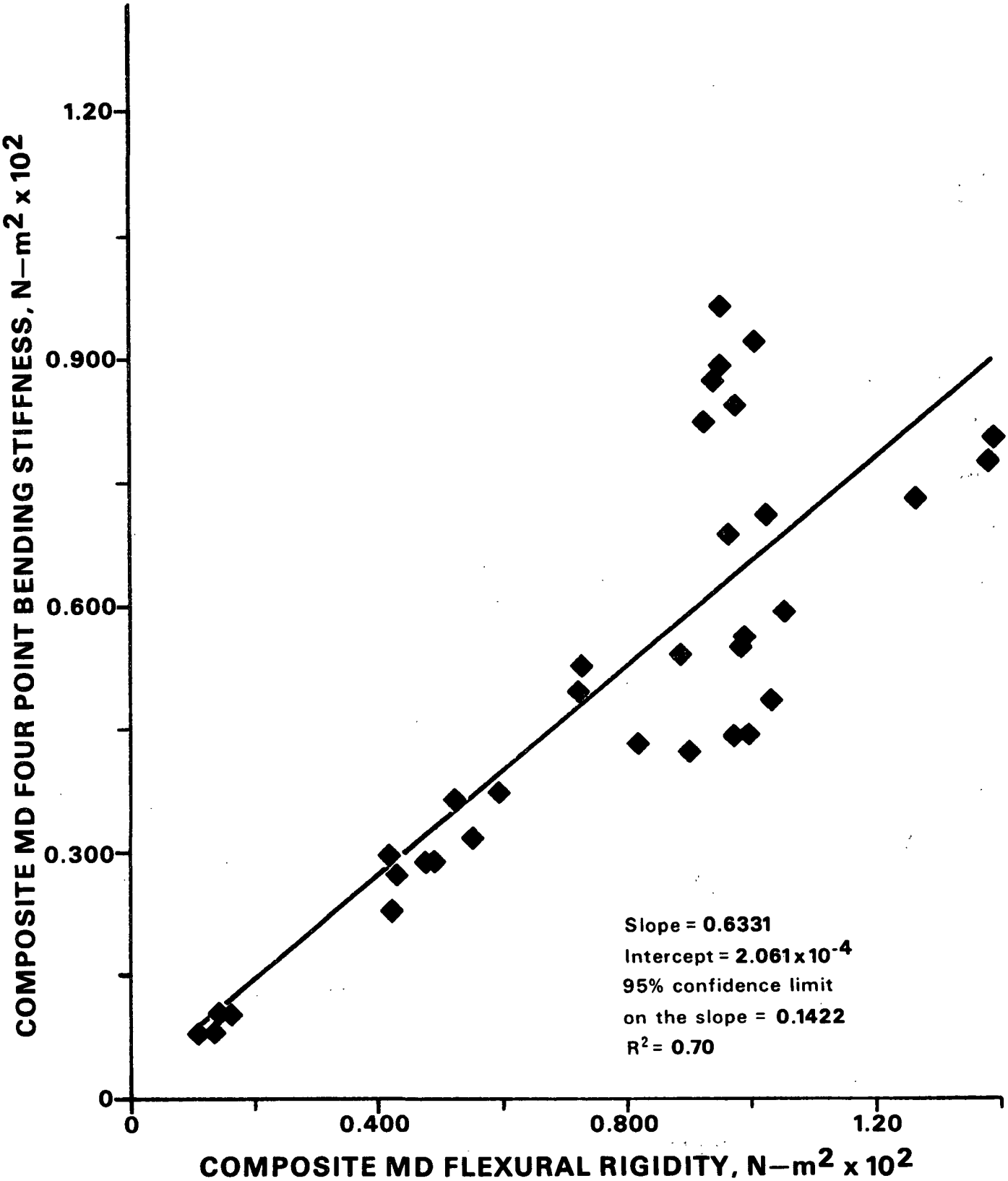

Figure 55. Composite MD four point bending stiffness versus composite MD flexural rigidity (E measured ultrasonically). Data for both the 1182 and 883 series of samples.

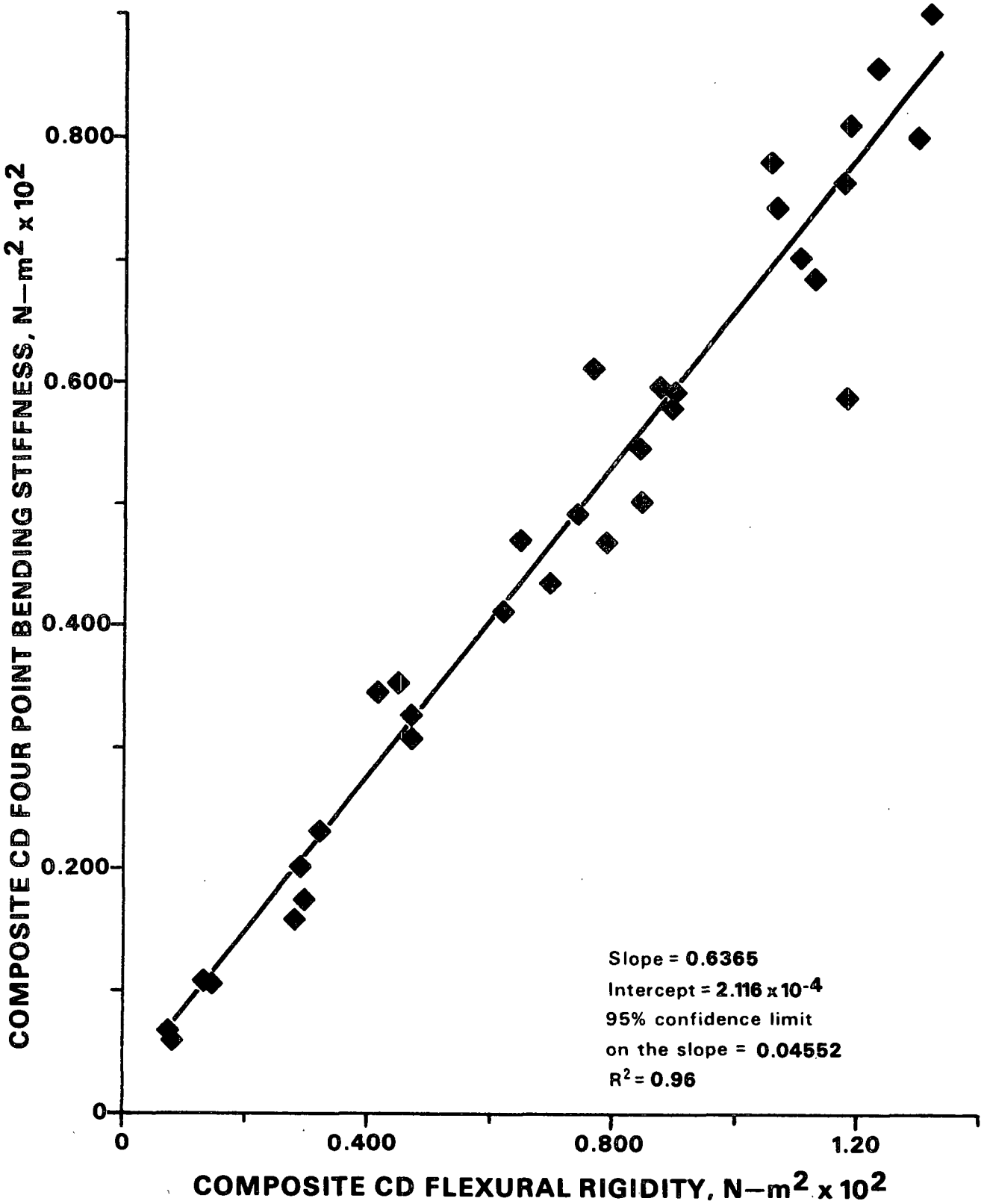

Figure 56. Composite CD four point bending stiffness versus composite CD flexural rigidity (E measured ultrasonically). Data for both the 1182 and 883 series of samples.

Figures 57 and 58 show the EI values for the composite, measured using the four point bending technique, plotted against the sum of the single layer EI values. As with the Taber stiffness data, the layered model improves the fit of the machine direction data considerably. It appears that, at least for the three-layer composites, a layered model is required to satisfactorily describe the bending behavior.

Examination of both the Taber and the four point bending data suggests that a layered model is most desirable for describing the bending properties of a layered composite material. However, it also appears that the cross machine data could be described satisfactorily using a single layer model, at least for the samples used here. Since one rarely possesses information about the individual layers within a commercially produced composite, it is comforting that the bending properties of many of the composites were accurately predicted by a single-layer model. For the composites studied here, it appears that the bending properties can be predicted from velocity data measured on the composites. For composites in which one or more of the layers is some distance from the neutral axis, as the differences between the properties of the individual layers increase, the measured values of the composite's bending stiffness will depart from the predictions of the composites ultrasonic data.

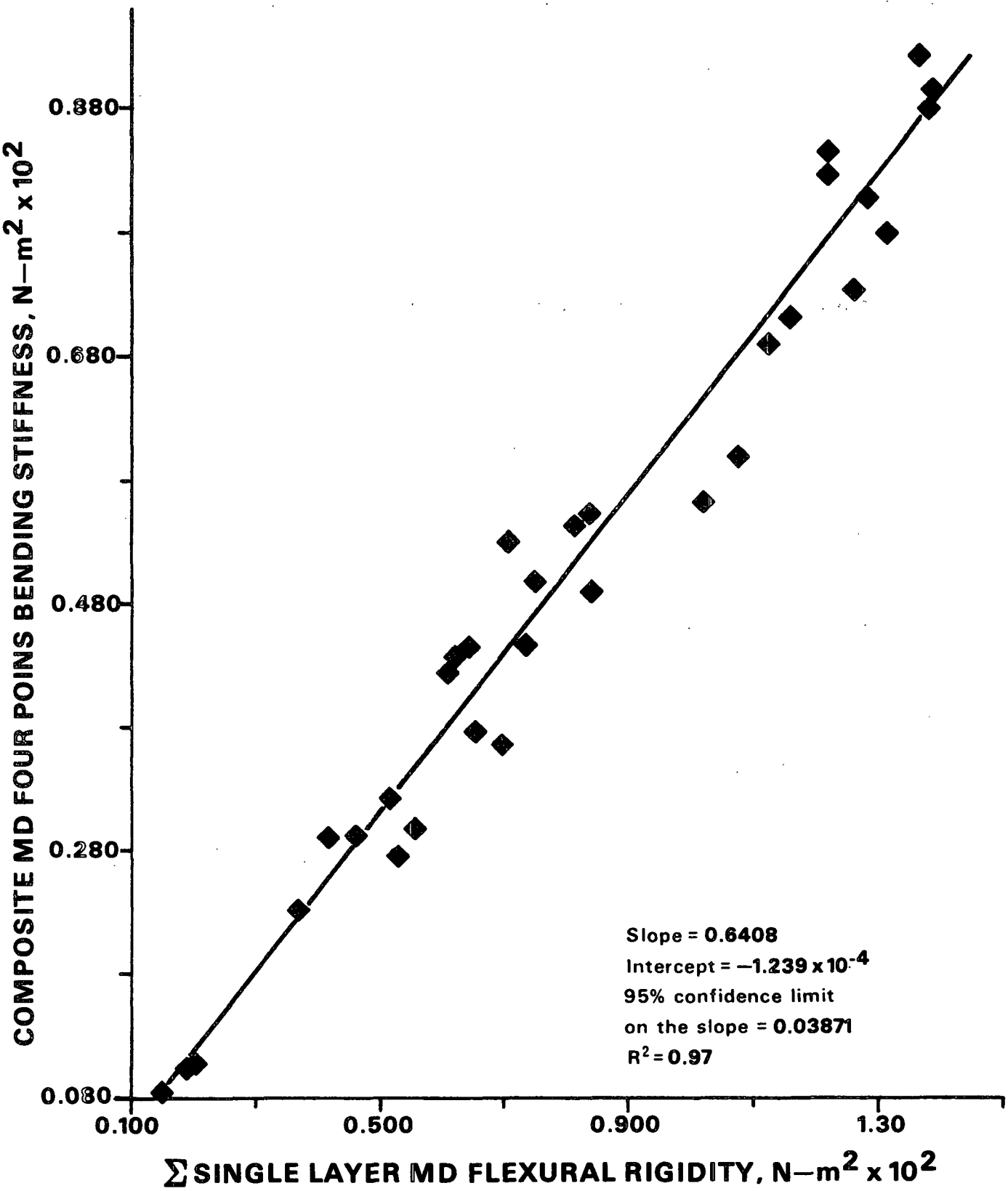

Figure 57. Composite MD four point bending stiffness versus Σ single layer MD flexural rigidity (E measured ultrasonically). Data for both the 1182 and 883 series of samples.

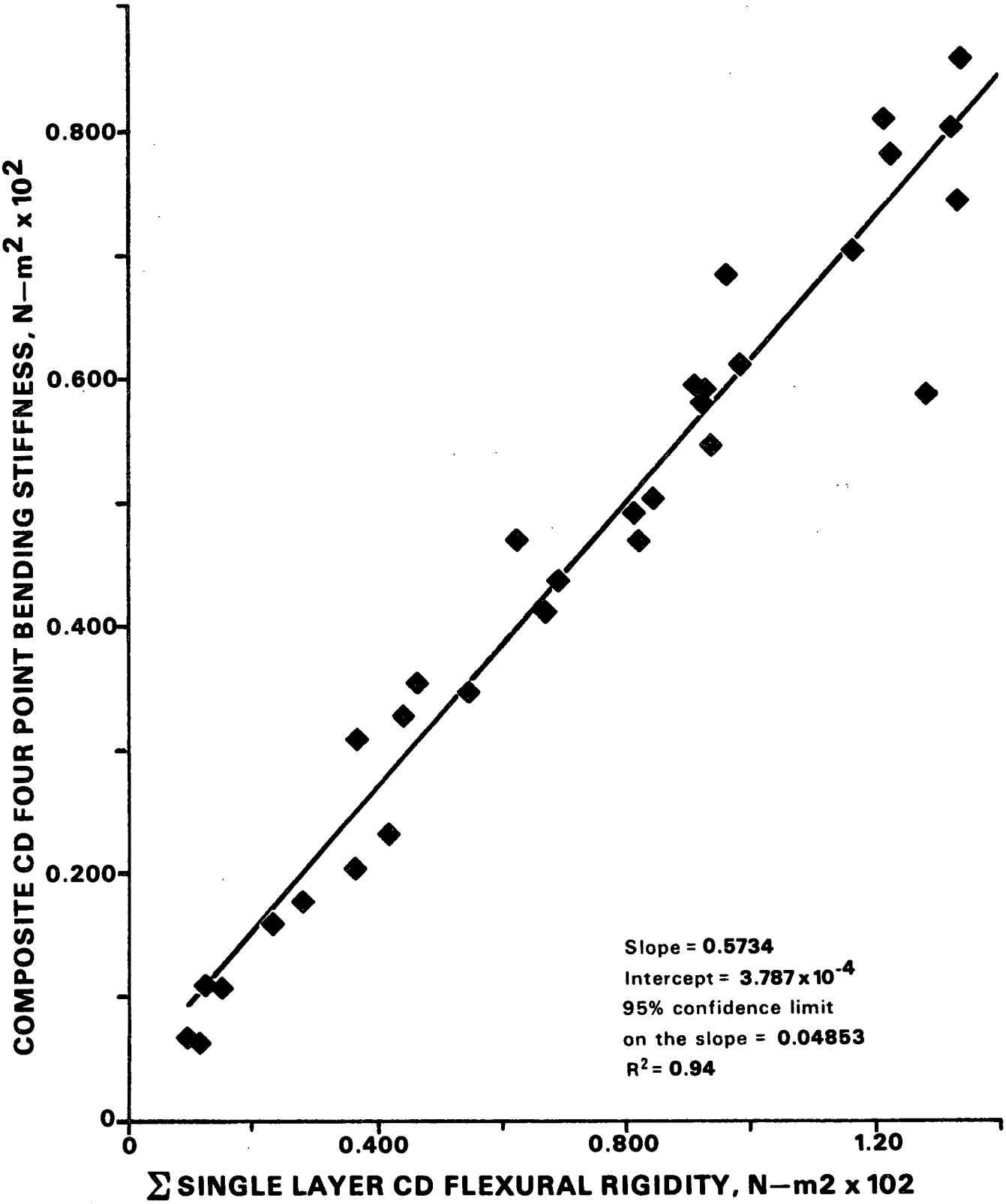

Figure 58. Composite CD four point bending stiffness versus the sum of single layer CD flexural rigidity (E measured ultrasonically). Data for both the 1182 and 883 series of samples.

SUMMARY

Correlations have been found between elastic constants which are measured ultrasonically and a number of physical properties; namely, tensile strength, compressive strength, and bending stiffness. In the case of tensile strength or compressive strength, these correlations are not improved by using the individual layer elastic constants. However, for bending stiffness, a layered model yields the best correlation.

For ultrasonic measurement of tensile strength and compressive strength, it is possible to treat a layered composite as though it were a single layer material. Ultrasonic techniques used to measure these properties on-machine should therefore need no special modification for use on layered composites. Considering the difficulties involved in measuring individual layer properties, the option to use a single layer approach is most appealing.

CONCLUSIONS

Layered paper composites are often assumed to behave as homogeneous orthotropic materials. Although this assumption serves as a useful approximation, it cannot yield a fair description of the material. To accurately characterize a layered composite, the properties of the individual layers must be known.

Two models have been presented for determining the elastic properties of a composite from the elastic properties of the individual layers. The in-plane elastic constants follow a basis weight average of the layers to yield the in-plane properties of the composite, while the out-of-plane constants follow a caliper average to yield the values of the composite. The longitudinal constants (C_{11}, C_{22}, and C_{33}) follow these models quite well. The shear constants (C_{44}, C_{55}, and C_{66}), however, do not fit quite as well. Either some additional factor affects the measured shear constants in the composite, or the properties at the interfaces between layers are somehow important.

Correlations exist between several physical tests and the elastic constants determined ultrasonically. Tensile and compressive strengths are equally well described by either single layer or composite models. Bending stiffness tests, however, correlate better with the ultrasonic data when using a layered model. The layered model apparently accounts for differences in the flexural rigidity of the three layer samples due to layer composition and construction, whereas the single layer model cannot account for these variations.

The plate wave resonance method for generating plate waves is not sensitive to air currents if a lock-in amplifier is used. The plate wave resonance device, therefore, no longer needs to be enclosed. Aside from making the plate

wave measurements easier to perform, the lock-in amplifier may allow new applications for this measurement technique. One of these applications may be as a noncontacting on-machine test method.

The theoretical layered orthotropic models developed in this study accurately describe the dispersion of plate waves in the layered composites studied. The models predict the location of the highly dispersive "fall-off" regions of the dispersion curves better than the single layer orthotropic model developed by others. The lack of bonding at an interface in the composite seems to affect the low frequency SO region of the dispersion curve, but does not alter the low velocity or fall-off regions of the dispersion curves.

ACKNOWLEDGMENTS

I would like to express my sincere thanks to my advisory committee of Gary Baum and Chuck Habeger for their assistance and counsel throughout the course of this work. I also wish to thank Fred Ahrens, who, until recently, was also a member of my committee. These three gentlemen made this work both interesting and enjoyable.

I would also like to thank The Institute of Paper Chemistry and its member companies for their support of this research. I wish to thank all of the faculty, staff, and students of The Institute of Paper Chemistry for their camaraderie. friendship, and help.

I would like to thank my parents, Walter and Doris, for their support, their love, and their encouragement to continue my education.

I especially wish to thank my wife Ronda for all of her help and support. Without her faith and love, this work would never have been possible.

LITERATURE CITED

1. Carlin, B., Ultrasonics, New York, McGraw-Hill, 1949.

2. Mann, R. W. Elastic wave propagation in paper. Doctoral Dissertation, Appleton, Wisconsin, The Institute of Paper Chemistry, 1978. 171 p.

3. Mann, R. W.; Baum, G. A.; Habeger, C. C., Tappi 62(8):115-18(1979).

4. Mann, R. W.; Baum, G. A.; Habeger, C. C., Tappi 63(2):163-6(1980).

5. Craver, J. K.; Taylor, D. L., Tappi 48(3):142-7(1965).

6. Taylor, D. L.; Craver, J. K., In Bolam's Consolidation of the Paper Web. Vol. 2, p. 852-72. London, Technical Section of the British Paper and Board Makers' Association, 1966.

7. Baum, G. A.; Bornhoeft, L. R., Tappi 62(5):87-90(1979).

8. Luukkala, M.; Heikkila, P.; Surakka, J., Ultrasonics 9(3):201-8(1971).

9. Baum, G. A.; Habeger, C. C., Tappi 63(7):63-6(1980).

10. Habeger, C. C.; Mann, R. W.; Baum, G. A., Ultrasonics 17:57-61(May, 1979).

11. Shepard, W., A-291 Research Topic. Appleton, Wisconsin, The Institute of Paper Chemistry, 1980.

12. ASTM Standard F 89-68, Part 21, p. 345-51.

13. Chatterjee, P. K., Tappi 52(4):699-704(1969).

14. Waterhouse, J. The ultimate strength of paper. IPC Technical Paper Series No. 146, Nov., 1984.

15. Papadakis, E. P., Tappi 56(2):74-7(1973).

16. Lu, M. T., Tappi 58(6):80(1975).

17. Fleischman, E. H. An investigation of the elastic and dielectric anisotropy of paper. Doctoral Dissertation, Appleton, Wisconsin, The Institute of Paper Chemistry, 1981. 155 p.

18. Solie, L. P.; Auld, B. A., J. Acoust. Soc. Am. 54:50(1973).

19. Kolsky, H. Stress waves in solids. Oxford, Clarendon Press, 1953.

20. Popov, E. P. Introduction to mechanics of solids. Englewood Cliffs, New Jersey, Prentice-Hall, Inc., 1968.

21. Carlsson, L.; Fellers, C., Fiber Sci. Technol. 13(3):213(1980).

22. The Institute of Paper Chemistry, Testing-Stiffness, Project 1108-4, Report Two, 1955.

23. TAPPI Standard Method T 535 pm-79.

24. The Institute of Paper Chemistry, Testing-Stiffness, Project 1108-4, Report Four, 1959.

25. Baum, G. A., The Institute of Paper Chemistry, personal communication.

26. Gray, D. W., American Institute of Physics Handbook, McGraw-Hill, Inc., 1957.

27. Baum, G. A. Procedures for measuring the in-plane orthotropic elastic constants of paper using ultrasonic techniques. IPC Technical Paper Series No. 119, Dec., 1981.

28. Habeger, C. C.; Van Zummeren, M. L. A cross-correlation technique for velocity of sound measurements in planar materials, internal memo.

29. The Institute of Paper Chemistry. Ultrasonic velocity measurements in the thickness direction of paper. Project 3467, Report One, Feb., 1984.

30. Jacoby, S. L. S.; Kowalik, J. S.; Pizzo, J. T. Iterative methods for non-linear optimization problems. Englewood Cliffs, New Jersey, Prentice-Hall, Inc., 1972.

31. Hardacker, K. W. The IPC paper thickness gage. IPC Technical Paper Series No. 138, Jan., 1984.

32. Baum, G. A.; Wink, W. A., Tappi 66(9):131(1983).

33. Victorov, I. A. Rayleigh and Lamb waves. New York, Plenum Press, 1967.

34. Habeger, C. C., The Institute of Paper Chemistry, personal communication, 1984.

35. Habeger, C. C.; Whitsitt, W. J., Fiber Sci. Technol. 19:215-39(1983).

APPENDIX I

Appendix I contains the ultrasonic data for all of the single layer and composite sheets. The caliper values presented here were obtained using the IPC rubber platen caliper method.[31] The column labeled "Composition" for the composite sheets gives the single layer sheets used to construct the composite. The "Basis Weight-Orientation" column for the single layers gives the basis weight and orientation levels for the sheet. Further information regarding sheet construction appears in Tables 1 and 2.

The 1182 Series of Samples

Single Layer Sheets

Sample	Basis Weight, g/m^2	Caliper, μm	Density, g/cm^3
G1	195.0	255.1	0.764
G2	427.0	552.2	0.773
G3	205.0	288.0	0.712
G4	422.0	579.6	0.728
S1	259.0	277.1	0.935
S2	523.0	480.1	1.089
S3	208.0	263.9	0.788
S4	430.0	411.0	1.046

Two Layer Samples

		Composite Values			Calculated from Layer Values		
Sample	Composition	Basis Weight, g/m^2	Caliper μm	Density g/cm^3	Basis Weight, g/m^2	Caliper, μm	Density g/cm^3
GS1	G1S1	456.0	496.7	0.918	454.0	532.2	0.853
GS2	G2S1	683.0	775.5	0.881	686.0	829.3	0.827
GS3	G3S1	463.0	524.0	0.884	464.0	565.1	0.821
GS4	G4S1	687.0	839.8	0.818	681.0	856.7	0.795
GS5	G1S2	705.0	767.5	0.919	718.0	735.2	0.977
GS6	G2S2	932.0	1041.5	0.895	950.0	1032.3	0.920
GS7	G3S2	714.0	770.0	0.927	728.0	768.1	0.948
GS8	G4S2	936.0	1107.5	0.845	945.0	1059.7	0.892
GS9	G1S3	396.0	448.3	0.883	403.0	519.0	0.776
GS10	G2S3	623.0	724.5	0.860	635.0	816.1	0.778
GS11	G3S3	405.0	478.1	0.847	413.0	551.9	0.748
GS12	G4S3	627.0	767.8	0.817	630.0	843.5	0.747
GS13	G1S4	620.0	671.2	0.924	625.0	666.1	0.938
GS14	G2S4	847.0	960.2	0.882	857.0	963.2	0.890
GS15	G3S4	629.0	701.4	0.897	635.0	699.0	0.908
GS16	G4S4	851.0	992.5	0.857	852.0	990.6	0.860

Ultrasonic Velocities for the 1182 Series of Two Layer Samples

Single Layer Sheets - all velocities in km/sec

Sample	Basis Weight Orientation	V_{LX}	V_{LY}	V_{LZ}	V_{SYZ}	V_{SXZ}	V_{SXY}	V_{S45}
G1	BW-OR-	2.864	2.928	0.491	0.481	0.480	1.764	1.759
G2	BW+OR-	2.736	2.851	0.480	0.532	0.525	1.708	1.703
G3	BW-OR+	3.232	2.231	0.431	0.428	0.486	1.624	1.638
G4	BW+OR+	3.140	2.348	0.429	0.482	0.541	1.651	1.659
S1	BW-OR-	3.238	3.226	0.794	0.593	0.598	1.955	1.970
S2	BW+OR-	3.209	3.338	0.823	0.645	0.694	2.011	2.015
S3	BW-OR+	3.986	2.774	0.699	0.478	0.519	2.064	2.035
S4	BW+OR+	3.961	2.896	0.765	0.593	0.648	2.088	2.032

Two Layer Sheets - all velocities in km/sec

Sample	Composition	V_{LX}	V_{LY}	V_{LZ}	V_{SYZ}	V_{SXZ}	V_{SXY}	V_{S45}
GS1	G1S1	3.110	3.180	0.596	0.556	0.564	1.916	1.939
GS2	G2S1	2.894	2.860	0.542	0.537	0.536	1.787	1.800
GS3	G3S1	3.202	2.902	0.539	0.510	0.553	1.890	1.910
GS4	G4S1	3.136	2.731	0.472	0.497	0.551	1.768	1.788
GS5	G1S2	3.032	3.016	0.649	0.606	0.600	1.866	1.879
GS6	G2S2	2.890	2.959	0.602	0.591	0.599	1.777	1.817
GS7	G3S2	3.225	2.989	0.613	0.593	0.643	1.890	1.913
GS8	G4S2	3.105	2.806	0.533	0.558	0.608	1.786	1.808
GS9	G1S3	3.321	2.930	0.567	0.551	0.589	1.979	1.937
GS10	G2S3	3.204	2.814	0.547	0.558	0.579	1.805	1.806
GS11	G3S3	3.512	2.550	0.509	0.486	0.545	1.861	1.806
GS12	G4S3	3.369	2.515	0.474	0.495	0.552	1.752	1.769
GS13	G1S4	3.487	2.923	0.605	0.537	0.567	1.927	1.923
GS14	G2S4	3.187	2.843	0.581	0.567	0.586	1.793	1.824
GS15	G3S4	3.552	2.695	0.579	0.528	0.589	1.896	1.894
GS16	G4S4	3.475	2.582	0.518	0.529	0.594	1.830	1.833

Elastic Stiffnesses for the 1182 Series of Two Layer Samples

Single Layer Sheets - all stiffnesses in GPa

Sample	Basis Weight Orientation	C_{11}	C_{22}	C_{33}	C_{44}	C_{55}	C_{66}	C_{12}
G1	BW-OR-	6.270	6.553	0.184	0.177	0.176	2.379	1.483
G2	BW+OR-	5.788	6.285	0.178	0.219	0.213	2.256	1.543
G3	BW-OR+	7.435	3.543	0.132	0.130	0.168	1.877	0.969
G4	BW+OR+	7.179	4.014	0.134	0.169	0.213	1.985	1.219
S1	BW-OR-	9.800	9.727	0.589	0.329	0.334	3.572	2.509
S2	BW+OR-	11.218	12.138	0.738	0.453	0.525	4.405	2.817
S3	BW-OR+	12.523	6.065	0.385	0.180	0.212	3.358	1.845
S4	BW+OR+	16.415	8.775	0.612	0.368	0.439	4.561	3.050

Two Layer Sheets - all stiffnesses in GPa

Sample	Composition	C_{11}	C_{22}	C_{33}	C_{44}	C_{55}	C_{66}	C_{12}
GS1	G1S1	8.880	9.284	0.326	0.284	0.292	3.370	2.175
GS2	G2S1	7.376	7.204	0.259	0.254	0.253	2.812	1.582
GS3	G3S1	9.059	7.441	0.257	0.230	0.270	3.156	1.737
GS4	G4S1	8.045	6.101	0.182	0.202	0.248	2.557	1.734
GS5	G1S2	8.444	8.356	0.387	0.337	0.331	3.198	1.914
GS6	G2S2	7.474	7.835	0.324	0.313	0.321	2.826	1.742
GS7	G3S2	9.644	8.284	0.348	0.326	0.383	3.312	2.135
GS8	G4S2	8.148	6.654	0.240	0.263	0.312	2.696	1.814
GS9	G1S3	9.742	7.583	0.284	0.268	0.306	3.460	1.927
GS10	G2S3	8.827	6.809	0.257	0.268	0.288	2.802	2.106
GS11	G3S3	10.448	5.508	0.219	0.200	0.252	2.934	1.853
GS12	G4S3	9.269	5.165	0.183	0.200	0.249	2.507	1.625
GS13	G1S4	11.232	7.892	0.338	0.266	0.297	3.430	2.500
GS14	G2S4	8.960	7.130	0.298	0.284	0.303	2.836	2.091
GS15	G3S4	11.314	6.513	0.301	0.250	0.311	3.224	1.950
GS16	G4S4	10.354	5.716	0.230	0.240	0.303	2.871	1.721

The 883 Series of Samples

Single Layer Sheets

Sample	Basis Weight, g/m^2	Caliper, μm	Density, g/cm^3
T1	113.0	222.8	0.507
T2	121.0	221.7	0.546
T3	246.0	453.8	0.542
T4	252.0	445.0	0.566
K1	115.0	156.5	0.735
K2	118.0	157.9	0.747
K3	233.0	310.3	0.715
K4	248.0	315.8	0.785

Three Layer Samples

		Composite Values			Calculated from Layer Values		
Sample	Composition	Basis Weight, g/m^2	Caliper μm	Density g/cm^3	Basis Weight, g/m^2	Caliper, μm	Density g/cm^3
TK1	T3-T3-T3	740.0	1299.1	0.570	738.0	1361.4	0.542
TK2	K3-K3-K3	711.0	914.6	0.777	699.0	930.9	0.751
TK3	T4-K4-T4	749.0	1162.0	0.645	752.0	1205.8	0.624
TK4	K4-T4-K4	738.0	1034.1	0.714	748.0	1076.6	0.695
TK5	T4-K4-K4	764.0	1059.1	0.721	748.0	1076.6	0.695
TK6	K4-T4-T4	752.0	1167.9	0.644	752.0	1205.8	0.624
TK7	K2-2T4-K2	756.0	1166.5	0.648	740.0	1305.8	0.567
TK8	T2-2K4-T2	748.0	1044.9	0.716	738.0	1075.0	0.687
TK9	T3-K4-T4	739.0	1161.4	0.636	746.0	1214.6	0.614
TK10	K3-T4-K4	733.0	1037.4	0.707	733.0	1071.1	0.684
TK11	T4-K3-K4	739.0	1049.1	0.704	733.0	1071.1	0.684
TK12	K4-T3-T4	728.0	1163.6	0.626	746.0	1214.6	0.614
TK13	2T2-2K2-2T2	732.0	1133.2	0.646	720.0	1202.6	0.599
TK14	6T1	688.0	1245.9	0.552	678.0	1336.8	0.507
TK15	6K1	695.0	891.1	0.780	690.0	939.0	0.735
TK16	2T2-K3-2T2	739.0	1126.4	0.656	717.0	1197.1	0.599
TK17	2K2-T3-2K2	724.0	1032.6	0.701	718.0	1085.4	0.662
TK18	2K2-2T2-2K2	733.0	1015.5	0.722	714.0	1075.0	0.664

Ultrasonic Velocities for the 883 Series of Three Layer Samples

Single Layer Sheets - all velocities in km/sec

Sample	Basis Weight Orientation	V_{LX}	V_{LY}	V_{LZ}	V_{SYZ}	V_{SXZ}	V_{SXY}	V_{S45}
T1	BW-OR-	2.914	2.846	0.314	0.604	0.630	1.717	1.697
T2	BW-OR+	3.451	2.276	0.343	0.588	0.788	1.680	1.678
T3	BW+OR-	2.996	2.749	0.322	0.540	0.564	1.761	1.742
T4	BW+OR+	3.315	2.401	0.353	0.508	0.616	1.704	1.727
K1	BW-OR-	3.063	2.972	0.585	0.709	0.675	1.805	1.800
K2	BW-OR+	3.461	2.616	0.603	0.614	0.666	1.805	1.793
K3	BW+OR-	3.227	2.946	0.614	0.605	0.640	1.847	1.866
K4	BW+OR+	3.457	2.730	0.630	0.582	0.670	1.849	1.835

Three Layer Sheets - all velocities in km/sec

Sample	Composition	V_{LX}	V_{LY}	V_{LZ}	V_{SYZ}	V_{SXZ}	V_{SXY}	V_{S45}
TK1	T3-T3-T3	2.746	2.984	0.333	0.534	0.504	1.729	1.724
TK2	K3-K3-K3	3.121	2.952	0.654	0.627	0.696	1.799	1.801
TK3	T4-K4-T4	2.775	3.253	0.411	0.619	0.522	1.717	1.773
TK4	K4-T4-K4	3.113	2.983	0.498	0.609	0.604	1.805	1.848
TK5	T4-K4-K4	3.026	2.806	0.499	0.639	0.620	1.797	1.797
TK6	K4-T4-T4	2.747	3.185	0.407	0.597	0.535	1.770	1.835
TK7	K2-2T4-K2	2.726	3.041	0.413	0.403	0.546	1.740	1.810
TK8	T2-2K4-T2	3.119	2.741	0.499	0.638	0.605	1.810	1.826
TK9	T3-K4-T4	2.880	2.915	0.409	0.604	0.560	1.778	1.811
TK10	K3-T4-K4	3.069	3.025	0.492	0.609	0.604	1.717	1.810
TK11	T4-K3-K4	2.958	2.964	0.492	0.626	0.600	1.798	1.845
TK12	K4-T3-T4	2.893	2.943	0.390	0.562	0.536	1.771	1.824
TK13	2T2-2K2-2T2	2.772	3.236	0.401	0.605	0.524	1.773	1.838
TK14	6T1	2.706	2.979	0.315	0.498	0.486	1.765	1.752
TK15	6K1	3.254	3.001	0.637	0.637	0.661	1.853	1.884
TK16	2T2-K3-2T2	2.644	3.353	0.407	0.607	0.533	1.768	1.824
TK17	2K2-T3-2K2	3.235	2.773	0.463	0.573	0.611	1.838	1.813
TK18	2K2-2T2-2K2	3.151	2.993	0.484	0.602	0.577	1.835	1.819

Elastic Stiffnesses for the 883 Series of Three Layer Samples

Single Layer Sheets - all stiffnesses in GPa

Sample	Basis Weight Orientation	C_{11}	C_{22}	C_{33}	C_{44}	C_{55}	C_{66}	C_{12}
T1	BW-OR-	4.307	4.103	0.050	0.185	0.201	1.495	1.284
T2	BW-OR+	6.500	2.827	0.064	0.189	0.339	1.540	0.995
T3	BW+OR-	4.866	4.097	0.056	0.158	0.172	1.681	1.165
T4	BW+OR+	6.223	3.265	0.071	0.146	0.215	1.644	0.977
K1	BW-OR-	6.894	6.491	0.251	0.369	0.335	2.394	1.926
K2	BW-OR+	8.925	5.114	0.272	0.282	0.331	2.435	1.815
K3	BW+OR-	7.450	6.209	0.270	0.262	0.293	2.441	1.892
K4	BW+OR+	9.385	5.853	0.312	0.266	0.353	2.685	2.009

Three Layer Sheets - all stiffnesses in GPa

Sample	Composition	C_{11}	C_{22}	C_{33}	C_{44}	C_{55}	C_{66}	C_{12}
TK1	T3-T3-T3	4.295	5.072	0.063	0.162	0.145	1.703	1.272
TK2	K3-K3-K3	7.572	6.774	0.333	0.306	0.377	2.516	2.113
TK3	T4-K4-T4	4.964	6.821	0.109	0.247	0.176	1.900	1.722
TK4	K4-T4-K4	6.916	6.350	0.177	0.265	0.260	2.325	1.749
TK5	T4-K4-K4	6.605	5.608	0.180	0.295	0.277	2.329	1.455
TK6	K4-T4-T4	4.859	6.532	0.107	0.229	0.184	2.017	1.254
TK7	K2-2T4-K2	4.816	5.993	0.111	0.105	0.193	1.962	1.102
TK8	T2-2K4-T2	6.964	5.378	0.178	0.291	0.262	2.345	1.312
TK9	T3-K4-T4	5.278	5.407	0.106	0.232	0.200	2.012	1.168
TK10	K3-T4-K4	6.655	6.466	0.171	0.262	0.258	2.282	1.930
TK11	T4-K3-K4	6.163	6.188	0.171	0.276	0.254	2.277	1.380
TK12	K4-T3-T4	5.236	5.419	0.095	0.198	0.180	1.962	1.163
TK13	2T2-2K2-2T2	4.964	6.764	0.104	0.236	0.177	2.031	1.383
TK14	6T1	4.044	4.901	0.055	0.137	0.130	1.720	1.049
TK15	6K1	8.258	7.024	0.316	0.316	0.341	2.678	2.065
TK16	2T2-K3-2T2	4.586	7.376	0.109	0.242	0.186	2.051	1.340
TK17	2K2-T3-2K2	7.338	5.391	0.150	0.230	0.262	2.369	1.639
TK18	2K2-2T2-2K2	7.167	6.466	0.169	0.262	0.240	2.431	2.026

APPENDIX II

Appendix II contains the tensile strength, STFI compressive strength, Taber stiffness, and four point bending stiffness data for the single layers and composites.

Tensile Strength Data for the 1182 Series of Samples

Single Layer Sheets

	MD				CD			
Sample	Mod. GPa	TS, nm/g	TEA, kL/m^2	Elong., %	Mod. GPa	TS, nm/g	TEA, kJ/m^2	Elong., %
G1	1.654	40.17	1.268	2.721	1.719	41.26	1.247	2.612
G2	2.055	32.40	2.164	3.266	2.142	33.88	2.274	3.054
G3	1.662	57.45	2.048	2.864	1.263	28.20	1.309	3.290
G4	2.721	48.89	4.219	4.108	1.256	26.92	2.627	3.969
S1	3.777	52.20	3.078	3.071	3.507	52.56	3.257	4.310
S2	3.329	50.48	7.077	3.849	3.598	47.66	6.802	4.740
S3	4.451	91.83	4.871	5.034	1.611	44.71	3.114	4.921
S4	4.489	85.50	10.56	4.402	3.041	45.07	6.506	5.612

Layered Composites

	MD				CD			
Sample	Mod. GPa	TS, nm/g	TEA, kL/m^2	Elong., %	Mod. GPa	TS, nm/g	TEA, kJ/m^2	Elong., %
GS1	3.363	47.81	5.878	4.507	3.005	49.23	5.771	4.792
GS2	2.428	39.83	6.951	4.434	1.491	42.78	9.020	4.428
GS3	3.494	51.42	5.296	3.859	1.612	41.92	5.099	3.830
GS4	2.533	48.39	7.631	3.968	1.628	38.34	7.257	4.028
GS5	2.732	45.91	10.11	4.917	2.454	46.41	10.15	4.406
GS6	2.092	40.33	12.55	5.114	1.915	37.77	13.40	5.271
GS7	2.840	40.60	8.761	4.161	2.112	43.92	11.73	5.240
GS8	2.447	44.40	12.85	4.548	2.571	26.85	5.236	1.619
GS9	3.912	69.29	7.432	5.029	1.742	41.52	4.260	4.042
GS10	2.900	55.14	8.507	4.283	2.084	36.29	2.505	3.517
GS11	3.666	73.43	6.588	3.817	2.244	47.11	5.214	4.263
GS12	2.820	65.15	9.739	3.818	1.306	33.20	6.643	4.574
GS13	3.342	72.14	12.65	4.923	2.299	41.90	7.673	4.755
GS14	2.692	54.55	13.620	4.890	2.321	37.30	8.668	4.215
GS15	3.565	68.49	11.11	3.906	1.976	39.79	8.769	5.455
GS16	3.151	61.23	15.37	4.237	1.775	34.76	9.445	4.965

Tensile Strength Data for the 883 Series of Samples

Single Layer Sheets

Sample	MD Mod. GPa	MD TS, nm/g	MD TEA, kL/m^2	MD Elong., %	CD Mod. GPa	CD TS, nm/g	CD TEA, kJ/m^2	CD Elong., %
T1	--	45.43	0.747	2.312	--	47.73	0.783	2.298
T2	1.879	62.09	0.975	2.234	1.579	28.82	0.498	2.055
T3	1.523	44.15	1.833	3.343	1.187	40.27	1.546	2.616
T4	2.404	63.33	2.442	3.300	1.088	33.70	1.531	2.875
K1	2.090	39.71	1.078	3.167	--	37.68	0.963	3.014
K2	2.479	52.20	1.510	3.508	--	26.44	0.656	2.530
K3	1.612	44.78	2.641	3.724	1.717	36.11	1.856	3.184
K4	1.804	50.65	2.967	3.494	1.546	33.17	2.445	4.285

Layered Composites

Sample	MD Mod. GPa	MD TS, nm/g	MD TEA, kL/m^2	MD Elong., %	CD Mod. GPa	CD TS, nm/g	CD TEA, kJ/m^2	CD Elong., %
TK1	1.376	41.01	5.346	3.396	1.681	46.01	6.160	3.477
TK2	2.553	46.39	10.38	4.837	1.980	41.12	7.439	4.100
TK3	1.746	40.55	6.997	3.981	2.147	53.64	8.030	3.654
TK4	2.310	50.71	10.98	4.830	2.067	44.53	7.317	3.914
TK5	2.094	47.47	10.84	4.777	1.831	40.10	6.937	3.850
TK6	1.452	40.24	8.483	5.114	1.708	46.81	13.40	5.271
TK7	1.613	40.71	7.485	3.789	2.004	56.68	9.896	4.190
TK8	--	44.39	9.419	4.313	1.926	45.38	7.740	4.055
TK9	1.639	41.86	7.434	4.016	1.860	50.08	6.782	3.529
TK10	2.035	45.80	9.176	4.353	1.934	45.62	7.491	3.712
TK11	2.032	45.04	9.321	4.455	1.872	42.54	7.104	4.027
TK12	1.516	42.54	7.071	3.835	1.731	48.73	7.127	3.643
TK13	1.512	41.84	8.132	4.415	2.086	56.33	7.885	3.508
TK14	1.577	48.50	5.886	3.440	1.343	40.65	5.384	3.509
TK15	2.358	48.95	1.214	5.369	2.043	40.48	8.328	4.440
TK16	1.359	36.36	7.276	4.102	2.292	57.23	8.266	3.724
TK17	2.186	52.70	11.10	4.614	2.060	48.20	7.613	3.959
TK18	2.084	50.50	11.54	4.877	1.875	45.85	7.607	3.768

Breaking Lengths for the 1182 and 883 Series of Samples

Single Layer Sheets

Sample	1182 Series Breaking Length		Sample	883 Series Breaking Length	
	MD, m	CD, m		MD, m	CD, m
G1	4099	4210	T1	4636	4871
G2	3306	3457	T2	6336	2941
G3	5862	2878	T3	4504	4110
G4	4989	2747	T4	6463	3439
S1	5327	5363	K1	4052	3845
S2	5151	4863	K2	5327	2698
S3	9370	4568	K3	4570	3685
S4	8724	4599	K4	5169	3385

Composites

Sample	1182 Series Breaking Length		Sample	883 Series Breaking Length	
	MD, m	CD, m		MD, m	CD, m
GS1	4879	5023	TK1	4185	4695
GS2	4064	4365	TK2	4734	4196
GS3	5247	4289	TK3	4138	5473
GS4	4938	3912	TK4	5174	4544
GS5	4685	4736	TK5	4844	4092
GS6	4115	3854	TK6	4106	4777
GS7	4143	4482	TK7	4154	5784
GS8	4531	2740	TK8	4530	4631
GS9	7070	4237	TK9	4271	5110
GS10	5627	3703	TK10	4673	4655
GS11	7493	4807	TK11	4596	4341
GS12	6648	3388	TK12	4341	4972
GS13	7361	4276	TK13	4269	5748
GS14	5566	3806	TK14	4949	4148
GS15	6989	4060	TK15	4995	4131
GS16	6248	3547	TK16	3710	5840
			TK17	5378	4918
			TK18	5153	4679

Compressive Strength Data for the 1182 Series of Samples

Single Layer Sheets

Sample	Compressive Strength MD, nm/g	Compressive Strength CD, nm/g	Compression Length MD, m	Compression Length CD, m
G1	23.81	18.36	2428	1872
G2	21.02	16.62	2143	1695
G3	28.21	11.82	2877	1205
G4	25.85	12.28	2636	1252
S1	28.40	27.80	2896	2835
S2	29.09	34.12	2966	3479
S3	35.46	19.49	3616	1987
S4	35.17	26.54	3586	2706

Layered Composites

Sample	Compressive Strength MD, nm/g	Compressive Strength CD, nm/g	Compression Length MD, m	Compression Length CD, m
GS1	27.73	29.04	2828	2961
GS2	25.87	26.13	2638	2664
GS3	29.68	25.12	3026	2561
GS4	27.28	22.18	2782	2262
GS5	30.05	29.13	3064	2970
GS6	28.27	27.82	2883	2837
GS7	29.89	27.02	3048	2755
GS8	30.01	27.01	3060	2754
GS9	32.55	25.40	3319	2590
GS10	28.51	24.64	2907	2513
GS11	35.87	21.06	3658	2147
GS12	29.56	20.25	3014	2065
GS13	32.61	25.57	3325	2607
GS14	31.13	23.97	3174	2444
GS15	34.94	23.23	3563	2369
GS16	32.84	21.64	3349	2207

Compressive Strength Data for the 883 Series of Samples

Single Layer Sheets

Sample	Compressive Strength MD, nm/g	Compressive Strength CD, nm/g	Compression Length MD, m	Compression Length CD, m
T1	22.32	20.37	2276	2077
T2	29.20	17.03	2977	1737
T3	21.27	19.53	2169	1991
T4	28.95	16.72	2952	1705
K1	23.93	24.63	2440	2511
K2	28.50	21.62	2906	2205
K3	26.03	25.56	2654	2606
K4	28.69	23.09	2925	2354

Layered Composites

Sample	Compressive Strength MD, nm/g	Compressive Strength CD, nm/g	Compression Length MD, m	Compression Length CD, m
TK1	19.37	21.17	1975	2159
TK2	27.66	24.80	2820	2529
TK3	22.39	25.14	2283	2563
TK4	25.13	25.89	2562	2640
TK5	26.43	22.96	2695	2341
TK6	20.76	26.35	2117	2687
TK7	18.82	22.89	1919	2334
TK8	27.49	27.72	2803	2827
TK9	23.32	23.36	2378	2382
TK10	24.34	25.52	2482	2602
TK11	25.57	24.40	2607	2488
TK12	22.38	22.89	2282	2334
TK13	22.17	25.17	2261	2622
TK14	21.04	19.52	2145	1990
TK15	27.85	26.06	2840	2657
TK16	20.44	26.32	2084	2684
TK17	25.79	21.82	2630	2225
TK18	24.45	25.34	2493	2584

Bending Stiffness Data for the 1182 Series of Samples

Single Layer Sheets - all values in $N\text{-}M^2 \times 10^3$

Sample	Taber Stiffness		Four Point Bending Stiffness	
	MD	CD	MD	CD
G1	0.1320	0.1245	--	--
G2	0.9364	1.011	--	--
G3	0.1545	0.0740	--	--
G4	1.367	0.1002	--	--
S1	0.2004	0.2135	--	--
S2	1.404	1.442	--	--
S3	0.2416	0.1002	--	--
S4	1.367	0.7117	--	--

Two Layer Sheets - all values in $N\text{-}M^2 \times 10^3$

Sample	Taber Stiffness		Four Point Bending Stiffness	
	MD	CD	MD	CD
GS1	1.068	1.086	0.8302	1.083
GS2	3.146	3.184	2.744	3.472
GS3	1.376	0.9645	1.041	1.092
GS4	4.120	3.081	3.756	3.544
GS5	3.109	3.231	2.901	3.281
GS6	5.946	6.368	5.974	7.042
GS7	3.615	2.772	3.203	3.094
GS8	7.660	5.900	7.787	6.863
GS9	0.9458	0.6705	0.8200	0.6276
GS10	3.184	2.350	2.967	2.324
GS11	1.283	0.6546	1.065	0.6728
GS12	4.055	2.247	3.662	2.038
GS13	2.669	2.023	2.321	1.770
GS14	5.881	4.851	5.618	4.698
GS15	3.268	1.807	2.901	1.609
GS16	7.351	4.308	7.323	4.374

Bending Stiffness Data for the 883 Series of Samples

Single Layer Sheets - all values in $N\text{-}M^2 \times 10^3$

Sample	Taber Stiffness		Four Point Bending Stiffness	
	MD	CD	MD	CD
T1	0.0040	0.0039	--	--
T2	0.0057	0.0026	--	--
T3	4.317	3.971	--	--
T4	6.209	3.193	--	--
K1	0.0024	0.0023	--	--
K2	0.0030	0.0018	--	--
K3	2.500	2.154	--	--
K4	3.175	2.013	--	--

Three Layer Sheets - all values in $N\text{-}M^2 \times 10^3$

Sample	Taber Stiffness		Four Point Bending Stiffness	
	MD	CD	MD	CD
TK1	7.014	6.602	8.068	7.674
TK2	4.869	4.289	4.969	4.710
TK3	4.233	7.791	4.456	9.145
TK4	7.537	5.413	8.944	5.960
TK5	5.104	5.235	5.518	5.476
TK6	5.900	7.772	6.888	8.033
TK7	7.492	7.548	9.660	8.126
TK8	4.176	5.806	4.443	6.116
TK9	4.429	7.201	4.879	7.821
TK10	7.098	5.544	8.261	5.920
TK11	5.169	5.338	5.416	5.815
TK12	6.265	7.239	7.121	7.447
TK13	3.961	8.025	4.255	8.591
TK14	5.488	6.826	8.453	5.889
TK15	4.748	4.158	5.303	4.124
TK16	3.774	8.138	4.345	9.038
TK17	7.829	4.766	9.231	4.935
TK18	7.557	4.982	8.772	5.035

APPENDIX III

Appendix III contains the plate wave data and theoretical dispersion curves for the layered composites.

Sample 1182 GS1 MD

	Density, g/cm^3	Caliper, mm	C_{11} GPa	C_{33} GPa	C_{13} GPa	C_{55} GPa
Layer 1	0.764	0.2551	6.297	0.184	0.00003	0.176
Layer 2	0.935	0.2771	9.802	0.589	0.00003	0.334

SUM R2 = 0.0461

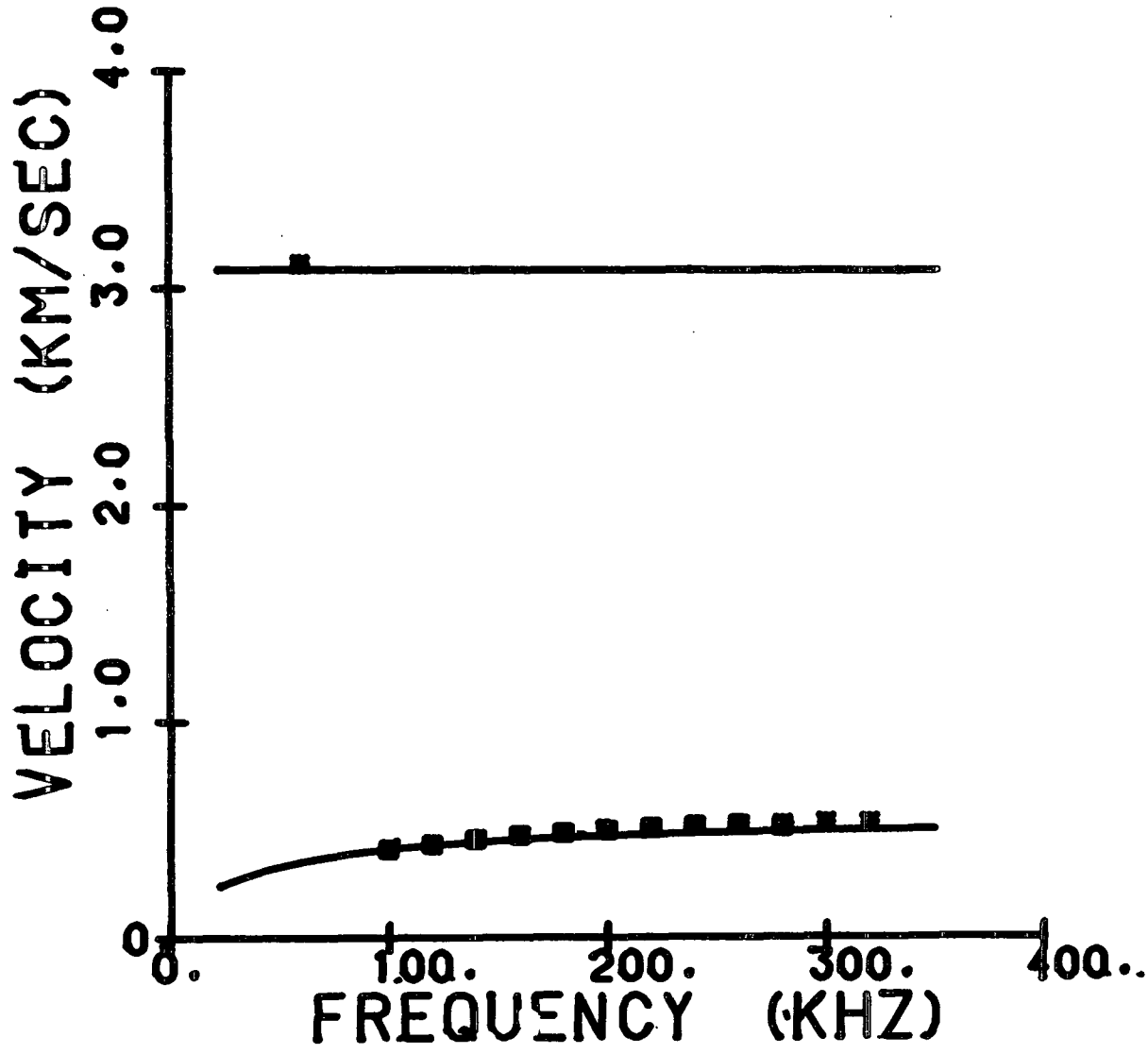

Sample 1182 GS2 MD

	Density, g/cm^3	Caliper, mm	C_{11} GPa	C_{33} GPa	C_{13} GPa	C_{55} GPa
Layer 1	0.773	0.5522	5.817	0.178	0.00003	0.213
Layer 2	0.935	0.2771	9.802	0.589	0.00003	0.334

SUM R2 = 0.0225

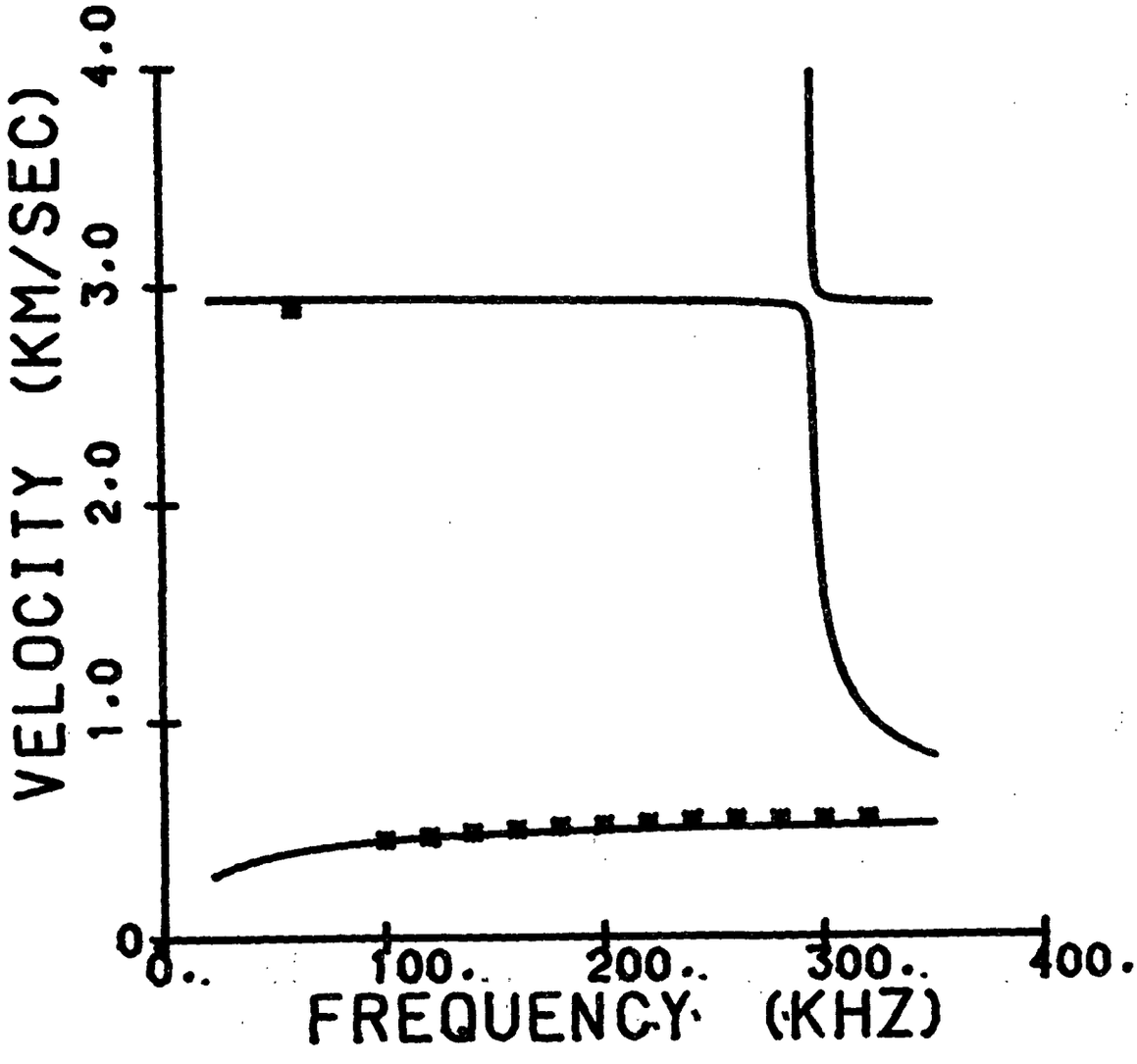

Sample 1182 GS3 MD

	Density, g/cm^3	Caliper, mm	C_{11} GPa	C_{33} GPa	C_{13} GPa	C_{55} GPa
Layer 1	0.712	0.2880	7.487	0.132	0.00003	0.168
Layer 2	0.935	0.2771	9.802	0.589	0.00003	0.334

SUM R2 = 0.0163

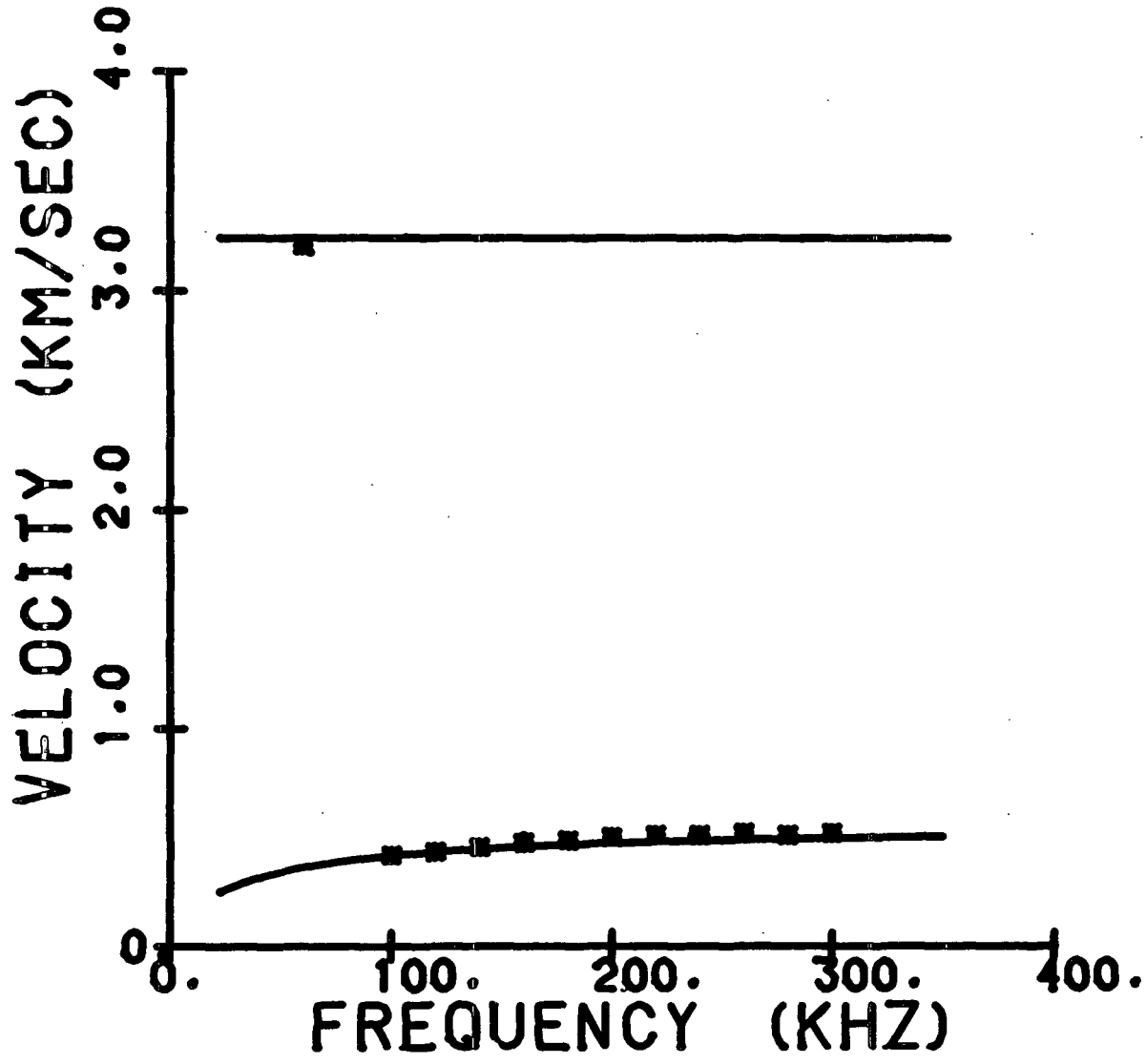

Sample 1182 GS4 MD

	Density, g/cm^3	Caliper, mm	C_{11} GPa	C_{33} GPa	C_{13} GPa	C_{55} GPa
Layer 1	0.728	0.5796	7.229	0.169	0.00003	0.213
Layer 2	0.935	0.2771	9.802	0.589	0.00003	0.334

SUM R2 = 1.2052

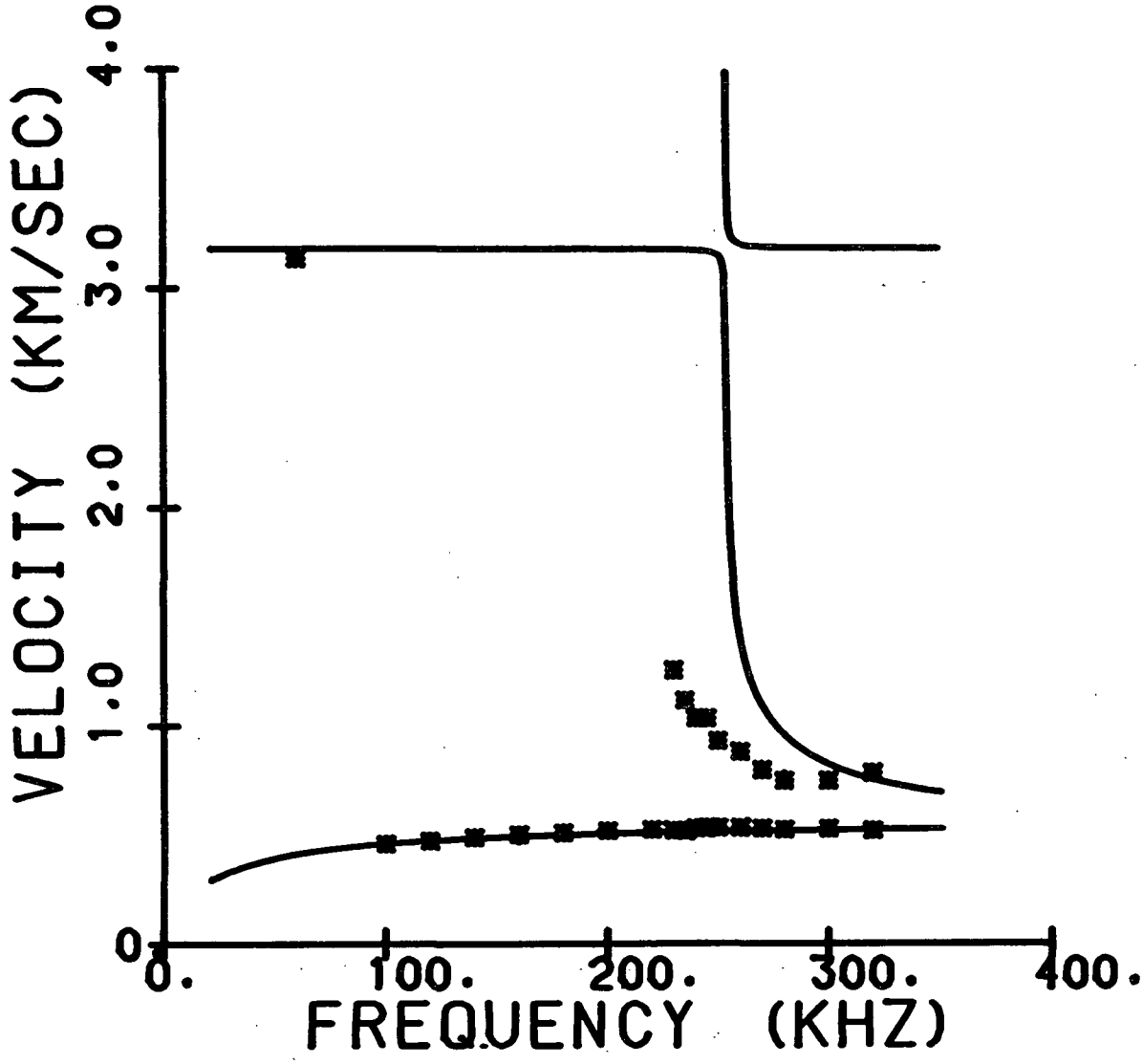

Sample 1182 GS5 MD

	Density, g/cm^3	Caliper, mm	C_{11} GPa	C_{33} GPa	C_{13} GPa	C_{55} GPa
Layer 1	0.764	0.2551	6.297	0.184	0.00003	0.176
Layer 2	1.089	0.4801	11.219	0.738	0.00003	0.525

SUM R2 = 0.0206

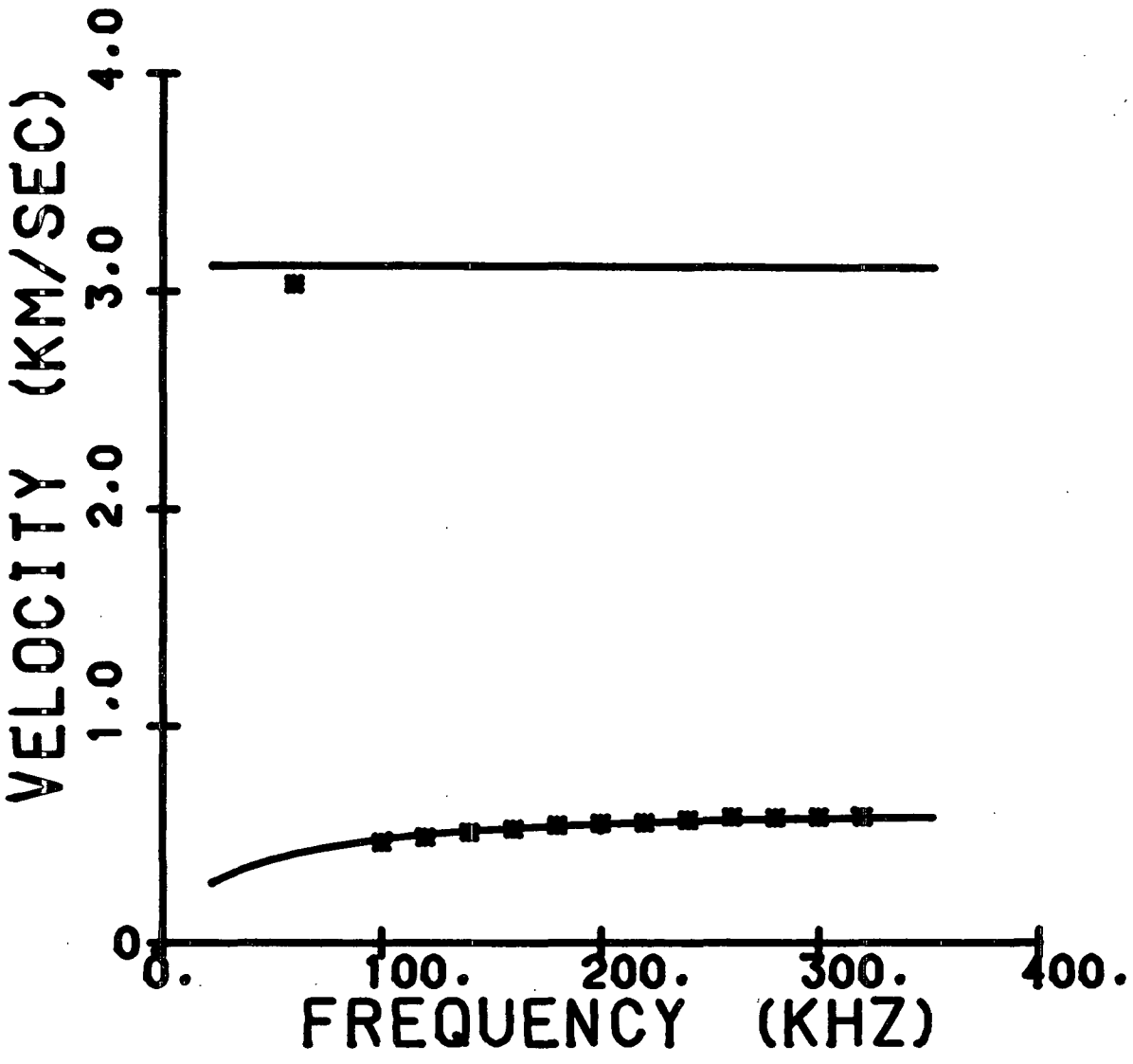

Sample 1182 GS6 MD

	Density, g/cm^3	Caliper, mm	C_{11} GPa	C_{33} GPa	C_{13} GPa	C_{55} GPa
Layer 1	0.773	0.5522	5.817	0.178	0.00003	0.213
Layer 2	1.089	0.4801	11.219	0.738	0.00003	0.525

SUM R2 = 0.3653

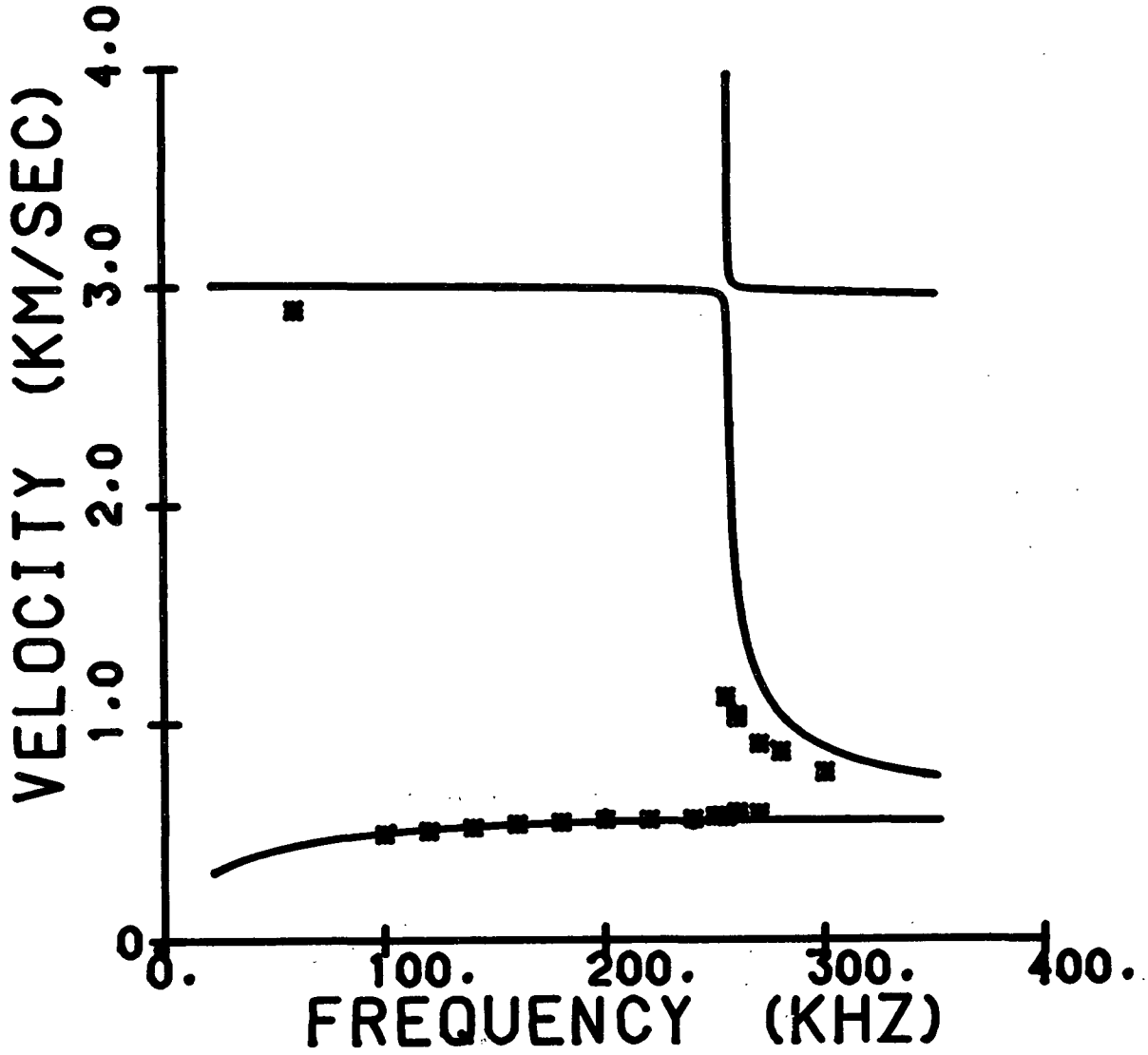

Sample 1182 GS7 MD

	Density, g/cm^3	Caliper, mm	C_{11} GPa	C_{33} GPa	C_{13} GPa	C_{55} GPa
Layer 1	0.712	0.2880	7.487	0.132	0.00003	0.168
Layer 2	1.089	0.4801	11.219	0.738	0.00003	0.525

SUM R2 = 0.0346

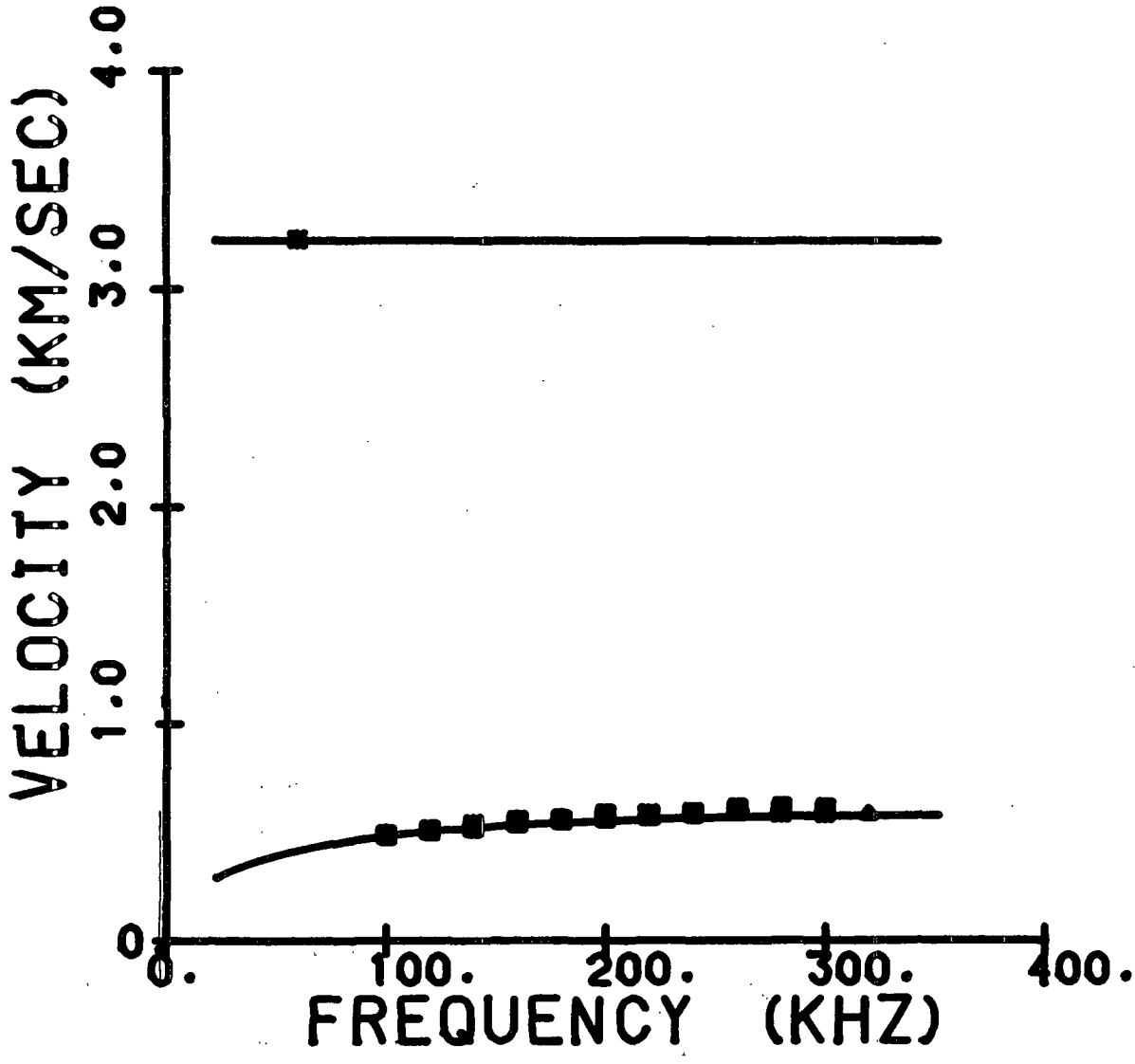

Sample 1182 GS8 MD

	Density, g/cm^3	Caliper, mm	C_{11} GPa	C_{33} GPa	C_{13} GPa	C_{55} GPa
Layer 1	0.728	0.5796	7.229	0.169	0.00003	0.213
Layer 2	1.089	0.4801	11.219	0.738	0.00003	0.525

SUM R2 = 2.9546

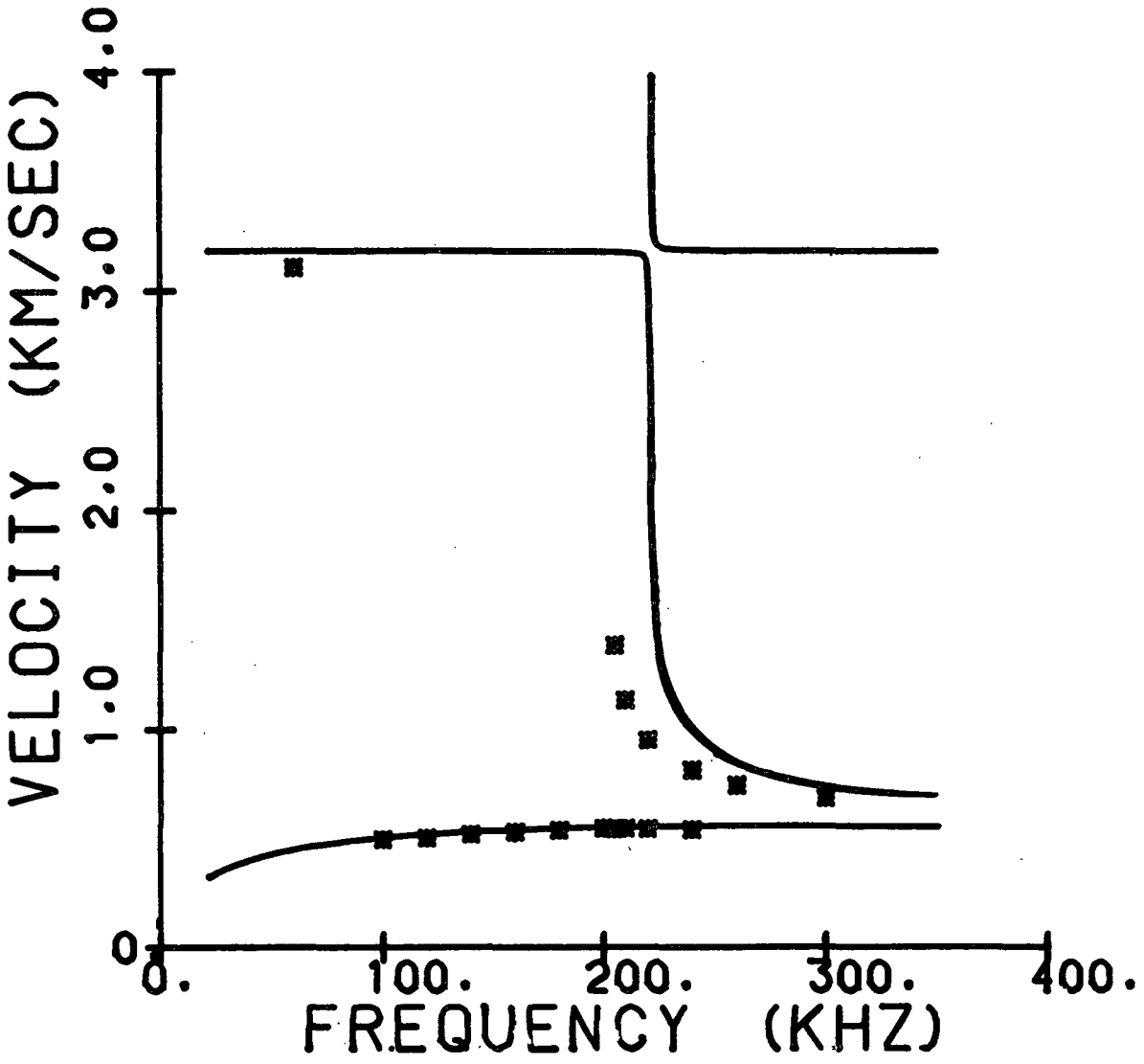

Sample 1182 GS9 MD

	Density, g/cm^3	Caliper, mm	C_{11} GPa	C_{33} GPa	C_{13} GPa	C_{55} GPa
Layer 1	0.764	0.2551	6.297	0.184	0.00003	0.176
Layer 2	0.788	0.2639	12.529	0.385	0.00003	0.212

SUM R2 = 0.1367

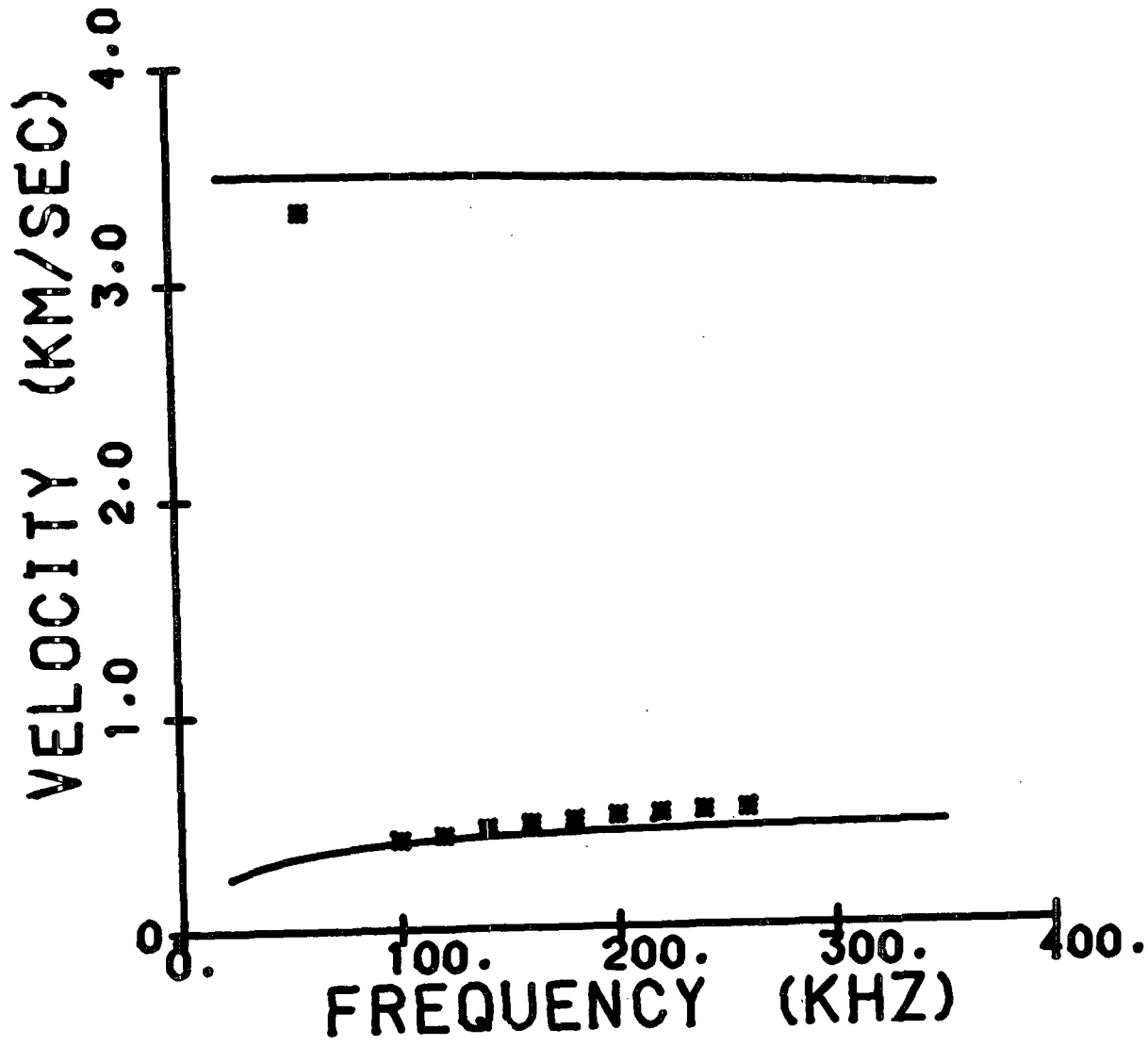

Sample 1182 GS10 MD

	Density, g/cm^3	Caliper, mm	C_{11} GPa	C_{33} GPa	C_{13} GPa	C_{55} GPa
Layer 1	0.773	0.5522	5.817	0.178	0.00003	0.213
Layer 2	0.788	0.2639	12.529	0.385	0.00003	0.212

SUM R2 = 0.2570

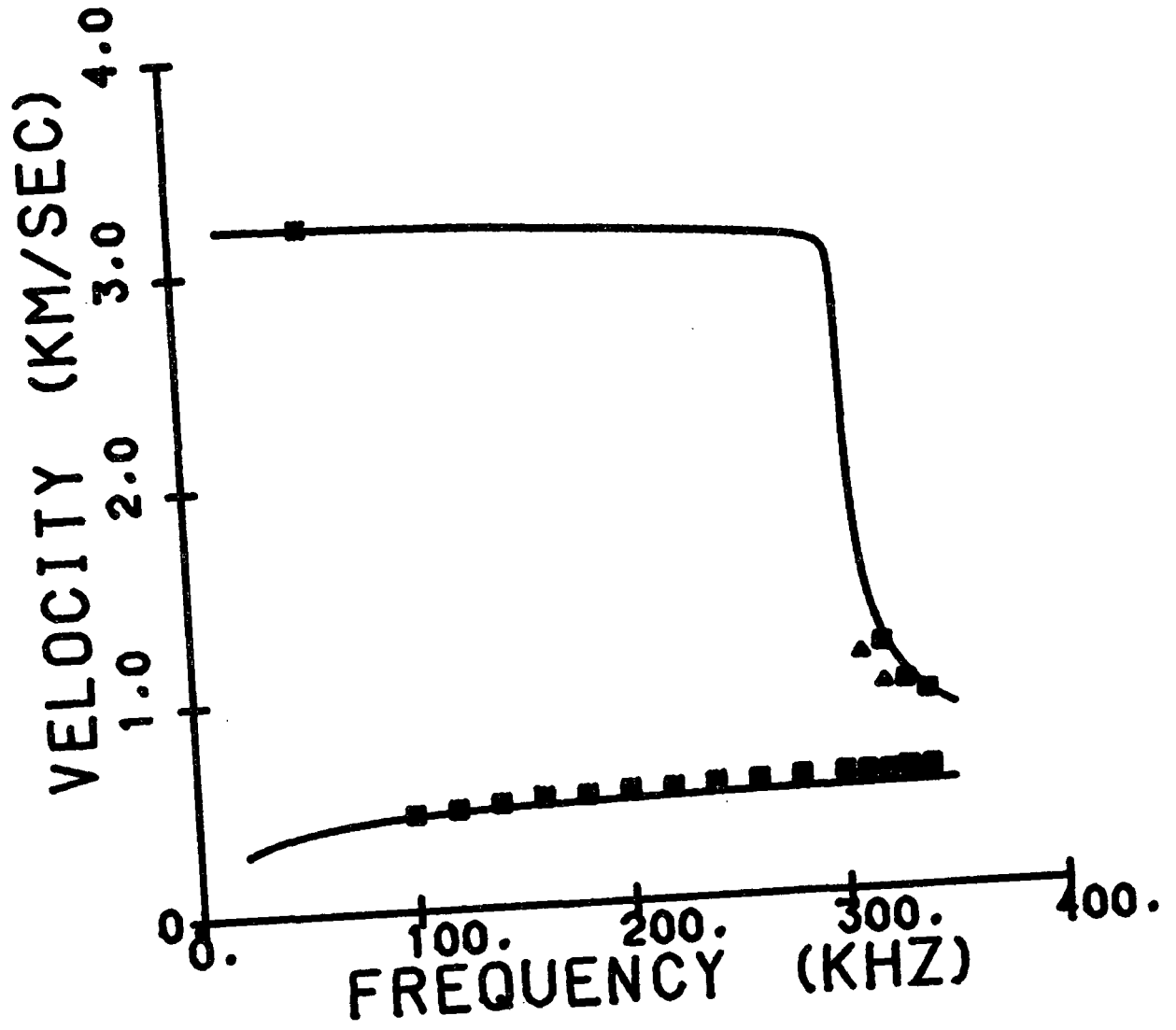

Sample 1182 GS11 MD

	Density, g/cm^3	Caliper, mm	C_{11} GPa	C_{33} GPa	C_{13} GPa	C_{55} GPa
Layer 1	0.712	0.2880	7.487	0.132	0.00003	0.168
Layer 2	0.788	0.2639	12.529	0.385	0.00003	0.212

SUM R2 = 0.1788

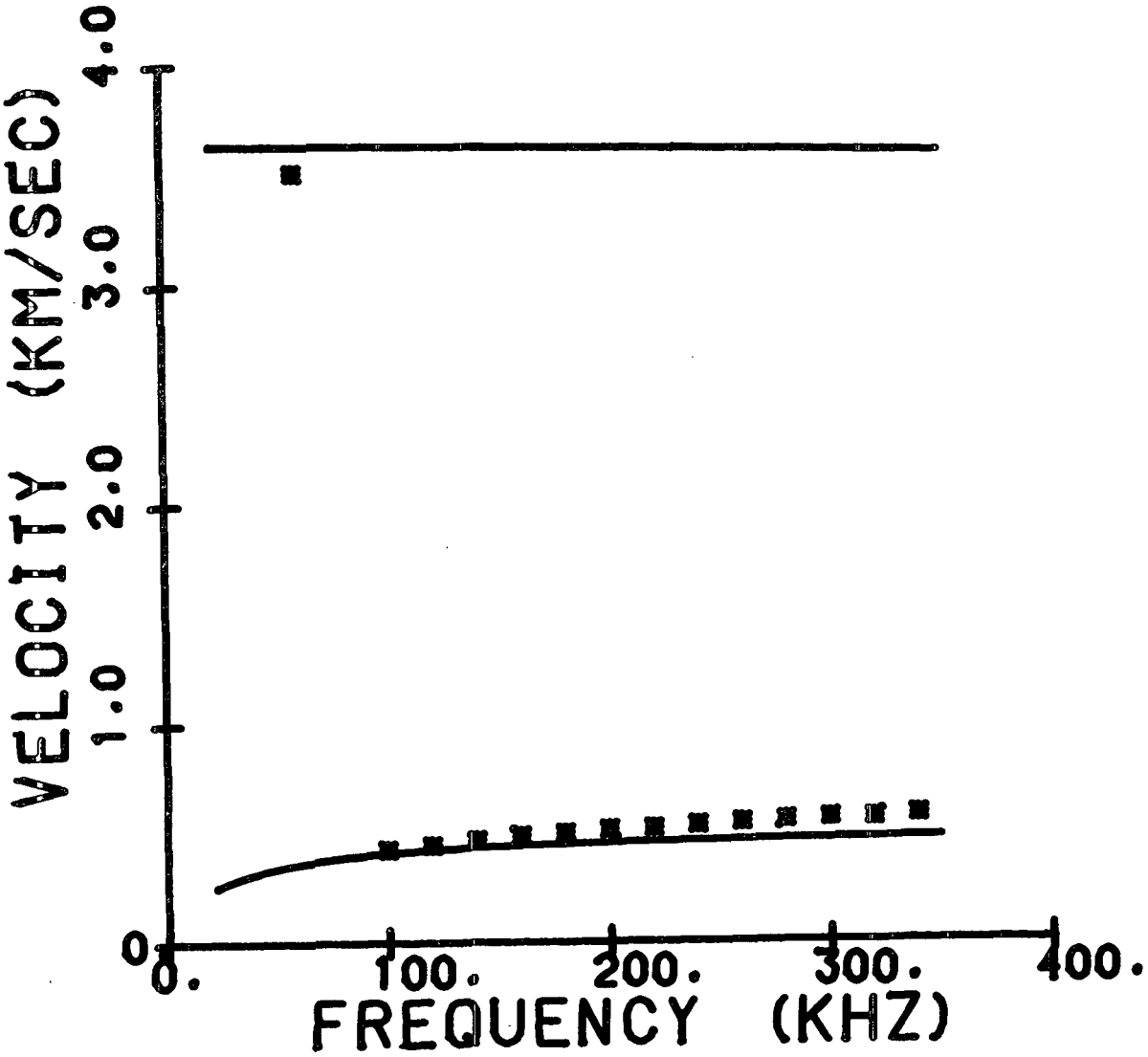

Sample 1182 GS12 MD

	Density, g/cm^3	Caliper, mm	C_{11} GPa	C_{33} GPa	C_{13} GPa	C_{55} GPa
Layer 1	0.728	0.5796	7.229	0.169	0.00003	0.213
Layer 2	0.788	0.2639	12.529	0.385	0.00003	0.212

SUM R2 = 0.1599

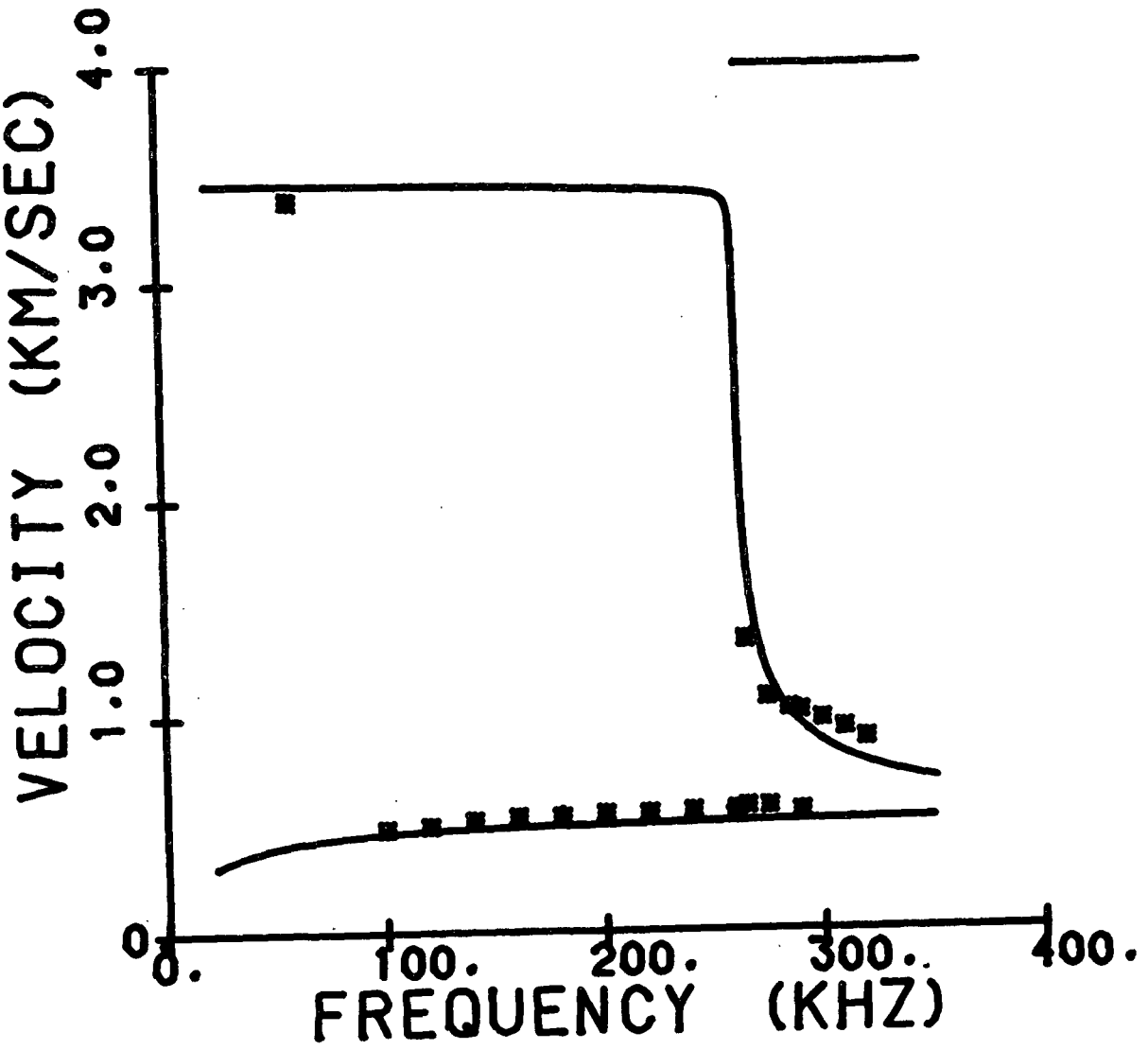

Sample 1182 GS13 MD

	Density, g/cm^3	Caliper, mm	C_{11} GPa	C_{33} GPa	C_{13} GPa	C_{55} GPa
Layer 1	0.764	0.2551	6.297	0.184	0.00003	0.176
Layer 2	10.046	0.9110	16.417	0.612	0.00003	0.439

SUM R2 = 0.0713

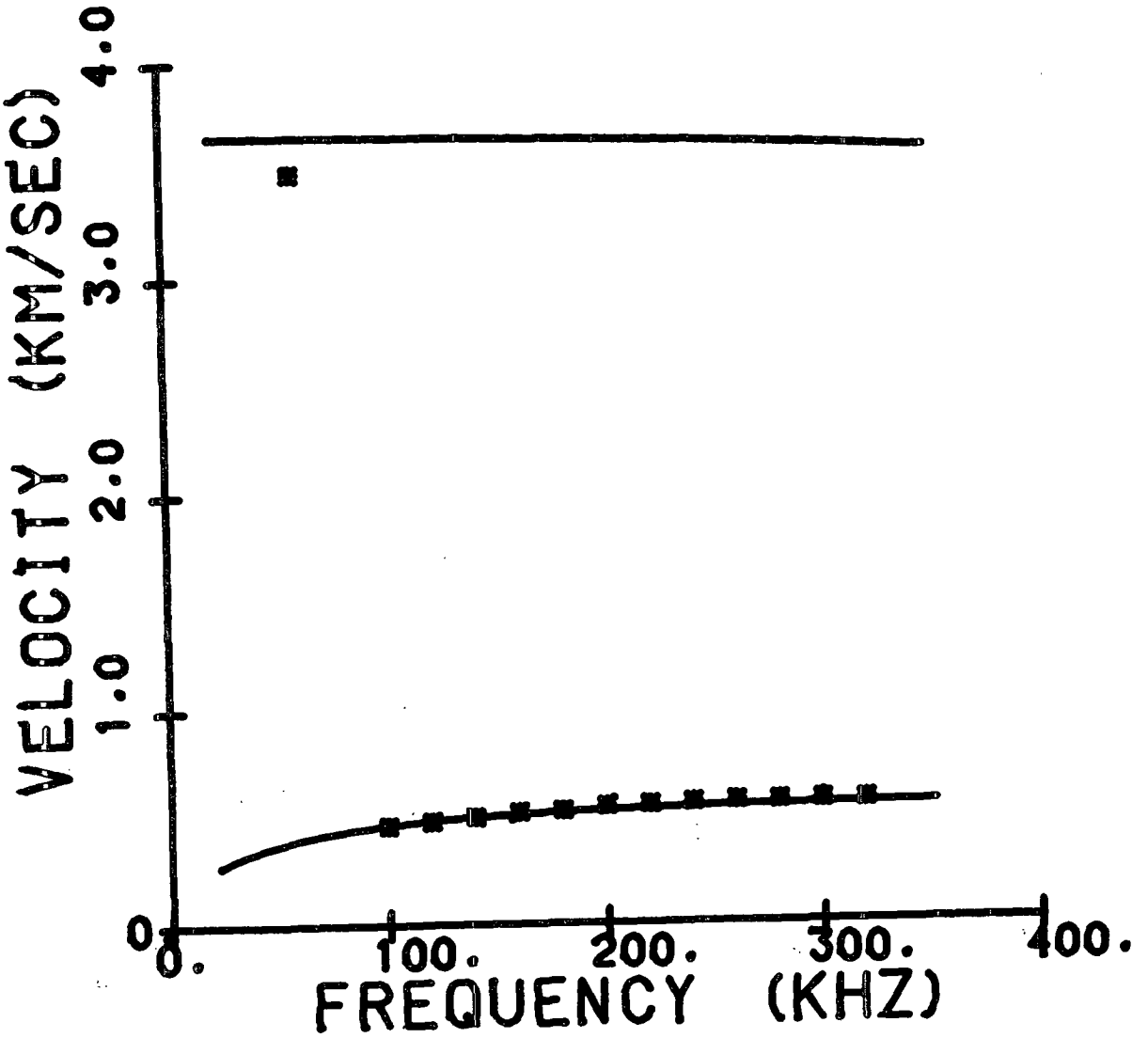

Sample 1182 GS14 MD

	Density, g/cm^3	Caliper, mm	C_{11} GPa	C_{33} GPa	C_{13} GPa	C_{55} GPa
Layer 1	0.773	0.5522	5.817	0.178	0.00003	0.213
Layer 2	10.046	0.9110	16.417	0.612	0.00003	0.439

SUM R2 = 0.4039

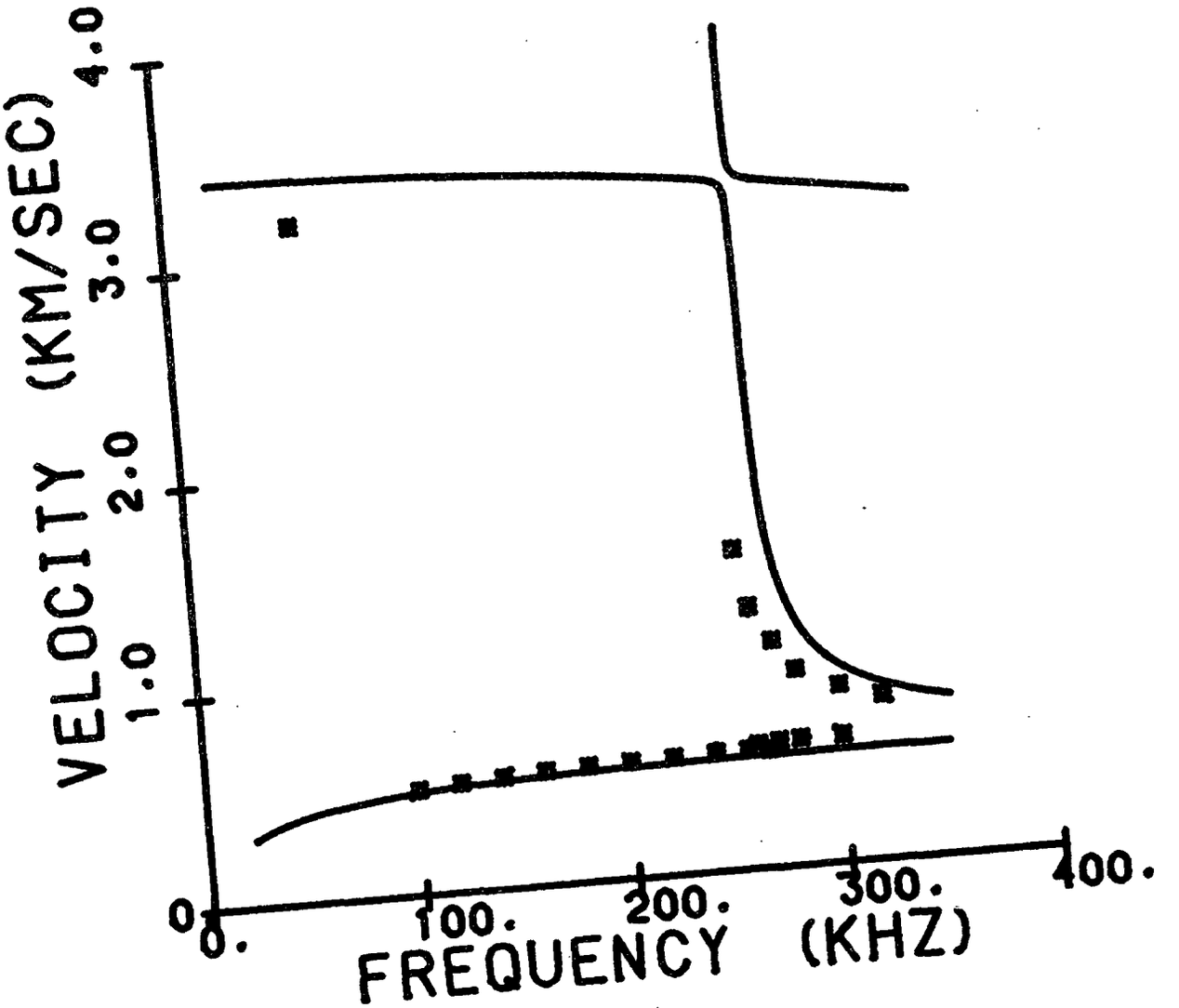

Sample 1182 GS15 MD

	Density, g/cm^3	Caliper, mm	C_{11} GPa	C_{33} GPa	C_{13} GPa	C_{55} GPa
Layer 1	0.712	0.2880	7.487	0.132	0.00003	0.168
Layer 2	10.046	0.9110	16.417	0.612	0.00003	0.439

SUM R2 = 0.1084

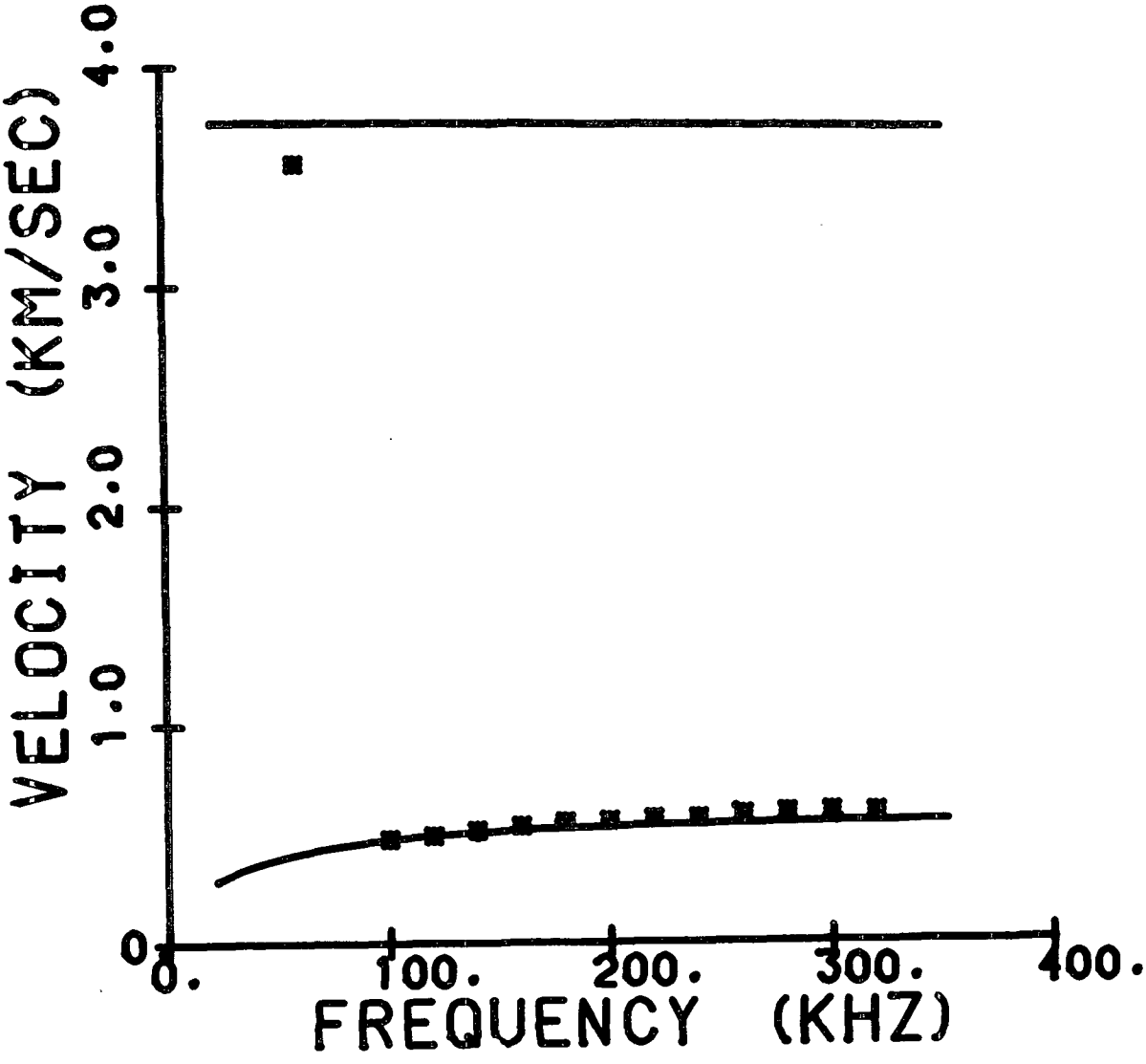

Sample 1182 GS16 MD

	Density, g/cm^3	Caliper, mm	C_{11} GPa	C_{33} GPa	C_{13} GPa	C_{55} GPa
Layer 1	0.728	0.5796	7.229	0.169	0.00003	0.213
Layer 2	10.046	0.9110	16.417	0.612	0.00003	0.439

SUM R2 = 0.3871

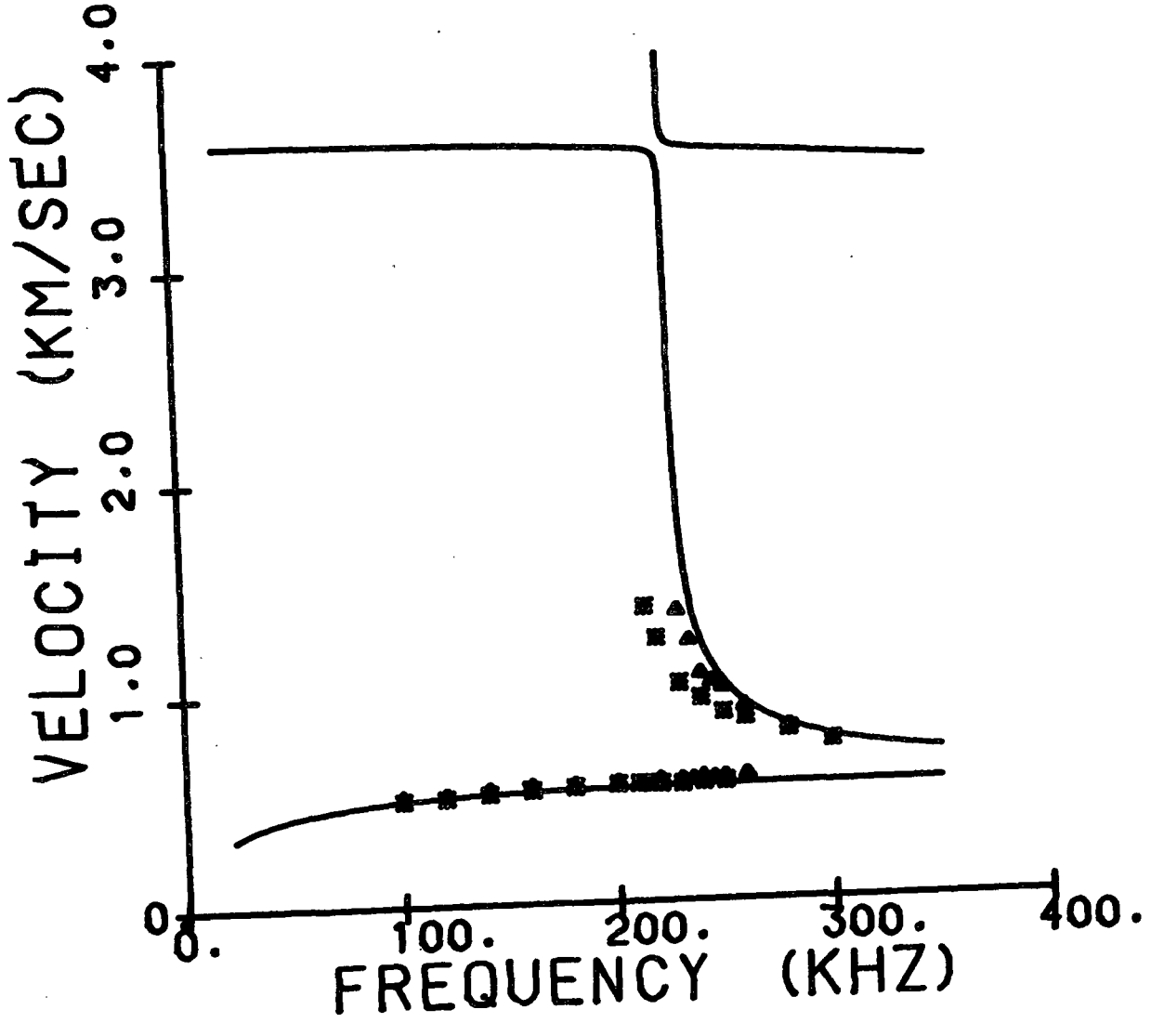

Sample 1182 GS1 CD

	Density, g/cm^3	Caliper, mm	C_{22} GPa	C_{33} GPa	C_{23} GPa	C_{55} GPa
Layer 1	0.764	0.2551	6.580	0.184	0.00003	0.177
Layer 2	0.935	0.2771	9.730	0.589	0.00003	0.329

SUM R2 = 1.1139

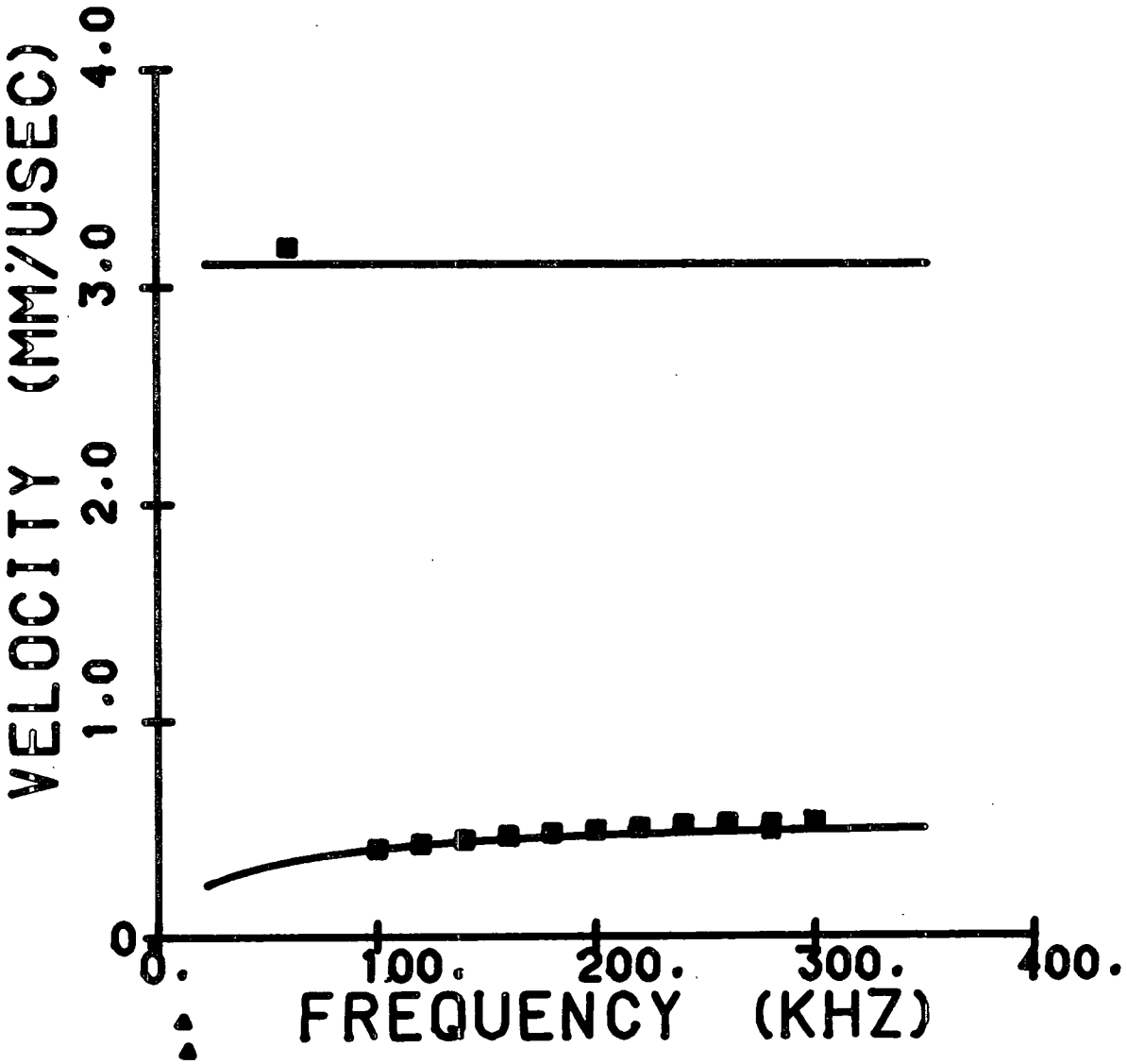

Sample 1182 GS2 CD

	Density, g/cm^3	Caliper, mm	C_{22} GPa	C_{33} GPa	C_{23} GPa	C_{55} GPa
Layer 1	0.773	0.5522	6.314	0.178	0.00003	0.219
Layer 2	0.935	0.2771	9.730	0.589	0.00003	0.329

SUM R2 = 0.0498

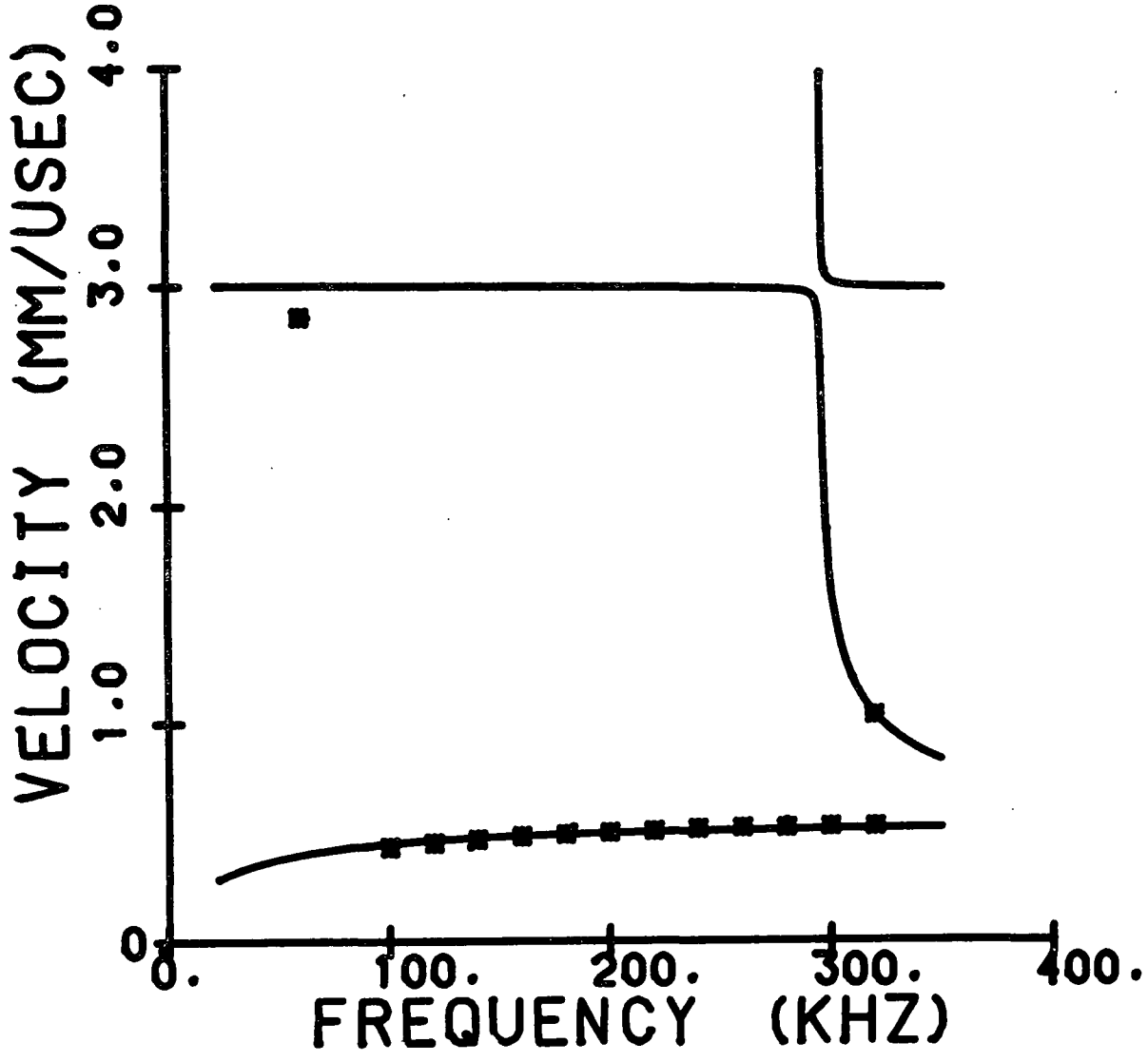

Sample 1182 GS3 CD

	Density, g/cm^3	Caliper, mm	C_{22} GPa	C_{33} GPa	C_{23} GPa	C_{55} GPa
Layer 1	0.712	0.2880	3.594	0.132	0.00003	0.130
Layer 2	0.935	0.2771	9.730	0.589	0.00003	0.329

SUM R2 = 0.0334

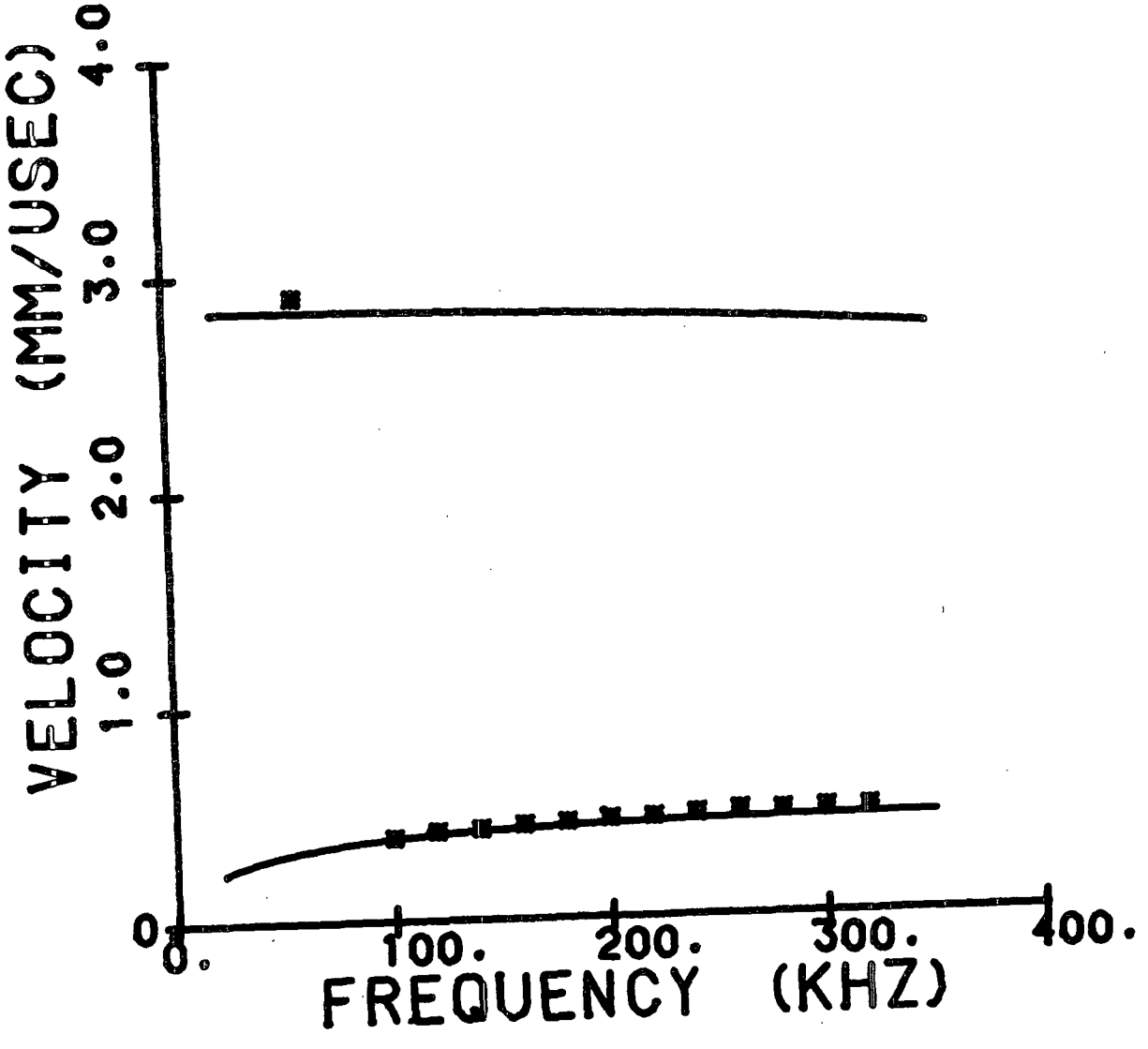

Sample 1182 GS4 CD

	Density, g/cm^3	Caliper, mm	C_{22} GPa	C_{33} GPa	C_{23} GPa	C_{55} GPa
Layer 1	0.728	0.5796	4.064	0.169	0.00003	0.169
Layer 2	0.935	0.2771	9.730	0.589	0.00003	0.329

SUM R2 = 1.3708

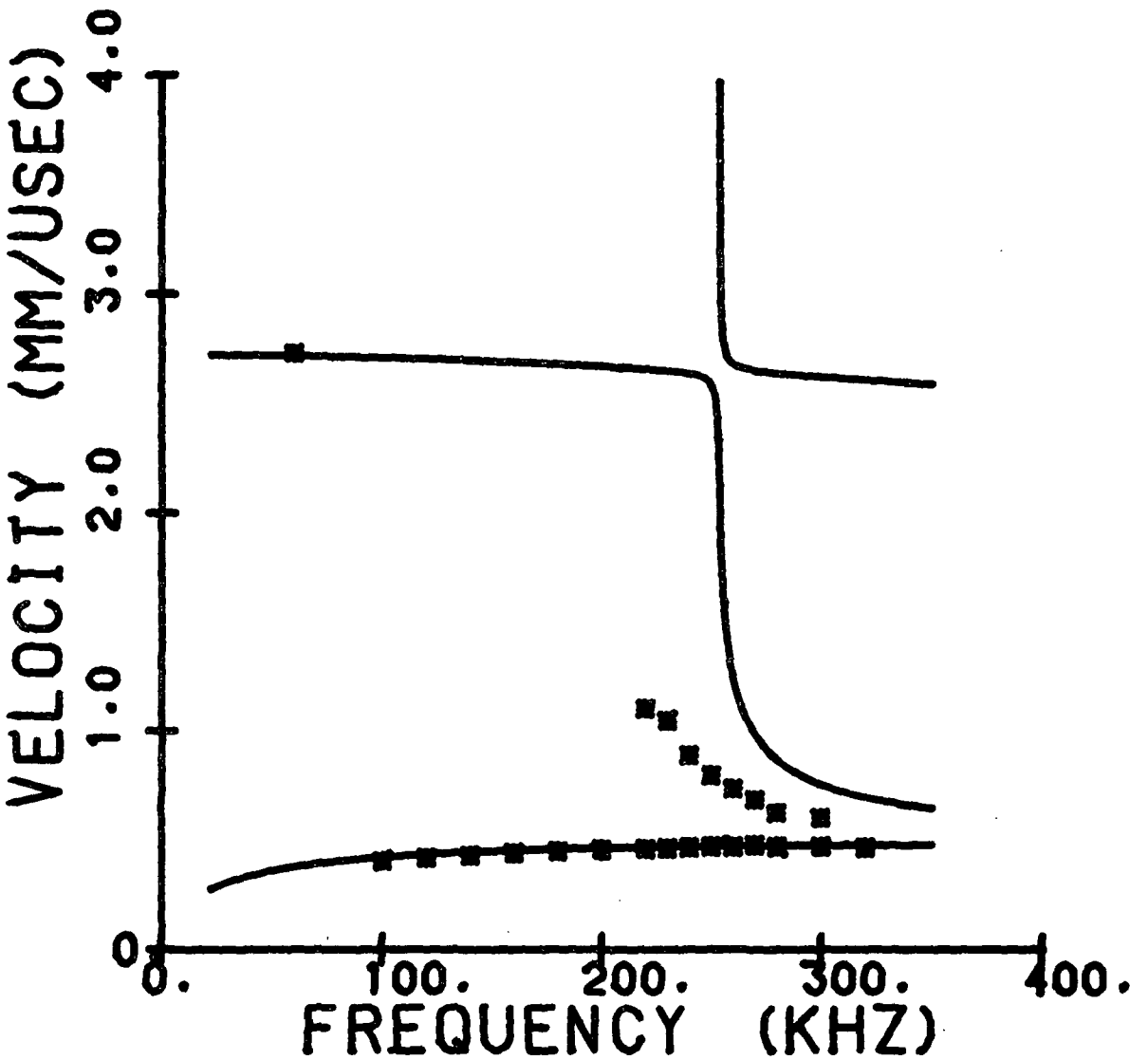

Sample 1182 GS5 CD

	Density, g/cm^3	Caliper, mm	C_{22} GPa	C_{33} GPa	C_{23} GPa	C_{55} GPa
Layer 1	0.764	0.2551	6.580	0.184	0.00003	0.177
Layer 2	1.089	0.4801	12.140	0.738	0.00003	0.453

SUM R2 = 0.3288

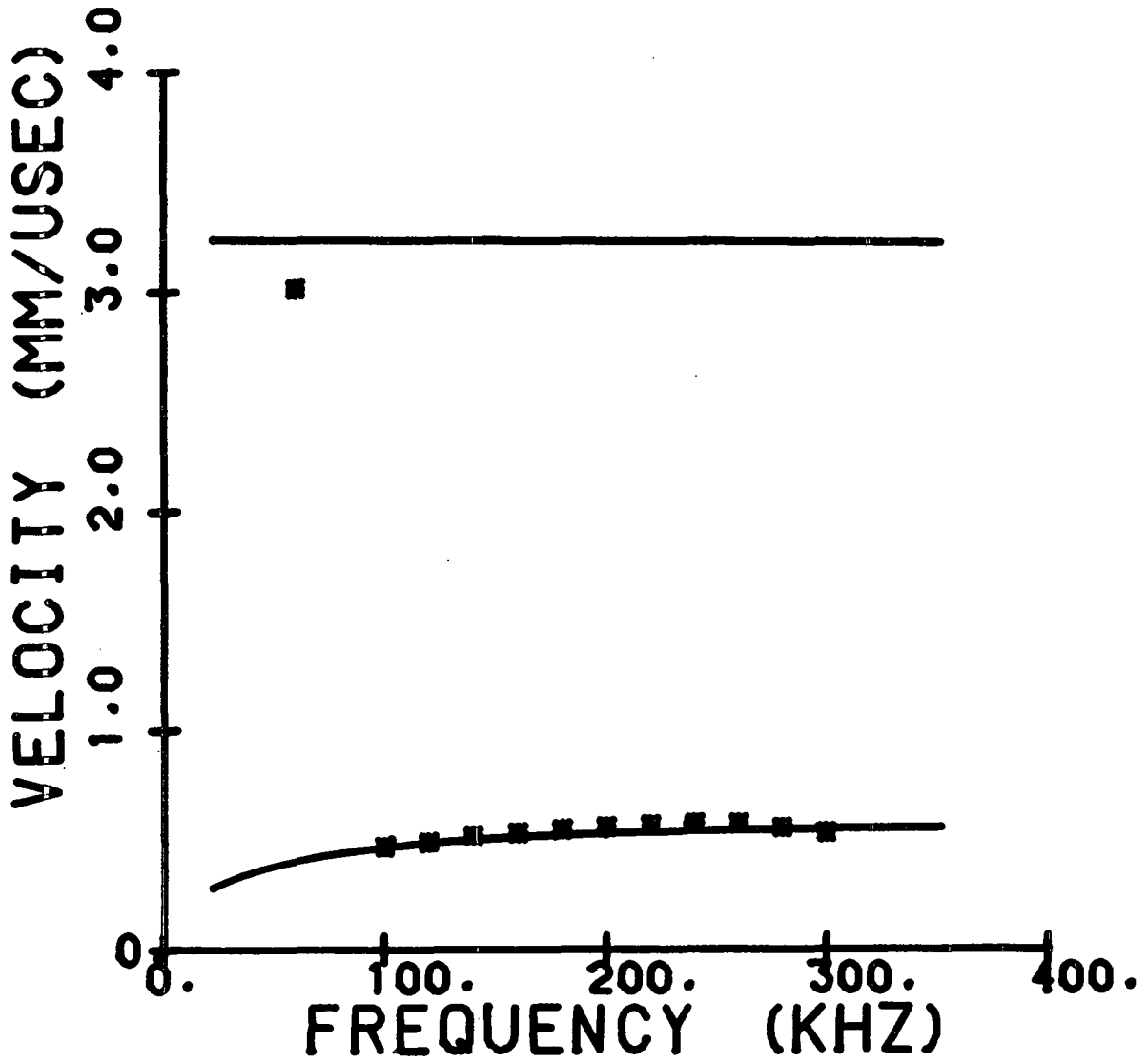

Sample 1182 GS6 CD

	Density, g/cm^3	Caliper, mm	C_{22} GPa	C_{33} GPa	C_{23} GPa	C_{55} GPa
Layer 1	0.773	0.5522	6.314	0.178	0.00003	0.219
Layer 2	1.089	0.4801	12.140	0.738	0.00003	0.453

SUM R2 = 0.2603

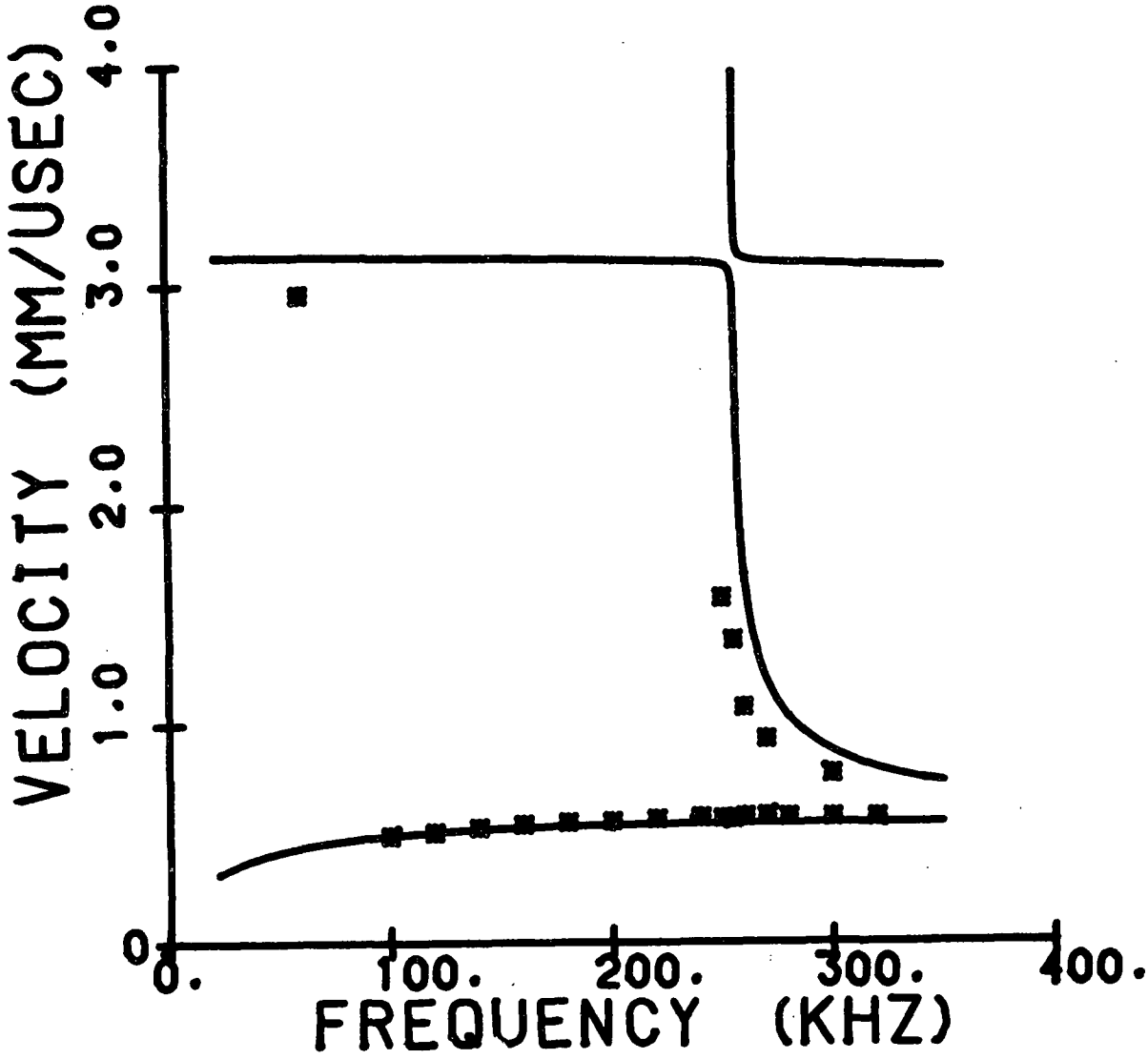

Sample 1182 GS7 CD

	Density, g/cm^3	Caliper, mm	C_{22} GPa	C_{33} GPa	C_{23} GPa	C_{55} GPa
Layer 1	0.712	0.2880	3.594	0.132	0.00003	0.130
Layer 2	1.089	0.4801	12.140	0.738	0.00003	0.453

SUM R2 = 1.4025

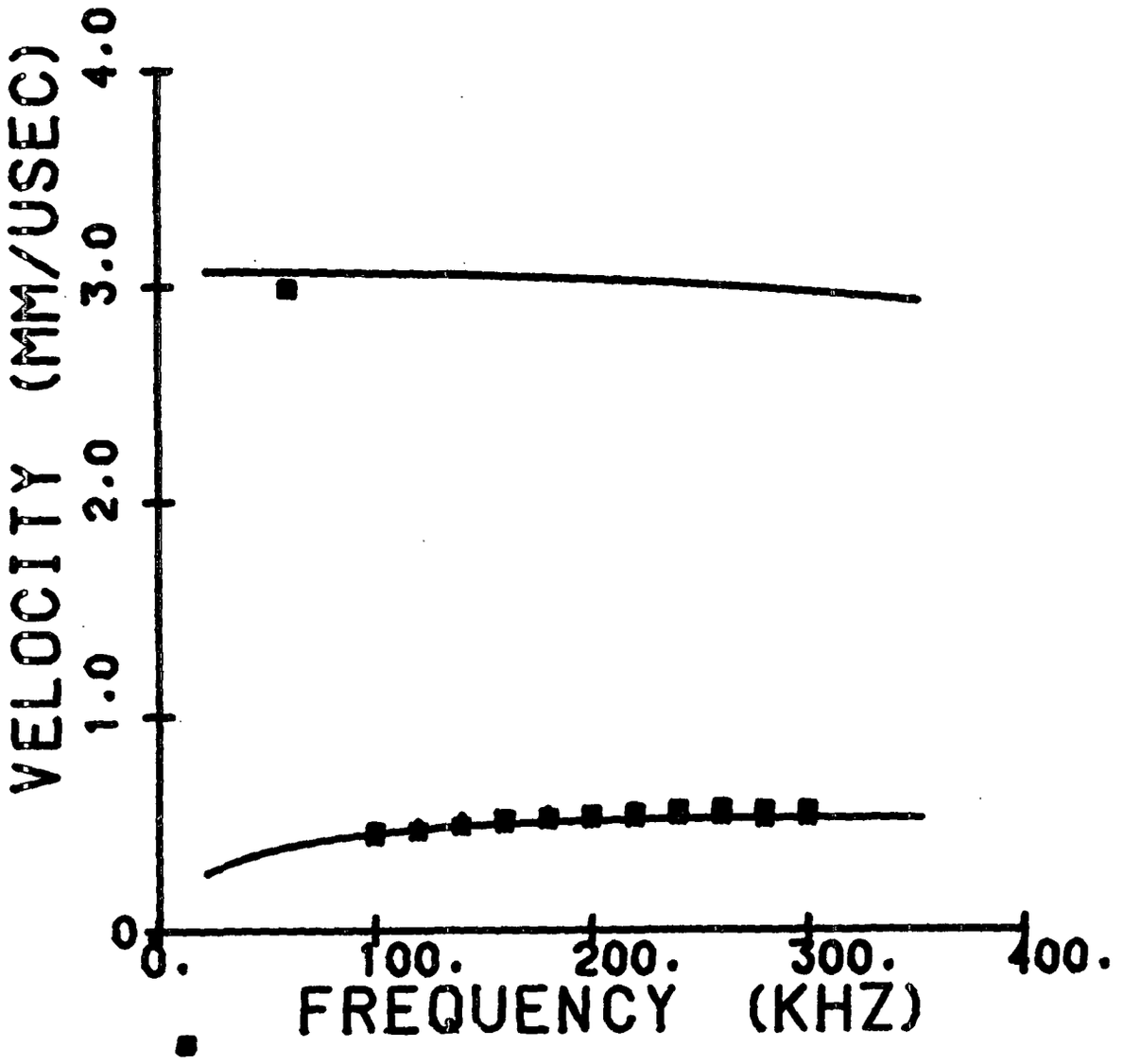

Sample 1182 GS8 CD

	Density, g/cm^3	Caliper, mm	C_{22} GPa	C_{33} GPa	C_{23} GPa	C_{55} GPa
Layer 1	0.728	0.5796	4.064	0.169	0.00003	0.169
Layer 2	1.089	0.4801	12.140	0.738	0.00003	0.453

SUM R2 = 0.8247

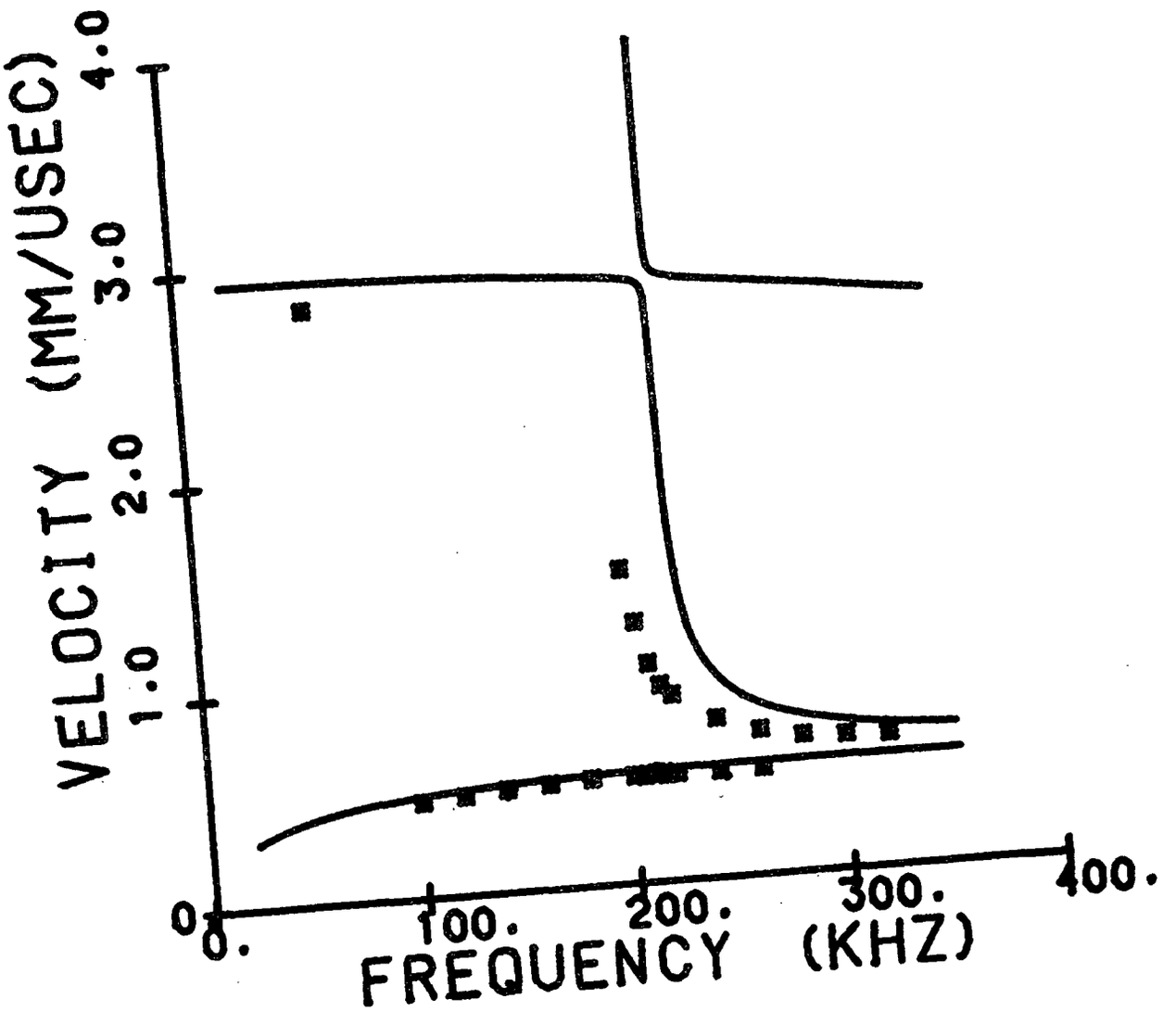

Sample 1182 GS9 CD

	Density, g/cm^3	Caliper, mm	C_{22} GPa	C_{33} GPa	C_{23} GPa	C_{55} GPa
Layer 1	0.764	0.2551	6.580	0.184	0.00003	0.177
Layer 2	0.788	0.2639	6.071	0.385	0.00003	0.180

SUM R2 = 0.0582

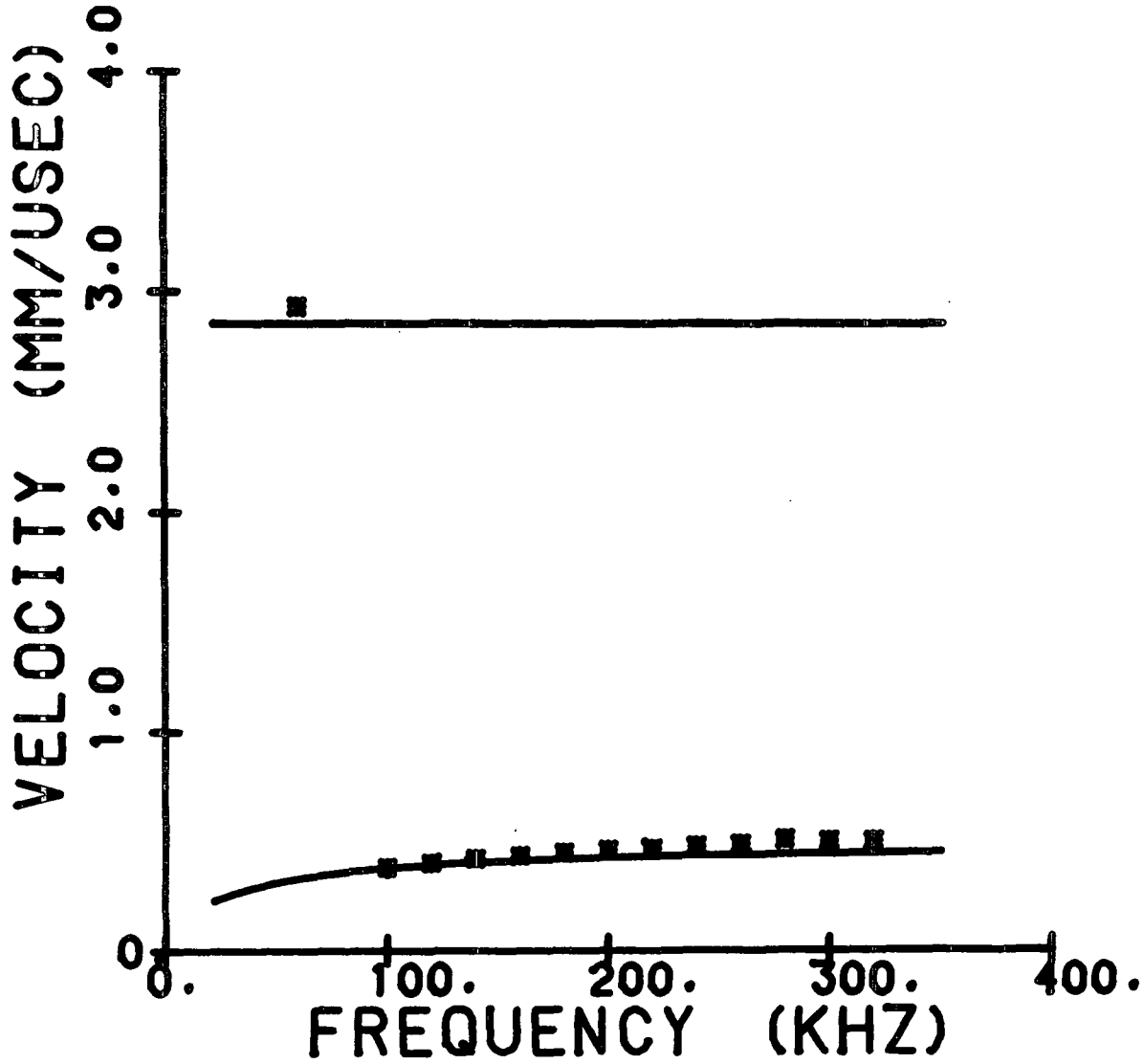

Sample 1182 GS10 CD

	Density, g/cm^3	Caliper, mm	C_{22} GPa	C_{33} GPa	C_{23} GPa	C_{55} GPa
Layer 1	0.773	0.5522	6.314	0.178	0.00003	0.219
Layer 2	0.788	0.2639	6.071	0.385	0.00003	0.180

SUM R2 = 0.3554

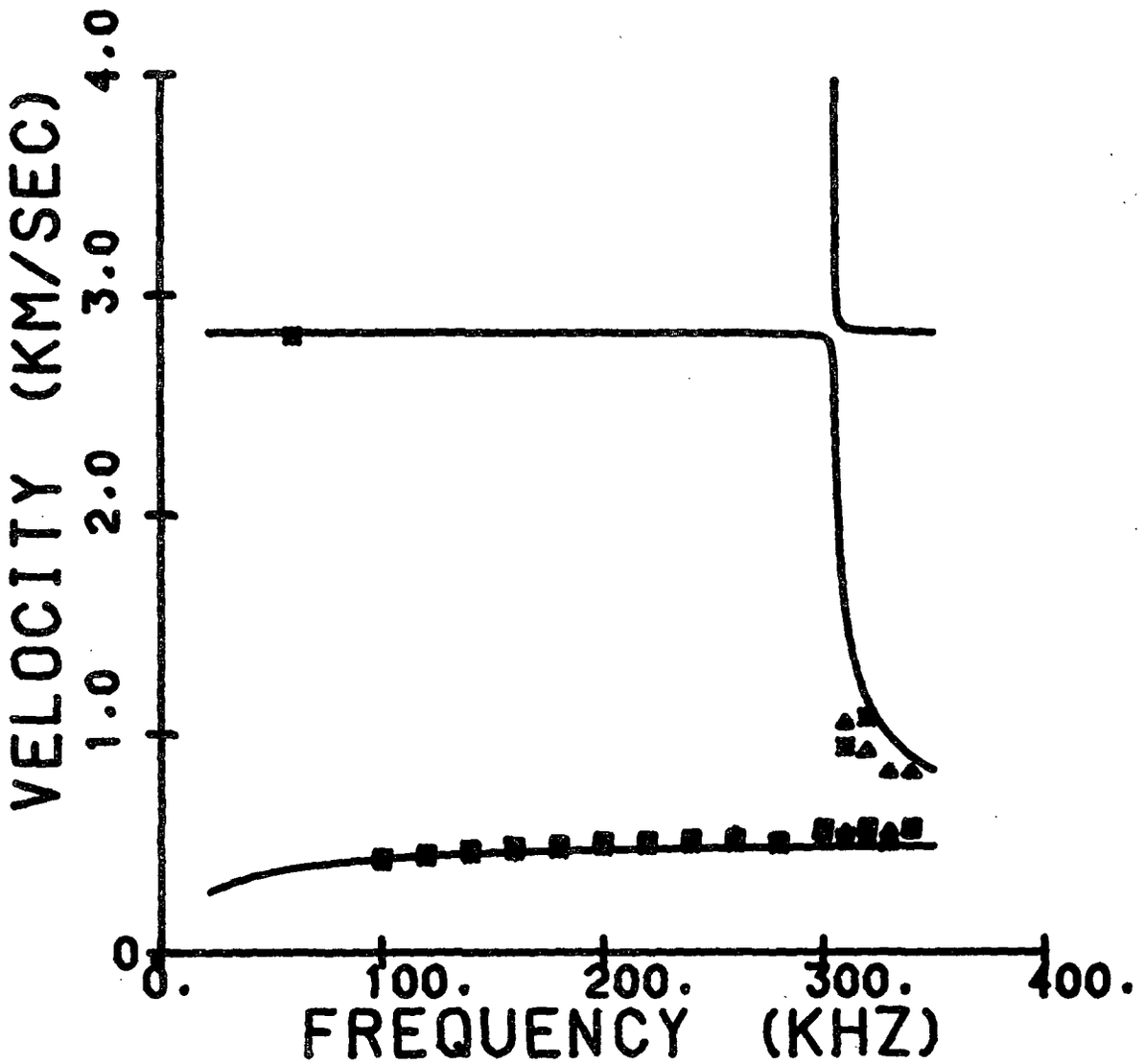

Sample 1182 GS11 CD

	Density, g/cm^3	Caliper, mm	C_{22} GPa	C_{33} GPa	C_{23} GPa	C_{55} GPa
Layer 1	0.712	0.2880	3.594	0.132	0.00003	0.130
Layer 2	0.788	0.2639	6.071	0.385	0.00003	0.180

SUM R2 = 0.0235

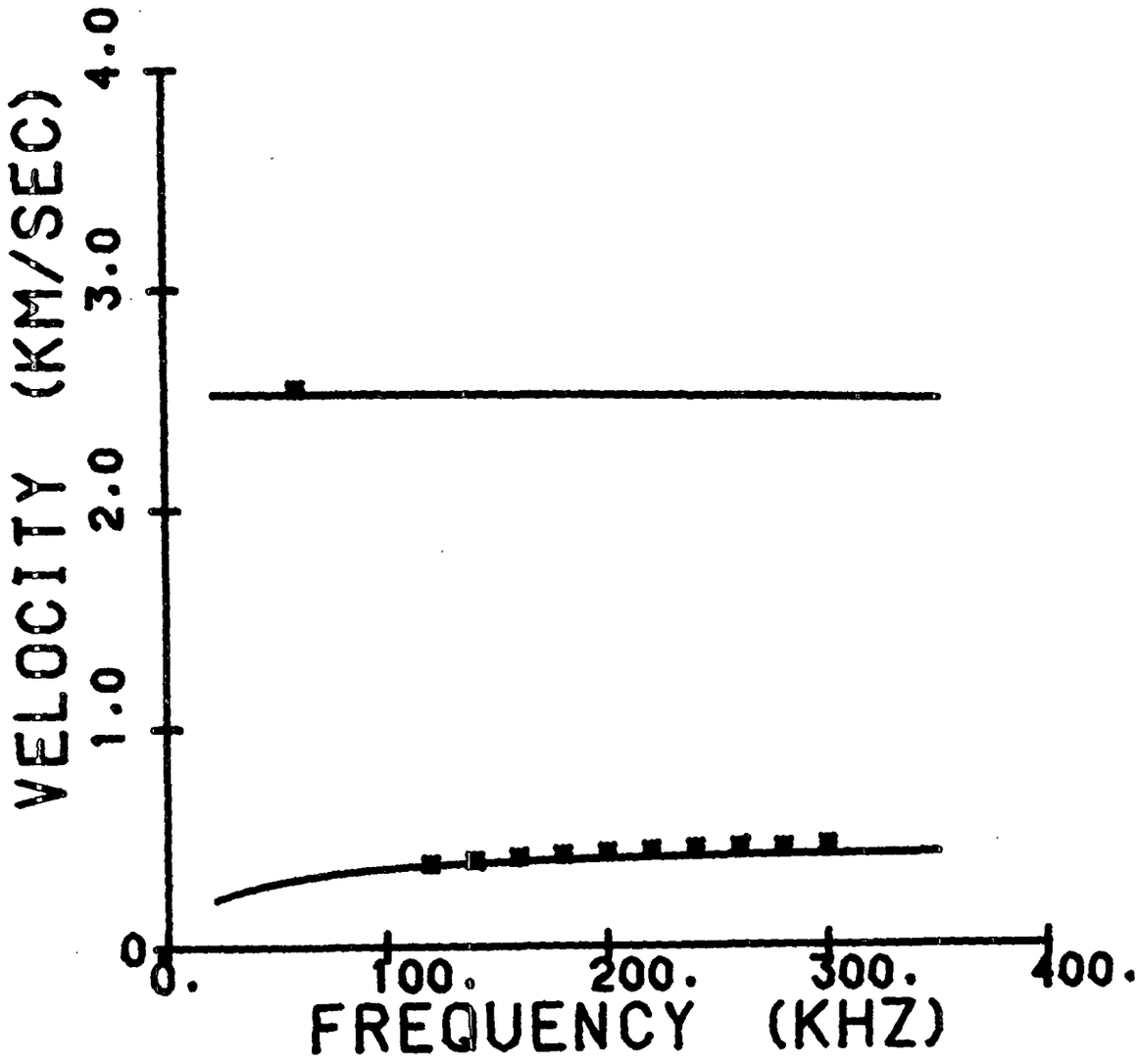

Sample 1182 GS12 CD

	Density, g/cm^3	Caliper, mm	C_{22} GPa	C_{33} GPa	C_{23} GPa	C_{55} GPa
Layer 1	0.728	0.5796	4.064	0.169	0.00003	0.169
Layer 2	0.788	0.2639	6.071	0.385	0.00003	0.180

SUM R2 = 0.1691

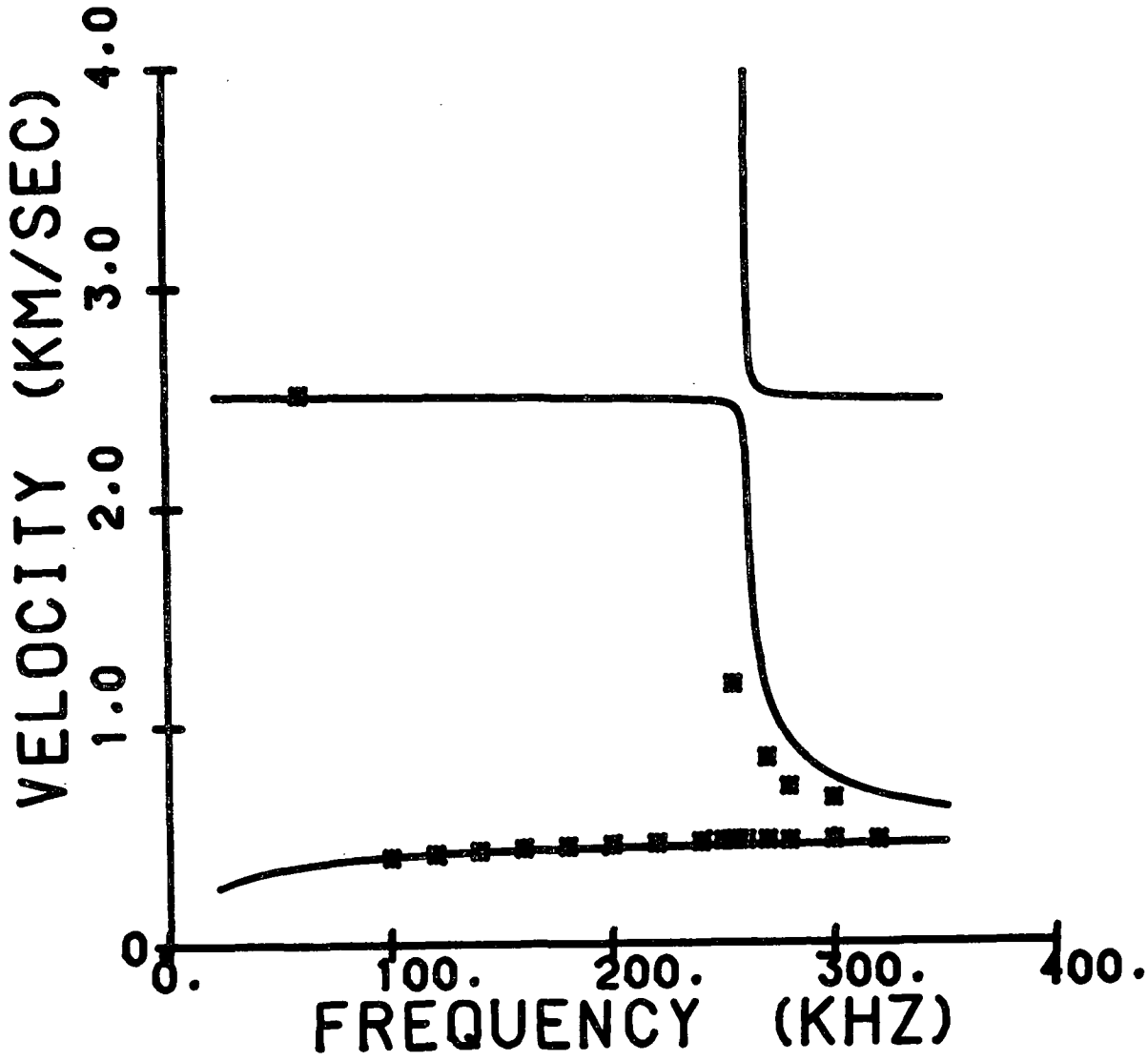

Sample 1182 GS13 CD

	Density, g/cm^3	Caliper, mm	C_{22} GPa	C_{33} GPa	C_{23} GPa	C_{55} GPa
Layer 1	0.764	0.2551	6.580	0.184	0.00003	0.177
Layer 2	10.046	0.9110	8.777	0.612	0.00003	0.368

SUM R2 = 0.0186

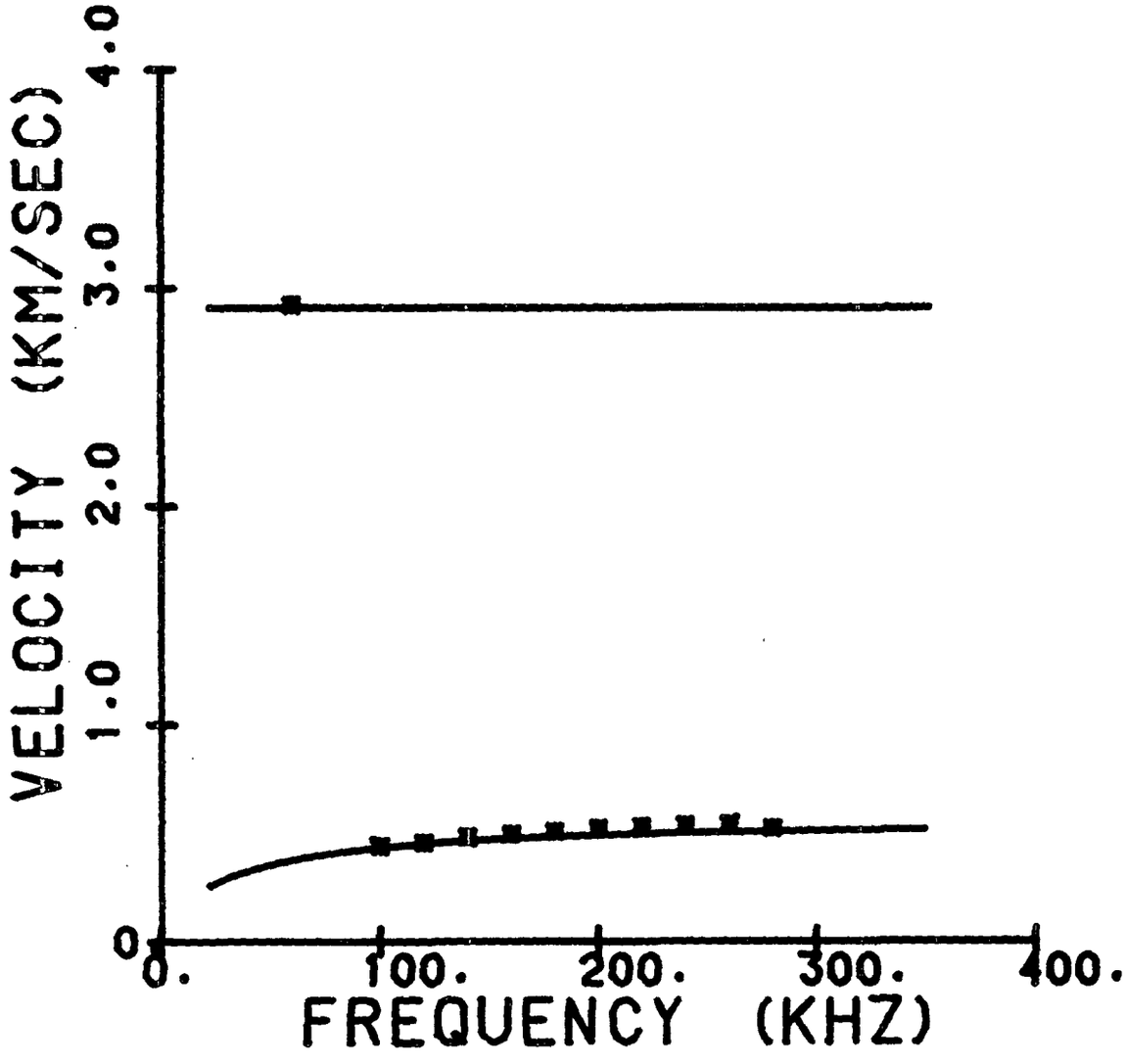

Sample 1182 GS14 CD

	Density, g/cm^3	Caliper, mm	C_{22} GPa	C_{33} GPa	C_{23} GPa	C_{55} GPa
Layer 1	0.773	0.5522	6.314	0.178	0.00003	0.219
Layer 2	10.046	0.9110	8.777	0.612	0.00003	0.368

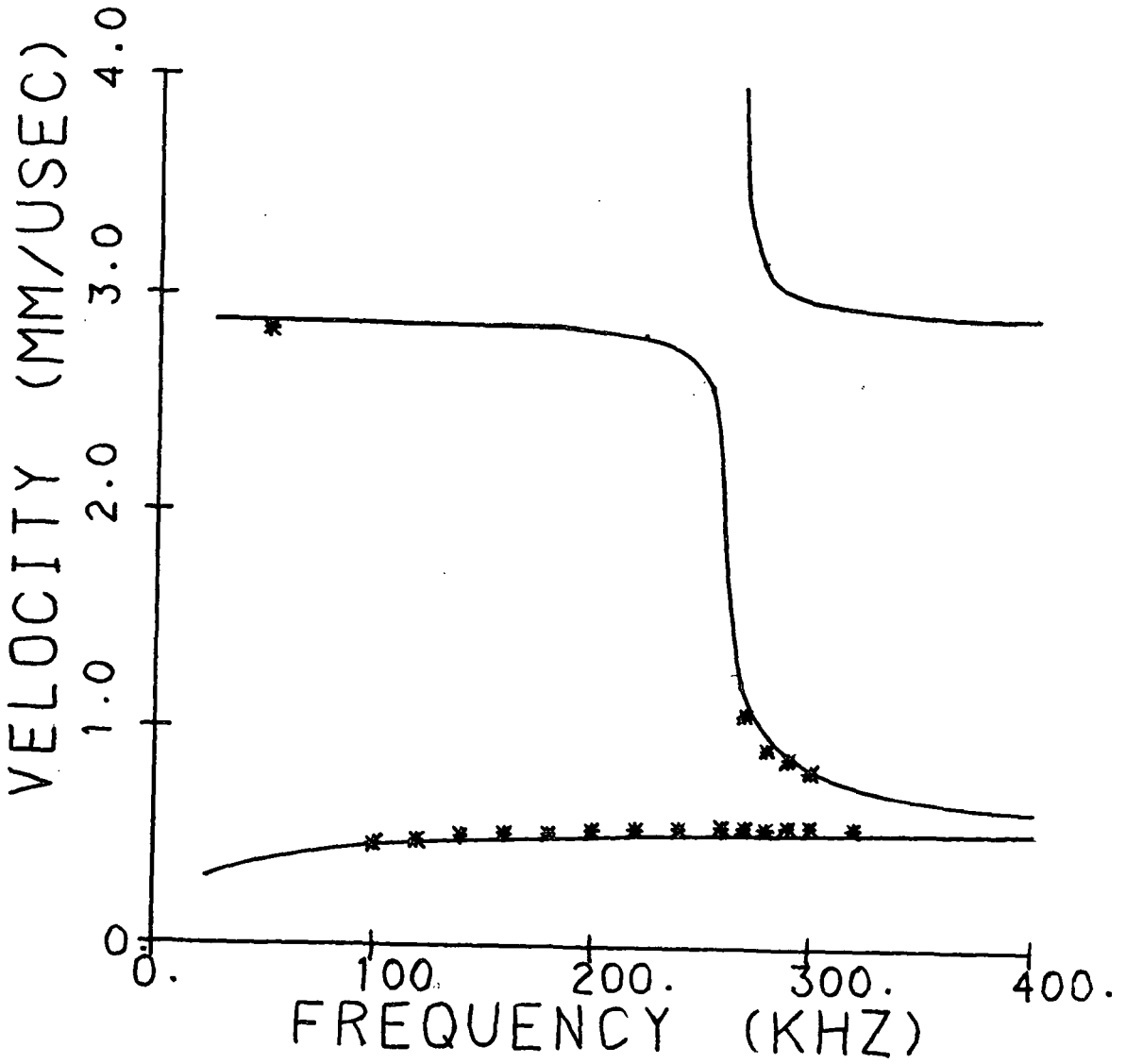

Sample 1182 GS15 CD

	Density, g/cm^3	Caliper, mm	C_{22} GPa	C_{33} GPa	C_{23} GPa	C_{55} GPa
Layer 1	0.712	0.2880	3.594	0.132	0.00003	0.130
Layer 2	10.046	0.9110	8.777	0.612	0.00003	0.368

SUM R2 = 0.0299

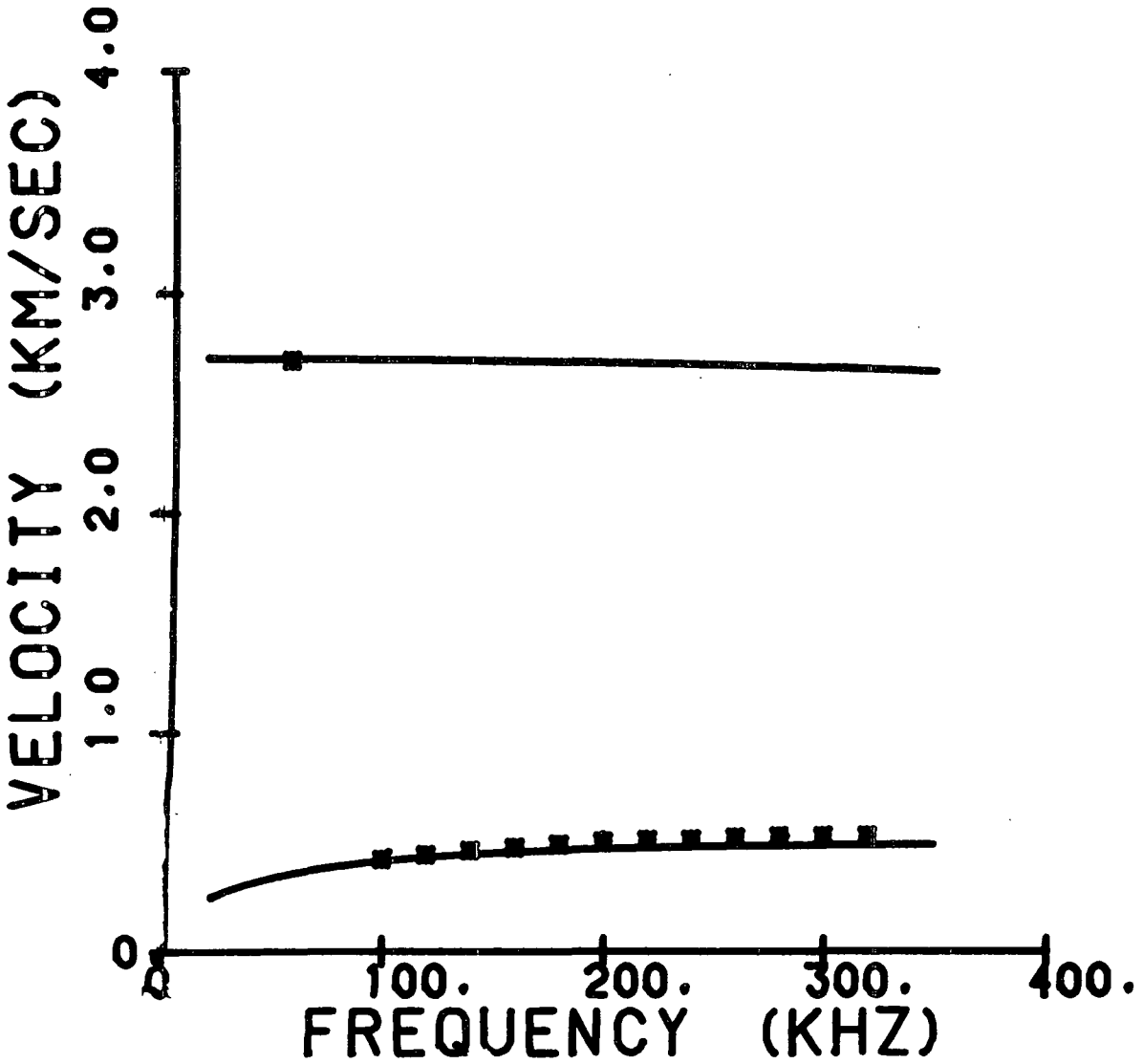

Sample 1182 GS16 CD

	Density, g/cm^3	Caliper, mm	C_{22} GPa	C_{33} GPa	C_{23} GPa	C_{55} GPa
Layer 1	0.728	0.5796	4.064	0.169	0.00003	0.169
Layer 2	10.046	0.9110	8.777	0.612	0.00003	0.368

SUM R2 = 0.3071

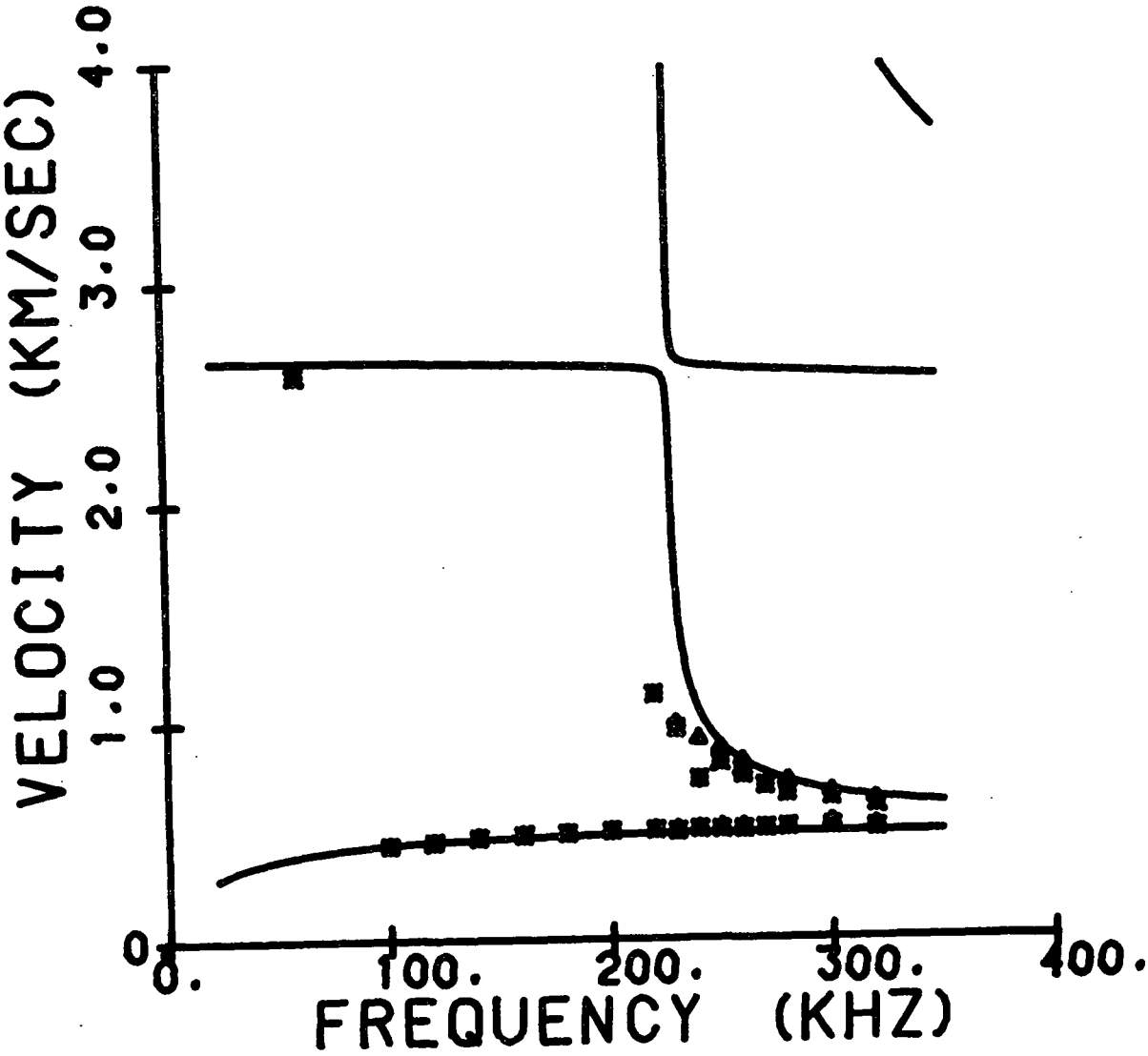

Sample 883 TK1 MD

	Density, g/cm^3	Caliper, mm	C_{11} GPa	C_{33} GPa	C_{13} GPa	C_{55} GPa
Layer 1	0.542	0.4538	4.381	0.056	0.00003	0.158
Layer 2	0.542	0.4538	4.381	0.056	0.00003	0.158
Layer 3	0.542	0.4538	4.381	0.056	0.00003	0.158

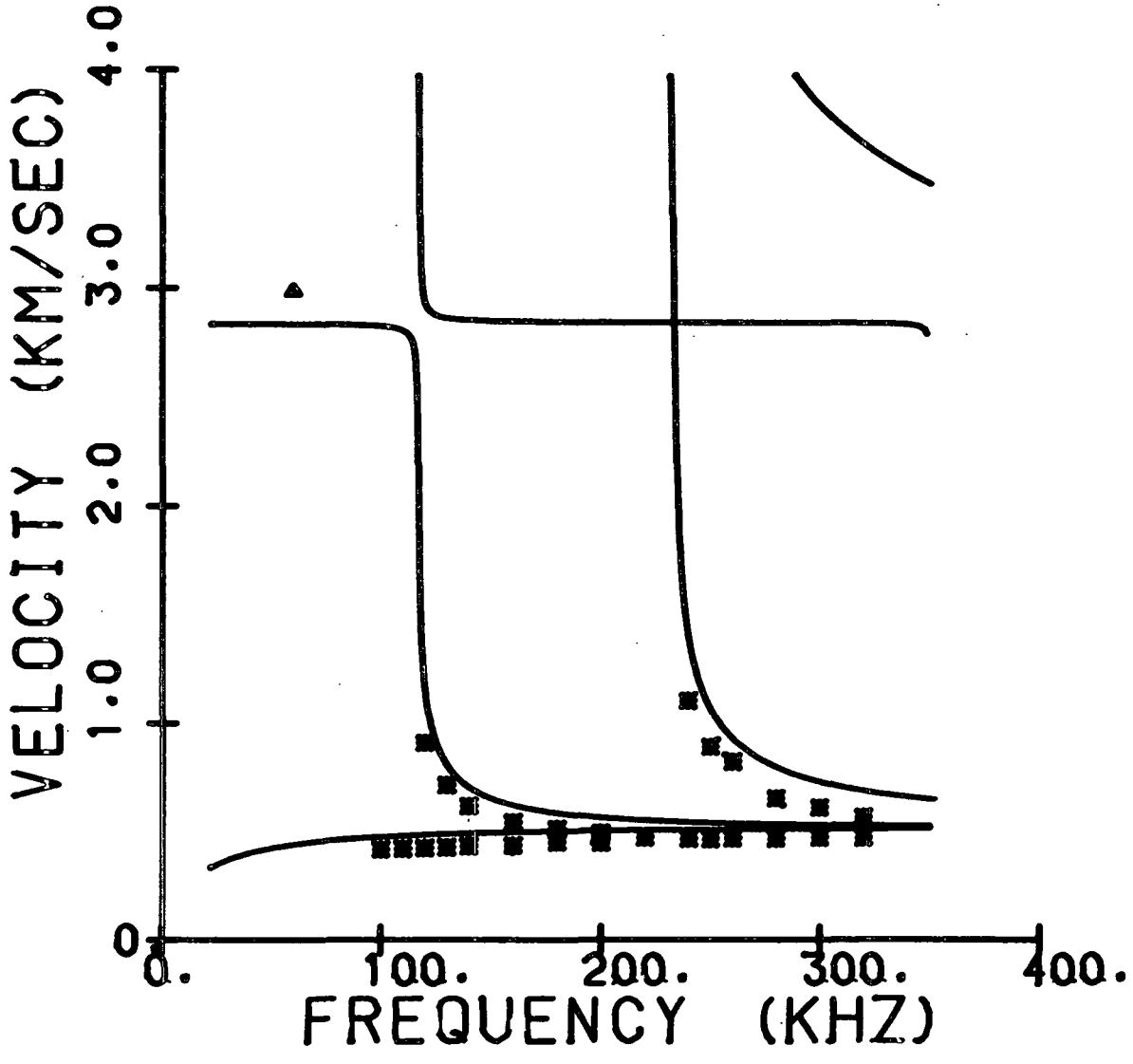

Sample 883 TK2 MD

	Density, g/cm^3	Caliper, mm	C_{11} GPa	C_{33} GPa	C_{13} GPa	C_{55} GPa
Layer 1	0.715	0.3103	7.463	0.270	0.00003	0.293
Layer 2	0.715	0.3103	7.463	0.270	0.00003	0.293
Layer 3	0.715	0.3103	7.463	0.270	0.00003	0.293

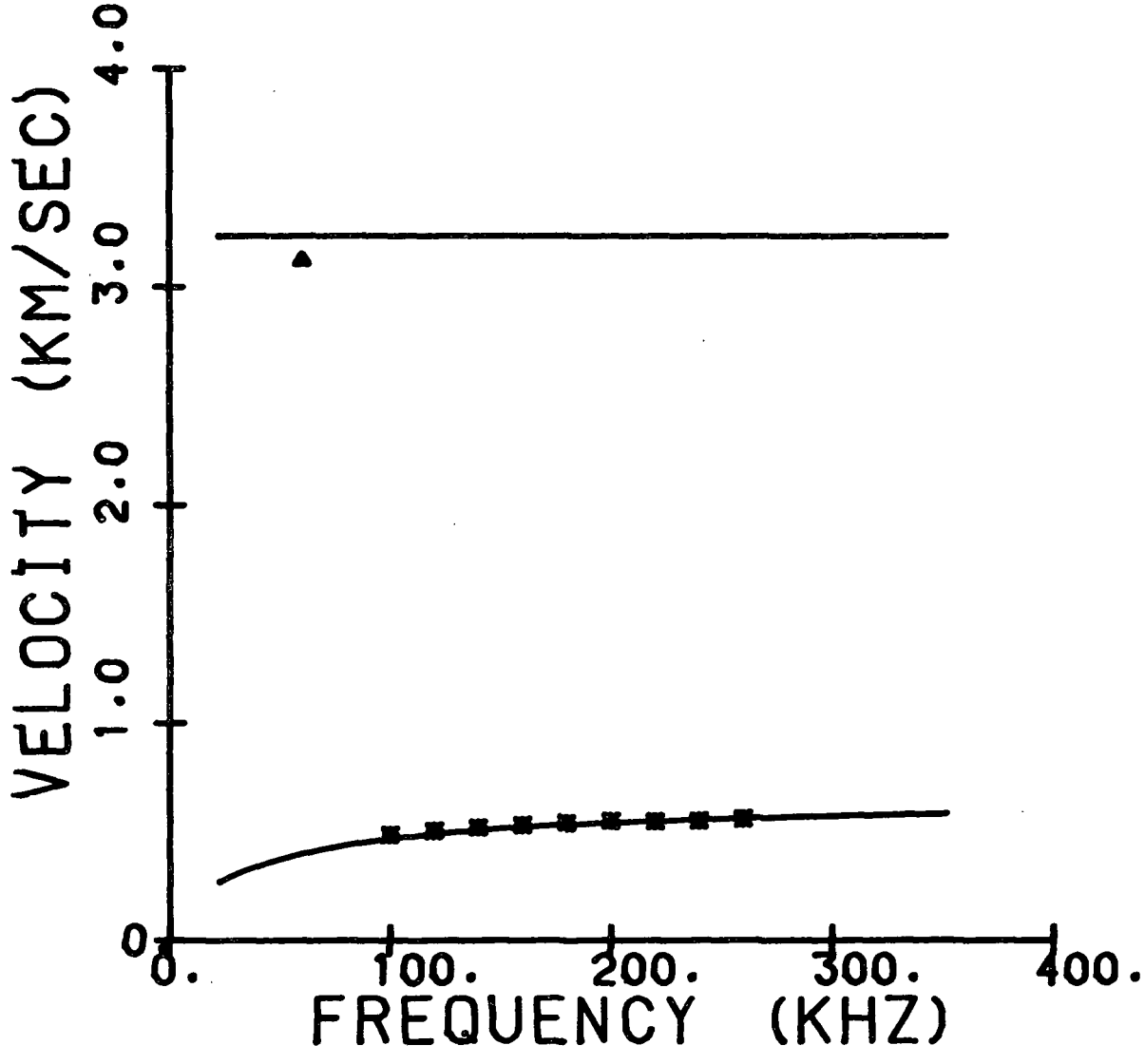

Sample 883 TK3 MD

	Density, g/cm^3	Caliper, mm	C_{11} GPa	C_{33} GPa	C_{13} GPa	C_{55} GPa
Layer 1	0.566	0.4450	3.445	0.071	0.00003	0.146
Layer 2	0.785	0.3158	9.394	0.312	0.00003	0.353
Layer 3	0.566	0.4450	3.445	0.071	0.00003	0.146

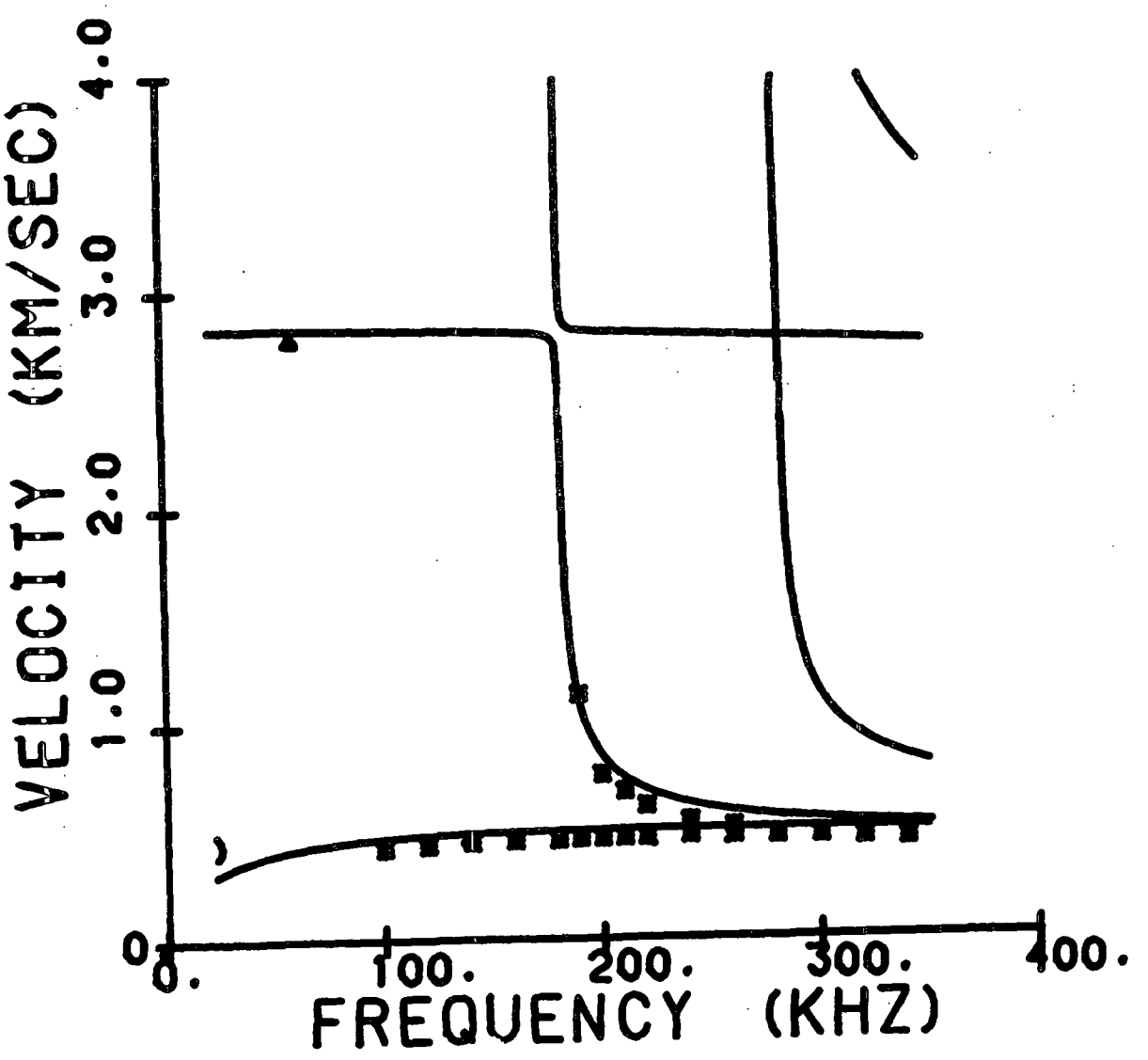

Sample 883 TK4 MD

	Density, g/cm^3	Caliper, mm	C_{11} GPa	C_{33} GPa	C_{13} GPa	C_{55} GPa
Layer 1	0.785	0.3158	9.394	0.312	0.00003	0.353
Layer 2	0.566	0.4450	3.445	0.071	0.00003	0.146
Layer 3	0.785	0.3158	9.394	0.312	0.00003	0.353

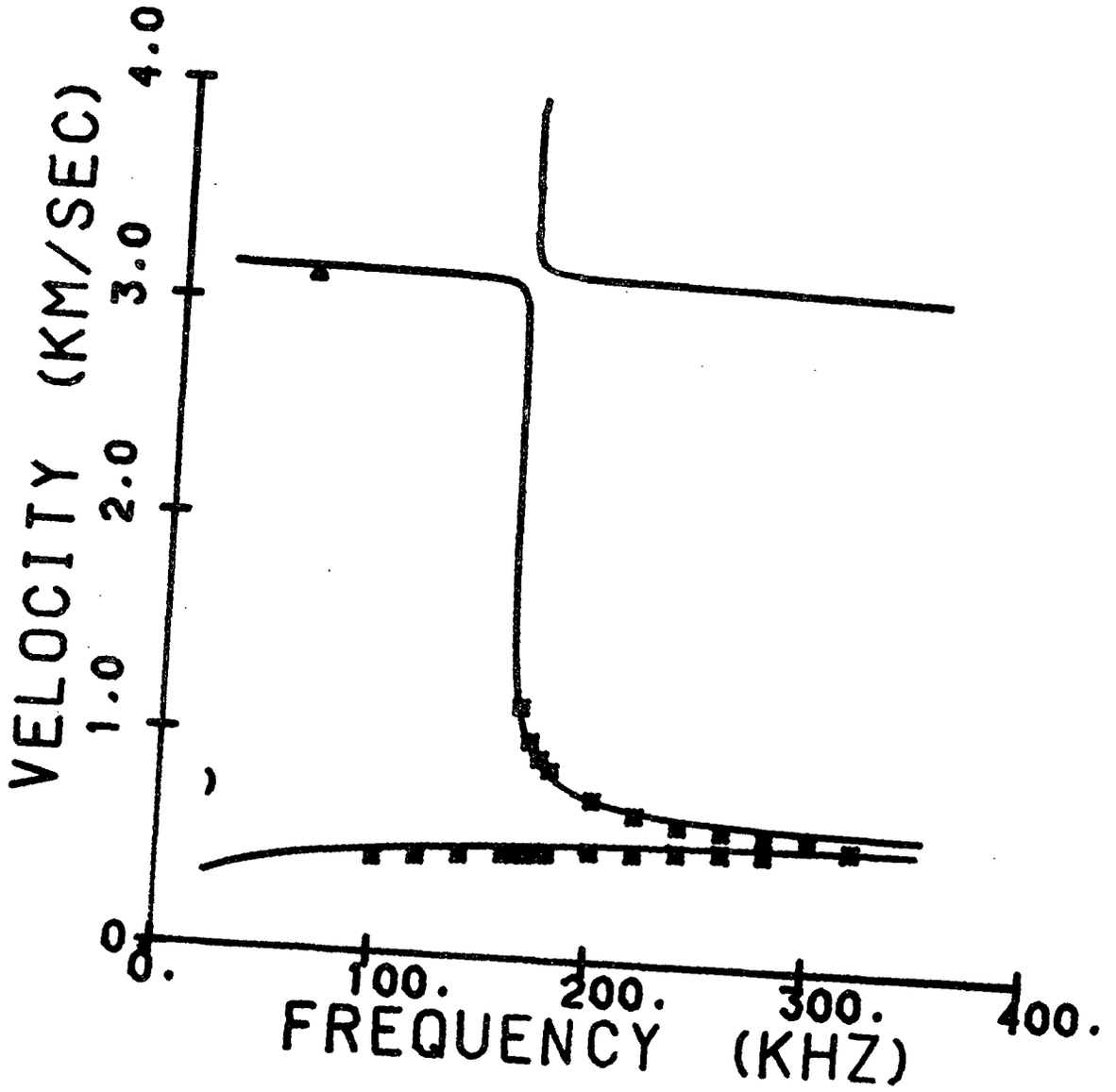

Sample 883 TK5 MD

	Density, g/cm^3	Caliper, mm	C_{11} GPa	C_{33} GPa	C_{13} GPa	C_{55} GPa
Layer 1	0.566	0.4450	3.445	0.071	0.00003	0.146
Layer 2	0.785	0.3158	9.394	0.312	0.00003	0.353
Layer 3	0.785	0.3158	9.394	0.312	0.00003	0.353

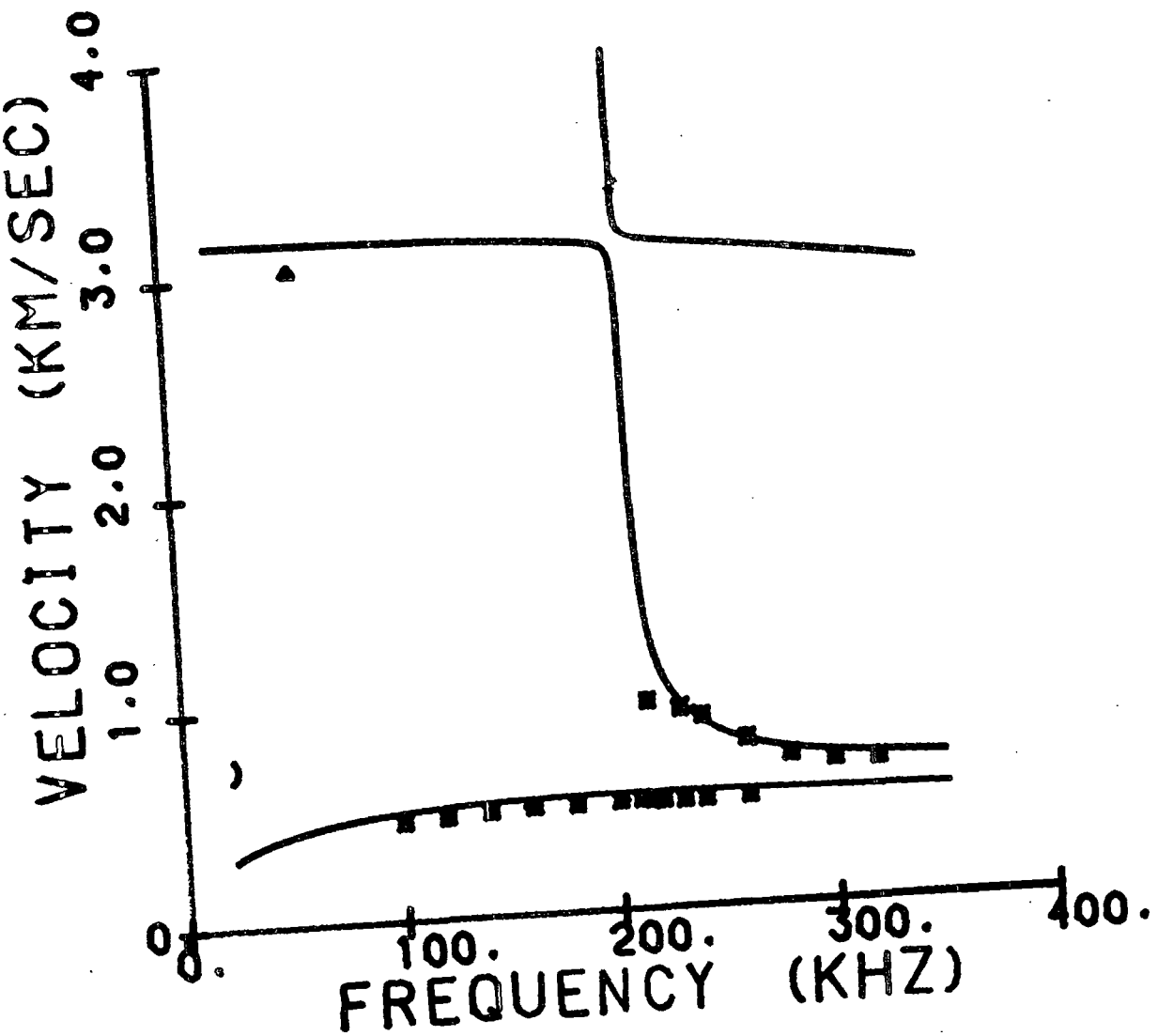

Sample 883 TK6 MD

	Density, g/cm^3	Caliper, mm	C_{11} GPa	C_{33} GPa	C_{13} GPa	C_{55} GPa
Layer 1	0.566	0.4450	3.445	0.071	0.00003	0.146
Layer 2	0.566	0.4450	3.445	0.071	0.00003	0.146
Layer 3	0.785	0.3158	9.394	0.312	0.00003	0.353

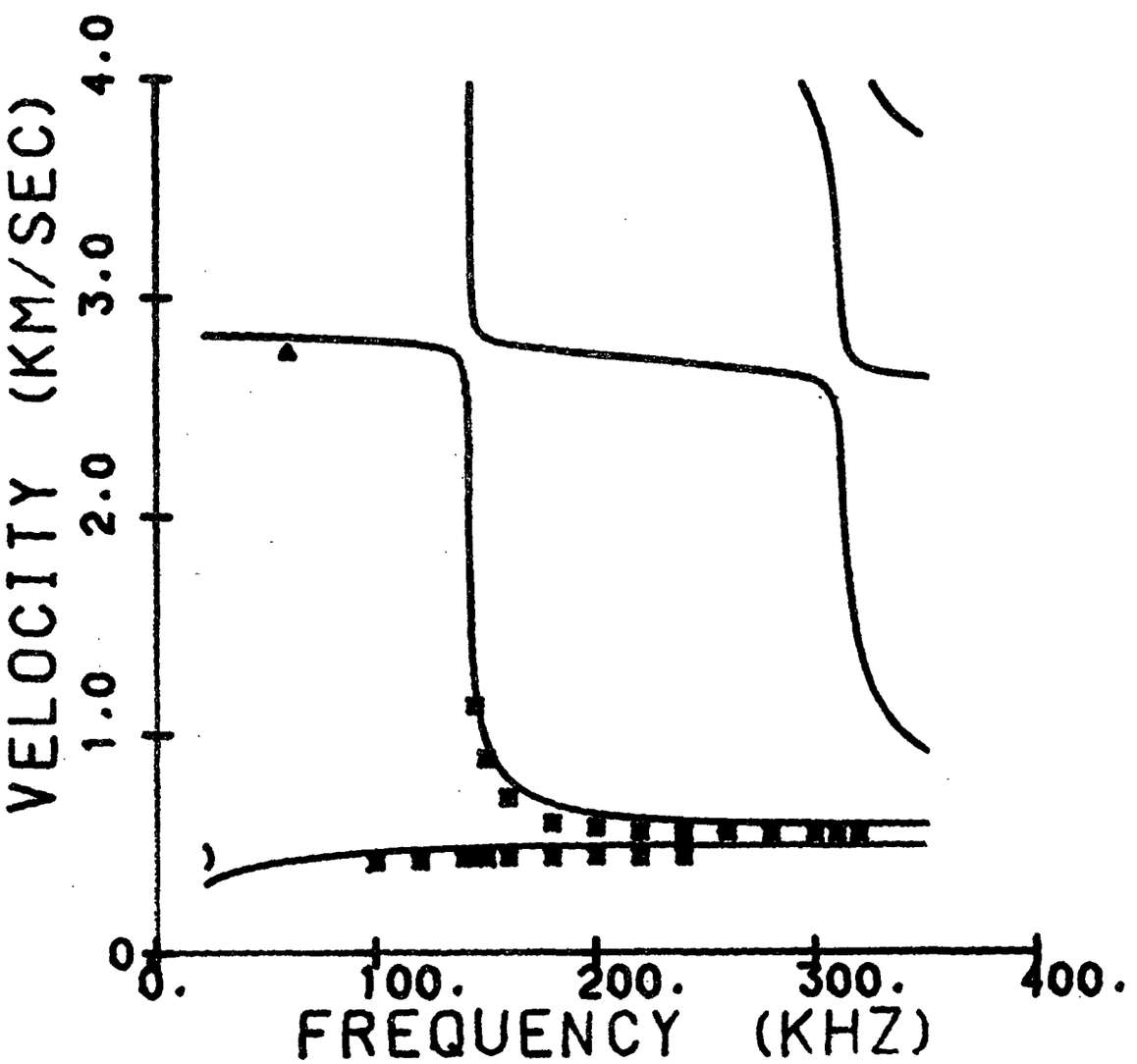

Sample 883 TK8 MD

	Density, g/cm^3	Caliper, mm	C_{11} GPa	C_{33} GPa	C_{13} GPa	C_{55} GPa
Layer 1	0.546	0.2217	3.046	0.064	0.00003	0.189
Layer 2	0.785	0.6316	9.394	0.312	0.00003	0.353
Layer 3	0.546	0.2217	3.046	0.064	0.00003	0.189

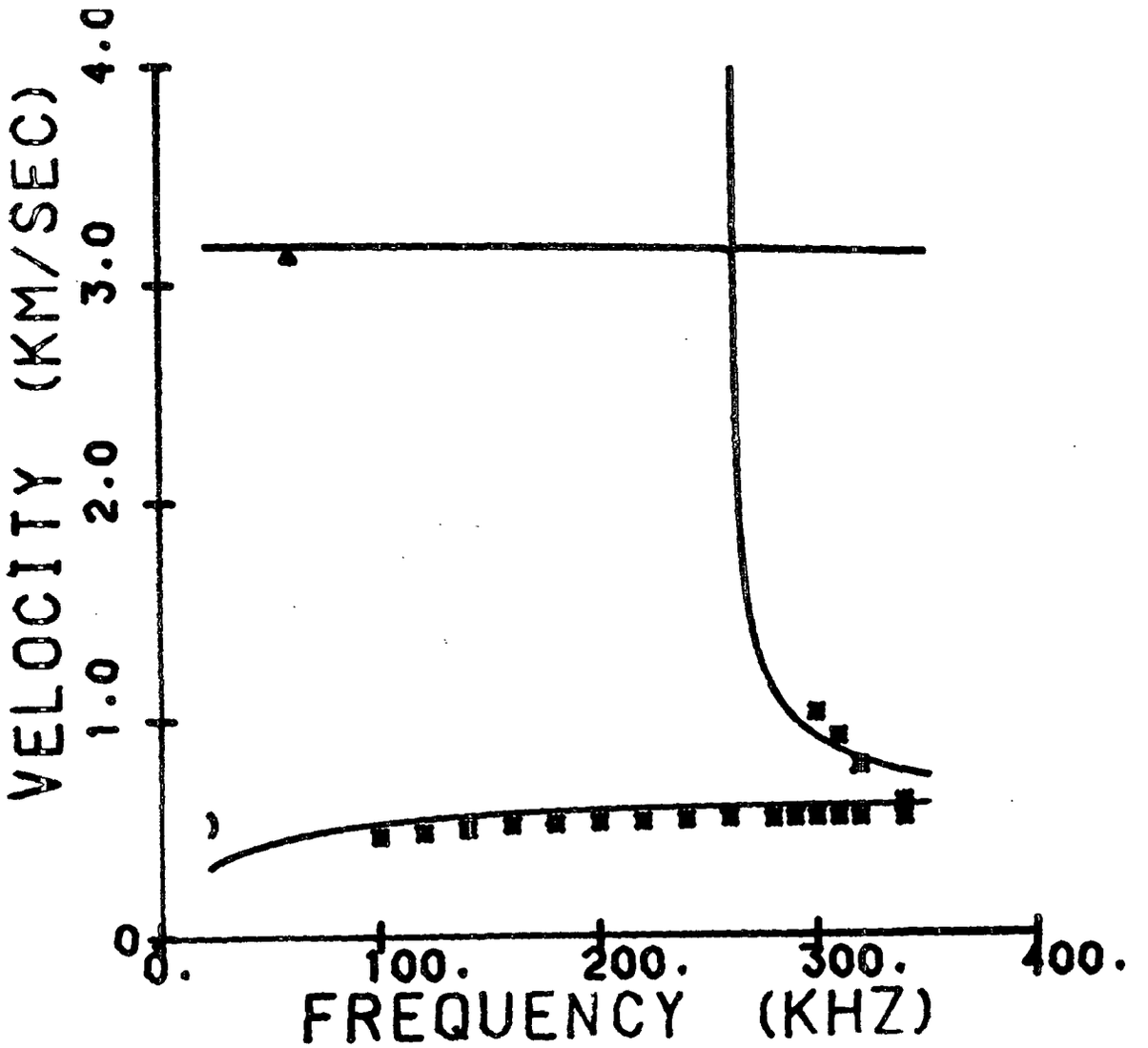

Sample 883 TK9 MD

	Density, g/cm^3	Caliper, mm	C_{11} GPa	C_{33} GPa	C_{13} GPa	C_{55} GPa
Layer 1	0.542	0.4538	4.381	0.056	0.00003	0.158
Layer 2	0.785	0.3158	9.394	0.312	0.00003	0.353
Layer 3	0.566	0.4450	3.445	0.071	0.00003	0.146

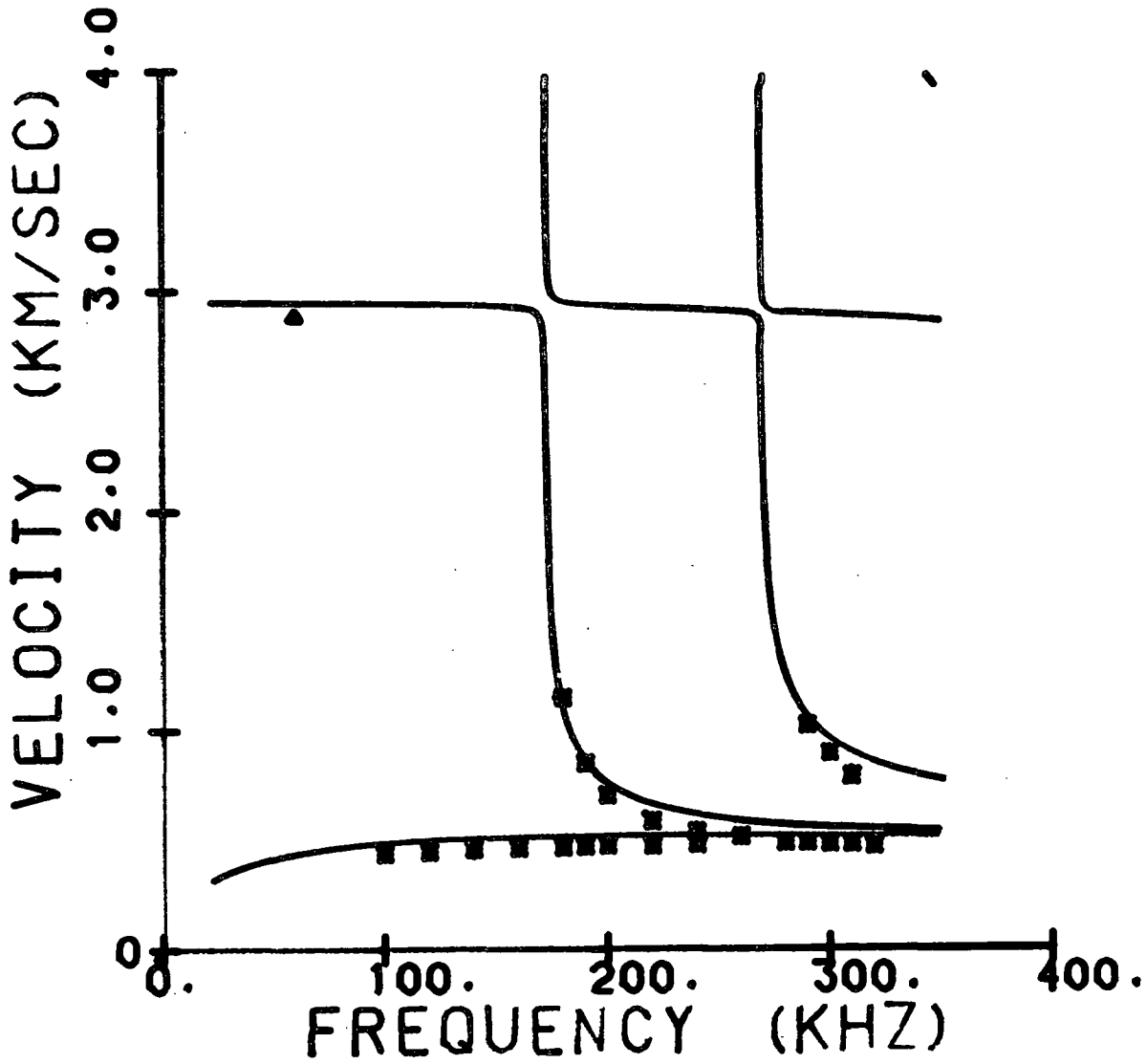

Sample 883 TK10 MD

	Density, g/cm^3	Caliper, mm	C_{11} GPa	C_{33} GPa	C_{13} GPa	C_{55} GPa
Layer 1	0.715	0.3103	7.463	0.071	0.00003	0.293
Layer 2	0.566	0.4450	3.445	0.071	0.00003	0.146
Layer 3	0.785	0.3158	9.394	0.312	0.00003	0.353

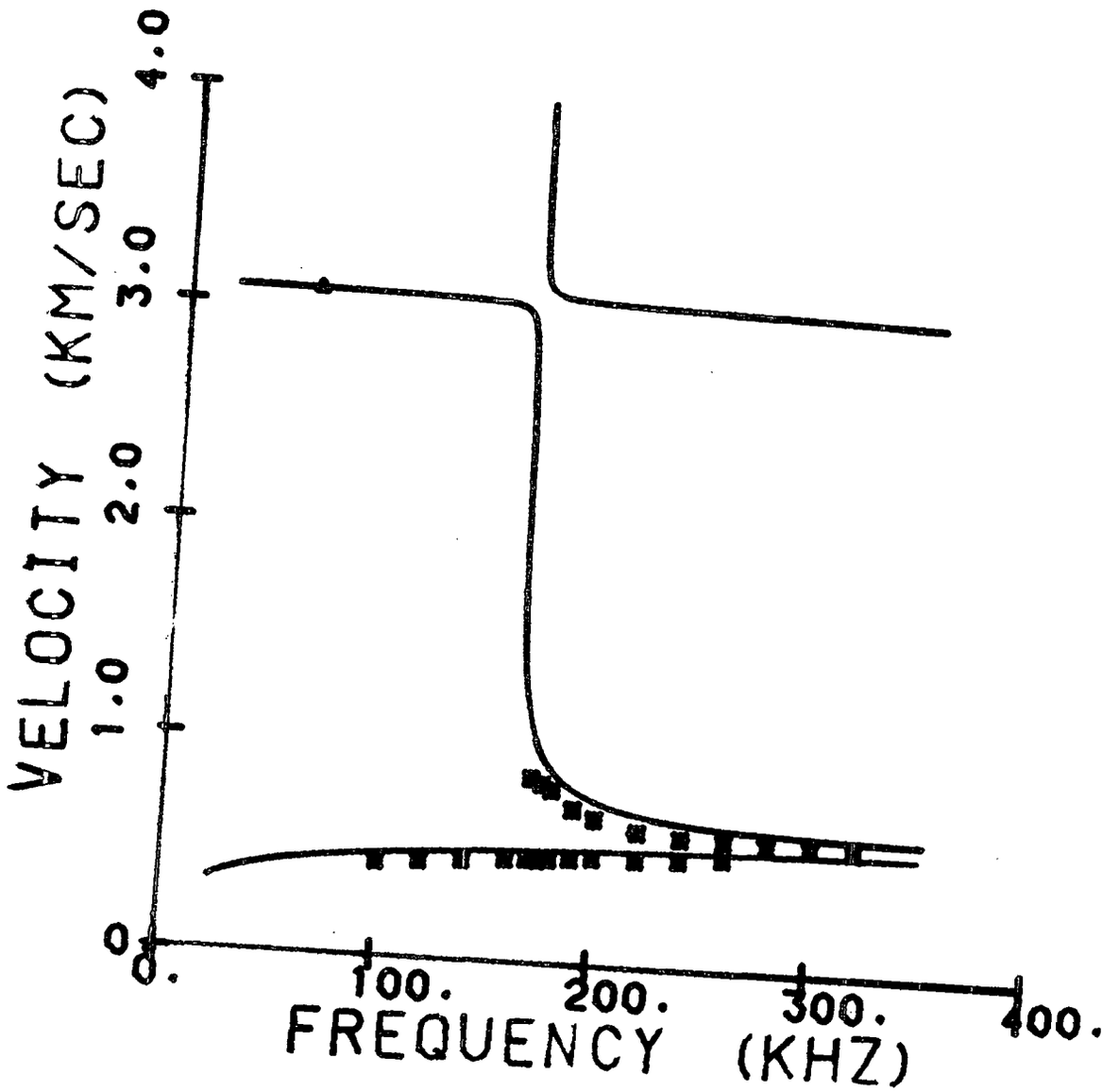

Sample 883 TK11 MD

	Density, g/cm^3	Caliper, mm	C_{11} GPa	C_{33} GPa	C_{13} GPa	C_{55} GPa
Layer 1	0.566	0.4450	3.445	0.071	0.00003	0.146
Layer 2	0.715	0.3103	7.463	0.071	0.00003	0.293
Layer 3	0.785	0.3158	9.394	0.312	0.00003	0.353

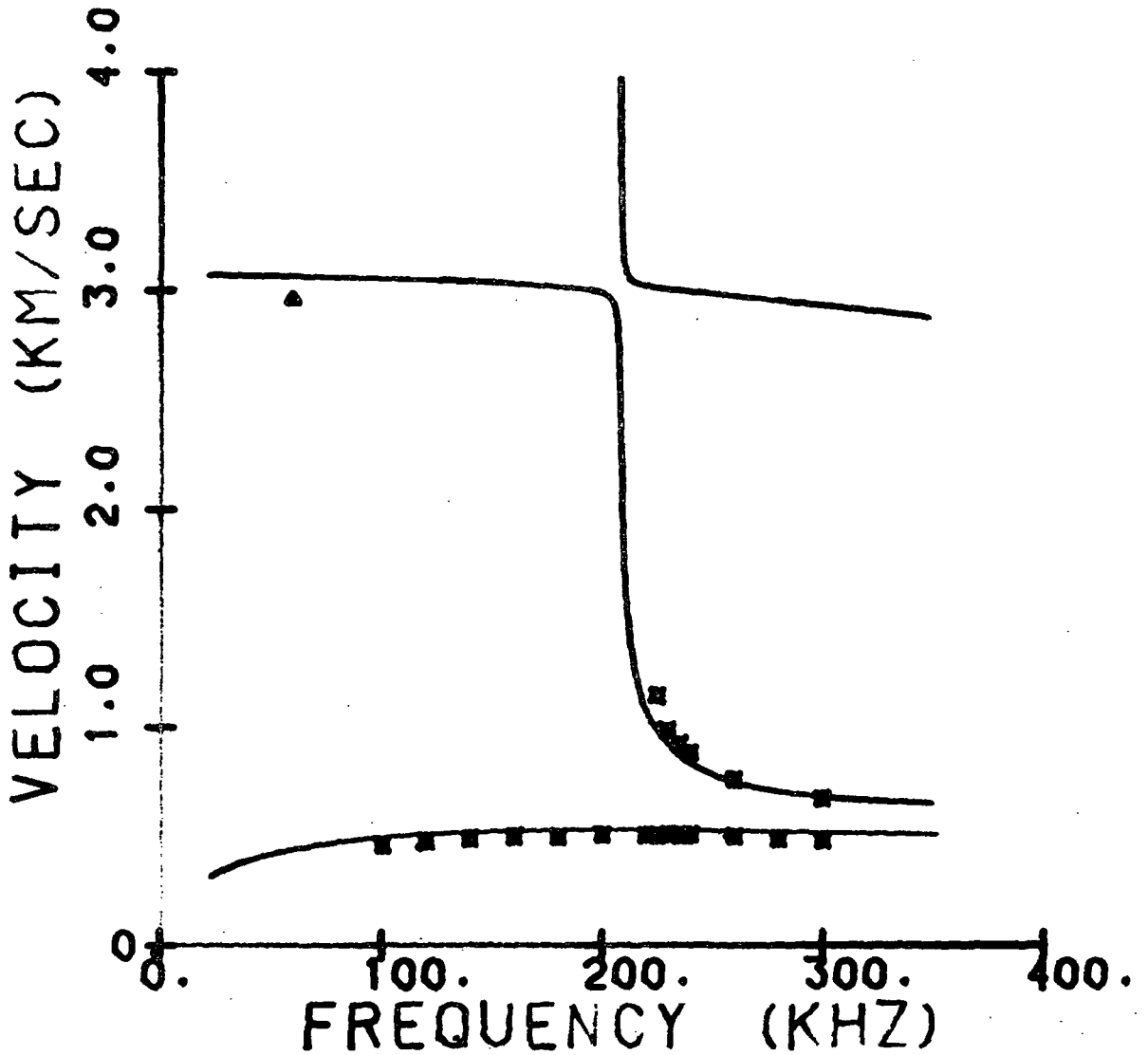

Sample 883 TK12 MD

	Density, g/cm^3	Caliper, mm	C_{11} GPa	C_{33} GPa	C_{13} GPa	C_{55} GPa
Layer 1	0.785	0.3158	9.394	0.312	0.00003	0.353
Layer 2	0.542	0.4538	4.381	0.056	0.00003	0.158
Layer 3	0.566	0.4450	3.445	0.071	0.00003	0.146

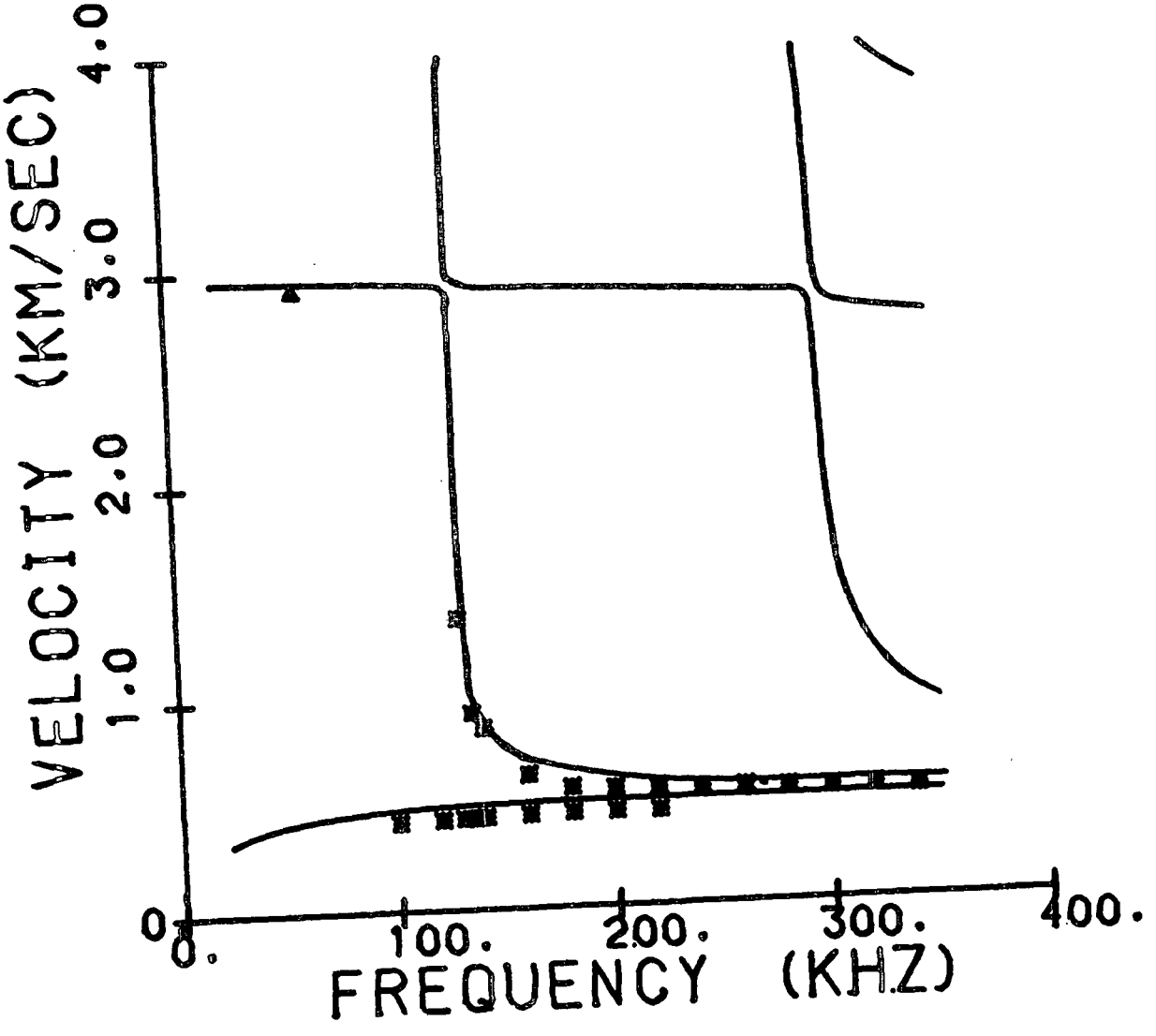

Sample 883 TK13 MD

	Density, g/cm^3	Caliper, mm	C_{11} GPa	C_{33} GPa	C_{13} GPa	C_{55} GPa
Layer 1	0.546	0.4434	3.046	0.064	0.00003	0.189
Layer 2	0.747	0.3158	8.964	0.272	0.00003	0.331
Layer 3	0.546	0.4434	3.046	0.064	0.00003	0.189

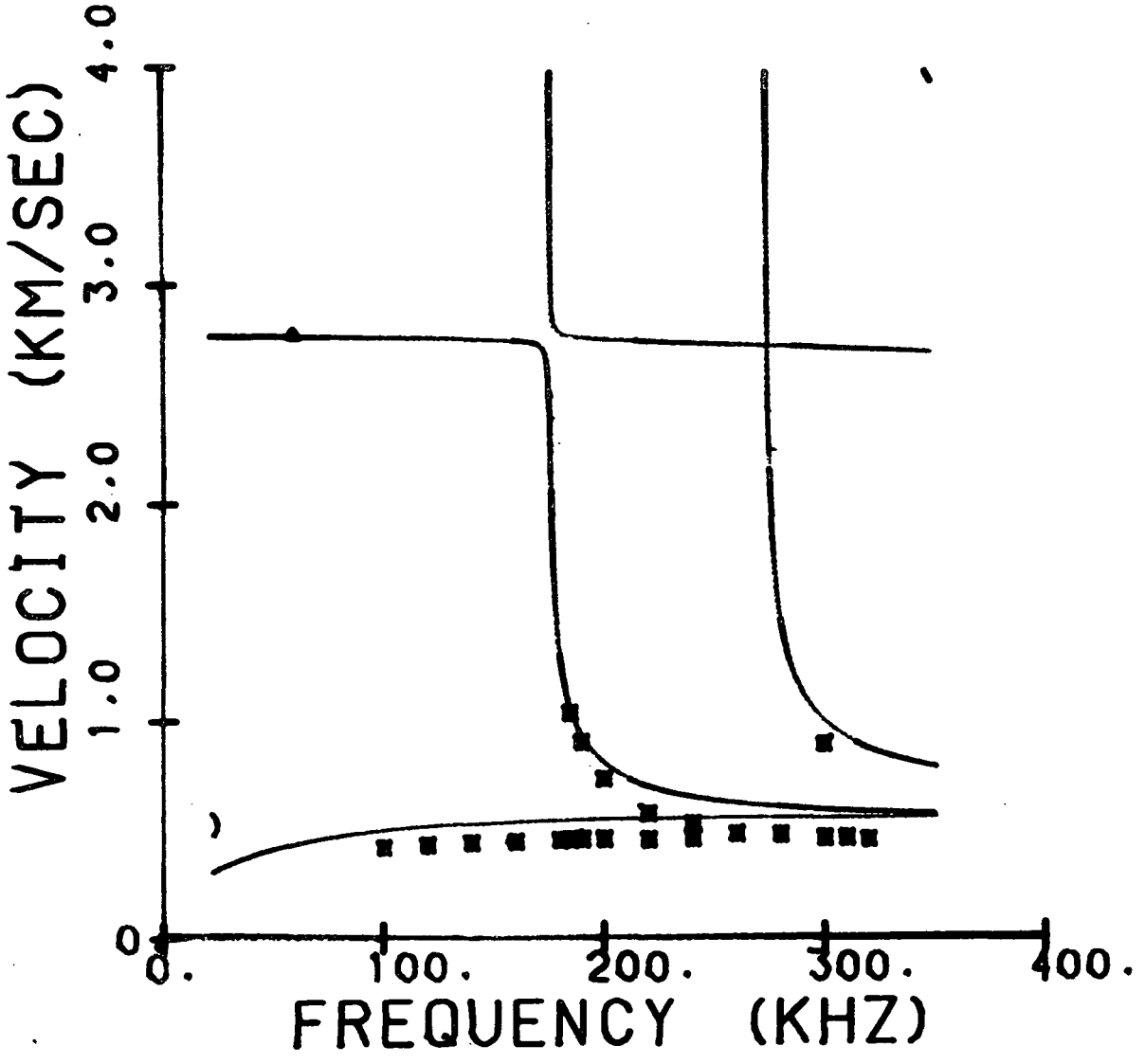

Sample 883 TK14 MD

	Density, g/cm^3	Caliper, mm	C_{11} GPa	C_{33} GPa	C_{13} GPa	C_{55} GPa
Layer 1	0.507	0.4456	4.468	0.050	0.00003	0.185
Layer 2	0.507	0.4456	4.468	0.050	0.00003	0.185
Layer 3	0.507	0.4456	4.468	0.050	0.00003	0.185

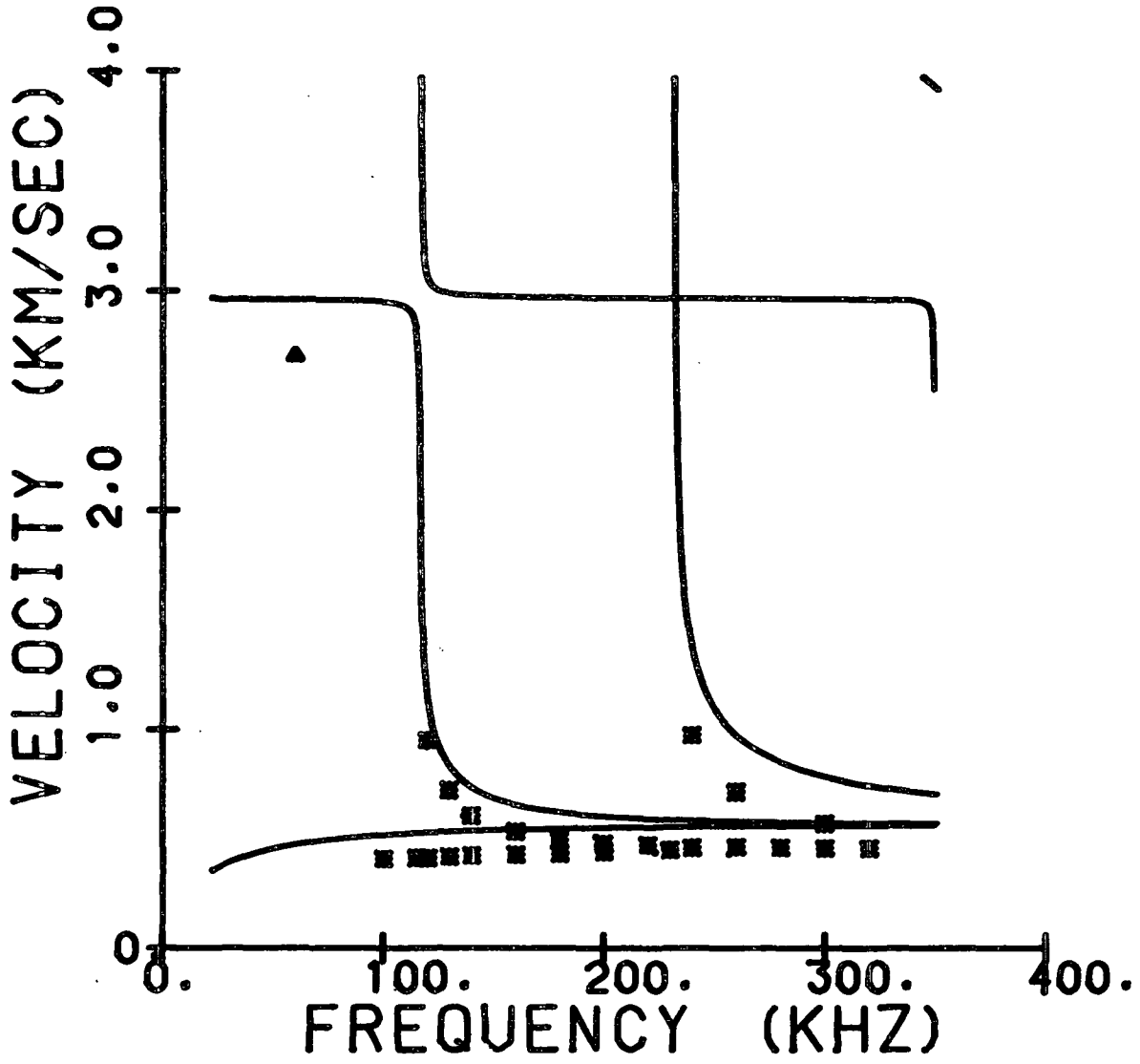

Sample 883 TK15 MD

	Density, g/cm^3	Caliper, mm	C_{11} GPa	C_{33} GPa	C_{13} GPa	C_{55} GPa
Layer 1	0.735	0.3130	6.908	0.251	0.00003	0.335
Layer 2	0.735	0.3130	6.908	0.251	0.00003	0.335
Layer 3	0.735	0.3130	6.908	0.251	0.00003	0.335

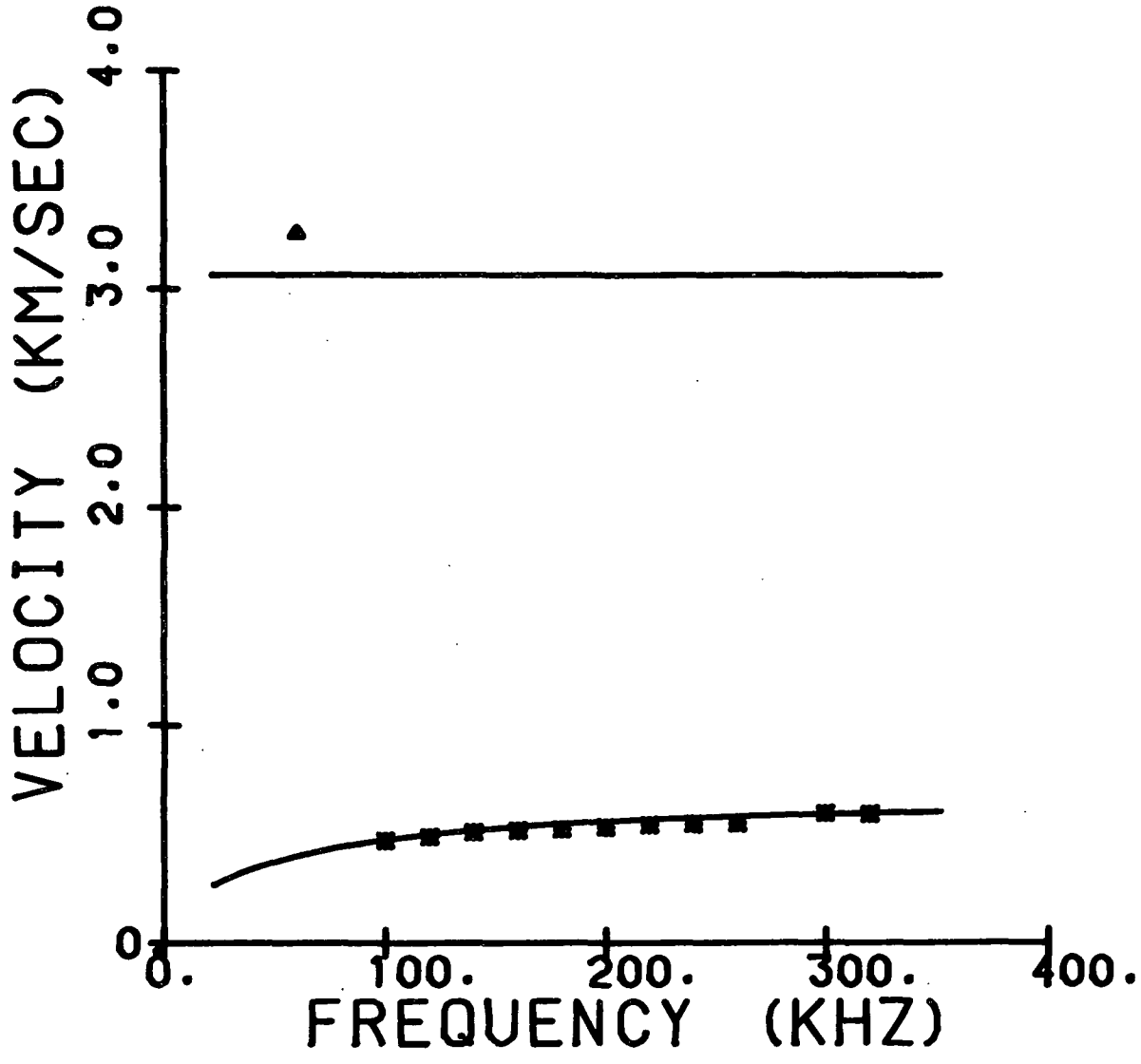

Sample 883 TK16 MD

	Density, g/cm^3	Caliper, mm	C_{11} GPa	C_{33} GPa	C_{13} GPa	C_{55} GPa
Layer 1	0.546	0.4434	3.046	0.064	0.00003	0.189
Layer 2	0.715	0.3103	7.463	0.071	0.00003	0.293
Layer 3	0.546	0.4434	3.046	0.064	0.00003	0.189

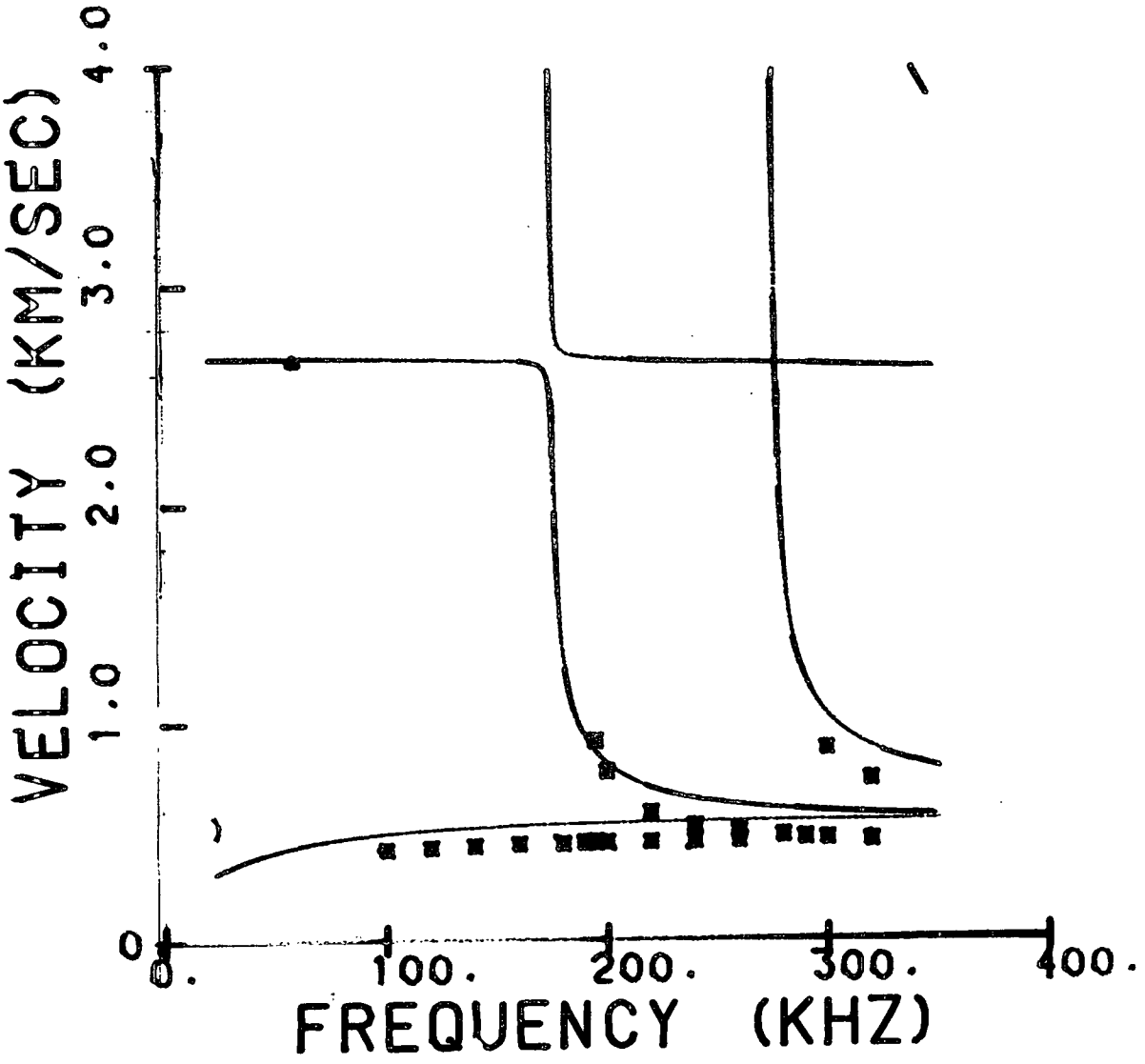

Sample 883 TK17 MD

	Density, g/cm^3	Caliper, mm	C_{11} GPa	C_{33} GPa	C_{13} GPa	C_{55} GPa
Layer 1	0.747	0.3158	8.964	0.272	0.00003	0.331
Layer 2	0.542	0.4538	4.381	0.056	0.00003	0.158
Layer 3	0.747	0.3158	8.964	0.272	0.00003	0.331

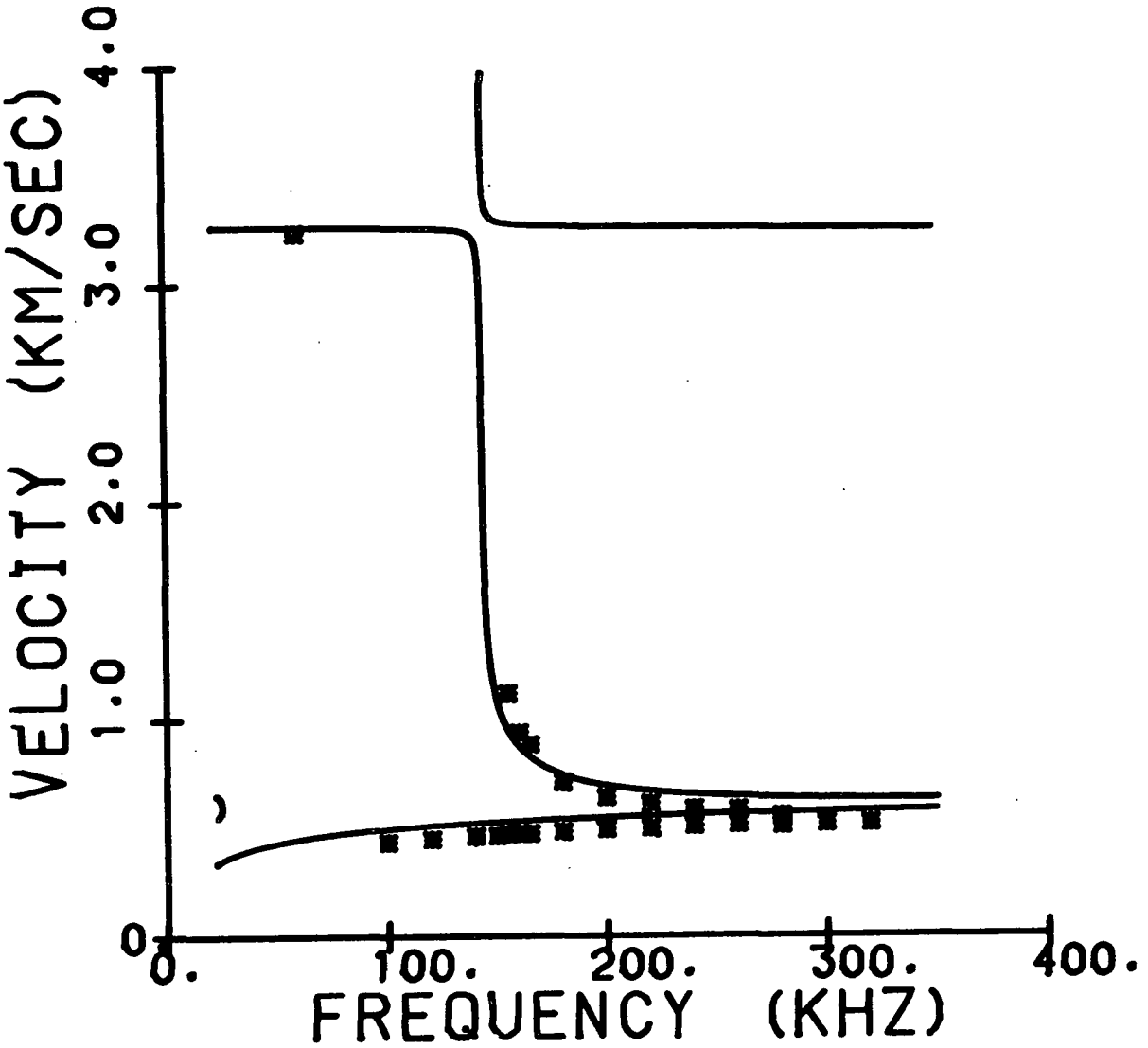

Sample 883 TK18 MD

	Density, g/cm^3	Caliper, mm	C_{11} GPa	C_{33} GPa	C_{13} GPa	C_{55} GPa
Layer 1	0.747	0.3158	8.964	0.272	0.00003	0.331
Layer 2	0.546	0.4434	3.046	0.064	0.00003	0.189
Layer 3	0.747	0.3158	8.964	0.272	0.00003	0.331

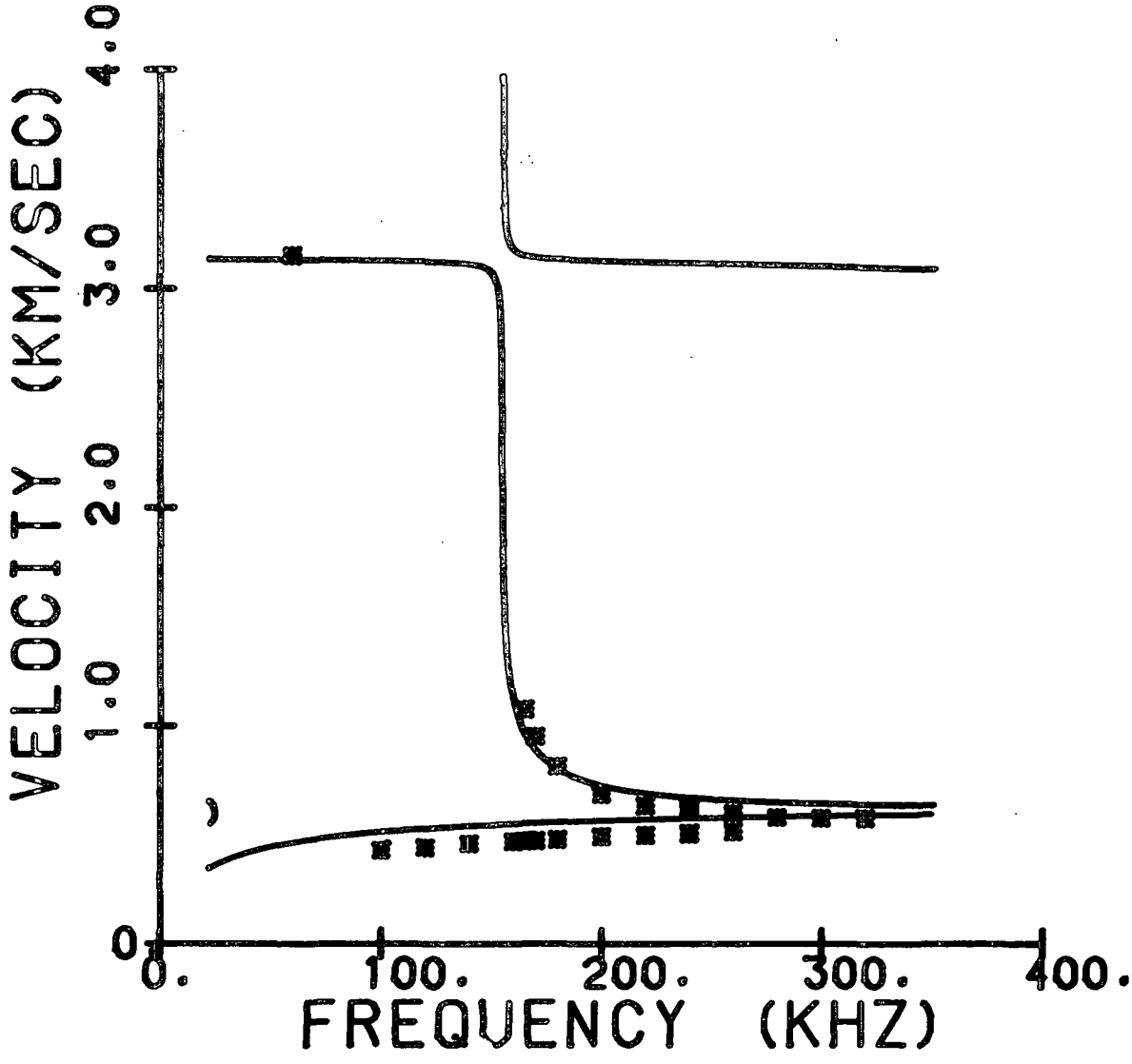

Sample 883 TK1 CD

	Density, g/cm^3	Caliper, mm	C_{22} GPa	C_{33} GPa	C_{23} GPa	C_{44} GPa
Layer 1	0.542	0.4538	5.151	0.056	0.00003	0.172
Layer 2	0.542	0.4538	5.151	0.056	0.00003	0.172
Layer 3	0.542	0.4538	5.151	0.056	0.00003	0.172

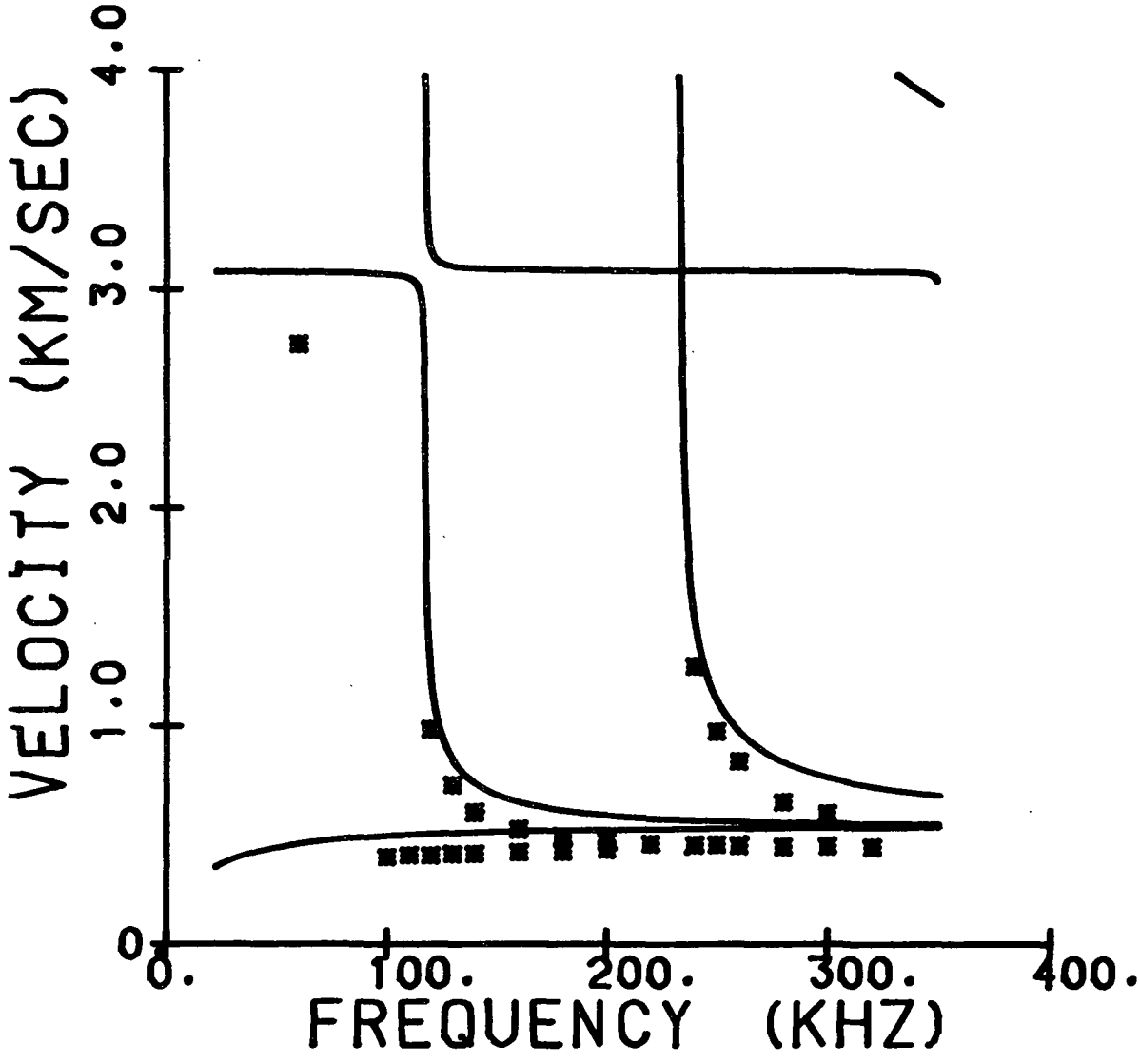

Sample 883 TK2 CD

	Density, g/cm^3	Caliper, mm	C_{22} GPa	C_{33} GPa	C_{23} GPa	C_{44} GPa
Layer 1	0.715	0.3103	6.222	0.270	0.00003	0.262
Layer 2	0.715	0.3103	6.222	0.270	0.00003	0.262
Layer 3	0.715	0.3103	6.222	0.270	0.00003	0.262

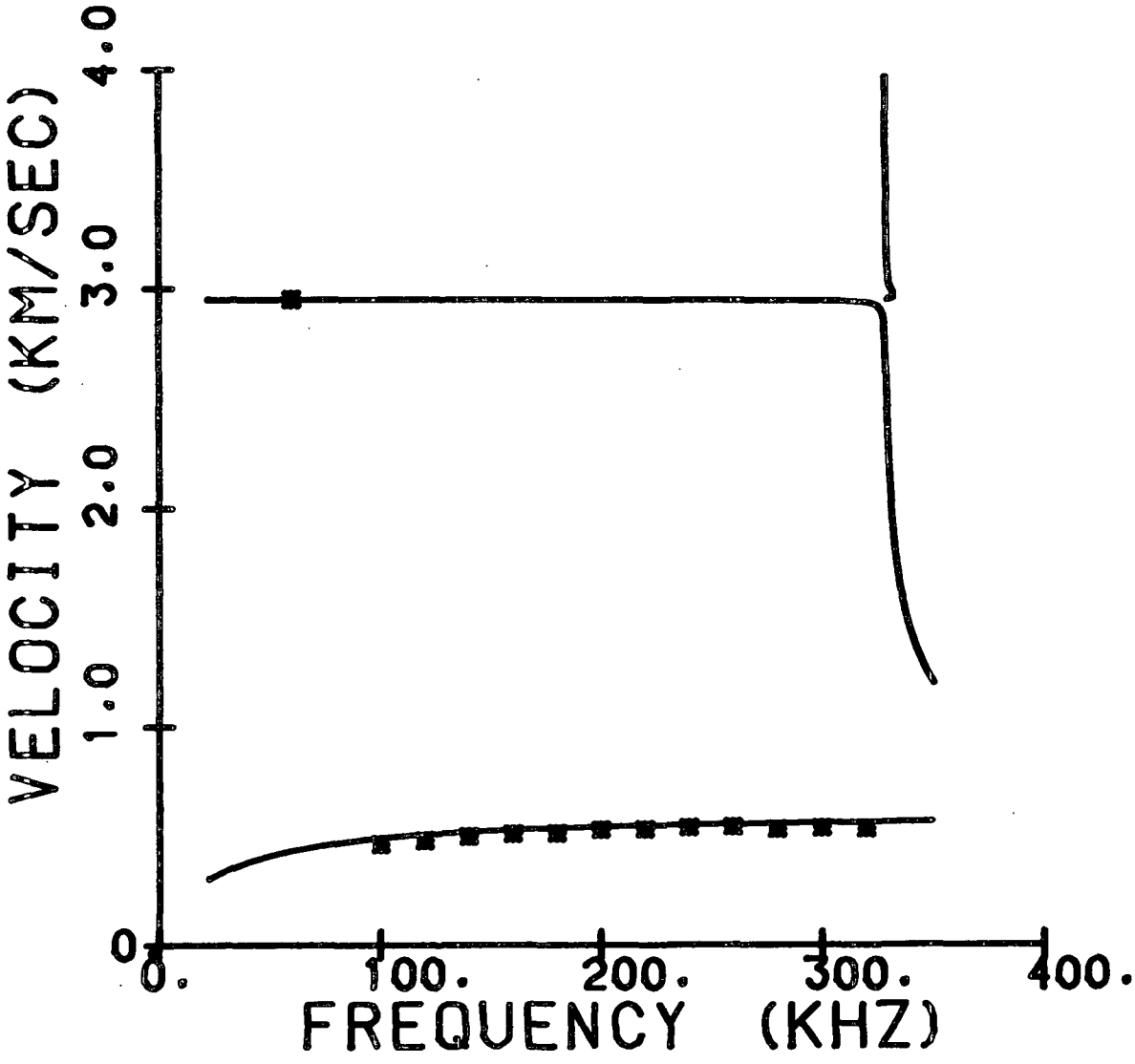

Sample 883 TK3 CD

	Density, g/cm^3	Caliper, mm	C_{22} GPa	C_{33} GPa	C_{23} GPa	C_{44} GPa
Layer 1	0.566	0.4450	6.404	0.071	0.00003	0.215
Layer 2	0.785	0.3158	5.862	0.312	0.00003	0.353
Layer 3	0.566	0.4450	6.404	0.071	0.00003	0.215

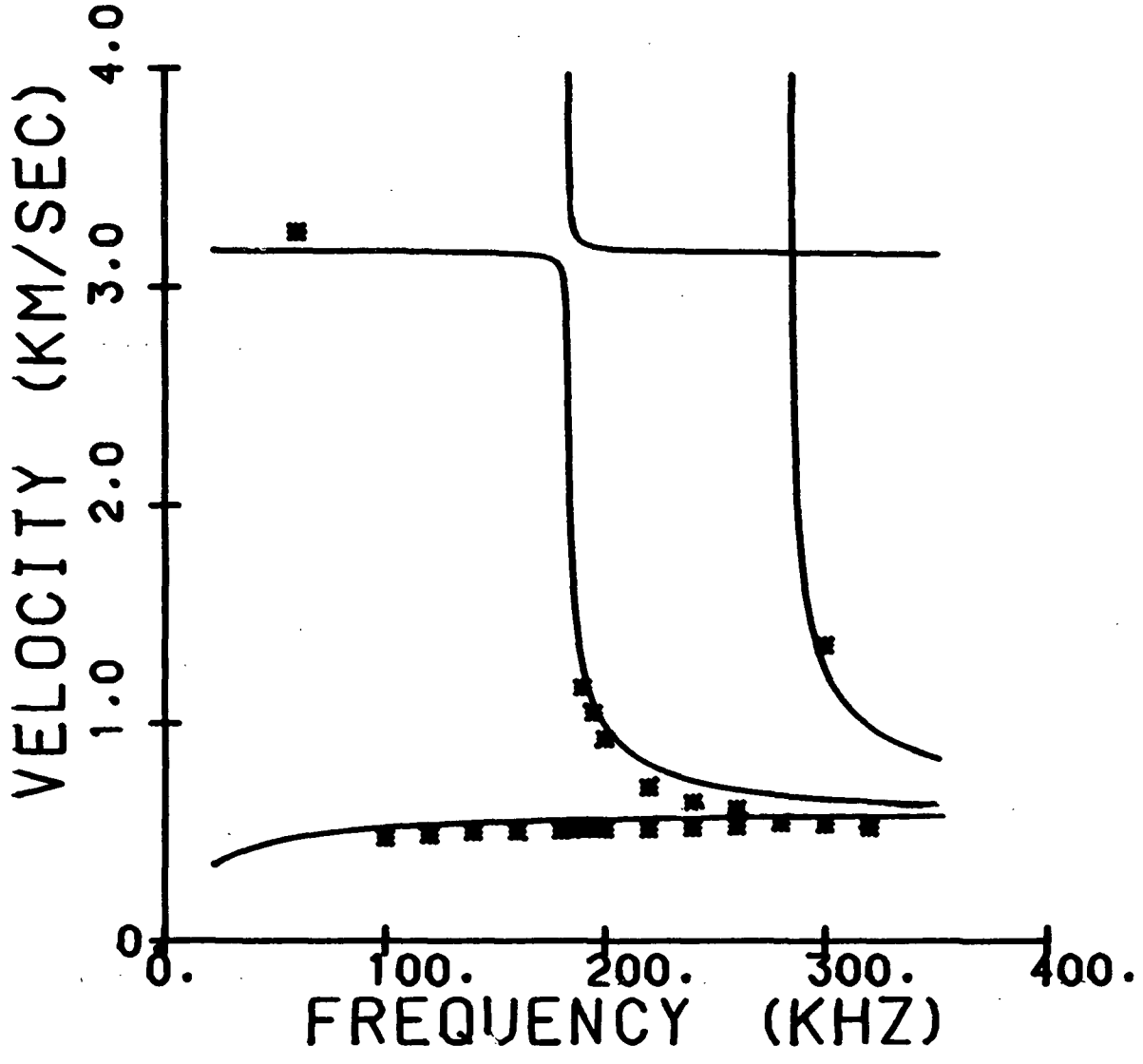

Sample 883 TK4 CD

	Density, g/cm^3	Caliper, mm	C_{22} GPa	C_{33} GPa	C_{23} GPa	C_{44} GPa
Layer 1	0.785	0.3158	5.862	0.312	0.00003	0.266
Layer 2	0.566	0.4450	6.404	0.071	0.00003	0.215
Layer 3	0.785	0.3158	5.862	0.312	0.00003	0.266

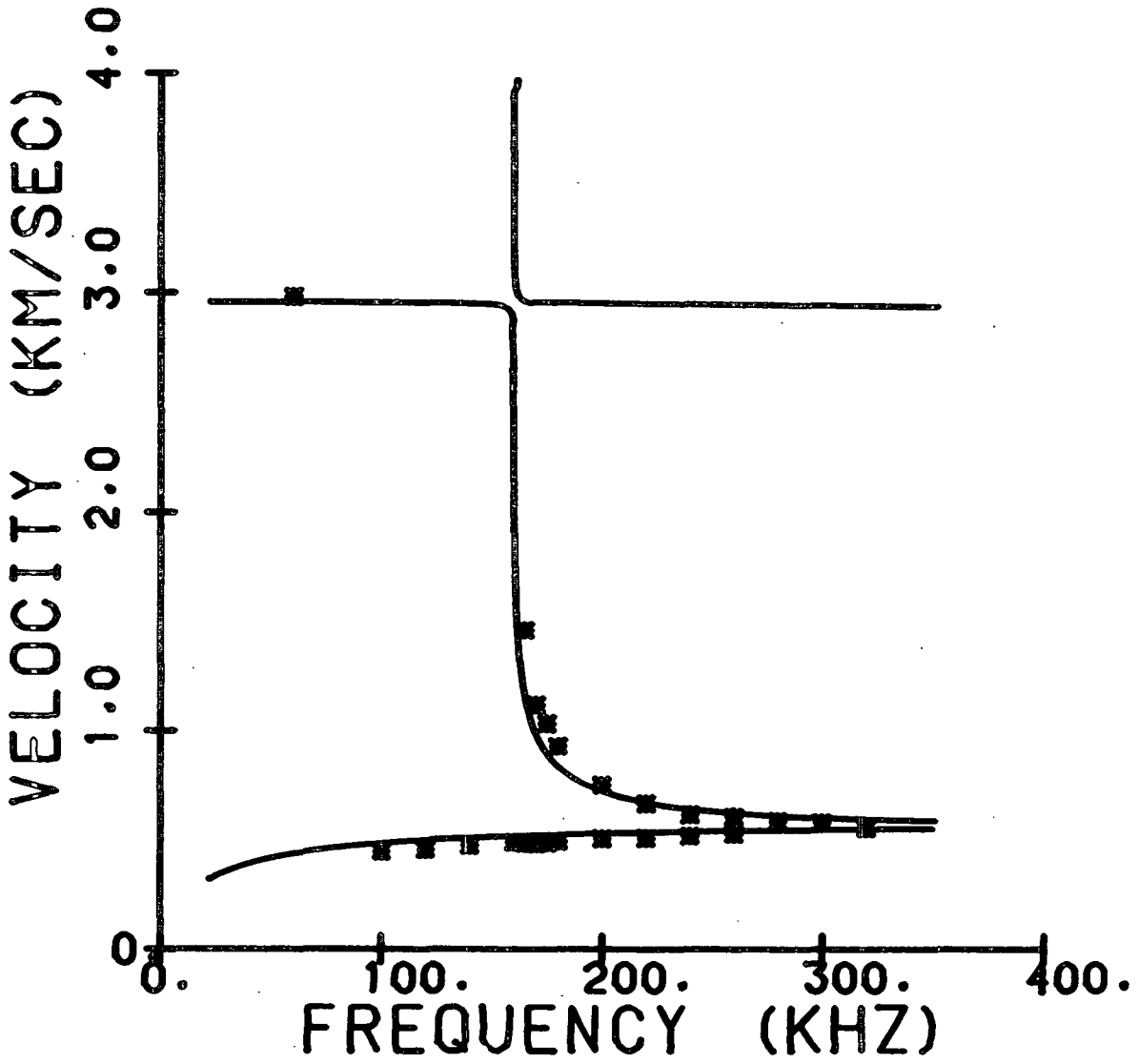

Sample 883 TK5 CD

	Density, g/cm^3	Caliper, mm	C_{22} GPa	C_{33} GPa	C_{23} GPa	C_{44} GPa
Layer 1	0.566	0.4450	6.404	0.071	0.00003	0.215
Layer 2	0.785	0.3158	5.862	0.312	0.00003	0.266
Layer 3	0.785	0.3158	5.862	0.312	0.00003	0.266

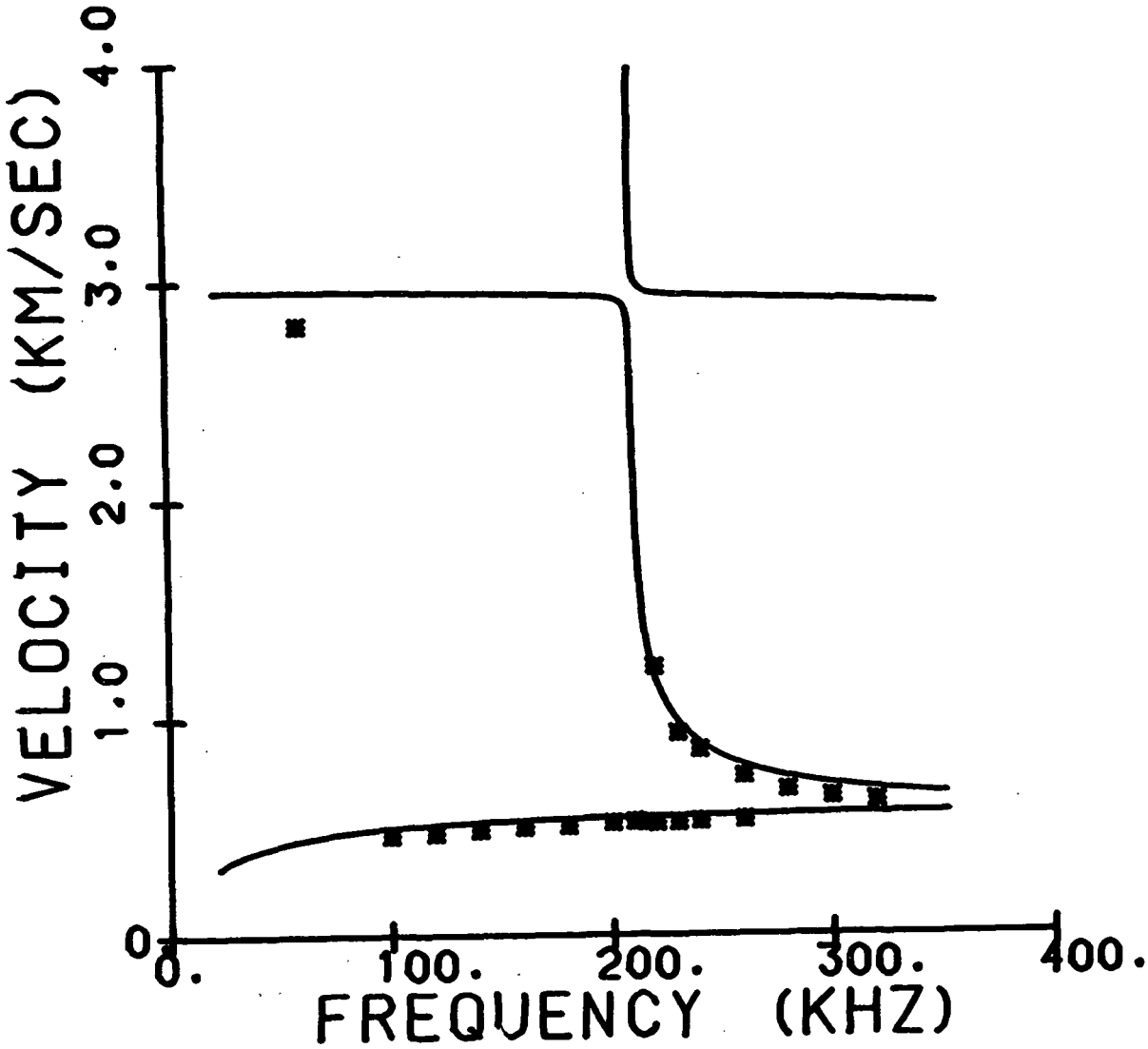

Sample 883 TK6 CD

	Density, g/cm^3	Caliper, mm	C_{22} GPa	C_{33} GPa	C_{23} GPa	C_{44} GPa
Layer 1	0.566	0.4450	6.404	0.071	0.00003	0.215
Layer 2	0.566	0.4450	6.404	0.071	0.00003	0.215
Layer 3	0.785	0.3158	5.862	0.312	0.00003	0.266

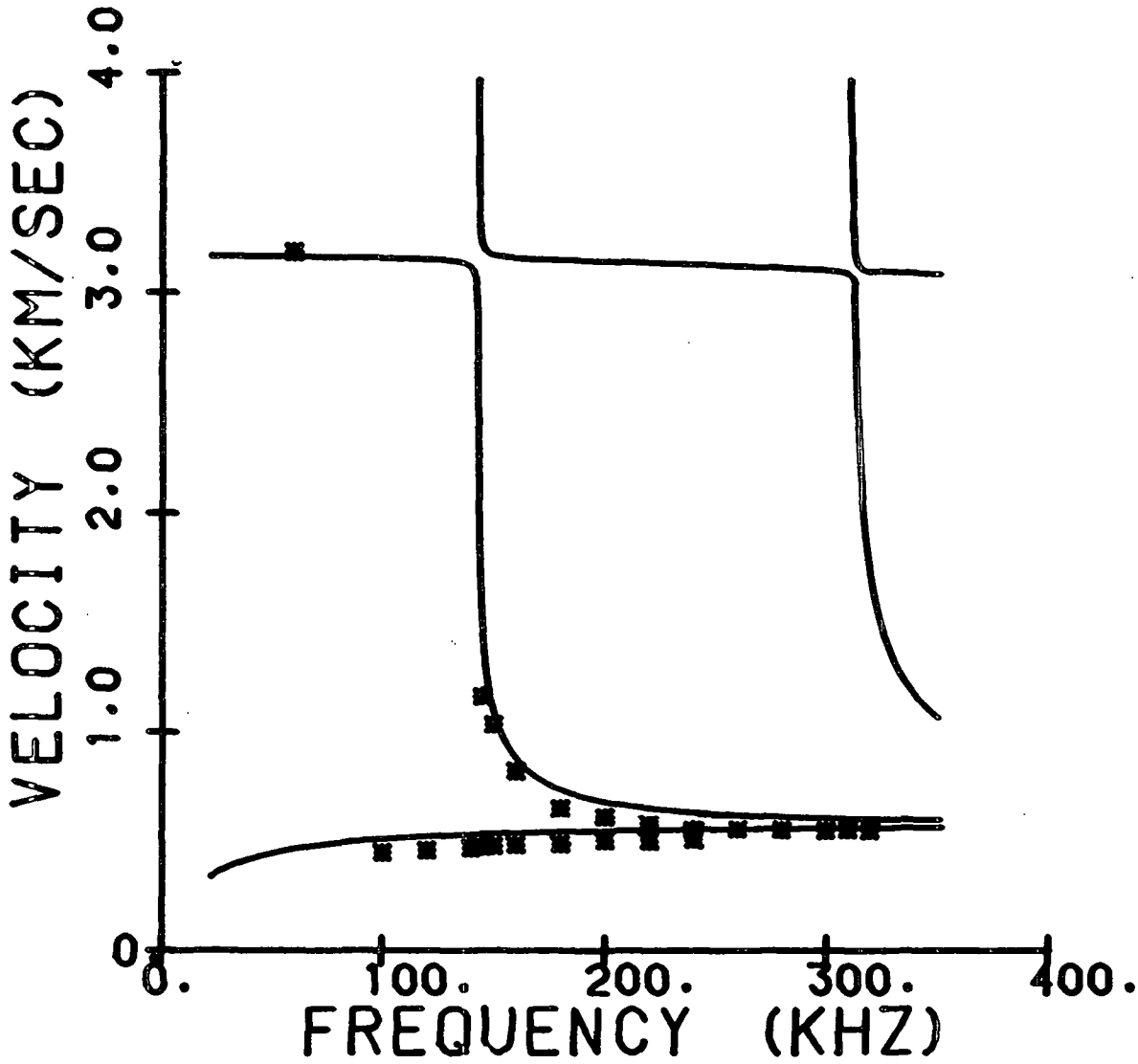

Sample 883 TK8 CD

	Density, g/cm^3	Caliper, mm	C_{22} GPa	C_{33} GPa	C_{23} GPa	C_{44} GPa
Layer 1	0.546	0.2217	6.718	0.064	0.00003	0.339
Layer 2	0.785	0.6316	5.862	0.312	0.00003	0.262
Layer 3	0.546	0.2217	6.718	0.064	0.00003	0.339

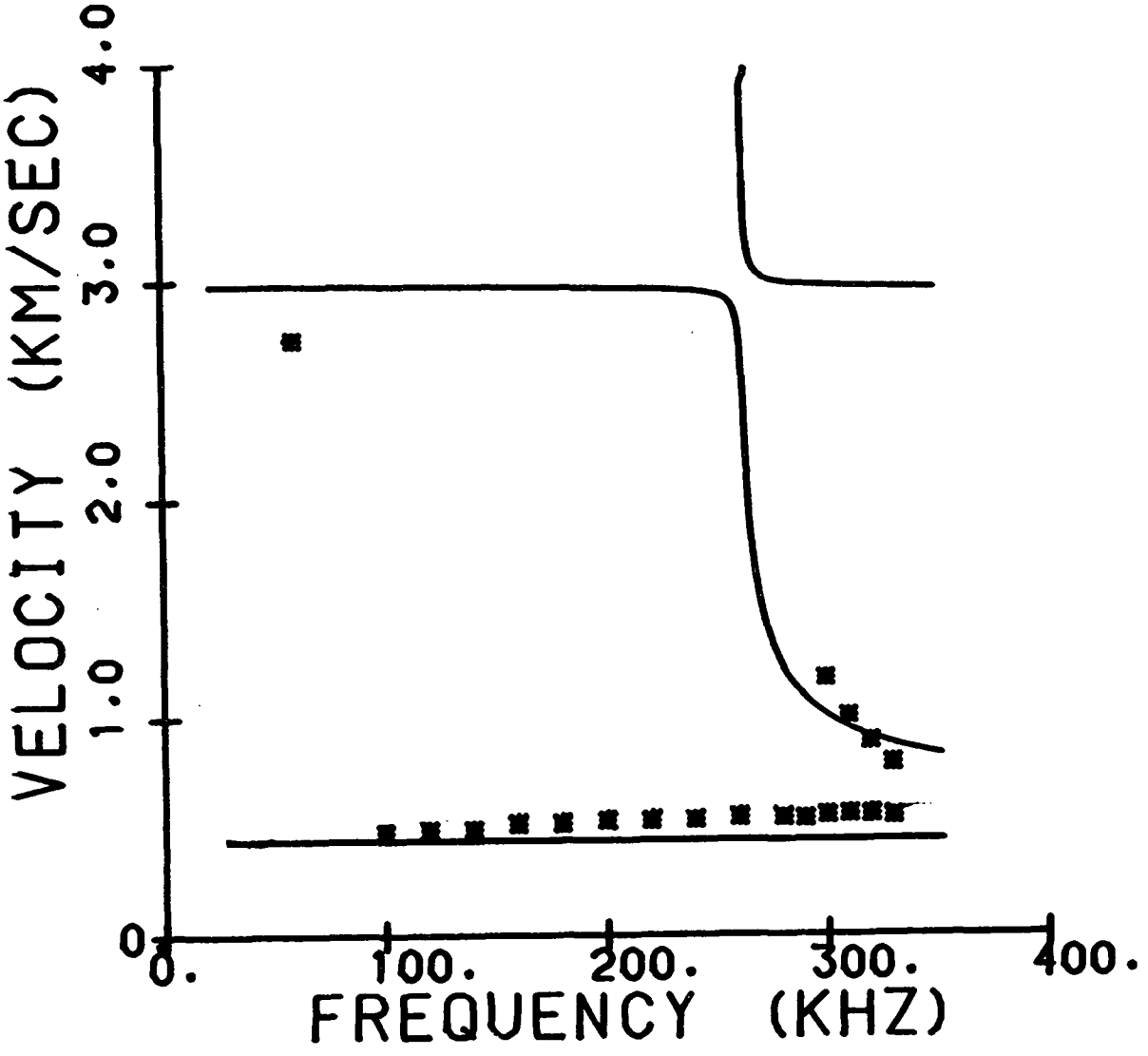

Sample 883 TK9 CD

	Density, g/cm^3	Caliper, mm	C_{22} GPa	C_{33} GPa	C_{23} GPa	C_{44} GPa
Layer 1	0.542	0.4538	5.151	0.056	0.00003	0.172
Layer 2	0.785	0.3158	5.862	0.312	0.00003	0.266
Layer 3	0.566	0.4450	6.404	0.071	0.00003	0.215

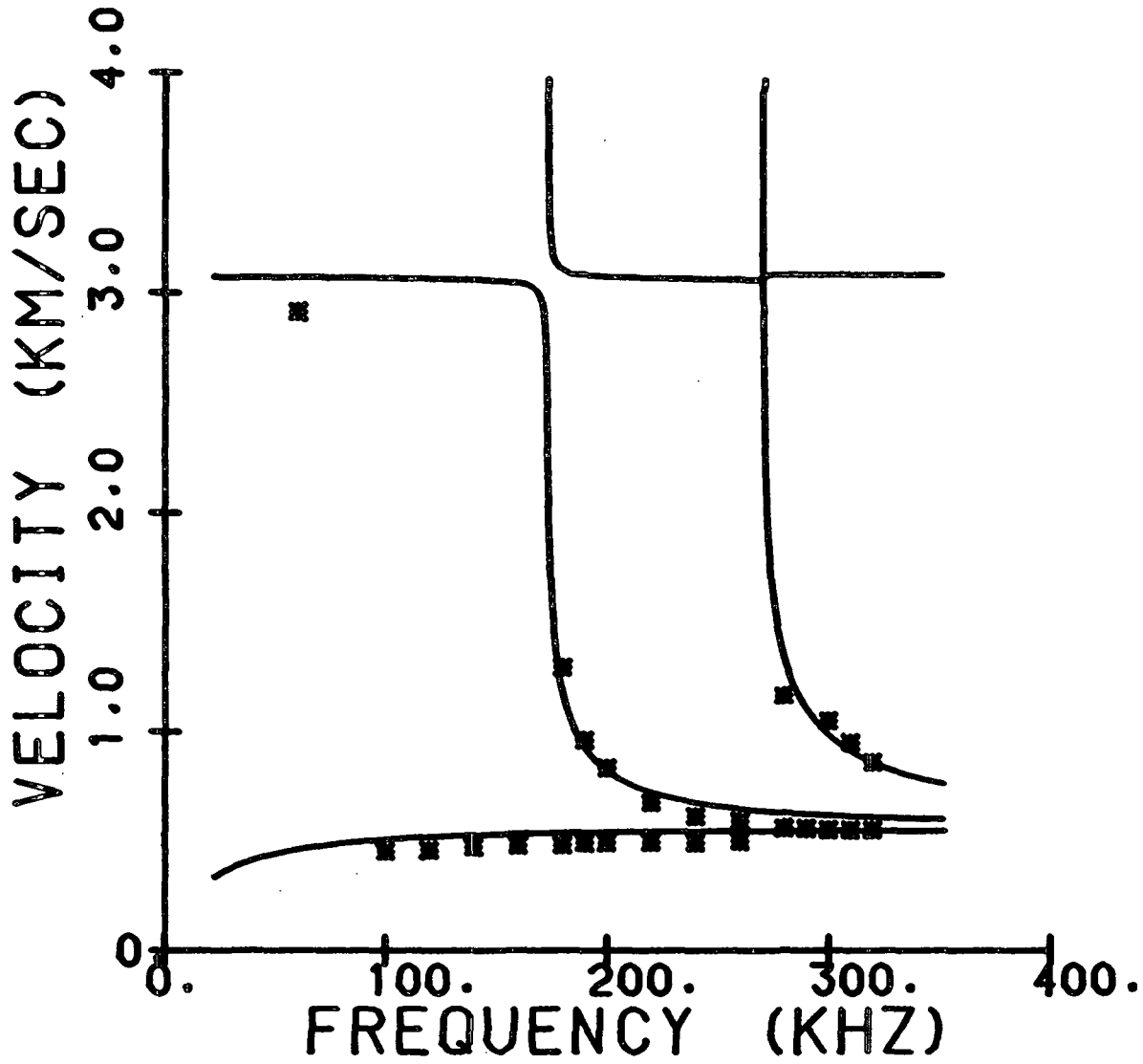

Sample 883 TK10 CD

	Density, g/cm^3	Caliper, mm	C_{22} GPa	C_{33} GPa	C_{23} GPa	C_{44} GPa
Layer 1	0.715	0.3103	6.222	0.270	0.00003	0.262
Layer 2	0.566	0.4450	6.404	0.071	0.00003	0.215
Layer 3	0.785	0.3158	5.862	0.312	0.00003	0.266

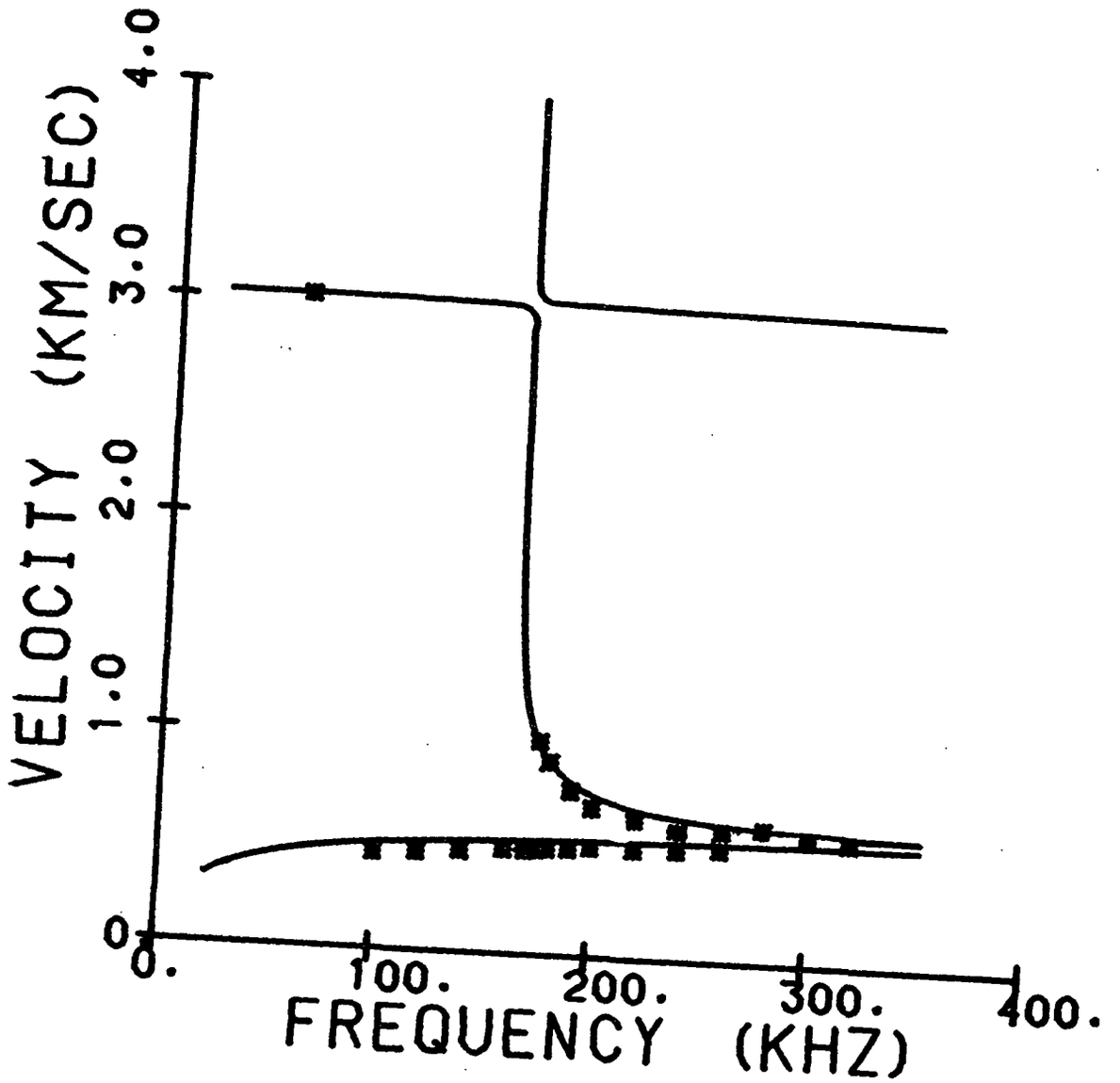

Sample 883 TK11 CD

	Density, g/cm^3	Caliper, mm	C_{22} GPa	C_{33} GPa	C_{23} GPa	C_{44} GPa
Layer 1	0.566	0.4450	6.404	0.071	0.00003	0.215
Layer 2	0.715	0.3103	6.222	0.071	0.00003	0.262
Layer 3	0.785	0.3158	5.862	0.312	0.00003	0.266

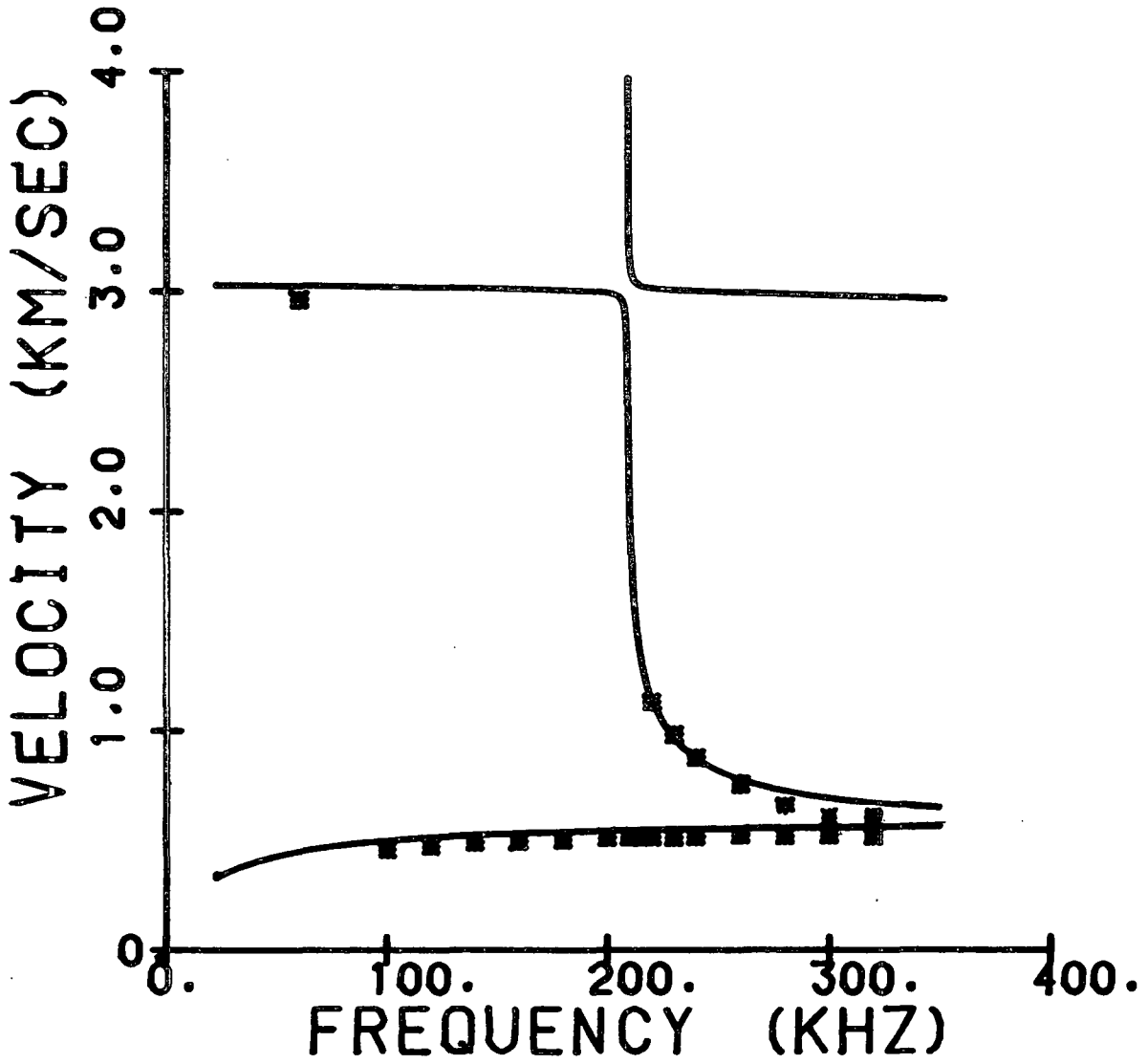

Sample 883 TK12 CD

	Density, g/cm^3	Caliper, mm	C_{22} GPa	C_{33} GPa	C_{23} GPa	C_{44} GPa
Layer 1	0.785	0.3158	5.862	0.312	0.00003	0.266
Layer 2	0.542	0.4538	5.151	0.056	0.00003	0.172
Layer 3	0.566	0.4450	6.404	0.071	0.00003	0.215

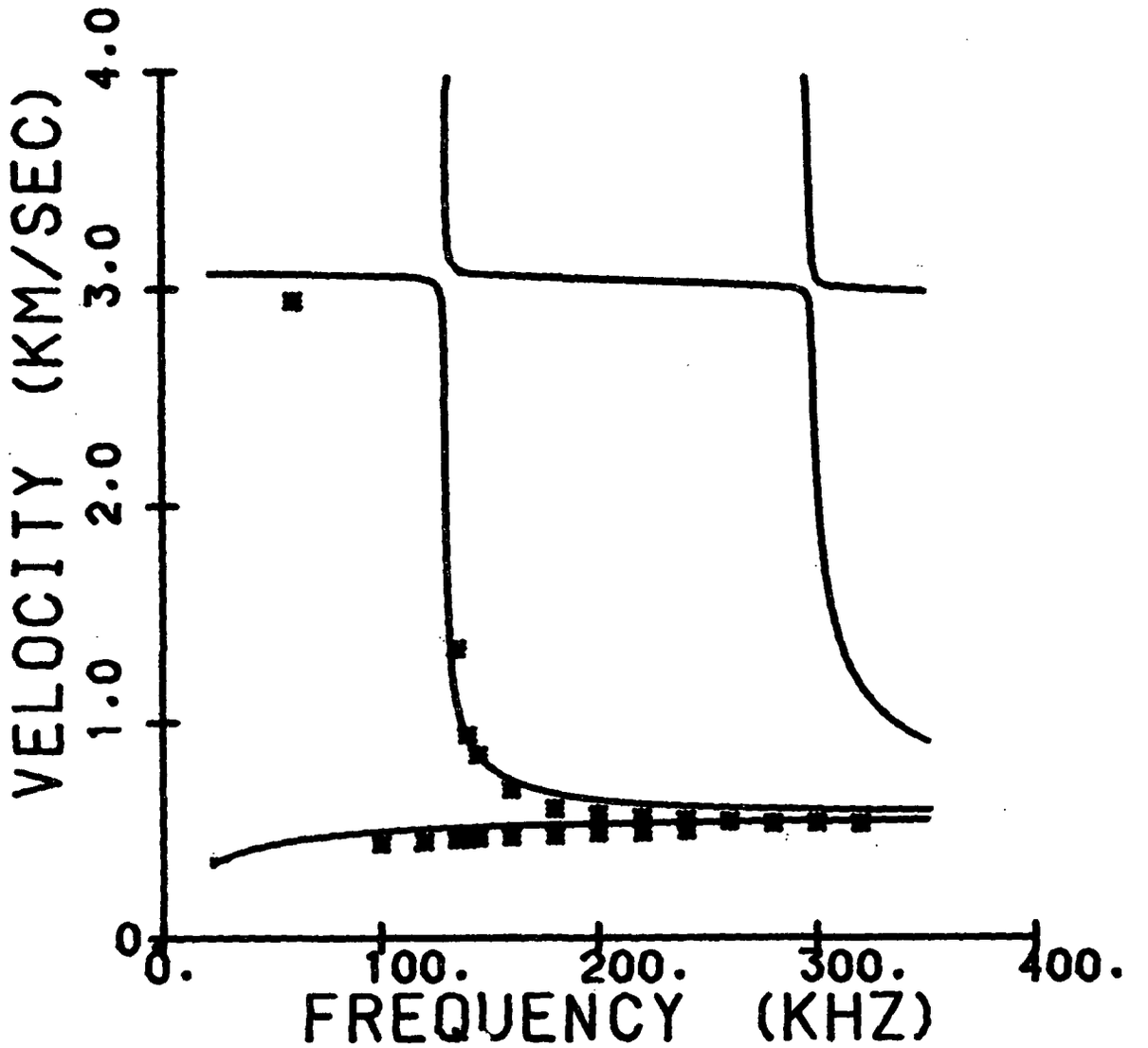

Sample 883 TK13 CD

	Density, g/cm^3	Caliper, mm	C_{22} GPa	C_{33} GPa	C_{23} GPa	C_{44} GPa
Layer 1	0.546	0.4434	6.718	0.064	0.00003	0.339
Layer 2	0.747	0.3158	5.126	0.272	0.00003	0.282
Layer 3	0.546	0.4434	6.718	0.064	0.00003	0.339

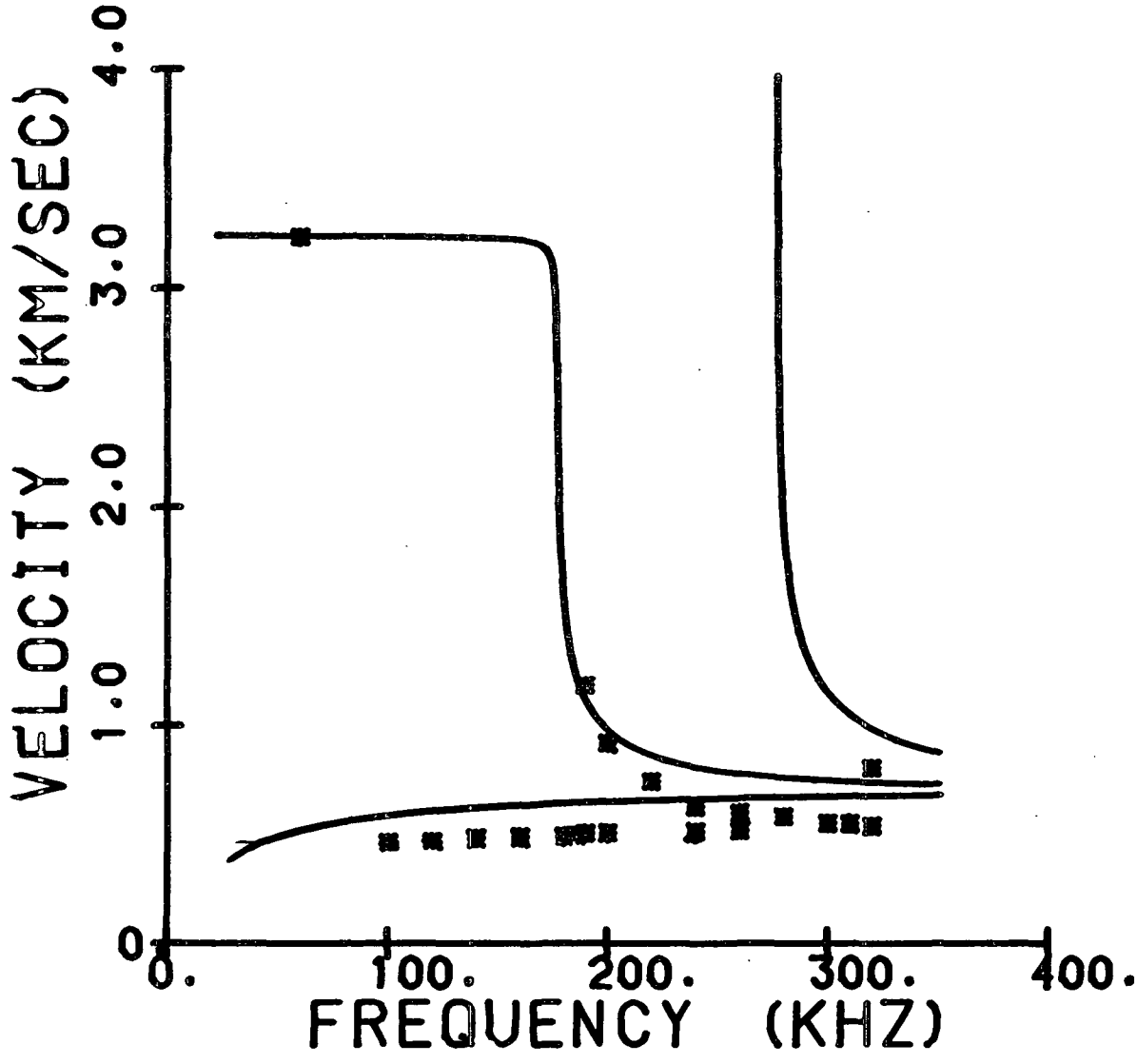

Sample 883 TK14 CD

	Density, g/cm^3	Caliper, mm	C_{22} GPa	C_{33} GPa	C_{23} GPa	C_{44} GPa
Layer 1	0.507	0.4456	4.667	0.050	0.00003	0.201
Layer 2	0.507	0.4456	4.667	0.050	0.00003	0.201
Layer 3	0.507	0.4456	4.667	0.050	0.00003	0.201

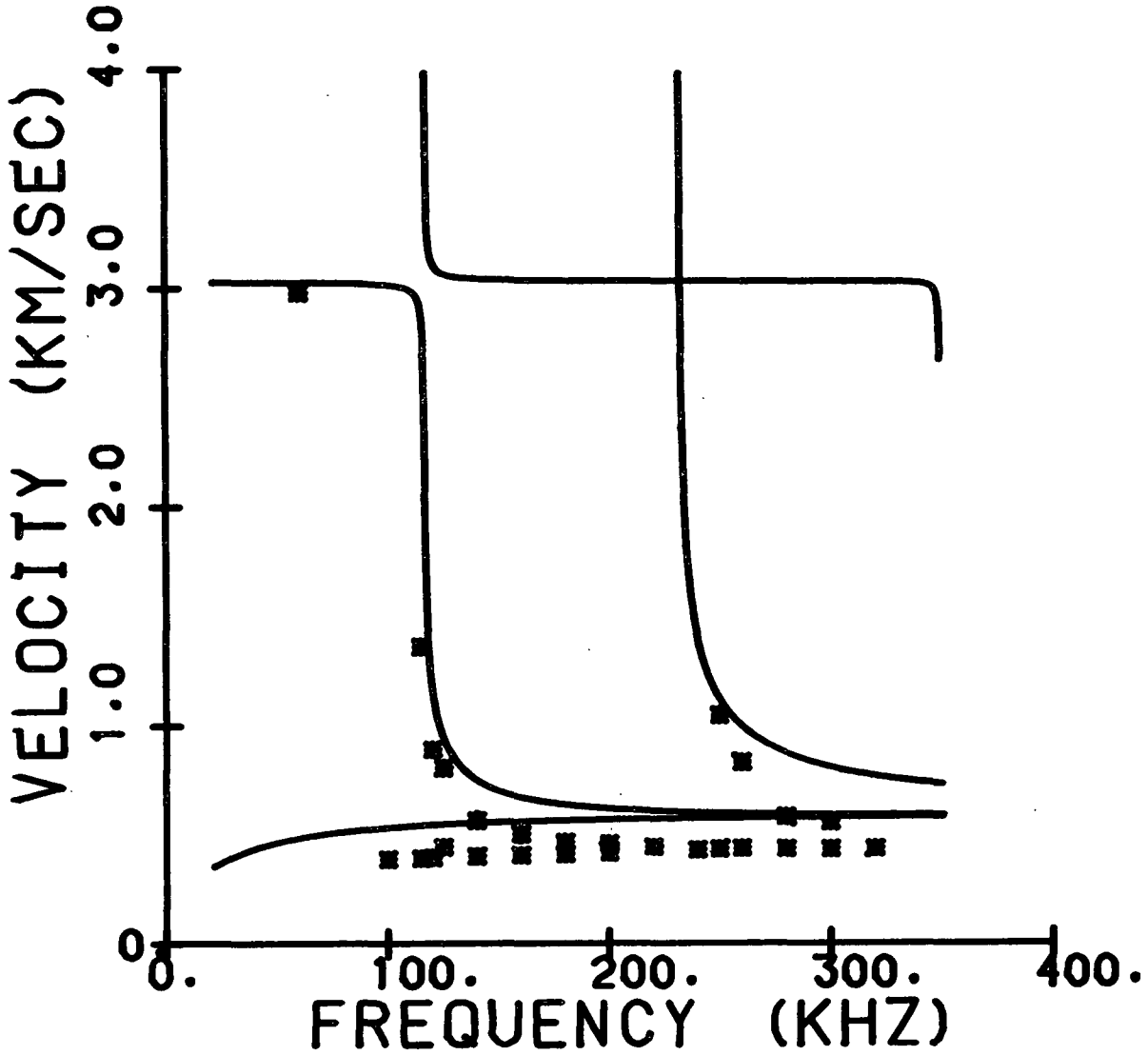

Sample 883 TK15 CD

	Density, g/cm^3	Caliper, mm	C_{22} GPa	C_{33} GPa	C_{23} GPa	C_{44} GPa
Layer 1	0.735	0.3130	6.505	0.251	0.00003	0.369
Layer 2	0.735	0.3130	6.505	0.251	0.00003	0.369
Layer 3	0.735	0.3130	6.505	0.251	0.00003	0.369

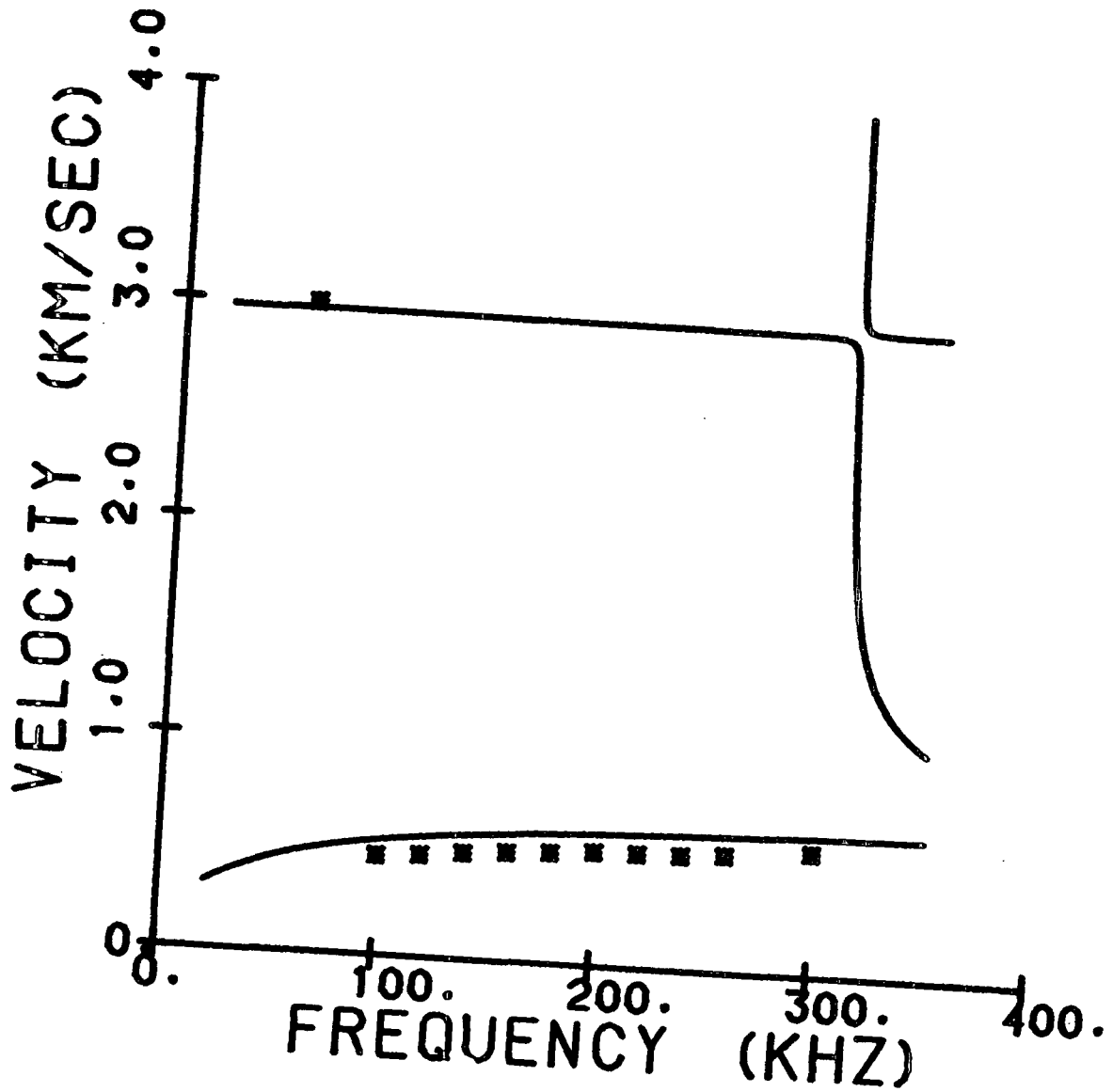

Sample 883 TK16 CD

	Density, g/cm^3	Caliper, mm	C_{22} GPa	C_{33} GPa	C_{23} GPa	C_{44} GPa
Layer 1	0.546	0.4434	6.718	0.064	0.00003	0.339
Layer 2	0.715	0.3103	6.222	0.071	0.00003	0.262
Layer 3	0.546	0.4434	6.718	0.064	0.00003	0.339

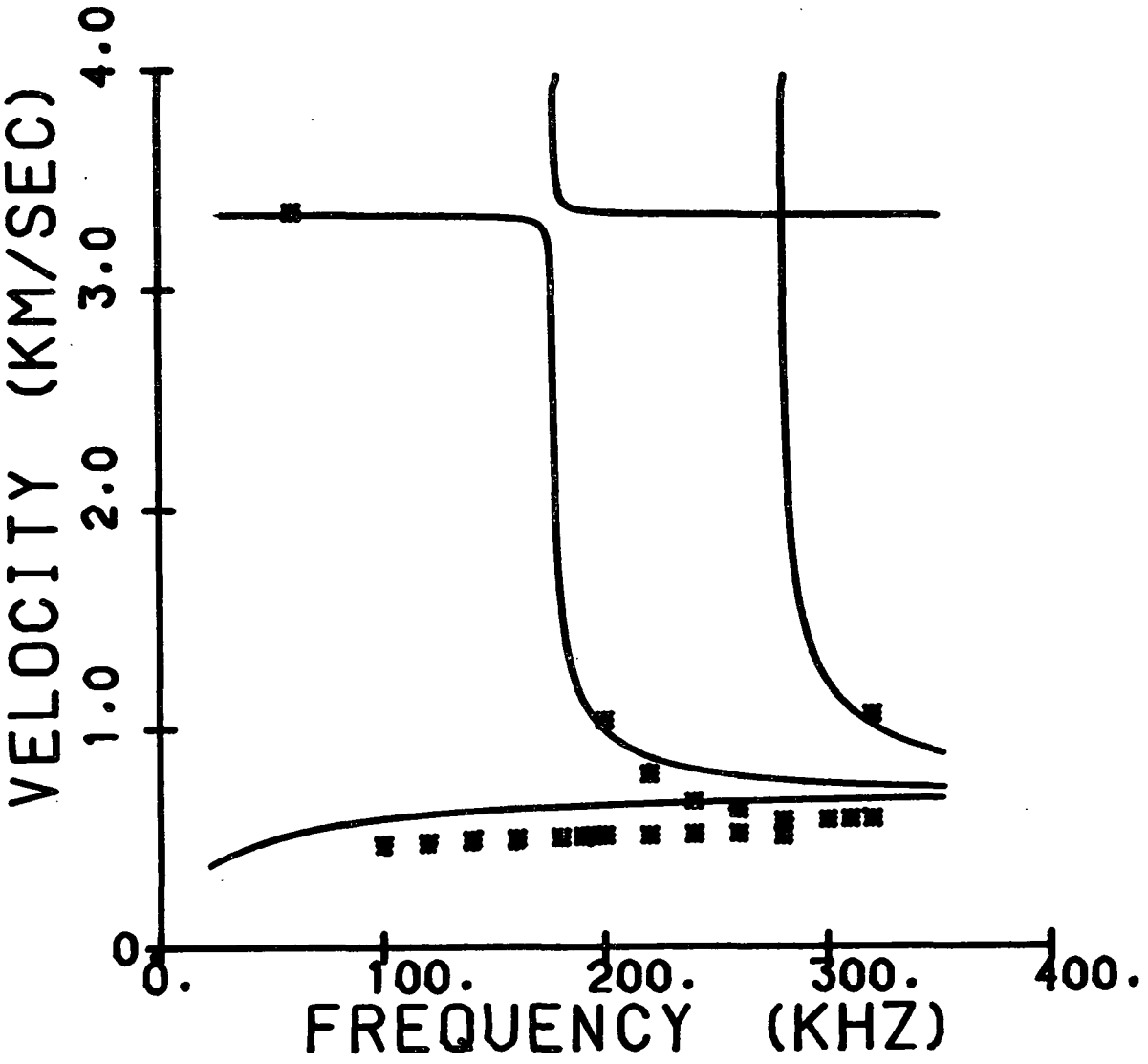

Sample 883 TK17 CD

	Density, g/cm^3	Caliper, mm	C_{22} GPa	C_{33} GPa	C_{23} GPa	C_{44} GPa
Layer 1	0.747	0.3158	5.126	0.272	0.00003	0.282
Layer 2	0.542	0.4538	5.151	0.056	0.00003	0.172
Layer 3	0.747	0.3158	5.126	0.272	0.00003	0.282

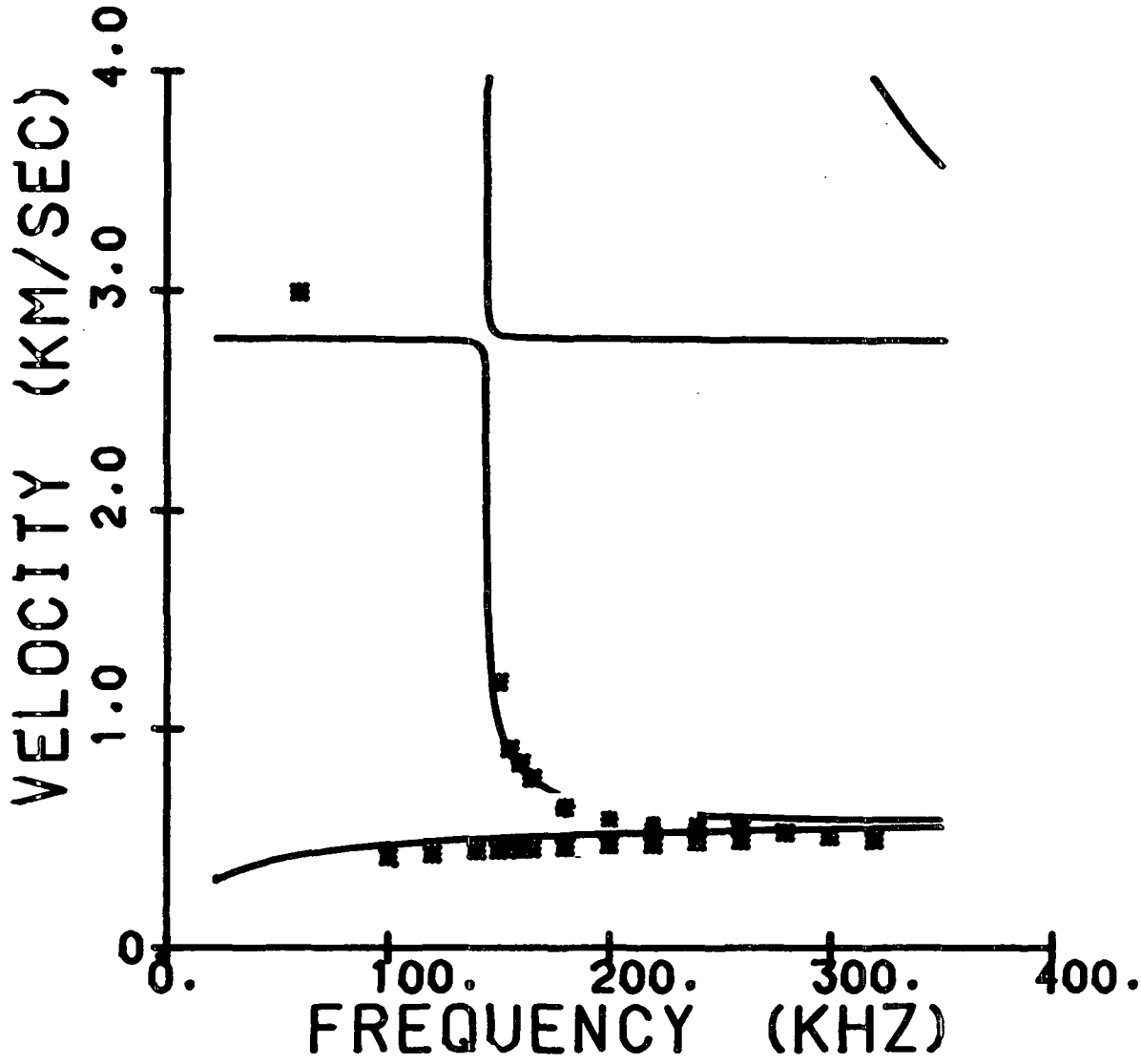

Sample 883 TK18 CD

	Density, g/cm^3	Caliper, mm	C_{22} GPa	C_{33} GPa	C_{23} GPa	C_{44} GPa
Layer 1	0.747	0.3158	5.126	0.272	0.00003	0.282
Layer 2	0.546	0.4434	6.718	0.064	0.00003	0.339
Layer 3	0.747	0.3158	5.126	0.272	0.00003	0.282

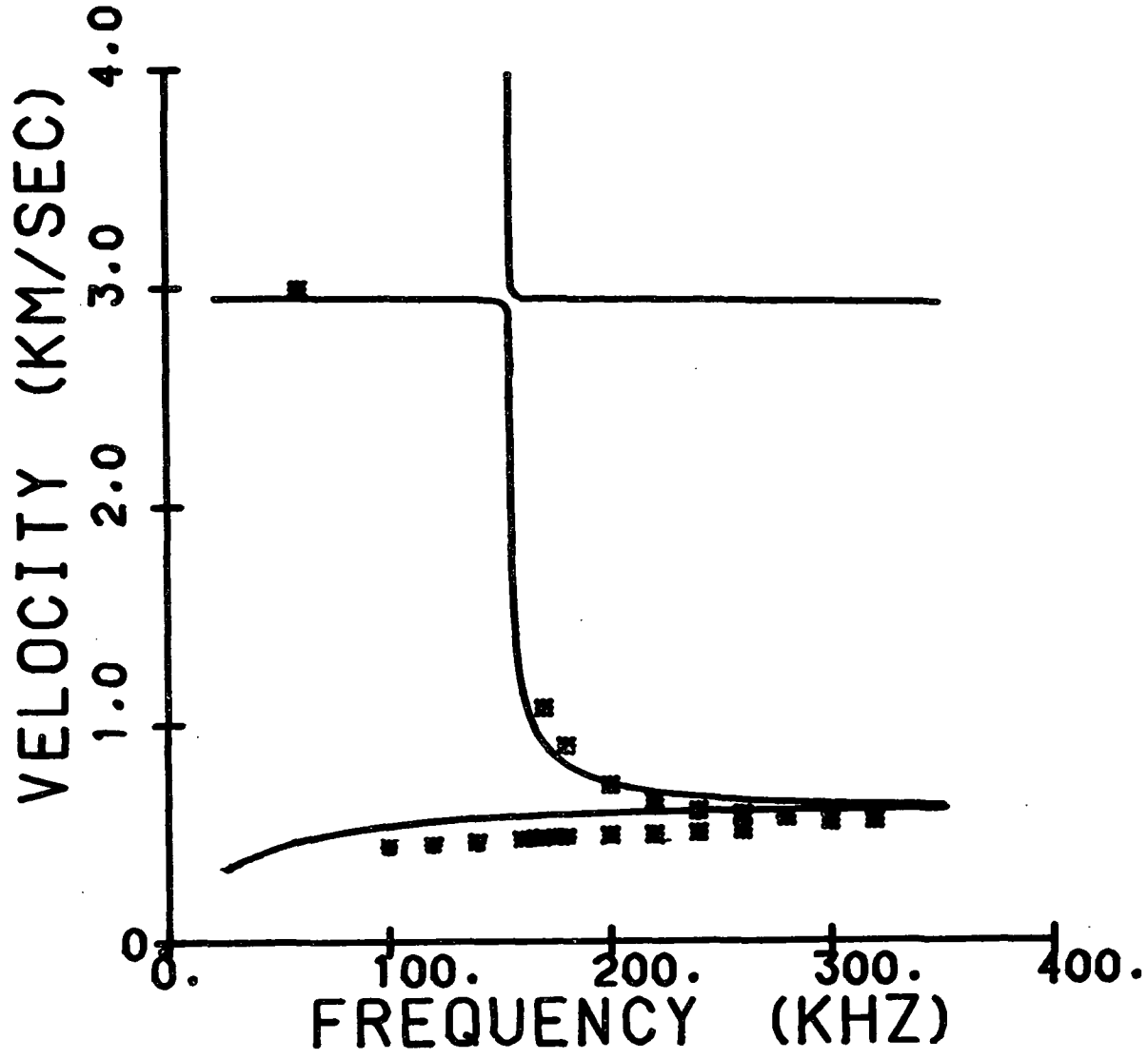

APPENDIX IV

Appendix IV contains the FORTRAN code for the two computer programs, RETRACE2 and RETRACE3. RETRACE2 calculates the dispersion curves for a two layer composite and RETRACE3 calculates the dispersion curves for a three layer composite.

```
WORKFILE: RETRACE2 (08/21/85)

      100     $RESET FREE
      200     $SET OWN
      300     FILE  1(TITLE="FILE1.",FILETYPE=7)
      400     FILE  2(TITLE="FILE2.",KIND=DISK,MAXRECSIZE=14,
      500           + AREAS=36000,AREASIZE=14,PROTECTION=SAVE)
      600     FILE  3(TITLE="FILE3.",KIND=DISK,MAXRECSIZE=14,
      700           + AREAS=36000,AREASIZE=14,PROTECTION=SAVE)
      800     $SET FREE
      900     DIMENSION F(1000),V(1000)
     1000     C-  THE PROGRAM RETRACE2 CALCULATES THE DISPERSION CURVES FOR A TWO
     1100     C-  LAYER COMPOSITE MATERIAL CONSTRUCTED FROM TWO ORTHOTROPIC LAYERS.
     1200     C-  THE LAYER DENSITIES (ARHO AND BRHO) ARE ENTERED IN G/MM3.  THE
     1300     C-  LAYER CALIPERS (AZ AND BZ) ARE ENTERED IN MM.  THE ELASTIC
     1400     C-  CONSTANTS (AC11,AC33,...BC13,BC55) ARE ENTERED IN GPA X 10-3.
     1500     C-  THE PROGRAM FINDS THE DISPERSION CURVES BY FIRST FINDING A
     1600     C-  POINT ON ONE OF THE CURVES, AND THEN TRACING THE OTHER POINTS
     1700     C-  ON THE CURVE.  THE CURVES ARE OBTAINED IN THE REGION OF
     1800     C-  VELOCITIES BETWEEN 0.2 AND 3.5 M/SEC AND FREQUENCIES BETWEEN
     1900     C-  0.2 AND 3.5 KHZ.  THE POINTS ON THE CURVES ARE LOCATED BY
     2000     C-  FINDING THE VALUES OF FREQUENCY AND VELOCITY WHICH SET THE
     2100     C-  DETERMINANT EQUAL TO ZERO.
     2200     C-  EPS= THE TOLERANCE ON THE ANGLE THETA
     2300     C-  THSP= THE INITIAL ANGLE SEARCHED RELATIVE TO THETA
     2400     C-  STEP= THE STEP LENGTH (RADIUS OF SEARCH ARC)
     2500     C-  AFTER FINDING A POINT ON THE CURVE, THE PROGRAM SEARCHES FOR
     2600     C-  THE NEXT POINT ALONG AN ARC OF RADIUS "STEP".  THE VALUES OF THE
     2700     C-  DETERMINANT ARE CALCULATED AT THREE ANGLES (THETA,THETAP,THETAN).
     2800     C-  THE SEARCH ROUTINE FINDS THE ANGLE WHICH MINIMIZES THE
     2900     C-  DETERMINANT.
     3000     COMPLEX DETERM
     3100     COMMON ARHO,AZ,AC11,AC33,AC13,AC55,C
     3200     COMMON BRHO,BZ,BC11,BC33,BC13,BC55
     3300     C-  READ INPUT DATA
     3400     READ(1,700) ARHO,AZ,AC11,AC33,AC13,AC55
     3500      700 FORMAT(6F12.8)
     3700     READ(1,700) BRHO,BZ,BC11,BC33,BC13,BC55
     3800     A=0.0
     3900     B=0.0
     4000     C=1.0
     4100     K=0
     4200     N=0
     4300     EPS=1.0E-03
     4400     THSP=0.01
     4500     STEP=0.01
     4600     C-  FIND POINTS ON THE CURVES NEAR THE VELOCITY AXIS
     4700     DO 5 I=20,400
     4800     VEL=I*0.01
     4900     FREQ=0.2
     5000     TMPR2=TMPR1
     5100     TMPI2=TMPI1
     5200     TMPR1=DETR
     5300     TMPI1=DETI
     5400     CALL DISP(DETERM,FREQ,VEL)
     5500     DETR=REAL(DETERM)*10000000000C00C0.
     5600     DETI=AIMAG(DETERM)*1CC0000000000000.
     5700     IF(C.LE.C.0) GO TO 30
     5800     C-  HAS A MINIMUM IN DETR ON DETI BEEN REACHED
     5900     IF((TMPR1.LT.DETR).AND.(TMPR1.LT.TMPR2)) GO TO 3
     6000     IF((ABS(TMPI1).LT.ABS(DETI)).AND.(ABS(TMPI1).LT.ABS(TMPI2)))
```

```
 6100     - GO TO 3
 6200     C-  HAVE DETR OR DETI CHANGED SIGN
 6300     IF((DETR*TMPR1).LT.0.0) GO TO 3
 6400     IF((DETI*TMPI1).LT.0.0) GO TO 3
 6500     GO TO 5
 6600     3 N=N+1
 6700     C-  INITIAL POINT A,B
 6800     F(N)=A
 6900     V(N)=B
 7000     C-  INITIAL VALUE OF THETA - START SEARCH ROUTINE
 7100     THETA=0.0
 7200      4 THETAP=THETA+THSP
 7300     THETAN=THETA-THSP
 7400     K=0
 7500     C-  IF CURVE TRACES BACK ON ITSELF, STOP SEARCH ROUTINE
 7600     IF(COS(THETA).LT.-0.05) GO TO 5
 7700     C-  IS THE ESTIMATE OF THE ANGLE CLOSE ENOUGH
 7800     200 IF((THETAP-THETAN).LE.EPS) GO TO 600
 7900     C-  FIND A NEW SET OF THREE ANGLES
 8000     FREQ2=FREQ+STEP*COS(THETA)
 8100     VEL2=VEL+STEP*SIN(THETA)
 8200     CALL DISP(DETERM,FREQ2,VEL2)
 8300     VAL=ABS(REAL(DETERM))+ABS(AIMAG(DETERM))
 8400     FREQ2=FREQ+STEP*COS(THETAP)
 8500     VEL2=VEL+STEP*SIN(THETAP)
 8600     CALL DISP(DETERM,FREQ2,VEL2)
 8700     VALP=ABS(REAL(DETERM))+ABS(AIMAG(DETERM))
 8800     FREQ2=FREQ+STEP*COS(THETAN)
 8900     VEL2=VEL+STEP*SIN(THETAN)
 9000     CALL DISP(DETERM,FREQ2,VEL2)
 9100     VALN=ABS(REAL(DETERM))+ABS(AIMAG(DETERM))
 9200     IF(VAL.GT.VALN) GO TO 300
 9300     IF(VAL.GT.VALP) GO TO 400
 9400     IF(VALP.GT.VALN) GO TO 500
 9500     THETAN=THETA
 9600     THETA=(THETAN+THETAP)/2.
 9700     K=1
 9800     GO TO 200
 9900     500 THETAP=THETA
10000     THETA=(THETAP+THETAN)/2.
10100     K=1
10200     GO TO 200
10300      300  THETAP=THETA
10400     THETA=THETAN
10500     THETAN=THETAN-THSP
10600     IF(K.GT.0) THETAN=THETA-ABS(THETAP-THETA)
10700     GO TO 200
10800      400  THETAN=THETA
10900     THETA=THETAP
11000     THETAP=THETAP+THSP
11100     IF(K.GT.0) THETAP=THETA+ABS(THETA-THETAN)
11200     GO TO 200
11300     C-  NEXT POINT HAS BEEN FOUND
11400     600 FREQ=FREQ+STEP*COS(THETA)
11500     VEL=VEL+STEP*SIN(THETA)
11600     N=N+1
11700     F(N)=FREQ
11800     V(N)=VEL
11900     2000 FORMAT(2F20.8)
12000     C-  IS THE NEW POINT WITHIN THE SEARCH AREA
12100     IF(FREQ.GT.3.5) GO TO 7
12200     IF(FREQ.LT.0.0) GO TO 7
```

```
      IF(VEL.GT.4.0) GO TO 7
      IF(VEL.LT.0.0) GO TO 7
      GO TO 4
       7 DETR=0.0
      DETI=0.0
      C=0.
      GO TO 5
       30 C=1.0
      I=I+50
      5 CONTINUE
C-   SEARCH FOR A CURVE AT VELOCITY 3.5 M/SEC
C-   FREQUENCY 0.2-3.5 KHZ
C-   SEARCH METHOD IS SAME AS USED ABOVE
      DO 15 I=10,2000
      VEL=4.0
      FREQ=I*0.002
      TMPR1=DETR*10000000000000000.
      TMPI1=DETI*10000000000000000.
      CALL DISP(DETERM,FREQ,VEL)
      IF(C.EQ.0.0) GO TO 31
      DETR=REAL(DETERM)
      DETI=AIMAG(DETERM)
      IF(TMPR1*DETR) 13,12,12
      12 IF(TMPI1*DETI)13,15,15
      13 N=N+1
      F(N)=A
      V(N)=B
      FREQ=FREQ-0.001
      THETA=-0.785398163
      14 THETAP=THETA+THSP
      THETAN=THETA-THSP
      IF(COS(THETA).LT.-0.3) GO TO 15
      1200 IF((THETAP-THETAN).LE.EPS) GO TO 1600
      FREQ2=FREQ+STEP*COS(THETA)
      VEL2=VEL+STEP*SIN(THETA)
      CALL DISP(DETERM,FREQ2,VEL2)
      VAL=ABS(REAL(DETERM)+AIMAG(DETERM))
      FREQ2=FREQ+STEP*COS(THETAP)
      VEL2=VEL+STEP*SIN(THETAP)
      CALL DISP(DETERM,FREQ2,VEL2)
      VALP=ABS(REAL(DETERM)+AIMAG(DETERM))
      FREQ2=FREQ+STEP*COS(THETAN)
      VEL2=VEL+STEP*SIN(THETAN)
      CALL DISP(DETERM,FREQ2,VEL2)
      VALN=ABS(REAL(DETERM)+AIMAG(DETERM))
      IF(VAL.GT.VALN) GO TO 1300
      IF(VAL.GT.VALP) GO TO 1400
      IF(VALP.GT.VALN) GO TO 1500
      THETAN=THETA
      THETA=(THETAN+THETAP)/2.
      K=1
      GO TO 1200
      1500 THETAP=THETA
      THETA=(THETAP+THETAN)/2.
      K=1
      GO TO 1200
      1300 THETAP=THETA
      THETA=THETAN
      THETAN=THETAN-THSP
      IF(K.GT.0) THETAN=THETA-ABS(THETAP-THETA)
      GO TO 1200
      1400 THETAN=THETA
```

```
18500     THETA=THETAP
18600     THETAP=THETAP+THSP
18700     IF(K.GT.0) THETAP=THETA+ABS(THETA-THETAN)
18800     GO TO 1200
18900      1600 FREQ=FREQ+STEP*COS(THETA)
19000     VEL=VEL+STEP*SIN(THETA)
19100     N=N+1
19200     K=0
19300     F(N)=FREQ
19400     V(N)=VEL
19500     IF(FREQ.GT.3.5) GO TO 17
19600     IF(FREQ.LT.0.0) GO TO 17
19700     IF(VEL.GT.4.0) GO TO 17
19800     IF(VEL.LT.0.0) GO TO 17
19900     GO TO 14
20000      17 DETR=0.0
20100     DETI=0.0
20200      31 C=1.0
20300     15 CONTINUE
20400     F(1)=N
20500     V(1)=N
20600     DO 16 I=1,N
20700     C-  WRITE THE POINTS AND INPUT DATA TO OUTPUT FILE
20800     16 WRITE(2,2000) F(I),V(I)
20900     WRITE(2,700) ARHO,AZ,AC11,AC33,AC13,AC55
21000     WRITE(2,700) BRHO,BZ,BC11,BC33,BC13,BC55
21100     STOP
21200     END
21250     C-  CALC CALCULATES THE VALUE OF THE DETERMINANT
21300     SUBROUTINE CALC(A,DETERM)
21400     COMMON ARHO,AZ,AC11,AC33,AC13,AC55,C
21500     COMMON BRHO,BZ,BC11,BC33,BC13,BC55
21600     INTEGER X,Y
21700     COMPLEX Z,A,RATIO,DETERM
21800     DIMENSION CA(8),Z(8),A(8,8)
21900     K=2
22000     L=1
22100     1 DO 2 I=L,8
22200     2 CA(I)=CDABS(A(I,L))
22300     3 IF(CA(L)) 9,4,9
22400     4 M=L+1
22500     DO 8 X=M,8
22600     5 IF(CA(X)) 6,8,6
22700     6 DO 7 Y=1,8
22800     Z(Y)=A(L,Y)
22900     A(L,Y)=A(X,Y)
23000     7 A(X,Y)=Z(Y)
23100     GO TO 9
23200     8 CONTINUE
23300     DETERM=(0.0,0.0)
23400     9 DO 10 I=K,8
23500     RATIO=A(I,L)/A(L,L)
23600     DO 10 J=K,8
23700     10 A(I,J)=A(I,J)-A(L,J)*RATIO
23800     IF(K-8) 11,12,12
23900     11 L=K
24000     K=K+1
24100     GO TO 1
24200     12 DETERM=(1,0)
24300     DO 13 L=1,8
24400     13 DETERM=DETERM*A(L,L)
24500     RETURN
```

```
24600     END
24700     C-  DISP CALCULATES THE VALUES OF THE ELEMENTS OF THE
24800     C-  MATRIX
24900     SUBROUTINE DISP(DETERM,FREQ,VEL)
25000     IMPLICIT COMPLEX(G-H,T,Z)
25100     DIMENSION A(8,8)
25200     COMPLEX KZAP,KZAN,KZBP,KZBN,A,DETERM,ISIN,Y,KZAS,KZBS
25300     COMMON ARHO,AZ,AC11,AC33,AC13,AC55,C
25400     COMMON BRHO,BZ,BC11,BC33,BC13,BC55
25500     REAL KX,G,F
25600     ISIN(Y)=CMPLX(-AIMAG(CSIN(Y)),REAL(CSIN(Y)))
25700     DO 25 I=1,8
25800     DO 25 J=1,8
25900      25 A(I,J)=0.0
26000     W=FREQ*2.0*3.14159265410.
26100     KX=W/VEL
26200     G=AZ
26300     F=BZ
26400     BA=(ARHO/(AC33*AC55))*(AC33*(AC11/ARHO-W**2/KX**2)-AC13*
26500     -(2.*AC55+AC13)/ARHO-AC55*W**2/KX**2)
26600     DA=(ARHO**2/(AC33*AC55))*(W**2/KX**2-AC55/ARHO)*(W**2/KX**2-AC11/
26700     -ARHO)
26800     ZA=BA**2-4*DA
26900     KZAP=CSQRT(0.5*(KX**2)*(-BA+CSQRT(ZA)))
27000     KZAN=CSQRT(0.5*(KX**2)*(-BA-CSQRT(ZA)))
27100     BB=(BRHO/(BC33*BC55))*(BC33*(BC11/BRHO-W**2/KX**2)-BC13*
27200     -(2.*BC55+BC13)/BRHO-BC55*W**2/KX**2)
27300     DB=(BRHO**2/(BC33*BC55))*(W**2/KX**2-BC55/BRHO)*(W**2/KX**2-BC11/
27400     -BRHO)
27500     ZB=BB**2-4*DB
27600     KZBP=CSQRT(0.5*(KX**2)*(-BB+CSQRT(ZB)))
27700     KZBN=CSQRT(0.5*(KX**2)*(-BB-CSQRT(ZB)))
27800     IF(KZAP.EQ.0.0) GO TO 10
27900     IF(KZAN.EQ.0.0) GO TO 10
28000     IF(KZBP.EQ.0.0) GO TO 10
28100     IF(KZBN.EQ.0.0) GO TO 10
28200     TANAP=(ARHO*W**2-AC11*KX**2-AC55*KZAP**2)/
28300     -((AC55+AC13)*KX*KZAP)
28400     TANAN=(ARHO*W**2-AC11*KX**2-AC55*KZAN**2)/
28500     -((AC55+AC13)*KX*KZAN)
28600     TANBP=(BRHO*W**2-BC11*KX**2-BC55*KZBP**2)/
28700     -((BC55+BC13)*KX*KZBP)
28800     TANBN=(BRHO*W**2-BC11*KX**2-BC55*KZBN**2)/
28900     -((BC55+BC13)*KX*KZBN)
29000     GAP=AC33*KZAP*TANAP+CMPLX(AC13*KX,0.0)
29100     GAN=AC33*KZAN*TANAN+CMPLX(AC13*KX,0.0)
29200     GBP=BC33*KZBP*TANBP+CMPLX(BC13*KX,0.0)
29300     GBN=BC33*KZBN*TANBN+CMPLX(BC13*KX,0.0)
29400     HAP=KZAP+KX*TANAP
29500     HAN=KZAN+KX*TANAN
29600     HBP=KZBP+KX*TANBP
29700     HBN=KZBN+KX*TANBN
29800     C-  THE VALUES OF THE MATRIX
29900     A(1,1)=(2.0,0.0)
30000     A(1,3)=(2.0,0.0)
30100     A(1,5)=(-2.0,0.0)
30200     A(1,7)=(-2.0,0.0)
30300     A(2,2)=-TANAP
30400     A(2,4)=-TANAN
30500     A(2,6)=TANBP
30600     A(2,8)=TANBN
30700     A(3,1)=2*GAP
```

```
30800     A(3,3)=2*GAN
30900     A(3,5)=-2*GBP
31000     A(3,7)=-2*GBN
31100     A(4,2)=-AC55*HAP
31200     A(4,4)=-AC55*HAN
31300     A(4,6)=BC55*HBP
31400     A(4,8)=BC55*HBN
31500     A(5,1)=2*GAP*CCOS(KZAP*G)
31600     A(5,2)=-GAP*ISIN(KZAP*G)
31700     A(5,3)=2*GAN*CCOS(KZAN*G)
31800     A(5,4)=-GAN*ISIN(KZAN*G)
31900     A(6,1)=2*HAP*ISIN(KZAP*G)
32000     A(6,2)=-HAP*CCOS(KZAP*G)
32100     A(6,3)=2*HAN*ISIN(KZAN*G)
32200     A(6,4)=-HAN*CCOS(KZAN*G)
32300     A(7,5)=2*GBP*CCOS(KZBP*F)
32400     A(7,6)=GBP*ISIN(KZBP*F)
32500     A(7,7)=2*GBN*CCOS(KZBN*F)
32600     A(7,8)=GBN*ISIN(KZBN*F)
32700     A(8,5)=-2*HBP*ISIN(KZBP*F)
32800     A(8,6)=-HBP*CCOS(KZBP*F)
32900     A(8,7)=-2*HBN*ISIN(KZBN*F)
33000     A(8,8)=-HBN*CCOS(KZBN*F)
33100     CALL CALC(A,DETERM)
33200     GO TO 20
33300      10 C=0.0
33400      20 RETURN
33500     END
```

WORKFILE: RETRACE3 (08/21/85)

```
      100     $RESET FREE
      200     $SET OWN
      300     FILE  1(TITLE="FILE1.",FILETYPE=7)
      400     FILE  2(TITLE="FILE2.",KIND=DISK,MAXRECSIZE=14,
      500          + AREAS=36000,AREASIZE=14,PROTECTION=SAVE)
      600     FILE  3(TITLE="FILE3.",KIND=DISK,MAXRECSIZE=14,
      700          + AREAS=36000,AREASIZE=14,PROTECTION=SAVE)
      800     $SET FREE
      900     DIMENSION F(2000),V(2000)
     1000     COMPLEX DETERM
     1001     C-  THE PROGRAM RETRACE2 CALCULATES THE DISPERSION CURVES FOR A 3
     1002     C-  LAYER COMPOSITE MATERIAL CONSTRUCTED FROM 3 ORTHOTROPIC LAYERS
     1003     C-  THE LAYER DENSITIES (ARHO,BRHO,CRHO) ARE ENTERED IN G/MM3.  THE
     1004     C-  LAYER CALIPERS (AZ,BZ,CZ) ARE ENTERED IN MM.  THE ELASTIC
     1005     C-  CONSTANTS (AC11,AC33,...CC13,CC55) ARE ENTERED IN GPA X 10-3.
     1006     C-  THE PROGRAM FINDS THE DISPERSION CURVES BY FIRST FINDING A
     1007     C-  POINT ON ONE OF THE CURVES, AND THEN TRACING THE OTHER POINTS
     1008     C-  ON THE CURVE.  THE CURVES ARE OBTAINED IN THE REGION OF
     1009     C-  VELOCITIES BETWEEN 0.2 AND 3.5 M/SEC AND FREQUENCIES BETWEEN
     1010     C-  0.2 AND 3.5 KHZ.  THE POINTS ON THE CURVES ARE LOCATED BY
     1011     C-  FINDING THE VALUES OF FREQUENCY AND VELOCITY WHICH SET THE
     1012     C-  DETERMINANT EQUAL TO ZERO.
     1013     C-  EPS= THE TOLERANCE ON THE ANGLE THETA
     1014     C-  THSP= THE INITIAL ANGLE SEARCHED RELATIVE TO THETA
     1015     C-  STEP= THE STEP LENGTH (RADIUS OF SEARCH ARC)
     1016     C-  AFTER FINDING A POINT ON THE CURVE, THE PROGRAM SEARCHES FOR
     1017     C-  THE NEXT POINT ALONG AN ARC OF RADIUS "STEP".  THE VALUES OF THE
     1018     C-  DETERMINANT ARE CALCULATED AT THREE ANGLES (THETA,THETAP,THETAN).
     1019     C-  THE SEARCH ROUTINE FINDS THE ANGLE WHICH MINIMIZES THE
     1020     C-  DETERMINANT.
     1100     COMMON ARHO,AZ,AC11,AC33,AC13,AC55,C
     1200     COMMON BRHO,BZ,BC11,BC33,BC13,BC55
     1300     COMMON CRHO,CZ,CC11,CC33,CC13,CC55
     1350     C-  READ INPUT DATA
     1400     READ(1,700) ARHO,AZ,AC11,AC33,AC13,AC55
     1500      700 FORMAT(6F12.8)
     1600     READ(1,700) BRHO,BZ,BC11,BC33,BC13,BC55
     1700     READ(1,700) CRHO,CZ,CC11,CC33,CC13,CC55
     1800     STEP=0.03
     1900     THSP=0.03
     2000     A=0.0
     2100     B=0.0
     2200     MAX=15
     2300     L=0
     2400     C=1.0
     2500     K=0
     2600     N=1
     2700     EPS=1.0E-03
     2750     C-  FIND POINTS ON THE CURVES NEAR THE VELOCITY AXIS
     2800     DO 5 I=20,400
     2900     VEL=I*0.01
     3000     FREQ=0.20
     3050     TMPR2=TMPR1
     3060     TMPI2=TMPI1
     3100     TMPR1=DETR
     3200     TMPI1=DETI
     3300     CALL DISP(DETERM,FREQ,VEL)
     3400     DETR=REAL(DETERM)*10000000000000000.
     3500     DETI=AIMAG(DETERM)*10000000000000000.
```

```
3550     IF(C.LE.C.0) GO TO 6
3560     C-  HAS A MINIMUM IN DETR OR DETI BEEN REACHED
3580     IF((TMPR1.LT.DETR).AND.(TMPR1.LT.TMPR2)) GO TO 3
3590     IF((ABS(TMPI1).LT.ABS(DETI)).AND.(ABS(TMPI1).LT.ABS(TMPI2)))
3595     - GO TO 3
3598     C-  HAVE DETR OR DETI CHANGED SIGN
3600     IF((DETR*TMPR1).LT.C.0) GO TO 3
3650     IF((DETI*TMPI1).LT.0.0) GO TO 3
3700     GO TO 5
3900     3 N=N+1
3950     C-  INITIAL POINT A,B
4000     F(N)=A
4100     V(N)=B
4200     VEL=VEL-C.005
4250     C-  INITIAL VALUE OF THETA - START SEARCH ROUTINE
4300     THETA=0.C
4400     4 THETAP=THETA+THSP
4500     THETAN=THETA-THSP
4550     C-  IF CURVE TRACES BACK ON ITSELF - STOP SEARCH ROUTINE
4600     IF(COS(THETA).LT.-0.3) GO TO 5
4650     C-  IS THE ESTIMATE OF THE ANGLE CLOSE ENOUGH
4700     200 IF((THETAP-THETAN).LE.EPS) GO TO 600
4800     L=L+1
4900     IF(L.GT.MAX) GO TO 600
4950     C-  FIND A NEW SET OF THREE ANGLES
5000     FREQ2=FREQ+STEP*COS(THETA)
5100     VEL2=VEL+STEP*SIN(THETA)
5200     CALL DISP(DETERM,FREQ2,VEL2)
5300     VAL=ABS(REAL(DETERM))+ABS(AIMAG(DETERM))
5400     FREQ2=FREQ+STEP*COS(THETAP)
5500     VEL2=VEL+STEP*SIN(THETAP)
5600     CALL DISP(DETERM,FREQ2,VEL2)
5700     VALP=ABS(REAL(DETERM))+ABS(AIMAG(DETERM))
5800     FREQ2=FREQ+STEP*COS(THETAN)
5900     VEL2=VEL+STEP*SIN(THETAN)
6000     CALL DISP(DETERM,FREQ2,VEL2)
6100     VALN=ABS(REAL(DETERM))+ABS(AIMAG(DETERM))
6200     IF(VAL.GT.VALN) GO TO 300
6300     IF(VAL.GT.VALP) GO TO 400
6400     IF(VALP.GT.VALN) GO TO 500
6500     THETAN=THETA
6600     THETA=(THETA+THETAP)/2.
6700     K=1
6800     GO TO 200
6900     500 THETAP=THETA
7000     THETA=(THETA+THETAN)/2.
7100     K=1
7200     GO TO 200
7300     300 THETAP=THETA
7400     THETA=THETAN
7500     THETAN=THETAN-THSP
7600     IF(K.GT.0) THETAN=THETA-ABS(THETAP-THETA)
7700     GO TO 200
7800     400 THETAN=THETA
7900     THETA=THETAP
8000     THETAP=THETAP+THSP
8100     IF(K.GT.0) THETAP=THETA+ABS(THETA-THETAN)
8200     GO TO 200
8250     C-  THE NEXT POINT HAS BEEN FOUND
8300     600 FREQ=FREQ+STEP*COS(THETA)
8400     VEL=VEL+STEP*SIN(THETA)
8500     N=N+1
```

```
 8600     L=0
 8700     K=0
 8800     F(N)=FREQ
 8900     V(N)=VEL
 9000     2000 FORMAT(2F20.8)
 9050     C-  IS THE NEW POINT WITHIN THE SEARCH AREA
 9100     IF(FREQ.GT.3.5) GO TO 7
 9200     IF(FREQ.LT.0.0) GO TO 7
 9300     IF(VEL.GT.4.0) GO TO 7
 9400     IF(VEL.LT.0.0) GO TO 7
 9500     GO TO 4
 9600      7 DETR=0.0
 9700     DETI=0.0
 9800     C=0.0
 9900     GO TO 5
10000      6 C=1.0
10050     I=I+60.
10100     5 CONTINUE
10150     C-  SEARCH FOR CURVE AT VELOCITY 3.5 M/SEC
10160     C-  FREQUENCY 0.2-3.5 KHZ
10170     C-  SEARCH ROUTINE IS THE SAME AS ABOVE
10200     DO 15 I=1,200
10300     VEL=4.0
10400     FREQ=I*0.02
10500     TMPR1=DETR*10000000CC00000.
10600     TMPI1=DETI*10000000CC00000.
10700     CALL DISP(DETERM,FREQ,VEL)
10800     DETR=REAL(DETERM)
10900     DETI=AIMAG(DETERM)
11000     IF(C.EQ.0.0) GO TO 18
11100     IF(TMPR1*DETR) 13,12,12
11200     12 IF(TMPI1*DETI)13,15,15
11300     13 N=N+1
11400     K=0
11500     F(N)=A
11600     V(N)=B
11700     FREQ=FREQ-0.01
11800     THETA=-0.785398163
11900     14 THETAP=THETA+THSP
12000     THETAN=THETA-THSP
12100     IF(COS(THETA).LT.-0.5) GO TO 15
12200     1200 IF((THETAP-THETAN).LE.EPS) GO TO 1600
12300     L=L+1
12400     IF(L.GT.MAX) GO TO 1600
12500     FREQ2=FREQ+STEP*COS(THETA)
12600     VEL2=VEL+STEP*SIN(THETA)
12700     CALL DISP(DETERM,FREQ2,VEL2)
12800     VAL=ABS(REAL(DETERM))+ABS(AIMAG(DETERM))
12900     FREQ2=FREQ+STEP*COS(THETAP)
13000     VEL2=VEL+STEP*SIN(THETAP)
13100     CALL DISP(DETERM,FREQ2,VEL2)
13200     VALP=ABS(REAL(DETERM))+ABS(AIMAG(DETERM))
13300     FREQ2=FREQ+STEP*COS(THETAN)
13400     VEL2=VEL+STEP*SIN(THETAN)
13500     CALL DISP(DETERM,FREQ2,VEL2)
13600     VALN=ABS(REAL(DETERM))+ABS(AIMAG(DETERM))
13700     IF(VAL.GT.VALP) GO TO 1400
13800     IF(VAL.GT.VALN) GO TO 1300
13900     IF(VALP.GT.VALN) GO TO 1500
14000     THETAN=THETA
14100     THETA=(THETA+THETAP)/2.
14200     K=1
```

```
14300     GO TO 1200
14400     1500 THETAP=THETA
14500     THETA=(THETA+THETAN)/2.
14600     K=1
14700     GO TO 1200
14800      1300 THETAP=THETA
14900     THETA=THETAN
15000     THETAN=THETAN-THSP
15100     IF(K.GT.0) THETAN=THETA-ABS(THETAP-THETA)
15200     GO TO 1200
15300      1400 THETAN=THETA
15400     THETA=THETAP
15500     THETAP=THETAP+THSP
15600     IF(K.GT.0) THETAP=THETA+ABS(THETA-THETAN)
15700     GO TO 1200
15800      1600 FREQ=FREQ+STEP*COS(THETA)
15900     VEL=VEL+STEP*SIN(THETA)
16000     N=N+1
16100     F(N)=FREQ
16200     V(N)=VEL
16300     L=0
16400     IF(FREQ.GT.3.5) GO TO 17
16500     IF(FREQ.LT.0.0) GO TO 17
16600     IF(VEL.GT.4.0) GO TO 17
16700     IF(VEL.LT.0.0) GO TO 17
16800     GO TO 14
16900      17 DETR=0.0
17000     DETI=0.0
17100     C=0.0
17200     GO TO 15
17300      18 C=1.0
17400     15 CONTINUE
17500     F(1)=N
17600     V(1)=N
17650     C-   WRITE THE POINTS AND INPUT DATA TO OUTPUT FILE
17700     DO 16 I=1,N
17800     16 WRITE(2,2000) F(I),V(I)
17900     WRITE(2,700) ARHO,AZ,AC11,AC33,AC13,AC55
18000     WRITE(2,700) BRHO,BZ,BC11,BC33,BC13,BC55
18100     WRITE(2,700) CRHO,CZ,CC11,CC33,CC13,CC55
18200     STOP
18300     END
18350     C-   CALC CALCULATES THE VALUE OF THE DETERMINANT
18400     SUBROUTINE CALC(A,DETERM)
18500     COMMON ARHO,AZ,AC11,AC33,AC13,AC55,C
18600     COMMON BRHO,BZ,BC11,BC33,BC13,BC55
18700     COMMON CRHO,CZ,CC11,CC33,CC13,CC55
18800     INTEGER X,Y
18900     COMPLEX Z,A,RATIO,DETERM
19000     DIMENSION CA(12),Z(12),A(12,12)
19100     K=2
19200     L=1
19300      1 DO 2 I=L,12
19400     2 CA(I)=CDABS(A(I,L))
19500     3 IF(CA(L)) 9,4,9
19600     4 M=L+1
19700      DO 8 X=M,12
19800     5 IF(CA(X)) 6,8,6
19900      6 DO 7 Y=1,12
20000     Z(Y)=A(L,Y)
20100     A(L,Y)=A(X,Y)
20200     7 A(X,Y)=Z(Y)
```

```
      GO TO 9
    8 CONTINUE
      DETERM=(C.0,0.0)
    9 DO 10 I=K,12
      RATIO=A(I,L)/A(L,L)
      DO 10 J=K,12
   10 A(I,J)=A(I,J)-A(L,J)*RATIO
      IF(K-12) 11,12,12
   11 L=K
      K=K+1
      GO TO 1
   12 DETERM=(1,0)
      DO 13 L=1,12
   13 DETERM=DETERM*A(L,L)
      RETURN
      END
C-  DISP CALCULATES THE VALUES OF THE ELEMENTS OF THE
C-  MATRIX
      SUBROUTINE DISP(DETERM,FREQ,V)
      IMPLICIT COMPLEX(G-H,T,Z)
      DIMENSION A(12,12)
      COMPLEX KZAP,KZAN,KZBP,KZBN,A,DETERM,ISIN,Y,KZCP,KZCN
      COMMON ARHO,AZ,AC11,AC33,AC13,AC55,C
      COMMON BRHO,BZ,BC11,BC33,BC13,BC55
      COMMON CRHO,CZ,CC11,CC33,CC13,CC55
      REAL KX,G,F
      ISIN(Y)=CMPLX(-AIMAG(CSIN(Y)),REAL(CSIN(Y)))
      DO 25 I=1,12
      DO 25 J=1,12
   25 A(I,J)=0.0
      W=FREQ*2.0*3.141592654/10.0
      KX=W/V
      G=AZ+BZ
      F=CZ
      BA=ARHO/(AC33*AC55)*(AC33*(AC11/ARHO-W**2/KX**2)-AC13*
     -(2.*AC55+AC13)/ARHO-AC55*W**2/KX**2)
      DA=ARHO**2/(AC33*AC55)*(W**2/KX**2-AC55/ARHO)*(W**2/KX**2-AC11/
     -ARHO)
      ZA=BA**2-4*DA
      KZAP=CSQRT(0.5*(KX**2)*(-BA+CSQRT(ZA)))
      KZAN=CSQRT(0.5*(KX**2)*(-BA-CSQRT(ZA)))
      BB=BRHO/(BC33*BC55)*(BC33*(BC11/BRHO-W**2/KX**2)-BC13*
     -(2.*BC55+BC13)/BRHO-BC55*W**2/KX**2)
      DB=BRHO**2/(BC33*BC55)*(W**2/KX**2-BC55/BRHO)*(W**2/KX**2-BC11/
     -BRHO)
      ZB=BB**2-4*DB
      KZBP=CSQRT(0.5*(KX**2)*(-BB+CSQRT(ZB)))
      KZBN=CSQRT(0.5*(KX**2)*(-BB-CSQRT(ZB)))
      BC=CRHO/(CC33*CC55)*(CC33*(CC11/CRHO-W**2/KX**2)-CC13*
     -(2.*CC55+CC13)/CRHO-CC55*W**2/KX**2)
      DC=CRHO**2/(CC33*CC55)*(W**2/KX**2-CC55/CRHO)*(W**2/KX**2-CC11/
     -CRHO)
      ZC=BC**2-4*DC
      KZCP=CSQRT(0.5*(KX**2)*(-BC+CSQRT(ZC)))
      KZCN=CSQRT(0.5*(KX**2)*(-BC-CSQRT(ZC)))
      IF(KZAP.EQ.0.0) GO TO 10
      IF(KZAN.EQ.0.0) GO TO 10
      IF(KZBP.EQ.0.0) GO TO 10
      IF(KZBN.EQ.0.0) GO TO 10
      IF(KZCP.EQ.0.0) GO TO 10
      IF(KZCN.EQ.0.0) GO TO 10
      TANAP=(ARHO*W**2-AC11*KX**2-AC55*KZAP**2)/
```

```
26300      -((AC55*AC13)*KX*KZAP)
26400      TANAN=(ARHO*W**2-AC11*KX**2-AC55*KZAN**2)/
26500      -((AC55+AC13)*KX*KZAN)
26600      TANBP=(BRHO*W**2-BC11*KX**2-BC55*KZBP**2)/
26700      -((BC55+BC13)*KX*KZBP)
26800      TANBN=(BRHO*W**2-BC11*KX**2-BC55*KZBN**2)/
26900      -((BC55+BC13)*KX*KZBN)
27000      TANCP=(CRHO*W**2-CC11*KX**2-CC55*KZCP**2)/
27100      -((CC55+CC13)*KX*KZCP)
27200      TANCN=(CRHO*W**2-CC11*KX**2-CC55*KZCN**2)/
27300      -((CC55+CC13)*KX*KZCN)
27400      GAP=AC33*KZAP*TANAP+CMPLX(AC13*KX,0.0)
27500      GAN=AC33*KZAN*TANAN+CMPLX(AC13*KX,0.0)
27600      GBP=BC33*KZBP*TANBP+CMPLX(BC13*KX,0.0)
27700      GBN=BC33*KZBN*TANBN+CMPLX(BC13*KX,0.0)
27800      GCP=CC33*KZCP*TANCP+CMPLX(CC13*KX,0.0)
27900      GCN=CC33*KZCN*TANCN+CMPLX(CC13*KX,0.0)
28000      HAP=KZAP+KX*TANAP
28100      HAN=KZAN+KX*TANAN
28200      HBP=KZBP+KX*TANBP
28300      HBN=KZBN+KX*TANBN
28400      HCP=KZCP+KX*TANCP
28500      HCN=KZCN+KX*TANCN
28550     C-   THE VALUES OF THE MATRIX
28600     A(1,1)=2.0*CCOS(KZAP*BZ)
28700     A(1,2)=-ISIN(KZAP*BZ)
28800     A(1,3)=2.0*CCOS(KZAN*BZ)
28900     A(1,4)=-ISIN(KZAN*BZ)
29000     A(1,5)=-2.0*CCOS(KZBP*BZ)
29100     A(1,6)=ISIN(KZBP*BZ)
29200     A(1,7)=-2.0*CCOS(KZBN*BZ)
29300     A(1,8)=ISIN(KZBN*BZ)
29400      A(2,5)=(-2.0,0.0)
29500      A(2,7)=(-2.0,0.0)
29600      A(2,9)=(2.0,0.0)
29700      A(2,11)=(2.0,0.0)
29800     A(3,1)=2.*TANAP*ISIN(KZAP*BZ)
29900     A(3,2)=-TANAP*CCOS(KZAP*BZ)
30000     A(3,3)=2.*TANAN*ISIN(KZAN*BZ)
30100     A(3,4)=-TANAN*CCOS(KZAN*BZ)
30200     A(3,5)=-2.*TANBP*ISIN(KZBP*BZ)
30300     A(3,6)=TANBP*CCOS(KZBP*BZ)
30400     A(3,7)=-2.*TANBN*ISIN(KZBN*BZ)
30500     A(3,8)=TANBN*CCOS(KZBN*BZ)
30600      A(4,6)=TANBP
30700      A(4,8)=TANBN
30800      A(4,10)=-TANCP
30900      A(4,12)=-TANCN
31000     A(5,1)=2.0*GAP*CCOS(KZAP*BZ)
31100     A(5,2)=-GAP*ISIN(KZAP*BZ)
31200     A(5,3)=2.0*GAN*CCOS(KZAN*BZ)
31300     A(5,4)=-GAN*ISIN(KZAN*BZ)
31400     A(5,5)=-2.0*GBP*CCOS(KZBP*BZ)
31500     A(5,6)=GBP*ISIN(KZBP*BZ)
31600     A(5,7)=-2.0*GBN*CCOS(KZBN*BZ)
31700     A(5,8)=GBN*ISIN(KZBN*BZ)
31800      A(6,5)=-2.0*GBP
31900      A(6,7)=-2.0*GBN
32000      A(6,9)=2.0*GCP
32100      A(6,11)=2.0*GCN
32200     A(7,1)=2.*AC55*HAP*ISIN(KZAP*BZ)
32300     A(7,2)=-AC55*HAP*CCOS(KZAP*BZ)
```

```
      A(7,3)=2.*AC55*HAN*ISIN(KZAN*BZ)
      A(7,4)=-AC55*HAN*CCOS(KZAN*BZ)
      A(7,5)=-2.*BC55*HBP*ISIN(KZBP*BZ)
      A(7,6)=BC55*HBP*CCOS(KZBP*BZ)
      A(7,7)=-2.*BC55*HBN*ISIN(KZBN*BZ)
      A(7,8)=BC55*HBN*CCOS(KZBN*BZ)
       A(8,6)=BC55*HBP
       A(8,8)=BC55*HBN
       A(8,10)=-CC55*HCP
       A(8,12)=-CC55*HCN
       A(9,1)=2.0*GAP*CCOS(KZAP*G)
       A(9,2)=-GAP*ISIN(KZAP*G)
       A(9,3)=2.0*GAN*CCOS(KZAN*G)
       A(9,4)=-GAN*ISIN(KZAN*G)
       A(10,9)=2.0*GCP*CCOS(KZCP*F)
       A(10,10)=GCP*ISIN(KZCP*F)
       A(10,11)=2.0*GCN*CCOS(KZCN*F)
       A(10,12)=GCN*ISIN(KZCN*F)
       A(11,1)=2.0*HAP*ISIN(KZAP*G)
       A(11,2)=-HAP*CCOS(KZAP*G)
      A(11,3)=2.0*HAN*ISIN(KZAN*G)
       A(11,4)=-HAN*CCOS(KZAN*G)
       A(12,9)=-2.0*HCP*ISIN(KZCP*F)
       A(12,10)=-HCP*CCOS(KZCP*F)
       A(12,11)=-2.0*HCN*ISIN(KZCN*F)
       A(12,12)=-HCN*CCOS(KZCN*F)
       CALL CALC(A,DETERM)
      GO TO 20
       10 C=0.0
       20 RETURN
       END
```